Spring 2017

Chemical characterization of biomass burning and sea spray aerosol

Thilina Jayarathne
University of Iowa

CHEMICAL CHARACTERIZATION OF BIOMASS BURNING AND SEA SPRAY AEROSOL

by

Thilina Jayarathne

A thesis submitted in partial fulfillment
of the requirements for the Doctor of Philosophy
degree in Chemistry in the
Graduate College of
The University of Iowa

May 2017

Thesis Supervisor: Associate Professor Elizabeth A. Stone

Graduate College
The University of Iowa
Iowa City, Iowa

CERTIFICATE OF APPROVAL

_____

PH.D. THESIS

_____

This is to certify that the Ph.D. thesis of

Thilina Jayarathne

has been approved by the Examining Committee for
the thesis requirement for the Doctor of Philosophy degree
in Chemistry at the May 2017 graduation.

Thesis Committee:_____
Elizabeth A. Stone, Thesis Supervisor

_____
Gary W. Small

_____
Alexei V. Tivanski

_____
Amanda J. Haes

_____
Keri C. Hornbuckle

To my loving wife and beloved parents

ACKNOWLEDGEMENTS

First and foremost, I would like to thank my advisor, Professor Betsy Stone for all the opportunities and guidance provided me during my graduate studies. I also acknowledge my past and present committee members, Professors Gary Small, Amanda Haes, Alexei Tivanski, Keri Hornbuckle and Tori Forbes, for their commitment, support, and encouragement. I also thank current and past Stone group members, especially my undergraduate mentees Austin Kammerer, Michael Dolan, Ashley Gilbert and Kaitlyn Daugherty for their assistance during my research projects. I would like to thank the organizers of fire lab at Missoula experiment (FLAME-4), Nepal ambient monitoring and source testing experiment (NAMaSTE) and Indonesia field campaigns. I also thank center for aerosol impacts on climate and environment (CAICE) team for their help and guidance. My sincere thanks to my undergraduate supervisor Professor Upul Subasinghe and all the faculty members of the Department of Forestry and Environmental Science, University of Sri Jayewardenepura, Sri Lanka, for all the knowledge and support given me as an undergraduate. I would also like to thank all my teachers from kindergarten to high school for inspiring me to pursue the goals in my life.

Most importantly, I thank my loving wife Aruni who stood by me through thick and thin for the last six years. I thank my loving mother and father for their constant and endless support and love given me from the day I was born until this moment to become the person who I am today. I also thank my loving sister for her endless support. I also thank all of my friends in Iowa City for always being there for me no matter what. I am truly grateful to you all for being great friends and making this far away land a home away from home.

ABSTRACT

Particulate matter (PM) suspended in air varies in size from nanometers to micrometers and contains a wide range of chemical components, including organic compounds, black carbon (soot), inorganic minerals and metals. Atmospheric aerosols are generated from either primary sources like volcanic eruptions, re-suspended soil dust, sea spray, vegetative detritus, fossil fuel and biomass combustion emissions; or secondary atmospheric reactions via gas-to-particle conversion of atmospheric gases. Particle size, abundance, and chemical composition determine how a particle interacts with light and other atmospheric constituents (e.g. gases, water vapor) in addition to its impact on human health. While atmospheric scientists have been working on characterizing atmospheric aerosols for many years, major gaps persist in understanding the properties of many globally-important sources. This dissertation provides new understanding of the chemical composition of biomass burning and sea spray aerosols.

PM emissions from biomass burning vary by fuel, and depend on fuel type and composition, moisture content, and combustion conditions. Although biomass smoke is critically important in global climate and local-regional health impacts, the physical and chemical composition of biomass burning aerosol is still not fully understood in the case of peat, agricultural residues and cooking fires. The Fire Laboratory at Missoula Experiments (FLAME) were designed to fulfill these gaps to improve our understanding in both historically undersampled and well-studied fuels while adding new instrumentation and experimental methods to provide previously unavailable information on chemical properties of biomass burning emissions. Globally-important biomass fuels were combusted in a controlled environment, and PM was chemically characterized to

compute fuel based emission factors (EF) as the amount of chemical species released per unit mass of fuel burned. We showed that chemical composition of PM varies for different fuel types and certain fuels types (e.g., peat and ocote) emit considerably high concentrations of polycyclic aromatic compounds that are associated with negative health effects. We also showed that PM from biomass smoke contains fluoride for the first time, at approximately 0.1% by weight. With respect to the annual global emissions of PM due to biomass burning, this makes biomass burning an important source of fluoride to the atmosphere. Further, peatland fire emissions are one of the most understudied atmospheric aerosol sources but are a major source of greenhouse gases globally and cause severe air quality problems in Asia. This thesis provides the first field-based emissions characterization study, for samples collected at peat burning sites in Central Kalimantan, Indonesia. Using these EFs and estimates of the mass of fuel burned, it was estimated that 3.2 - 11 Tg of $PM_{2.5}$ were emitted to atmosphere during 2015 El Niño peat fire episode which is ~10 % of estimated total annual PM flux for biomass burning. Overall, these studies computed more representative EFs for previously undersampled sources like peat, and previously unidentified chemical species like fluoride that can be used to update regional and global emission inventories.

The concentration and composition of organic compounds in sea spray aerosol (SSA) alters its optical properties, hygroscopicity, cloud condensation, and ice nucleation properties and thus affects Earth's radiative budget. In the past, SSA has been difficult to characterize, because of low concentrations relative to background pollutants. Nascent SSA was generated during a mesocosm, using a wave-flume at the University of California, San Diego and was characterized for saccharides and inorganic ions in order

to assess their relative enrichment in fine ($PM_{2.5}$) and coarse ($PM_{10-2.5}$) SSA and sea surface microlayer (SSML) relative to seawater. For the first time, we showed that saccharides comprise a significant fraction of organic matter in fine and coarse SSA contributing 11 % and 27 %, respectively. Relative to sodium, saccharides were enriched 14-1314 times in fine SSA, 3-138 times in coarse SSA, but only up to 1.0-16.2 times in SSML. The saccharide and ion concentration in SSML and persistent whitecap foam was quantitatively assessed by another mesocosm study performed under controlled conditions. We demonstrated that relative to sodium, saccharides were enriched 1.7-6.4 times in SSML and 2.1-12 times in foam. Higher enrichment of saccharides in foam over the SSML indicates that surface active organic compounds become increasingly enriched on aged bubble film surfaces. Similarly, we showed that fine SSA contains saccharides characteristic of energy-related polysaccharides, while coarse SSA contains saccharides that are characteristic of structure-related polysaccharides. The ultrafiltration studies showed that structure-related polysaccharides effectively coagulate to form large particulate organic matter and size is likely the reason for their exclusion from small SSA. The enrichment of organic species in SSML, foam and SSA led to an enrichment of inorganic ions probably through chelation with organic molecules. Mean enrichment factors for major ions demonstrated the highest enrichment in fine SSA for potassium (1.3), magnesium (1.4), and calcium (1.7). Consequently, due to these organic and inorganic enrichments, SSA develops a significantly different chemical profile compared to seawater. These improved chemical profiles of SSA should be used to develop laboratory proxies to further study the transfer of organic matter across the ocean-air interface and the physical properties of SSA. .

Overall, the results presented in this dissertation provide new chemical profiles for previously understudied emission sources like peatland fire emissions, and previously unquantified chemical species like F^- in biomass burning emissions and enrichment of saccharides and ions in SSA. These data could be used in updating regional and global emission inventories, atmospheric modeling and human exposure studies.

PUBLIC ABSTRACT

The air around us contains very small particles that vary in size and chemical composition. These particles can scatter sunlight reducing the amount that reaches to the Earths' surface and overall cool the earth. Human exposures to atmospheric particles are linked to negative health impacts. Because the properties of particles determine their climate and health impacts, my research focuses on understanding the chemical composition and fluxes of particles emitted to the atmosphere from biomass fuel burning and sea spray. New chemical profiles for the combustion of globally-important fuels, such as conifers, agricultural residues, grasses, peat and cookstoves were developed and fuel-based emission factors (the mass of particles emitted from burning one kilogram fuels) were determined. This allowed for estimation of the amount of particles emitted to the atmosphere during the 2015 Indonesian peatland fires and the role of biomass burning in the global fluorine cycle. The estimated F^- flux from biomass burning is comparable to total fluorine emissions from anthropogenic sources and biomass burning emissions were identified as a major source of fluorine to the atmosphere. In my work related to particles emitted from sea, we found that organic compounds such as carbohydrates and inorganic ions such as calcium are selectively transferred to atmosphere across the air-water interface. Therefore, chemical composition in sea spray is different than that of seawater. Further, some carbohydrates in seawater coagulate and we hypothesize due to their size, they are likely excluded from small aerosol particles, making carbohydrate composition in small and large aerosols distinct from one another. These chemical profiles will enable better representation of biomass burning and sea spray emissions and their chemical properties in atmospheric models and laboratory studies.

TABLE OF CONTENTS

LIST OF TABLES

LIST OF FIGURES

CHAPTER ONE

INTRODUCTION

1.1 Atmospheric Aerosols

Atmospheric aerosols or particulate matter (PM) are solid and/or liquid particles suspended in air. These aerosols vary in size from 1 nm to 100 µm. Aerosols are categorized based on their size. Broadly, atmospheric aerosols can be categorized into three major size categories, namely coarse, fine and ultra-fine. Fine particles correspond to those less than 2.5 µm and coarse particles refer to particles in the size range of 2.5 – 10 µm in diameter; these two fractions accounted for a substantial fraction of the aerosol mass.[1-3] Ultrafine particles have diameters <0.1 µm and dominate the particle number distribution of atmospheric aerosols.[2] In the troposphere, the typical total particle number concentration varies between 10^2-10^5 particles per cubic centimeter and mass concentration range 1-100 µg m^{-3}.[1] However, the size distribution, number and mass concentration of aerosols in the atmosphere are highly variable, both temporally and spatially due to different generation mechanisms, atmospheric aging, atmospheric dilution and long range transport.[4, 5]

Atmospheric aerosols are generated from either primary sources or secondary atmospheric reactions as shown in Figure 1.1.[6] Primary aerosols originate from a wide variety of natural and anthropogenic sources like periodic volcanic eruptions, wind-driven or traffic related resuspension of soil dust, sea spray, fossil fuel and biomass combustion. Secondary atmospheric aerosols are formed by gas-to-particle conversion of atmospheric precursor gasses via atmospheric reactions. Combustion generated particles, such as those from biomass burning, automobile engines and fossil fuel burning can be

small as few nanometers and as large as 1 μm. Secondary atmospheric aerosol is also found mainly smaller than 1 μm. On the other hand, windblown dust, plant pollens, vegetative detritus, bacterial and fungal spores are generally few micrometers in size and can be as large as 100 μm.[2] Generally, high particle concentration are observed near the source (e.g. near a busy road) and it decreases at remote locations due to atmospheric dilution.[1, 2]

PM originates from one location can be transported long distances by wind. During long range transport, the aerosol particles encounter different atmospheric gases, moisture and sunlight, and undergo surface and multi-phase chemical reactions altering the chemical and physical properties of the primary aerosol particle.[7-11] Further, gas phase molecules can nucleate new particles or condense on to existing primary particles to form secondary aerosols via various chemical reactions affecting the composition of the atmospheric PM.[12-17] Further, both chemical composition of the particle and number of particles changes significantly during the different time of the year.[18] Aerosol that are produced photochemically (e.g. ammonium sulfate, secondary organic aerosol) usually have higher concentrations during summer and lower concentration during winter due to elevated temperatures, relative humidity and daylight.[17]

1.2 Chemical Composition of Aerosol

Ambient aerosols are a complex chemical mixture of carbonaceous compounds, inorganic ions, crustal materials and water vapor.[2] Carbonaceous aerosols are divided into two categories named as elemental carbon (EC) and organic carbon (OC). EC (a.k.a. black carbon (BC)) enters the atmosphere exclusively as primary emissions due to incomplete combustion of fossil fuel and biomass. OC is comprised of aliphatic and

aromatic hydrocarbons with diverse functional groups that are produced from both direct emissions from sources like biomass and fossil fuel burning, and by atmospheric oxidation of precursor gases.[13, 17, 19-22] In general, EC and OC contribute 30-50 % of total PM mass.[4, 17, 23]Apart from the organic constituents, inorganic ions in the atmospheric aerosol also comprise 20-40 % of ambient $PM_{2.5}$ by mass.[4, 16, 17, 23, 24] Sulfate (SO_4^{2-}) and nitrate (NO_3^-) anions, the predominant forms of atmospheric acid derivatives, are formed in the atmosphere mainly as secondary products of sulfur oxides (SO_x) and nitrogen oxides (NO_x), respectively.[12] Atmospheric particles containing elements such as calcium (Ca), magnesium (Mg), aluminum (Al), iron (Fe), titanium (Ti) and silica (Si) primarily originate from earth crust that is generated by windblown soil.[12] Particles containing transition metals (e.g. Zn, Pb, Mn, Cr, Cu, Ni) are associated with anthropogenic emissions such as coal and fossil fuel combustion, and industrial activities.[5] The chemical composition of particles are directly related with its emission source: marine aerosols are dominated by NaCl, desert aerosols are dominated by silica, peatland fire emissions are dominated by OC, and remote-continental and free-tropospheric aerosols are dominated by secondary aerosols.[2, 25] Thus, the chemical composition of atmospheric aerosols can state important insights to their source.

The chemical composition of fine and coarse particles is also different. Fine particles contain primary particles from combustion emissions and secondary aerosols formed by chemical reactions resulting in gas-to-particle conversion.[16, 23, 26] Coarse particles are primarily produced either by mechanical processes like re-suspended soil dust, fly ash, ocean wave breaking and tire wear or biological particles like pollens, fungal spores and vegetative detritus.[12, 23, 27, 28]

1.3 Importance of Aerosol

Atmospheric aerosols play an important role in the environment due to its influence on atmospheric physio-chemical processes, the Earths' radiative balance and climate, and human health.[1, 12, 29]

1.3.1 Effects on Atmospheric Physio-chemical Processes, Radiative Balance and Climate

The size and chemical composition of PM affect its aerosol physical properties such as hygroscopicity, cloud condensation and ice nucleation activity, and radiative forcing.[30-33] The hygroscopicity of atmospheric aerosols describes how these particles interact with water vapor. When relative humidity (RH) exceeds the deliquescence relative humidity (DRH) water vapor spontaneously absorbs onto the particle and it substantially increases in size.[34] The hygroscopic properties of PM can vary based on their chemical composition. Hydrophobic soot particles do not change their size in the presence of water vapor while particles containing water soluble materials (e.g. inorganic ion, salt, water soluble organic compounds) effectively grow in size.[32, 35, 36] At supersaturation of water vapor (RH>100%) some aerosol particles can act as cloud condensation nuclei (CCN) or ice nuclei (IN) to form liquid cloud droplets or ice crystals that contribute to cloud formation that will ultimately bring precipitation to the Earth's surface.[37] Clouds as well as atmospheric aerosols scatter solar radiation and reduce the amount of solar radiation reach the Earth's surface that is known as indirect and direct radiative forcing.[38, 39] However, some aerosols such as black carbon can absorb solar radiation and contribute to global warming.[40] The magnitude of aerosol radiative forcing

ranges from +0.42 W m^{-2} to -1.8 W m^{-2} and this values are dependent on the chemical composition and physical properties of the PM.[38] Thus, understanding the chemical composition of PM will provide insights to understanding the physical properties of aerosol and their climate interactions, and in turn will guide towards the strategies to mitigate climate effects.

1.3.2 Effects on Human Health

Exposures to high levels of atmospheric aerosols have been linked to negative health effects and mortality around the world.[41-46] In particular, inhalation of PM can exacerbate respiratory and cardiovascular diseases and in extreme pollution conditions can even cause death.[42, 45, 47] Due to this underlying connection between atmospheric aerosols and human health, World Health Organization (WHO) has established a guideline of 25 μg m^{-3} averaged over a 24 hour period.[48] However, extreme pollution conditions such as forest fires can increase the ambient particulate matter concentration nearly two orders of magnitude higher than the levels recommended by WHO.[49] Usually, the majority of the ambient aerosol mass is comprised of low-toxicity compounds such as organic carbon, soil dust, inorganic minerals (e.g. $(NH_4)_2SO_4$, NH_4NO_3, KCl, NaCl) and particle bound water.[5, 17] Soot, polycyclic aromatic hydrocarbons (PAHs), transition metals and endotoxins have low atmospheric abundance, but are capable of contributing adverse health effects.[5, 17, 25, 27, 50-52] However, certain emissions from particular sources like exhaust smoke of plastic and tire burning, welding, coke-oven, aluminum smelting, diesel and gasoline engines contain harmful species such as PAHs and trace metals.[53-56] Therefore, the chemical composition of PM is expected to be an important determinant in

its health outcome and useful for setting up occupational exposure limits and human exposure studies.

1.4 Sea Spray Aerosol

Oceans cover 70 % of the Earth's surface and are a major source of primary aerosol emission.[57-61] The annual global flux of sea spray aerosol (SSA) has been estimated as 2-100 Pg yr^{-1} which is comparable to total annual dust emissions.[12, 58, 59, 61] SSA particles are formed via wave breaking at wind speeds greater than 5 m s^{-1} at which air is entrained into the ocean water and dispersed into small bubbles that rise through the water column to the surface and burst.[61] First, the bubble cap disintegrates into tiny droplets, typically less than 1 μm in diameter (film drops) and then inner bubble cap of the collapsed bubble retracts to a vertical cylindrical jet that create another set of droplets, typically 1 to 25 μm in size (jet drops) as shown in Figure 1.2.[60, 62-64] Film drops and jet drops together form SSA that have longer atmospheric lifetimes (~5 days) and consequently important in atmospheric chemistry and aerosol-climate interactions.[60]

Due to their hygroscopicity and size, SSA act as effective CCN and plays a significant role in cloud formation affecting earths' radiation budget.[32, 65, 66] It has been estimated that direct and indirect radiative forcing of SSA cause a reduction of the radiation reaching the ocean surface by 0.08-6 W m^{-2}.[63] However, most climate models still treat SSA as pure sea salt (NaCl) or similar in composition to seawater, thus the climate predictions by these models have large uncertainties and considerable deviations from observations.[58, 60, 63, 67, 68] This is primarily due to our limited understanding of the molecular level composition of SSA that alter the aerosol physical properties like

hygroscopic growth, cloud condensation and ice nucleation activity.[32, 69] Thus, characterizing the chemical composition of SSA is required for accurate modeling and estimation of aerosol radiative influence and cloud microphysical properties.[58, 63, 70]

The attempts taken to characterize SSA go as far back as 1940s. Scientists reported human respiratory irritants in the air blowing via areas with higher algal growth, implying the emission of seawater components to the atmosphere.[71] In the recent past, with improved analytical techniques and advanced instrumentation a significant effort has been put into physical and chemical characterization of SSA.[60] It was discovered that significant fraction of SSA could actually be organic matter and sometimes, contributing to more than 90 % of the particle mass depending on the particle size.[22] The relative amount of organic matter to salt in SSA is far higher than that of seawater, with the greatest organic-to-salt enrichment occurring in smaller particle sizes.[72, 73] The mechanism proposed for this enrichment is the scavenging of surface-active organic matter by rising bubbles and the rise of organic colloids through positive buoyancy. This leads to the accumulation of organic matter at the sea surface microlayer (SSML) and selectively transfers to SSA in the process of bubble bursting.[74-81] Further, organic molecules could complex with inorganic ions in seawater and selectively transfer them to SSA that can lead to a different salt composition in aerosol than bulk seawater.

1.5 Biomass Burning Aerosol

Fire has been used since early stages of human evolution as an effective tool for cooking, heating and lighting, and more recently as a land management tool and for industries.[82, 83] Biomass burning is a major source of atmospheric aerosols and annual

flux of total PM is estimated to be 82.4 Tg yr^{-1}.[84] In general, 80-90 % of biomass burning aerosols are in fine mode (typically d_p < 1 μm) and is the largest source of primary fine carbonaceous aerosols to the atmosphere.[26, 84, 85]

Typically, biomass burning aerosols are composed 50-60 % of organic carbon, 5-10 % of elemental carbon and 10-15 % of inorganic ions. These aerosols effectively scatter and absorb solar radiation due to high content of organic and black carbon, and could have both positive and negative radiative forcing effects. Further, smoke particles can act as effective CCNs and INs affecting the cloud formation and cloud properties. Higher smoke levels reduce visibility affecting day-today human activities and cause negative health and environmental impacts.[86-89]

Remote sensing techniques along with atmospheric transport and chemistry models are used to estimate the global biomass emissions (Figure 1.3).[90-93] In order to compute robust model estimates of biomass emissions, accurate data of aerosol emissions from biomass fires are required. Model input parameters require metrological and atmospheric conditions, total burned area and emissions per unit area during a fire event. The emissions per unit area is calculated using amount of biomass burned and fuel based emission factors (EF), the amount of chemical species released per unit mass of fuel burned which should be experimentally determined.[84, 94] However, the estimated fluxes of biomass burning aerosols using this approach show large variations (20-75 %) across different studies. The reason for this discrepancy is largely due to use of different EFs that are not representative to the emission source.[93] Since biomass smoke is an important source of atmospheric aerosols, in recent past number of studies focused on the characterization of biomass burning emissions in order to compute representative EFs

and build source profiles to use for atmospheric, climate and source apportionment molding.[93] Apart from traditionally measured forest and savanna fuels, these studies tested a wide range of fuel types collected from different ecosystems including some rarely studied sources like foliage, organic soil and fuels commonly burned in residential or industrial use (e.g. agricultural residue, fuelwood, cow dung). [94-100] However, up-to-date only few studies have focused on comprehensive measurements of both gas-phase and particulate-phase emissions.[50, 96, 98, 100] Further, EFs of biomass burning PM is highly dependent on fuel type (soft wood, hard wood, grass, organic soil), fuel moisture content and burning condition (flaming vs smoldering).[94, 98, 101] Thus, more studies are needed to understand the emission variation of PM under different burning conditions. Therefore, calculating representative EFs for biomass burning PM via laboratory and *in-situ* field measurements will advance the biomass burning emission inventories and global model estimates.

1.6 Overview of Thesis Chapters

The research presented in this dissertation focuses on chemical characterization of biomass burning and sea spray aerosol. The chapters on biomass burning aerosols discuss the emission factors of $PM_{2.5}$ mass, EC, OC, organic species, water-soluble inorganic ions and metals in biomass burning aerosols. The chapters on sea spray aerosol is focused on the enrichment of organic carbon, carbohydrates, divalent cations and metals in sea surface microlayer, whitecap foam and sea spray aerosols.

A variety of experimental procedures were utilized in this study. Chapter 2 discusses the experimental procedures including aerosol collection, instrumental analysis,

quality control, and data collection methods that are common across the studies reported herein.

Chapter 3 presents the chemical composition and computed EFs of $PM_{2.5}$ emitted from biomass combustion, representing seven different fuel categories including conifers, agricultural residues, grasses and other perennials, peat, cook stoves, trash and shredded auto tires which were rarely sampled in previous studies.

Chapter 4 discusses the emissions of fine particle water-soluble fluoride (F^-) from biomass burning which represents a major and previously uncharacterized source of F^- to the atmosphere.

Chapter 5 presents the first comprehensive chemical characterization of $PM_{2.5}$ which was collected from authentic *in-situ* peat smoke during the 2015 El Niño peatland fire episode in Central Kalimantan, Indonesia and total gas and particulate emission estimates for this fire episode.

Chapter 6 discusses the enrichment of OC, saccharides, and inorganic ions in nascent SSA, and how the selective transfer across the air-water interface leads to chemical differences in SSA from bulk seawater, and the influence of the ocean biology in this phenomenon.

Chapter 7 describes the enrichment of dissolved organic carbon (DOC), carbohydrate and metals in the sea surface microlayer and whitecap foam over a full phytoplankton bloom cycle and selective transfer of certain saccharide types from bulk seawater to bubble film surface where SSA is generated.

Finally, chapter 8 provides the conclusions and future directions for research on the chemical composition of biomass burning and sea spray aerosol.

The research projects described in chapters three to seven involved many collaborations, with me as the scientific leader of the work presented herein. The contributions of each co-author are listed in each respective chapter. In addition to the research findings presented in this thesis, I have contributed many other research projects during my graduate studies. The EC OC data presented in chapter 3 was used to parameterize aerosol single scattering albedo, absorption Ångström exponent and IN activity.[36, 86, 89, 102] The EF_{OC} and EF_{EC} data of *in-situ* peat fire emission study presented in chapter 5 were used to evaluate the aerosol optical properties and these were compared with online photoacoustic extinctiometeric (PAX) measurements.[49] The concentration and enrichment factors of OC, saccharides and inorganic ions presented in chapter 6 were used to explain the influence of ocean biology on SSA composition, selective transfer pathways of organics matter and inorganic ions to SSA and to assess physical properties of SSA.[66, 103, 104] Further, the seawater, SSML and SSA samples described in chapter 6 were extracted and analyzed for anionic surfactants in order to understand the selective transfer of surfactants to SSA.[105] Laboratory experiments were performed to investigate this selective transfer across the sea-air interface and led to the understanding that surface activity of the organic molecules play a key role in chemical selectivity.[72] My studies were also focused on chemical characterization of PM emitted from understudied emission sources in Nepal (e.g cookstoves, motorcycles, garbage burning, brick kilns).[50, 96] Apart from primary source-aerosol characterization, I contributed to sample and analyze secondary organic aerosols, tire burning smoke, and bioaerosols in Iowa[17, 18, 27, 56] and secondary organic aerosol in Centreville, Alabama.[106] Finally, these research work will help to fill certain knowledge gaps exist in current literature.

Figure 1.1: A schematic of the major sources contribute to atmospheric aerosols. This figure illustrates the examples of primary aerosol sources and atmospheric reactions to form secondary aerosols. The aerosol production sources could be natural (e.g. combustion, sea spray, dust) or anthropogenic (e.g. industrial). The figure is adapted from reference 6.

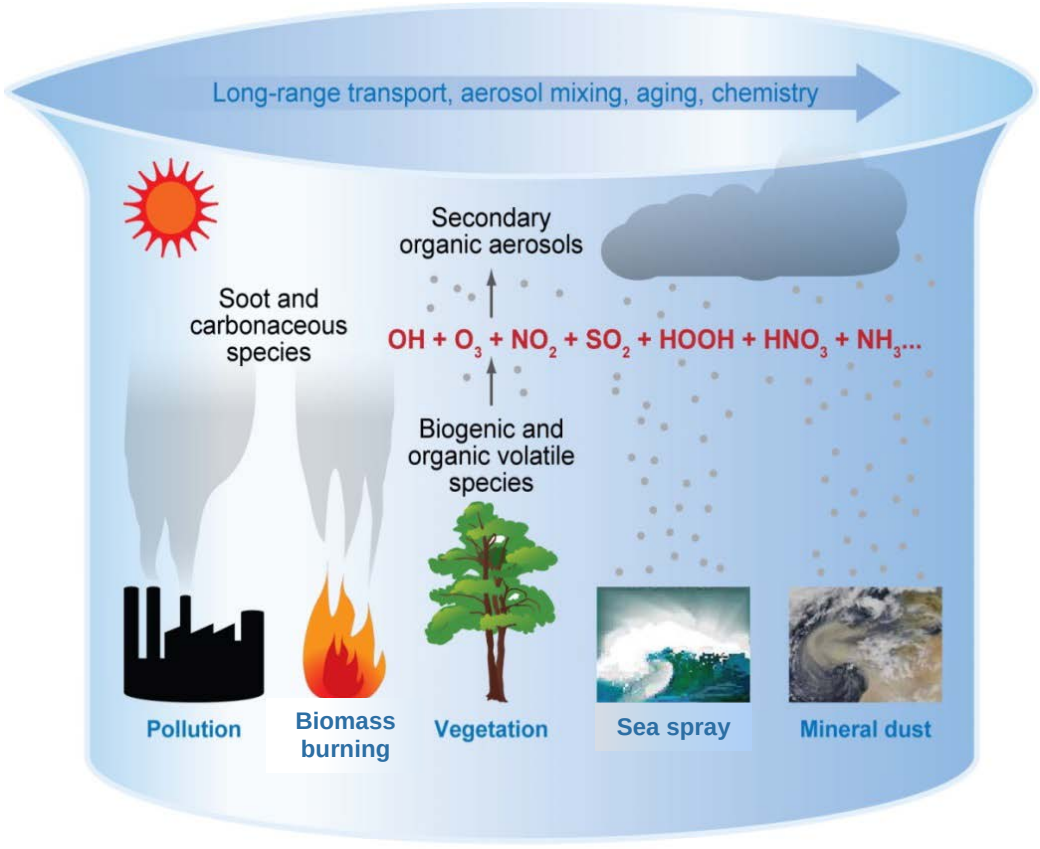

Figure 1.2: A schematic of SSA generation by bubble bursting mechanism via film drop and jet drop formation.

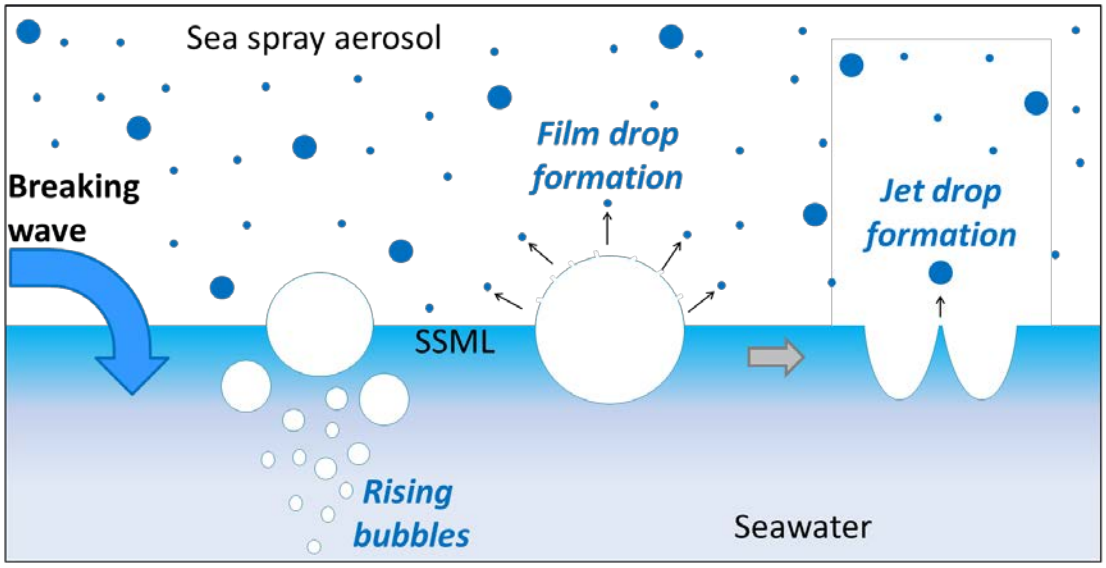

Figure 1.3: A fire map computed by NASA for the period of 28th September – 7th October, 2015 using Moderate Resolution Imaging Spectroradiometer (MODIS). The red colored dots are locations where fire was detected at least once during that period. Yellow color indicates areas with high fire count frequencies. (The image was downloaded from https://lance.modaps. eosdis.nasa.gov /cgi-bin/imagery/firemaps.cgi. Credits: Fire maps were created by Jacques Descloitres. Fire detection algorithm developed by Louis Giglio. Blue Marble background image created by Reto Stokli).

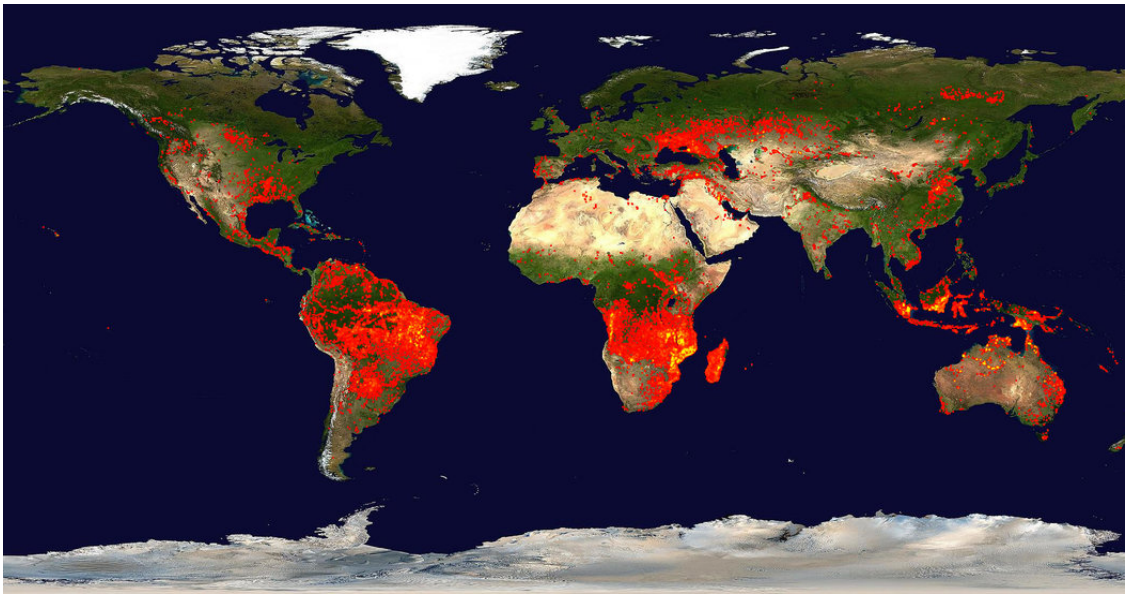

CHAPTER TWO

EXPERIMENTAL METHODS

Experimental procedures commonly utilized in sample collection, extraction and analysis of particulate matter are discussed here, with specific details of each study provided in the corresponding chapters.

2.1 Collection of Particulate Matter from Sea Spray and Biomass Burning Emissions

Fine ($PM_{2.5}$) and coarse ($PM_{10-2.5}$) particles were collected using commercial and custom-built aerosol samplers. A typical aerosol sampler consists with an air inlet, a particle separation device, a filter holder, an oil-free mechanical pump, a flow controller and a flow meter.[107] The mechanical pump draws the air through the sampler inlet at a constant flowrate that is typically measured by flow meters. The air flow is directed to a particle separation device that separates particles based on their aerodynamic diameter, defined as the diameter of a sphere with a unit density (1 g cm^{-3}) that has the same settling velocity in air as the considered particle. The particle separation device is typically a cyclone precipitator or an impactor.

A cyclone precipitator, a modification of the centrifuge technique, is based on introducing the air mass at a high velocity into a vessel that consists of an upper cylindrical part and a lower conical part. The tangential introduction of air into the cyclone creates a downward vortex inside the cyclone, and at the bottom of the lower conical part, the air vortex spirals upward through the center and leaves out from the top of the cyclone creating a double vortex inside the cyclone body (Figure 2.1). The

particles in the spinning air mass are subjected to a centrifugal force towards cyclone walls that is proportional to the particle mass. Simultaneously, particles undergo an opposite fluid drag force due to upward movement of air at the center of the cyclone. The centrifugal force towards the cyclone wall overcome the opposite drag force for larger particles with heavier mass due to their higher inertial momentum. Thus, they impact on cyclone wall and are removed from air and collect at the dust cup located at the bottom of the cyclone. Smaller particles have higher drag force than inertial momentum and follow the vortex and escape from the top of cyclone as shown in the Figure 2.1. The cyclone geometry and the velocity of the air mass together determine the cut-off particle diameter. Thus, adjusting the air mass velocity by changing the flow rate can regulate the particle size that is removed by the cyclone.[108]

Impactors typically contain an impaction surface placed across the path of the air stream that separate particles from the flowing air stream. The impaction inlet is positioned above the center of the impaction plate causing the air flow to stream around it. The larger particles with heavier mass have higher momentum, thus cannot bend sharply to follow the air flow path. Therefore, they impact on the plate and are removed from the air stream. The smaller particles that have lower masses have lower momentum and manage to follow the air flow path to the second impaction chamber. The second impaction inlet nozzle is narrower than the first, thus air velocity is higher than the first impaction chamber. Due to increased air velocity particles gain a higher momentum and the particles that cannot follow the air flow path impact on the second stage and are removed from the air stream. The rest of the particles follow the air flow path and continue to the next chamber and so on. The impactor dimensions and air velocity are

chosen such that particles smaller than the desired cut-size follow the air flow and escape the impaction plate, while larger particles deviate from the main air flow, impact and are removed from the main air steam as shown in Figure 2.2.[107]

The impaction plates are typically aluminum substrates, glass plates or filters. If particles do not stick on the impaction surface, they can bounce back into the main gas stream, break into fragments by collision and re-enter into the air stream or can re-suspend the previously impacted particles by continuous air flow. To overcome these issues virtual impaction is involved in atmospheric PM sampling in which the air stream impacts against a mass of relatively still air instead of a solid surface. The larger particles travel into the still air mass and are slowly collected on a filter. Smaller particles with less inertia follow the major air flow and deposit on another filter located in the main air flow downstream as shown in Figure 2.3. In atmospheric PM sampling virtual impactors are used to separate two size fractions simultaneously, typically fine and coarse.

Unlike cyclone precipitators that have single size-cut, impactors are used to separate several particle sizes into separate bins simultaneously. Dichotomous samplers and cascade impactor samplers (e.g. micro-orifice uniform deposit impactor (MOUDI)) are commonly used atmospheric particulate samples that use an impactor as a particle separation device.[107, 109]

2.2 Substrates for Particulate Matter Collection

Particles were collected on to quartz fiber filters (QFF) and Teflon filters (Pall, Life Sciences). QFF were pre-baked at 550 °C for 18 hours before sample collection to remove organic contaminants and stored in pre-cleaned aluminum foil-lined petri dishes

sealed with Teflon tape. Teflon filters were stored in plastic petri dishes sealed with Teflon tape and always handled with metal-free utensils. Field blank filters, that are collected in a similar way to sampled filters but without drawing air through it, were collected for every five sample filters to evaluate contamination from filter handling, transport and storage. Filters were stored in a freezer at -20 °C before and after sample collection. Specific details about sample collection in each study will be discussed in each corresponding chapters.

2.3 Determination of Aerosol Mass

Before and after sample collection Teflon filters were conditioned for 48 hours in a desiccator and weighed using an analytical microbalance (Mettler Toledo XP26) in a temperature (~25 °C) and humidity (~40%) controlled room. PM mass was calculated as the difference of pre-and post-sampling filter weights, which were determined in triplicate. The micro-balance is very stable over the replicate measurements and standard deviation is typically <5 μg. The uncertainty in the PM mass measurement was propagated using the standard deviation of triplicate measurements of pre- and post-sampling filter weights, the standard deviation field blank values, and 10 % of the PM mass concentration, which is a conservative estimate of the analytical error associated with this measurement.

2.4 Analysis of Organic Carbon and Elemental Carbon

Organic carbon (OC) and elemental carbon (EC) were determined following the NIOSH 5040 method or ACE-Asia protocol on 1.0 cm^2 punches of QFF (Sunset OC-EC

Aerosol Analyzer, Sunset Laboratories, Tigard, OR).[110, 111] Uncertainty in OC measurements was propagated from the standard deviation of the field blank OC levels and 5% the OC concentration, a conservative estimate of the precision error in replicate sample analysis.[110] Uncertainty in EC measurements was propagated from the instrumental uncertainty (0.05 μg cm^{-2}), 5% of the measured EC, and 5% of pyrolyzed carbon, which refers to organic carbon that charred during analysis.

2.5 Extraction and Analysis of Water-soluble Organic Carbon

A sub-sample of QFF filters was extracted into 15.0 mL of >18.2 MΩ resistivity ultra-pure water (Thermo, Barnstead Easypure II) using acid washed (10% nitric acid) and freshly pre-baked (550 °C for 5.5 hours) glassware and subsequently analyzed for water soluble organic carbon (WSOC) using a total organic carbon (TOC) analyzer (GE, Sievers 5310 C) in triplicate measurements. Inorganic carbon was removed by an inorganic carbon remover unit that equipped with the TOC analyzer (GE, Sievers ICR). Instrumental detection limits (IDLs) were determined as three times the standard deviation of ten replicate injections of the lowest calibration standard and were 35 μg C L^{-1}. The method detection limit (MDL) was 95 μg C L^{-1} which was determined as three times the standard deviation of seven replicate extractions and analyses of a sample to which a WSOC standard at three times the IDL was added. WSOC was quantified using a standard calibration curves prepared from potassium hydrogen phthalate (Ultra Scientific). The uncertainty of WSOC measurements was propagated from the standard deviation of the triplicate measurements, standard deviation of the field blank WSOC levels and 10% of the extract WSOC measurement. The water insoluble fraction of

organic carbon (WIOC) was calculated by subtracting the WSOC concentration by total OC concentration and uncertainty was propagated from individual uncertainties of the two values.

2.6 Extraction and Analysis of Carbohydrates

2.6.1 Materials for Standard Preparation

Xylitol, D-mannitol, L-arabinose, D-glucose, D-xylose, D-fructose (Sigma-Aldrich), erythritol, D-arabitol, D-trehalose, L-fucose, inulin (Alfa-Aesar), L-rhamnose, D-mannose, D-ribose, dextrin (Acros Organics), D-galactose, sucrose (Fisher) at > 99 % purity were used for standard solution preparation. Analytical grade sodium hydroxide (50 %) (Fisher) was used for mobile phase preparation and, hydrochloric (Fluka), nitric (Fisher), sulfuric (BDH) and trifluoroacetic acid (Reagent-World) used for hydrolysis. Ultra-pure water (Thermo, Barnsted EasyPure-II; 18.2 MΩ resistivity) was used in solution preparation.

2.6.2 Acid Hydrolysis

Four strong acids, hydrochloric, sulfuric, nitric and trifluoroacetic acids (TFA) were tested as hydrolyzing agents to break oligo- and polysaccharides into their monomers.[112] The use of hydrochloric, nitric and sulfuric acids led to chromatographic interferences at 8.8-10.2 minutes, interfering with measurement of ribose and sucrose. Therefore, TFA was selected as the hydrolyzing agent, because it did not exhibit this interference. Mild hydrolysis conditions of 0.1 M TFA and 100 ^{0}C were used based on the recommendations of prior studies.[112] The optimum hydrolysis time was determined

by kinetic experiments. In this regard, the standard solutions of glucose, sucrose, inulin, dextrin, and an aliquot of a marine sample (day 3 foam) were hydrolyzed and analyzed after 15, 30, 60, 120, 240, 480, 720 and 1440 minutes to monitor the release of glucose and/or fructose. Additional sample preparation steps such as neutralization and desalination were not carried out during sample preparation in order to minimize the analyte loss.[113, 114] The results of the kinetic experiment is given in Figure 2.4.

The concentration of glucose standard did not significantly change over the entire experiment confirming the stability of glucose under these conditions. Sucrose and inulin were completely hydrolyzed after 60 minutes while dextrin and day 3 foam sample slowly hydrolyzed and peaked after 720 minutes. Based on these results, 720 mins (12 hours) was determined to be the optimum hydrolysis time, which provided greater than 99% hydrolysis.

2.6.3 HPAEC-PAD Methodology

Instrumental analysis of carbohydrates was conducted using ion chromatography (Dionex-ICS 5000) with an electrochemical detector (ED) on a Dionex CarboPac^{TM} PA20 (3 × 150 mm) carbohydrate column, preceded by a guard column and Dionex AminoTrap^{TM} trap column. The mobile phase consisted of 27.5 mM aqueous sodium hydroxide, which was prepared with degassed ultra-pure water and stored under pressurized (30 psi) ultra-pure nitrogen environment. Isocratic elution was performed at a 0.480 mL min^{-1} flow rate and, column cleanup and regeneration was performed before each injection using 200 mM sodium hydroxide at the same flow rate over 15 minutes. The electrochemical detector, capable of pulsed amperometric measurements consisted of

a disposable gold working electrode and Ag|AgCl reference electrode applying the standard carbohydrate quadrupole potential waveform with following conditions: E1 = +0.05 V (0.0–0.4 s; integration 0.2–0.4 s); E2 = +0.75 V (0.41–0.6 s); and E3 = -0.15 V (0.61–1.0 s).[115] A constant temperature of 30 ^{0}C was maintained in both column and detector compartments. A DV-50 (Dionex) auto sampler and a 25 µL injection loop were used for sample injection.

The order of elution generally follows the pK_a values[116] of the carbohydrates and retention times were highly repeatable (Table 1, n = 17), with maximum peak shift less than 3% RSD. An HPAEC-PAD chromatogram for 1.0 µM carbohydrate standard is given in Figure 2.5. Peak resolution (R_s) was calculated from the distance between the peak maxima (d) and the peak width at half height (w_h) for two adjacent peaks (i and $(i-1)$)[117] using Equation 2.1.

$$R_s = \frac{2d}{1.70\,[(w_h)_i + (w_h)_{(i-1)}]} \quad \text{(Equation 2.1)}$$

Seven-point calibration curves ranging from 10 nM to 10 µM and based on peak area were used for quantification. IDLs were determined as three times the standard deviation of ten replicate injections of the lowest calibration standard. MDL were determined as three times the standard deviation of seven replicate extractions and analyses of a sample to which a carbohydrate standard at three times the IDL was added. The instrumental reproducibility was assessed as the RSD of the analyte concentration calculated from nine consecutive injections from the same vial, while the method repeatability (day-to-day variation) was evaluated from replicate measurements of 1.0 µM standard over 5 days. The efficiencies of sample preparation and hydrolysis were

examined using spike recovery assessment, in which a saccharide mixture of known concentration was added to ultra-pure water and then analyzed in the same way as samples. Spike recoveries were calculated by Equation 2.2.

$$Spike\ recovery\ (\%) = \frac{Observed\ concentration\ of\ the\ analyte}{Added\ concentration\ of\ the\ analyte} \times 100\% \quad \text{(Equation 2.2)}$$

Table 2.1 summarizes method performance metrics, including peak retention time, peak resolution, calibration range, coefficient of determination (R^2), IDLs, MDLs, instrumental reproducibility and average spike recovery. R_s ranged 0.59-5.9 with a clear separation of peak maxima of all the analytes (Table 1). Baseline separation ($R_s > 1.5$) was achieved for fucose, rhamnose, arabinose and fructose, and a peak overlap of less than 2% was observed for ribose and sucrose. All species met the threshold R_s of 0.54 have been proposed by Rodrigues et al. (1993) in order for two peak maxima to be clearly separated and were close to or above the threshold R_s of 0.6 proposed by and Miller (2005) for the same purpose.[117, 118] In comparison to prior studies by Kerherve et al. (1995), Mopper et al. (1995), and Engel and Handel (2011), this HPAEC method provides improved resolution for rhamnose, arabinose, glucose and mannose, all of which are important components of the marine carbohydrate pool.[77, 114, 119] Improvements to chromatographic resolution result from the use of a Dionex (Thermo) CarboPac PA-20 column with pellicular anion-exchange resin beads that are smaller (6.5 μm) than previously used columns, which were AS-6 in the case of Mopper et al., CarboPac PA-1 in the case of Kerherve et al. and CarboPac PA-10 in the case of Engel and Handel.[77, 114, 119]

Linear PAD response was observed from 10.0 nM to 10.0 µM with coefficients of determination (R^2) greater than 0.999. IDLs ranged from 1.4 - 6.0 nM, while MDLs ranging from 2.5 - 18.0 nM (Table 2.1). The RSDs of instrumental reproducibility (consecutive) and method repeatability (day to day variation) for individual carbohydrates were < 5% and <7%, respectively indicating the high precision of the optimized HPAEC method. Spike recoveries for most of the carbohydrates were greater than 90%, demonstrating efficient analyte recoveries. Ribose (83%), fructose (84%) and xylitol (84%) had the lowest recoveries, likely due to the destruction of those sugars during hydrolysis.[120] The performance metrics are equally as good as previously reported methods demonstrating high accuracy and precision of the optimized method for marine relevant carbohydrates.

Application of the optimized HPAEC-PAD protocol to quantify carbohydrates in actual marine samples is shown in Figures 6b and 6c, before and after hydrolysis, respectively. A shift to shorter retention times relative to carbohydrate standard chromatogram (6a) is attributed due to high salt content in the sample matrix and the addition of TFA to the hydrolyzed samples.[112] Therefore, peak identity was confirmed by method of standard addition; upon addition of carbohydrate standards to samples, a consistent growth in the carbohydrate peaks were observed as shown in Figure 2.7.

2.7 Extraction and Analysis of Water-soluble Inorganic Ions

Water soluble inorganic ion content was determined by Teflon filters. Prior to extraction, Teflon filters were cut in half using ceramic scissors and blades on a clean guided glass surface. The full and half-filter masses were measured on an analytical

balance (Mettler Toledo XS204) in order to accurately determine the fraction of filter extracted; results were scaled assuming uniform PM deposition. Half of the Teflon filter was uniformly wet with 100 µL of isopropyl alcohol and subsequently extracted into 15.0 mL ultra-pure water (Thermo, BARNSTED EasyPure-II; 18.2 MΩ resistivity) by shaking 12 hours at 125 rpm. For every 10 samples, 1 lab blank, 2 field blanks, and 1 spike recovery sample were prepared and analyzed. Extracts were filtered with 0.45 µm PTFE (Whatman) filters prior to analysis.

Aqueous extractions of filter samples were analyzed by ion exchange chromatography (Dionex-ICS5000). For anion analysis, a Dionex IonPac^{TM} AS22 anion column was used. The mobile phase consisted of 4.5 mM sodium carbonate (Na_2CO_3) and 1.4 mM sodium bicarbonate ($NaHCO_3$) at a flow rate of 1.2 mL min^{-1}. For cation analysis, a Dionex IonPac^{TM} CS12A cation column was used. The mobile phase consisted of 20 mM methane sulfonic acid and flowed at 0.5 mL min^{-1}. A conductivity detector (Thermo) was used for detection and was preceded by a self-regenerating suppressor (ASRS^{TM} 300 for anions and CSRS^{TM} 300 for cations). Anions and cations were identified against authentic standards (Dionex) and cation and anion standard chromatograms are given in Figure 2.8 and 2.9, respectively. Ions were quantified with seven point calibration curves and the analytical uncertainties of the measurements were propagated using the MDL, standard deviation of the field blank value and 10% of the measurement value.

IDL was determined as three times the standard deviation of the lowest detected concentration of each analyte through seven consecutive injections. MDL of analytes were obtained by performing seven spike recovery samples by spiking a lab blank filter

with a standard solution which prepared targeting a final concentration which will be 3-5 times higher than the IDL. The spiked filters were then extracted and analyzed in triplicate to determine the recovered concentrations and the MDL was determined as the average blank levels plus three times standard deviation of the recovered concentrations across seven extracts. The efficiency of analyte extraction were examined using spike recovery assessment, in which a standard mixture of known concentration was added to a Teflon filter, let dry and extracted into ultra-pure water and then analyzed in the same way as samples. Spike recoveries were calculated as Equation 1. The calibration range, coefficient of determination (R^2), IDLs, MDLs, and average spike recoveries for anions and cations are given in Table 2.2.

2.8 Extraction and Analysis of Total Metals

Teflon filters were cut into half using ceramic blades and total dissolution metals were extracted using an procedure adopted from US EPA Method 3052.[121] In brief, filters were digested in a mixture of 2:1 concentrated nitric and hydrochloric acid (TraceMetal Grade, Fisher Chemical) using a MARS 6 microwave assisted digestion system (CEM Corporation, Matthews, NC) at 200 °C for 13 minutes. Extracts were filtered by 0.45 µm PTFE filter (Whatman) and analyzed for metals using a Thermo X-Series II quadrupole ICP-MS instrument (Thermo Fisher Scientific Inc., Waltham, MA, USA).[122] The instrument was calibrated against IV-ICPMS-71A ICP-MS standard (Inorganic Ventures) for a range of 0.1 to 50 ppb. The MDL and spike recovery % were calculated as described in section 2.6 and values are reported in Table 2.3. The uncertainty of the

measurement was propagated using standard deviation of the filed blank measurements, MDL and 10% of the metal concentration.

2.9 Extraction and Analysis of Organic Species

Quartz fiber filters were sub-sampled to obtain ~200 µg C prior to organic species quantification by gas chromatography mass spectrometry (GC-MS). These sub-samples were spiked with deuterated internal standards which were used in quantification: pyrene-D_{10}, benz(a)anthracene-D_{12}, cholestane-D_4, pentadecane-$D_{32,}$ eicosane-D_{42}, tetracosane-D_{50}, triacontane-D_{62}, dotriacontane-D_{66}, hexatriacontane-D_{74} , levoglucosan-$^{13}C_6$ and cholesterol D_6. Each sub-sample was then stepwise extracted in 2×20 mL aliquots of hexane followed by 2×20 mL aliquots of acetone by ultra-sonication (60 sonics min^{-1}, 5510-Branson) for 15 minutes.[123] The solvent extracts were subsequently concentrated to a final volume of ~100 µL using Turbovap (Caliper Life Sciences, Turbo Vap LV Evaporator) and micro-scale nitrogen evaporation system (Reacti-Therm III TS-18824 and Reacti-Vap I 18825, Thermo Scientific) upon high-purity nitrogen (PRAXAIR Inc.). These extracted samples were stored at -20 °C until the chemical analysis.

Organic species in filter extracts were quantified using GC-MS (Agilent Technologies 7890A) equipped with an Agilent DB-5 column (30 m X 0.25 mm X 0.25 µm) with electron ionization (EI) source in the positive mode using a temperature range from 60 to 300 °C. Helium was utilized as the carrier gas, and the 3 µL aliquots of the extracts were injected in splitless mode.[123]

Hydroxyl-bearing polar compounds were analyzed following trimethylsilyl (TMS) derivatization.[124] Briefly, 10 µL of the extract was blown down to complete

dryness and reconstituted in 10 µL of pyridine (Burdick & Jackson, Anhydrous). A 20 µL of the silylation agent N,O-bis-(trimethylsilyl)trifluoroacetamide (Fluka Analytical, 99%) was added to the mixture, and was heated for 3 hours at 70 ˚C to complete the silylation reaction. The silylated samples were immediately analyzed for polar compounds.

Responses of analytes were normalized to the corresponding isotopically-labeled internal standard and five point linear calibration curves (with correlation coefficients, $R^2 \geq 0.995$) were utilized for the quantification of organic species. Compounds that were not in the standards were measured by assessing the response curve from the compound that is most analogous in structure and retention time. The analytical uncertainties for the measured species were propagated from the standard deviation of the field blanks, MDLs and 20% of the measured concentration. The MDLs and spike recoveries were calculated as described in section 2.6 and quantitative values are given in Table 2.4.

2.10 Scanning Electron Microscopy (SEM) Energy Dispersive X-ray (EDX) Microanalysis

SEM-EDX spectroscopy was used to confirm the presence of fluoride in biomass burning aerosol samples. A sub-sample of a quartz fiber filter was mounted on a SEM sampling stub using double-sided carbon tape. Morphology and $PM_{2.5}$ composition were examined using a scanning electron microscope (Hitachi S-3400N) coupled with an energy dispersive X-ray spectrometer (Bruker) at 15.0 kV accelerating voltage. EDX spectra were collected for the fluorine Kα line at 676.8 eV and were used to map elemental fluorine distributions in $PM_{2.5}$ samples.

2.11 Energy-dispersive X-ray Fluorescence Spectroscopy (XRF) Analysis

Metals in biomass burning aerosol samples were measured by Department of Biomedical Engineering and Environmental Sciences, National Tsing Hua University, Hsinchu, Taiwan using an energy-dispersive X-ray fluorescence spectrometer (ED-XRF, Epsilon 5, PANalytical), equipped with a 600 W power X-ray tube, following a protocol adopted from the US EPA Chemical Speciation Network.[125, 126] The relative bias of the ED-XRF analyses, calculated using NIST standards, and was within 15 %.

Figure 2.1: Schematic diagram of a cyclone precipitator (The figure is adapted from reference 107).

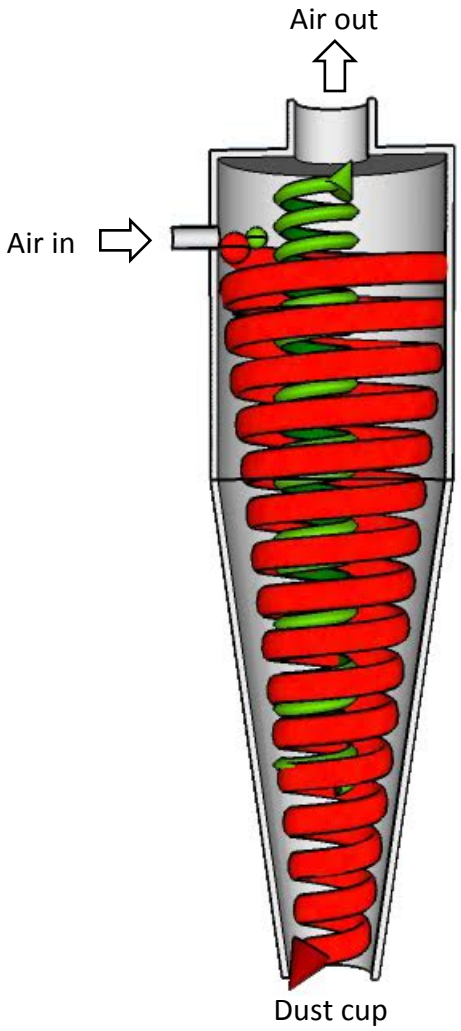

Figure 2.2: Schematic diagram of a cascade impactor (The figure is adapted from reference 107).

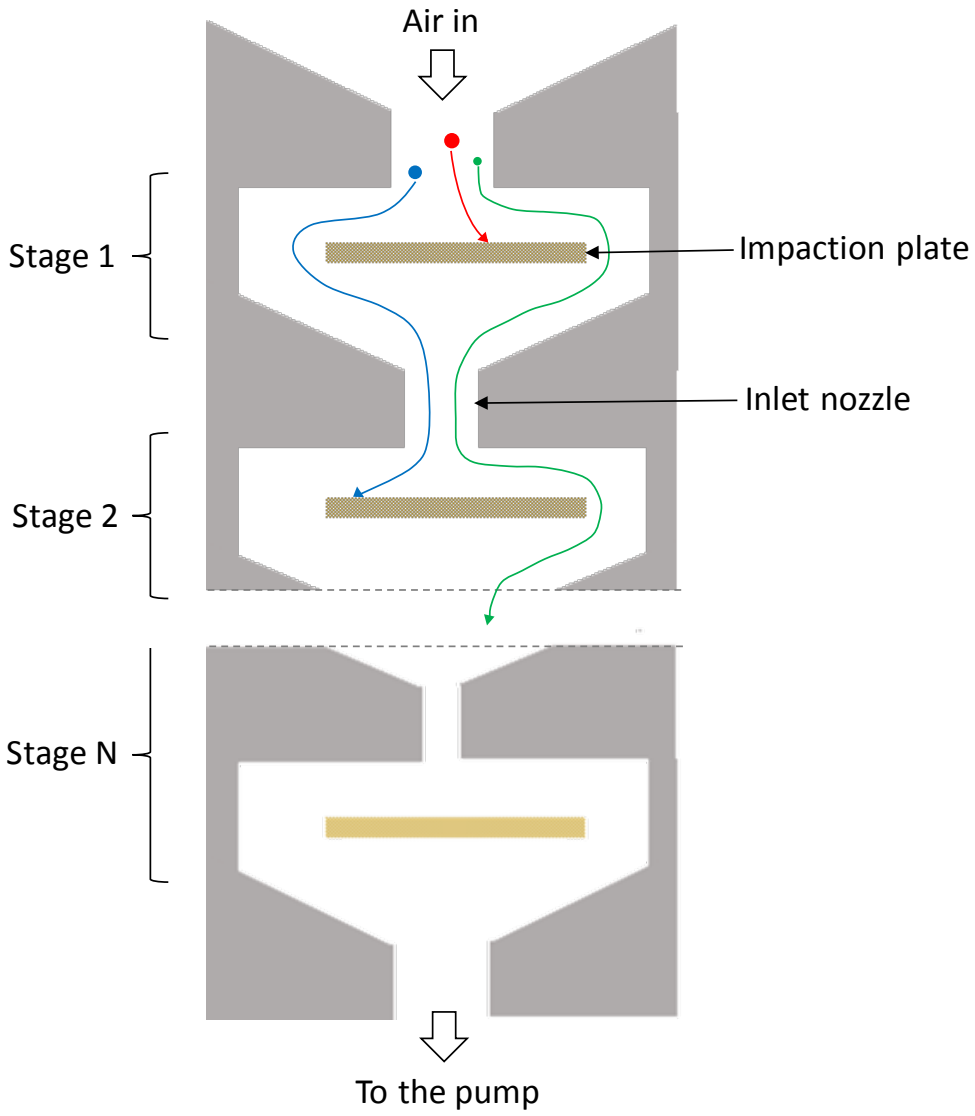

Figure 2.3: Schematic diagram of a virtual impactor (The figure is adapted from reference 107).

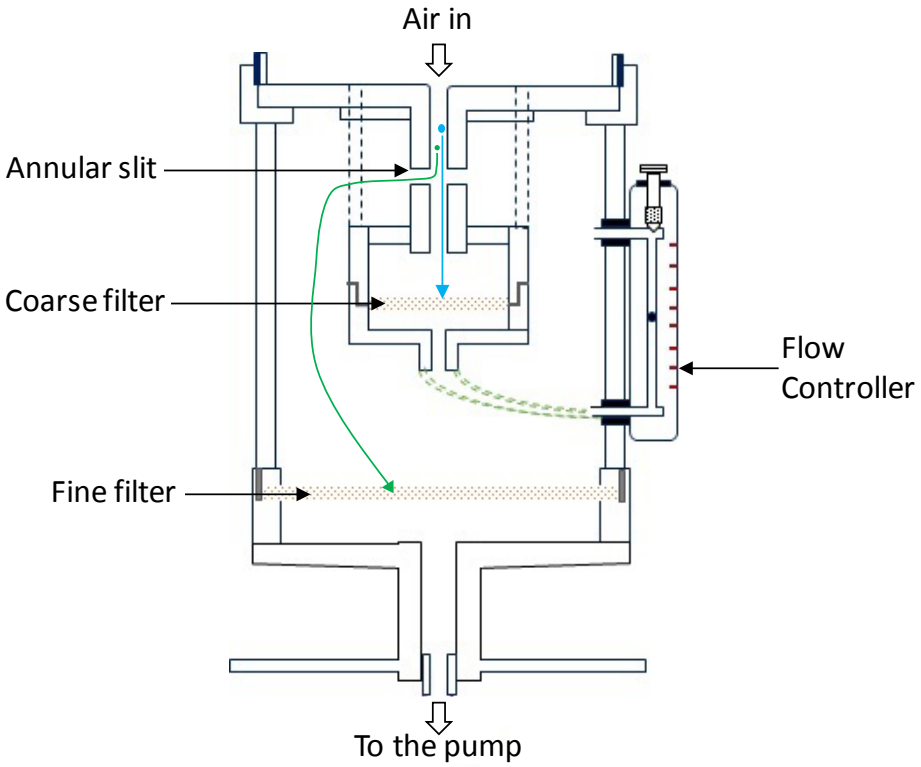

Figure 2.4: Concentrations of glucose or fructose in samples undergoing hydrolysis. Error bars show the propagated analytical uncertainty.

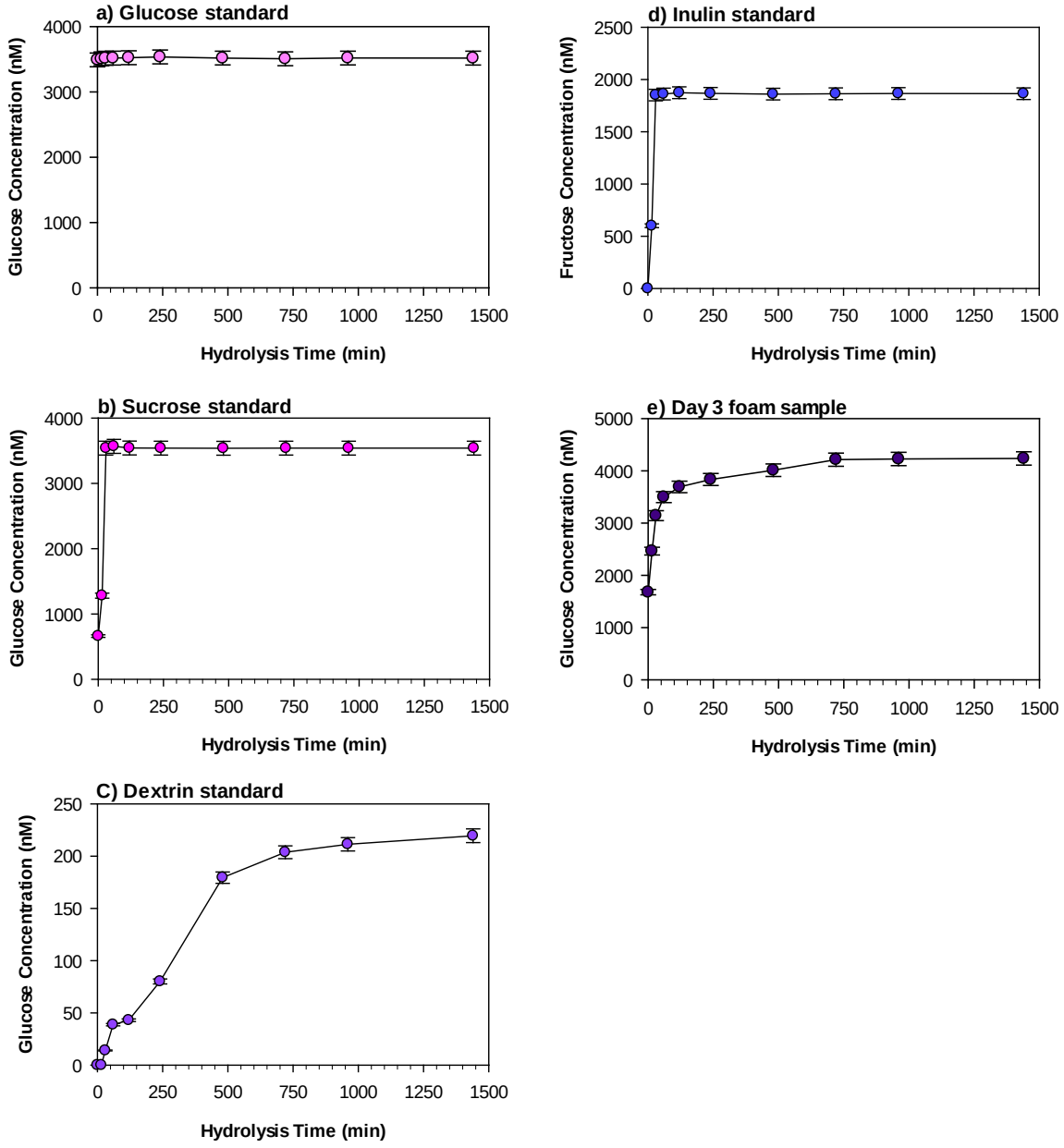

Figure 2.5: HPAEC-PAD chromatograms for a 1.0 µM carbohydrate standard. Numerical peak numbers correspond to the species listed in Table 2.1.

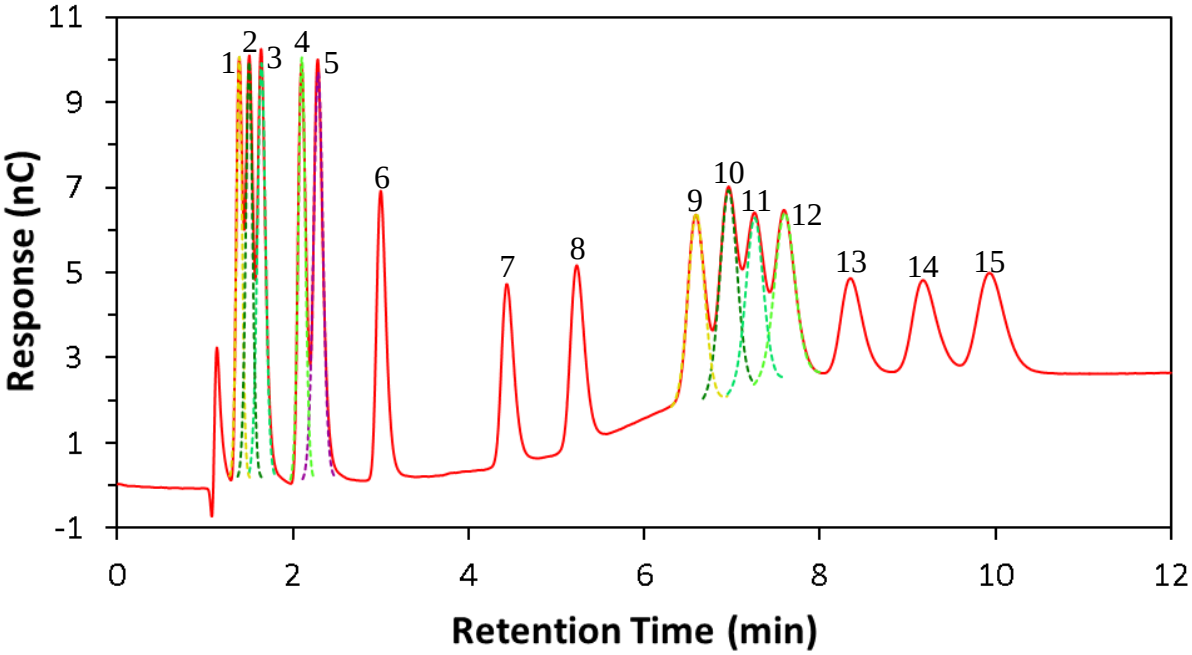

Figure 2.6: HPAEC-PAD chromatograms for a 1.0 µM saccharide standard (a) and day 3 foam sample before (b) and after (c) hydrolysis. Numerical peak numbers correspond to the species listed in Table 2.1.

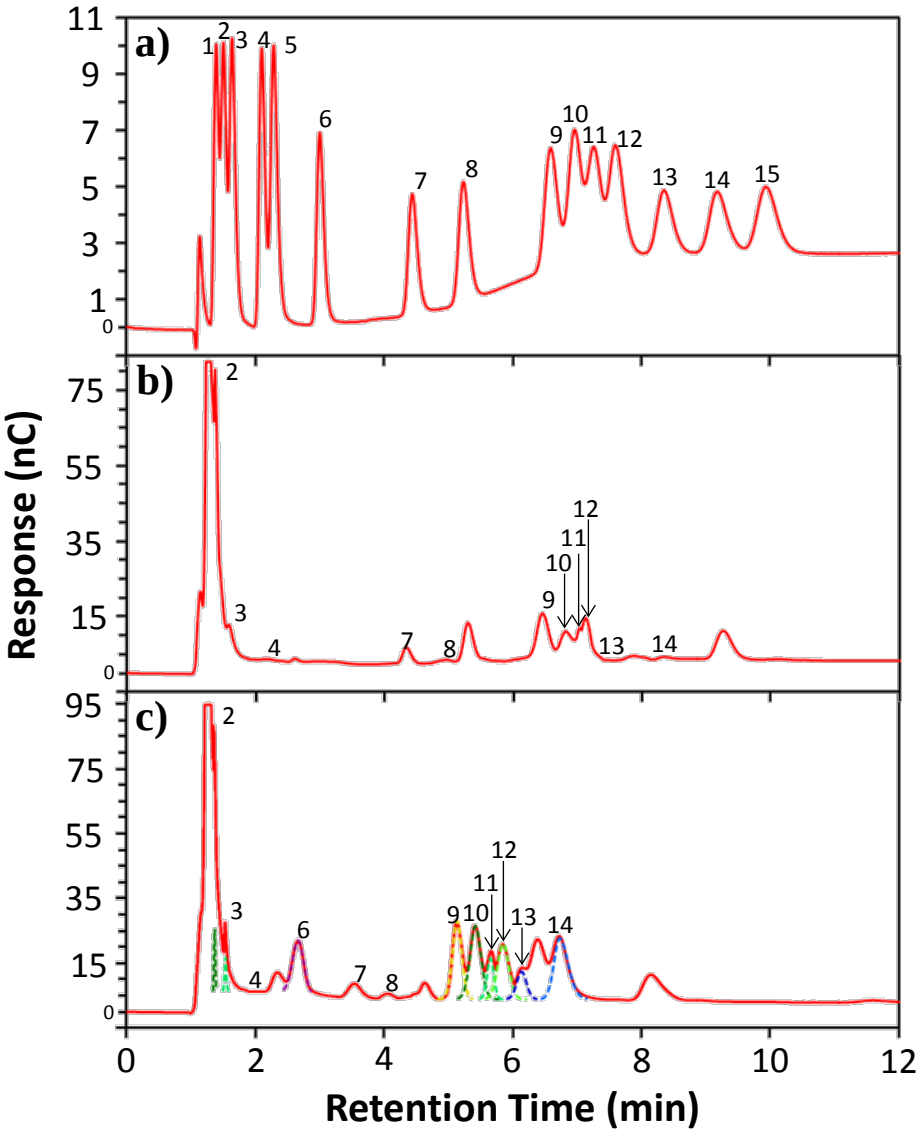

Figure 2.7: Identification of carbohydrate peaks using method of standard addition: a) day 3 hydrolyzed foam sample, with addition of b) arabinose, c) rhamnose and ribose, d) fucose and fructose, e) mannitol and xylose, f) arabitol and mannose, g) xylitol and glucose, and h) erythritol and galactose. Numerical peak numbers correspond to the species listed in Table 2.1.

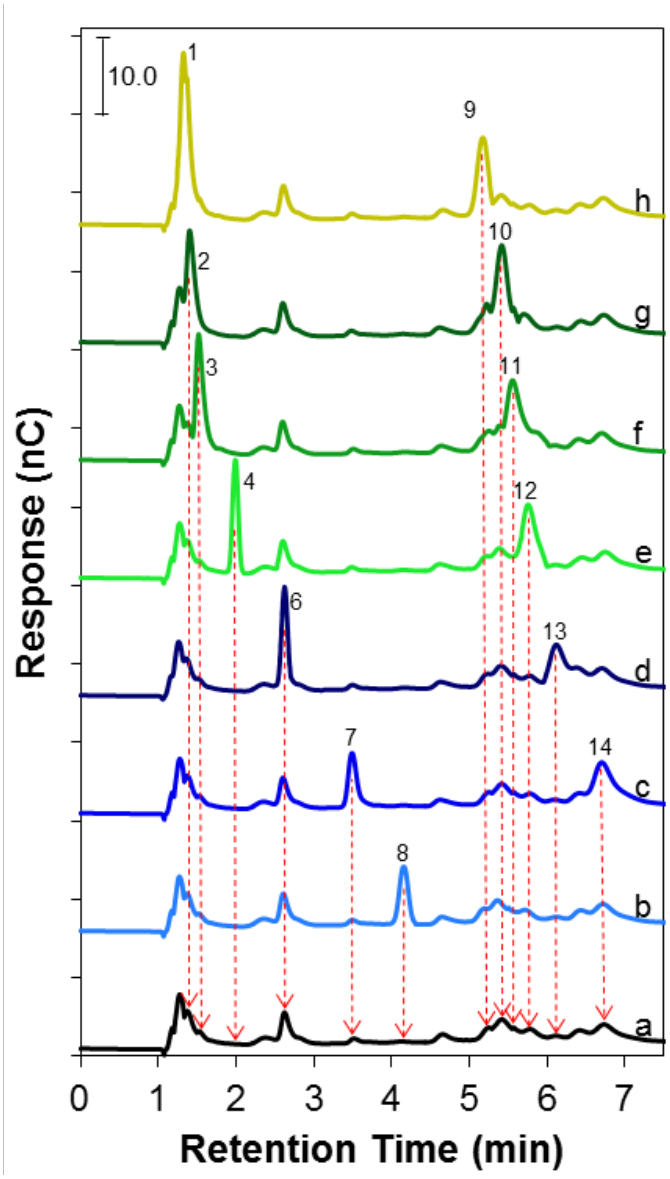

Figure 2.8: Separation of cations in Dionex CS12A column.

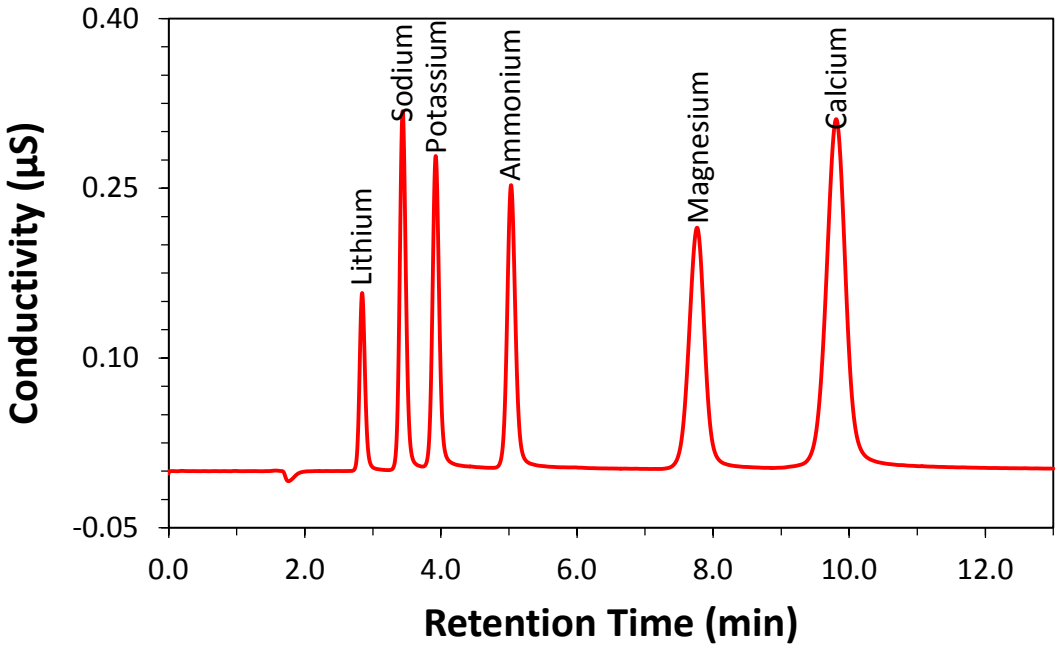

Figure 2.9: Separation of anions in Dionex AS22 column.

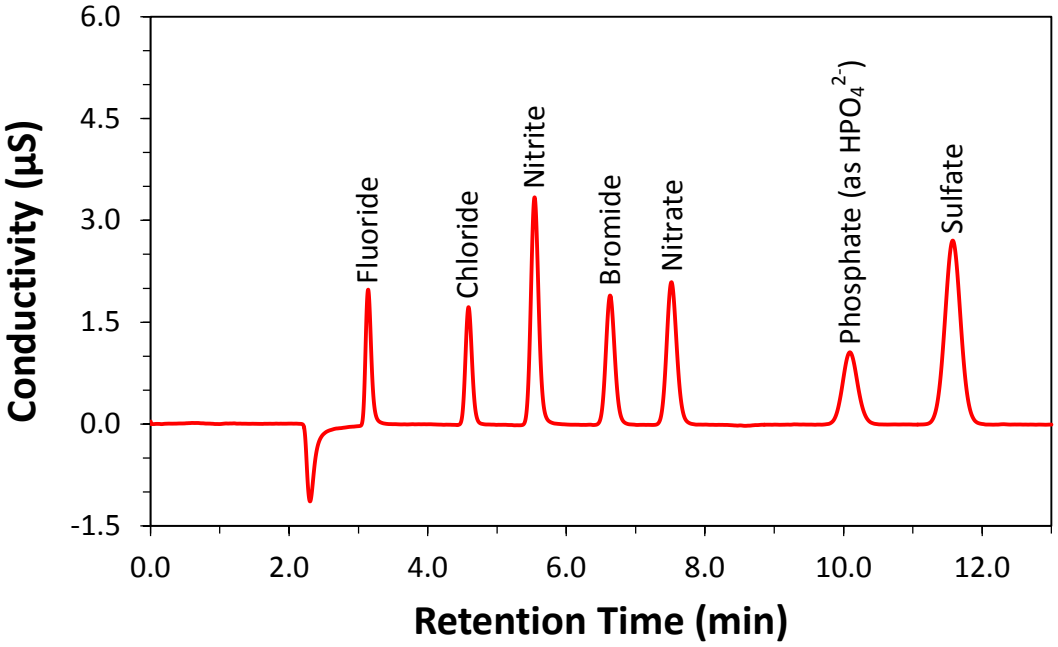

Table 2.1: Summary of method performance for HPAEC-PAD analysis, including peak retention time, peak resolution, calibration range, coefficient of determination, instrumental detection limits, method detection limits, instrumental reproducibility and average spike recovery (± 1 standard deviation) for the analysis method. Calibration range was 10 – 10,000 nM and R^2 was > 0.999 for all the analytes.

Peak No.	Analyte	Peak Retention Time (min)[a]	Peak Resolution	Detection Limits		Reproducibility (%)		Spike Recovery (%)	
				IDL (nM)	MDL (nM)	Consecutive[b]	Day to day variation[c]	Unhydrolyzed (n=5)	Hydrolyzed (n=3)
1	Erythritol	1.390 ± 0.003	-	2.4	5.0	1.7	1 ± 1	98 ± 4	109 ± 2
2	Xylitol	1.500 ± 0.002	0.59	3.3	4.2	2.4	4 ± 3	92 ± 6	84 ± 1
3	Arabitol	1.64 ± 0.01	0.74	1.4	2.5	1.0	3 ± 2	95 ± 7	94 ± 3
4	Mannitol	2.100 ± 0.003	2.4	1.6	3.2	1.1	2 ± 2	97 ± 6	94 ± 2
5	Trehalose	2.29 ± 0.02	0.89	1.6	3.8	1.1	3 ± 2	97 ± 3	NA[d]
6	Fucose	2.986 ± 0.008	3.4	4.6	9.3	3.3	5 ± 2	94 ± 2	99 ± 6
7	Rhamnose	4.46 ± 0.09	5.9	2.9	7.5	2.2	1.5 ± 0.8	98 ± 4	94 ± 6
8	Arabinose	5.26 ± 0.03	2.7	6.0	8.0	4.7	2.0 ± 0.9	96 ± 4	96 ± 3
9	Galactose	6.6 ± 0.2	3.8	3.9	8.4	3.3	2 ± 2	96 ± 2	100 ± 6
10	Glucose	6.96 ± 0.04	0.92	2.8	4.3	2.2	2 ± 1	97 ± 6	97 ± 3
11	Mannose	7.3 ± 0.2	0.64	4.8	11.9	4.4	3 ± 2	94 ± 6	98 ± 10
12	Xylose	7.60 ± 0.07	0.65	3.6	9.7	2.6	6 ± 3	97 ± 3	105 ± 7
13	Fructose	8.4 ± 0.2	1.6	5.2	11.6	4.5	7 ± 2	82 ± 4	84 ± 4
14	Ribose	9.2 ± 0.1	1.7	3.2	18.0	2.9	1.9 ± 0.8	101 ± 2	83 ± 3
15	Sucrose	10.0 ± 0.2	1.3	3.7	4.7	3.0	3 ± 3	100 ± 2	NA[d]

a) average peak retention time ± 1 SD (n=17); b) RSD of 9 consecutive injections from 50 nM standard solution; c) percent deviation of 1.0 µM check standard in 5 different days; d) not included in the spike

Table 2.2: Figures of merit for anion and cation analysis, including the range of seven-point calibration curves, coefficient of determination, instrument detection limit, method detection limit, and mean spike recovery (± 1 standard deviation) for 7 replicate samples.

Analyte	Calibration Range (mg L^{-1})	R^2	IDL (µg L^{-1})	MDL (µg L^{-1})	Spike Recovery (%)
Cations					
Na^+	0.050 – 10.0	> 0.999	1.6	28.3	92 ± 6
NH_4^+	0.062 – 12.0	NA[a]	1.3	20.9	99 ± 5
K^+	0.13 – 25.0	> 0.999	1.1	4.20	101 ± 2
Mg^{2+}	0.062 – 12.0	> 0.998	1.2	29.8	98 ± 2
Ca^{2+}	0.13 – 25.0	> 0.999	21.9	37.0	100 ± 3
Anions					
F^-	0.010 – 1.00	> 0.999	2.2	5.0	98 ± 1
Cl^-	0.030 – 3.00	> 0.999	3.6	7.8	103 ± 2
NO_2^-	0.10 – 10.0	> 0.998	6.7	30.2	101 ± 3
Br^-	0.10 – 10.0	> 0.999	4.5	22.9	101 ± 2
NO_3^-	0.10 – 10.0	> 0.999	7.9	22.6	102 ± 2
SO_4^{2-}	0.15 – 15.0	> 0.999	9.1	60.0	102 ± 2

a) non-linear calibration

Table 2.3: Figures of merit for total metal analysis; coefficient of determination, method detection limit, and mean spike recovery (± 1 standard deviation) for 5 replicate spike recovery samples.

Analyte	R^2	MDL (µg L^{-1})	Spike Recovery (%)
Al	> 0.999	6.95	86 ± 2
Ti	> 0.999	0.80	93 ± 8
V	0.998	1.27	96 ± 2
Cr	> 0.999	1.97	99 ± 2
Mn	> 0.999	0.77	98 ± 2
Fe	> 0.999	6.34	103 ± 2
Ni	> 0.999	0.30	99 ± 2
Cu	> 0.999	0.64	95 ± 2
Zn	> 0.999	8.20	100 ± 4
As	0.991	2.96	126 ± 2
Se	0.991	9.98	121 ± 2
Sr	> 0.999	1.20	92 ± 1
Cd	0.998	1.17	111 ± 1
Ba	> 0.999	0.76	97 ± 1
Pb	> 0.999	0.36	103 ± 1

Table 2.4: Method detection limit, and mean spike recovery (± 1 standard deviation) for 6 replicate spike recovery samples of organic species.

Analyte	Detection Limit (pg μL^{-1})	Spike Recovery (%)
Phenanthrene	4.44	92 ± 4
Anthracene	3.13	92 ± 4
Fluoranthene	4.89	100 ± 2
Pyrene	3.75	103 ± 4
9-Methylanthracene	6.26	76 ± 6
Benzo(GHI)fluoranthene	4.31	104 ± 2
Cyclopenta(cd)pyrene	3.14	41 ± 6
Benz(a)anthracene	3.69	99 ± 6
Chrysene	3.09	106 ± 3
1-Methylchrysene	2.95	112 ± 3
Retene	9.98	99 ± 4
Benzo(b)fluoranthene	8.03	112 ± 5
Benzo(k)fluoranthene	7.43	106 ± 3
Benzo(e)pyrene	4.87	109 ± 3
Benzo(a)pyrene	3.45	97 ± 5
Perylene	3.78	95 ± 8
Indeno(1,2,3-cd)pyrene	5.44	101 ± 3
Benzo(GHI)perylene	8.44	111 ± 4
Dibenz(ah)anthracene	5.01	114 ± 4
Picene	NA	124 ± 6
17α(H)-22,29,30-Trisnorhopane	1.49	97 ± 3
17β(H)-21α(H)-30-Norhopane	1.58	115 ± 7
17α(H)-21β(H)-Hopane	1.41	109 ± 4
ABB-20R-C27-Cholestane	4.51	114 ± 8
ABB-20S-C27-Cholestane	5.88	106 ± 2
ABB-20R-C28-Ergostane	2.43	102 ± 3
ABB-20R-C29-Sitostane	3.54	115 ± 7
Tetradecane	23.0	88 ± 7
Pentadecane	26.8	114 ± 19
Hexadecane	14.9	101 ± 7
Norpristane	50.4	94 ± 15
Heptadecane	16.6	92 ± 18
Pristane	28.6	92 ± 11
Octadecane	18.5	85 ± 3
Phytane	25.9	92 ± 6
Nonadecane	16.0	96 ± 5
Eicosane	10.6	96 ± 2
Heneicosane	23.8	107 ± 8
Docosane	35.8	120 ± 4
Tricosane	13.2	92 ± 5
Tetracosane	NA	112 ± 18
Squalane	NA	122 ± 19
Pentacosane	39.9	104 ± 12
Hexacosane	31.6	102 ± 12
Heptacosane	22.4	96 ± 8
Octacosane	49.1	88 ± 5
Nonacosane	47.8	92 ± 6
Triacontane	91.2	89 ± 5
Hentriacontane	70.9	88 ± 4
Dotriacontane	69.5	85 ± 4
Tritriacontane	56.2	85 ± 3
Tetratriacontane	64.2	88 ± 4
Pentatriacontane	84.5	87 ± 3

CHAPTER THREE

CHEMICAL CHARACTERIZATION OF BIOMASS BURNING AEROSOL FROM CONIFERS, GRASSES, CROP RESIDUE, PEAT AND COOKING FIRES[1]

3.1 Abstract

$PM_{2.5}$ emitted from 86 fuels during combustion were characterized, across five different fuel categories including conifers, agricultural residues, grasses and other perennials, peat and cookstoves during the fourth Fire Laboratory at Missoula experiment (FLAME-4). Fire-integrated emission factors (EFs) were computed for $PM_{2.5}$ mass, organic carbon (OC), elemental carbon (EC), water-soluble organic carbon (WSOC), water-soluble inorganic ions (K^+, NH_4^+, Na^+, Ca^{2+}, Mg^{2+}, F^-, Cl^-, NO_3^-, SO_4^{2-}), metals (Al, Si, Ti, Cr, Mn, Fe, Ni) and organic species (e.g. levoglucosan, polycyclic aromatic hydrocarbons). Generally, EFs varied with fuel type and the geographic location where it was harvested, burning condition (stack or room) and modified combustion efficiency (MCE). Generally, PM was dominated by OC (22-97 %) and EC (2-76 %). Anhydrosugars dominated the OC mass fraction of conifers, agricultural residues and grasses while n-alkanes dominated the OC mass fraction of peat. The OC emission profiles of cookstoves were depend on the fuel type more than the cookstove technology. Among tested fuels ocote showed the highest PAH mass fraction of OC contributing 5 % of OC mass. Inorganic ions contributed a significant fraction (4-69 %) of PM emitted by agricultural residues and grasses and other perennial plants with the major inorganic

[1] This chapter is in preparation to publish as Jayarathne, T.; Stockwell, C.; Dolan, M.; Engling, G.; Yokelson, R.; Stone, E.; "Chemical characterization of biomass burning aerosol from conifers, grasses, crop residue, peat and cooking fires" *Atmospheric Environment.*
Author Contributions
E.S. and R.Y. designed research and planned the experiments; T.J. collected extracted and analyzed PM samples, processed data and wrote the chapter; C.S. provided MCE and EF_{CO} data; M.D. analyzed WSOC; G.E. analyzed metals in PM.

compounds expected to be as KCl, NH_4Cl and K_2SO_4. Our measurements spanned over a variety of fuel types collected from different geographical locations which were burned under 2 different burning methods at a wide range of MCEs, and thus help to improve estimates of the variation of emissions for similar fuel types.

3.2 Introduction

Fire has been used since early stages of human evolution as an effective tool for cooking, heating, lighting and hunting, and more recently as a tool for land management and pest control, a method of waste disposal and for industrial use.[82, 83, 127, 128] Ecologically, forest and savanna fires were considered as essential natural phenomenon required maintaining the balance of ecosystems, which generally started due to a lighting strike or volcanic activity. But in recent years the contribution from anthropogenic fires are becoming more frequent due to extensive agricultural practices.[127, 129] At present biomass burning is not limited to natural forest and savanna fires, but also agricultural and crop residue fires, peatland fires, garbage burning, industrial and domestic use of biomass comprise to a significant fraction of global biomass burning budget.[93]

Biomass burning is recognized as a major source of atmospheric PM and annual flux of total PM is estimated to be ~80 Tg yr^{-1}.[84] In general, 80-90 % of biomass burning aerosols are in fine mode (typically d_p < 1 μm) and considered as the largest source of primary fine carbonaceous aerosols to the atmosphere.[26, 84, 85, 93] Biomass burning emissions not only elevated the PM levels at the source, it also can transport over long distance and lead to regional and global climate, socioeconomic and health effects.[130, 131] Biomass burning emissions primarily contain gaseous carbonaceous species (e.g. CO_2,

CO, CH_4) and also rich in particulate carbonaceous species, elemental carbon (EC) and organic carbon (OC).[84, 93, 100] Recent studies have demonstrated that biomass burning smoke is also a major source of brown carbon (BrC).[49, 96, 102] Annual global emission of EC due to biomass burning are estimated to be 4.8-5.7 Tg C yr^{-1}, which is comparable to estimated annual contribution from fossil fuel combustion emissions.[84, 93, 132] Biomass burning is also estimated to emit 38-54 Tg C yr^{-1} of OC which is ~40% of the total global OC budget.[84, 132, 133]

Usually, field studies or laboratory experiments are used to measure biomass burning emissions. *In-situ*, airborne and remote sensing measurements or sampling ambient aerosols at receptor sites impacted by biomass burning smoke are the major approaches used in field-based studies.[93] *In-situ* measurements are claimed to be the best approach among all as it can sample fresh smoke right after emitting from the source. However, *in-situ* measurements are limited by difficulties associated with accessing the actual burning sites with instrumentation and require portable or mobile battery-powered instruments.[134] Airborne measurements and sampling from receptor sites are typically made downwind of the emission source and sampled smoke is likely from a various fuel types, and is always mixed with ambient PM.[135] Therefore, burning individual biomass fuels in a laboratory under controlled conditions is used to study emissions from individual fuel types. Further, laboratory experiments allow for the measurement of physical (e.g. moisture content, mass of fuel, mass of residue) and chemical (e.g. elemental composition) properties of the fuel that actually burned which in turn facilitate to compute more robust emission factors via mass balance modeling.[135] However, fuel harvesting, handling, transport, storage and different burning conditions utilized in

laboratory experiments can significantly alter biomass and fire properties, thus, may not representative to natural emissions.[25, 49]

The efforts made to quantitatively estimate biomass burning emissions have a history nearly 40 years.[136] Chemical profiles developed through field and laboratory studies have supported the development of global and regional emission inventories of biomass burning.[93] Emission estimates are generally computed on a mass basis using the burned area, fuel loading and fuel-based emission factors (EF).[93] Major uncertainties of the model estimates have been attributed to inadequate data in EFs and fuel loading.[99] EFs reflect the mass of a chemical species (e.g. $PM_{2.5}$ mass, EC, OC) emitted to the mass of fuel burned and largely depend on biomass type and burning conditions.[137] Further, many important biomass types have not or rarely being studied (e.g. peat, cookstove, garbage); thus representative EFs are not available.[93] Therefore, comprehensive EFs for variety of fuel types representing different burning conditions are essential for more representative and robust model estimations in order to assess their influence on local and global scale.[26, 90, 93, 138] Therefore, in recent past number of studies focused on the comprehensive characterization of biomass burning emissions in order to build source profiles to use for emissions inventories and source apportionment modeling. Apart from commonly measured forest and savanna fuels these studies utilized some rarely studied sources like foliage, organic soil and fuels commonly burned in residential or industrial use (e.g. cooking fires, garbage, tires).[94-100]

The Fire Laboratory at Missoula Experiments (FLAME) were designed to fulfill these gaps to compute comprehensive EFs for both gaseous and particulate species for variety of under sampled fuel types. Previously three FLAME laboratory studies were

conducted in 2006 (FLAME-1), 2007 (FLAME-2), 2009 (FLAME-3), and this study (FLAME-4) was took place in 2012 at the U.S. Forest Service's Fire Science Laboratory (FSL), Missoula, Montana, USA with overall goal of burn both historically undersampled and well-studied fuels while adding new instrumentation and experimental methods to provide previously unavailable information on physical and chemical properties of biomass burning emissions. During this study more than 150 burns were performed representing wide variety of globally significant fuels including African and savanna grasses, crop residue, peat, conifers, cookstoves, shredded tires and trash under different burning conditions. This manuscript primarily focuses on chemical characterization of PM and several companion papers have already been published on gas-phase characterizations[94, 95, 139] and particulate fluoride emissions.[140] To this end 86 $PM_{2.5}$ samples were collected and chemically speciated with the primary objective of computing EFs for $PM_{2.5}$ mass, EC, OC, water soluble ions, metals and organic species across five different fuel categories including conifers, agricultural residues, grasses and other perennials, peat and cookstoves. To the best of our knowledge this is the first comprehensive cookstove study related to common fuels used in USA. Emissions from traditional 3-stone, and improved envirofit rocket, EZstove and Phillips gasifier were test using red oak, Douglas fir and ocote as firewood. Further, the computed EFs in this study were compared with previously published values, and emission profiles were compared across different fuel types.

3.3 Methods

3.3.1 Fuel Harvesting and Storage

A complete description of fuel harvesting and storage is given in Stockwell et al., (2014) and the geographical locations of the harvested fuels are indicated in Table S3.1.

3.3.2 Combustion Facility and Burn Procedure

The FSL is equipped with a combustion chamber and the design of the combustion chamber is described in detail elsewhere.[98] In brief, the combustion chamber is a square room with an exhaust stack in the middle. The fuel bed was positioned right below the exhaust stack and combustion emissions were drawn through the exhaust stack at a constant flowrate. These burns are referred to as "stack" burns. Apart from stack burns another type of experiments were performed, which we referred to as "room" burns. For room burns, the combustion chamber was sealed by closing the exhaust stack opening, and the fuel bed was positioned at the middle of exhaust stack and the chamber wall. A large circulation fan was operated to facilitate well mixing of smoke to distribute the burning emissions evenly throughout the room. Fuels (ranging in mass from 0.1 – 4 kg) were burned over the course of 2-30 minutes under conditions (e.g. loading, geometry, etc.) designed to mimic natural field burning.

3.3.3 $PM_{2.5}$ Sample Collection

$PM_{2.5}$ was collected using two custom-built PM samplers in parallel. The $PM_{2.5}$ samplers were positioned on the sampling platform with the sampler inlets located at the center of the exhaust stack for stack burns. For room burns, the $PM_{2.5}$ samplers were

positioned at the North side of the combustion chamber and smoke filled in the combustion chamber was sampled at ~2 m height from the floor. In both stack and room burn configurations, the biomass smoke was diluted significantly with room air to cool the smoke to ambient temperature to allow for gas-particle partitioning to equilibrate prior to sample collection. The PM was collected on pre-cleaned 37 mm quartz fiber filters (QFF) and pre-weighed Teflon filters (PALL, Life Sciences, Port Washington, NY) preceded by two 2.5 μm sharp-cut cyclones (URG). Field blanks (FB) were collected for every seventh sample and for some samples a second (backup) QFF filter (QBT) was placed in series behind the first (front) Teflon filter in order to assess the positive sampling artifacts from carbonaceous gas adsorption. Sampled filters were stored in dark and frozen (-20 °C) and were shipped frozen to the University of Iowa for chemical analysis.

3.3.4 $PM_{2.5}$ Mass, Elemental Carbon, Organic Carbon, Water-soluble Organic Carbon, Water-soluble Inorganic Ion and Organic Speciation Measurement

The procedures utilized in PM mass, organic carbon, elemental carbon, water-soluble organic carbon, water-soluble inorganic ion and organic speciation measurements are described in Chapter 2.

3.3.5 Total Metals

Metals in biomass burning aerosol samples were analyzed by an energy-dispersive X-ray fluorescence spectrometer (ED-XRF, Epsilon 5, PANalytical), equipped with a 600 W power X-ray tube, following a protocol adopted from the US EPA

Chemical Speciation Network.[125, 126] The relative bias of the ED-XRF analyses, calculated using NIST standards, and was within 15 %.

3.3.6 Emission Factor and MCE Calculation

The mixing ratios of CO and ~20 other gases were measured by an open-path Fourier transform infrared (OP-FTIR) spectrometer.[95] The carbon mass balance approach was used to determine the carbon monoxide emission factor (EF_{CO}) in the units of mass of CO per kilogram of fuel burned (g kg^{-1}).[95] CO was used as the reference species to calculate the EF of particulate species and the CO mass drawn through the filter (M_{CO}) was calculated using the CO concentration in the smoke. Then, the mass of the analyte (M_X) and EF_{CO} was used to calculate the emission factors of the desired analyte (EF_X) (e.g. PM mass, EC, OC, etc.) following equation 3.1.

$$EF_X = \frac{M_X}{M_{CO}} \times EF_{CO} \quad (3.1)$$

Uncertainty in EF_X was propagated from the relative uncertainty of EF_{CO}, conservatively estimated as 5 % of the value and the analytical uncertainty of the considered analyte. The modified combustion efficiency (MCE) was calculated as $MCE = \Delta CO_2/(\Delta CO + \Delta CO_2)$ and was used as an indicator of flaming combustion (MCE > 0.9) and smoldering combustion (~0.75-0.84).[137]

3.4 Results and Discussion

3.4.1 $PM_{2.5}$ Composition and Emission Factors

The average contribution of OC, EC water-soluble ions and metal oxides relative to total $PM_{2.5}$ mass for each fuel category is given in Figure 3.1a. For 9 biomass categories, sum of the speciated masses exceeded the gravimetrically measured $PM_{2.5}$ masses (e.g. Ponderosa pine), and 3 biomass categories $PM_{2.5}$ mass was below the detection limits (e.g. cookstoves). Therefore, $PM_{2.5}$ mass fractions of those burns were calculated using re-constructed mass; by summing OC, EC, ion and metal oxide masses. Higher OC contributions were observed for peat (83±18 %) and conifers (80±12 %) among all the studied fuel categories. In contrast, EC comprised to a significant fraction of PM emitted by cookstoves (61±17 %) and grasses (43±13 %) while water-soluble inorganic ions showed a higher mass fraction in agricultural residue burns (27±22 %) relative to other studied fuel categories.

Average $PM_{2.5}$ EFs for each biomass category is presented in Table 3.1 while individual $PM_{2.5}$ EFs for all the burns are given in Table S3.1. The induvial $EF_{PM2.5}$ for conifers ranged 4.5-93 g kg^{-1} averaging at 43±30 g kg^{-1}. The observed EF $PM_{2.5}$ for conifers in this study is comparable with average EFs, 4-167 g kg^{-1} reported in previous laboratory studies.[98-100, 141, 142]

The overall average $EF_{PM2.5}$ for grasses and other perennial plant category was 12±17 g kg^{-1} ranging from below the detection limits to 79 g kg^{-1} (Table S3.1). The overall average was dragged to a higher value due to relatively higher EFs of hay, alfalfa and manzanita than the grasses (Table 3.1). This is likely due to long smoldering phase of these perennials relative to instantly burn grasses. If we consider only the grass burns

(African grass, sawgrass and wiregrass), the average $EF_{PM2.5}$ decreased to 6.1±5.9 g kg^{-1}. These EFs are also similar to previously reported average EFs, 2.1-39 g kg^{-1} [21, 98-100] for savanna fires from laboratory and field studies.

The MCE of conifers and, grasses and other perennial plant categories ranged 0.848-0.970 and 0.911-0.984, respectively (Table S3.1). These MCEs indicate mixtures of flaming and smoldering combustion.[137] Previous studies have shown higher PM emissions at lower MCEs.[98, 143] Similarly, we observed a significant negative correlation with $EF_{PM2.5}$ and MCE for conifers, and grasses and other perennial plant fuel categories (Figure 3.2a). However, such a significant correlation was not observed for other fuel categories indicating MCE is not the only determinant factor for PM emission.

The average $EF_{PM2.5}$ for agricultural residue was 19±13 g kg^{-1} ranging from BDL to 42 g kg^{-1} (Table S3.1). Relatively higher $EF_{PM2.5}$ was observed for agricultural residue room burns (28±11 g kg^{-1}) than stack burns (9±7 g kg^{-1}) indicating the influence of combustion method on PM emissions. However, observed EFs are on par with previously reported EFs (12-30 g kg^{-1}) for agricultural fires.[98, 141]

Peat burns had the lowest MCE values, 0.683-0.832 which is indicative of smoldering combustion.[137] The overall average peat $EF_{PM2.5}$ was 61±44 g kg^{-1} and is higher than the average values, 5.9-46 previously reported for laboratory peat fire emission studies.[100, 144, 145] The recent *in-situ* measurements of peatland fire emissions reported more representative EFs for $PM_{2.5}$ (6.0 - 29.6 g kg^{-1}) and our study average is 3 times greater than their reported average (17.3±6.0 g kg^{-1}).[25] This is likely due to different burning conditions as evident by lower MCE values in this study (0.68-0.83) relative to Black et al., (0.80-0.88) and Jayarathne et al., (0.73-0.83).

3.4.2 EC and OC Emission Factors

The effects of negative sampling artifacts due to carbonaceous gas adsorption were assessed during this study using QBT approach.[146] EC was not detected on any of the backup filters indicating the efficient collection of EC on front filters. For the samples with QBT collected, the OC on the backup filter was directly subtracted. For the rest, the average OC concentration for the fuel type was used: rice straw (2.0±0.4 %), ponderosa pine (1.2 %), black spruce (2.9±1.6 %), and peat (3.1±0.8 %). For the fuel types without backup filters collected, the study average of OC artifact (2.4±1.2 %) was used for artifact correction. The FB subtracted backup filter OC concentration ranged from 0.8±0.6 µgC cm^{-2} to 5.6±0.7 µgC cm^{-2} and a significant (p=0.05) positive correlation (r=0.63) was observed with front filter OC loading (Figure 3.3). This indicates that the amount of carbonaceous gas adsorbed is proportional to the mass concentration of OC and, not yet reach to a level of backup filter saturation. Previously Turpin et al. [147] also showed similar quartz fiber filters become saturated above 6 µg OC cm^{-2}.

The computed average EC and OC emission factors are given in Table 3.1 and individual emission factors are given in Table S3.1. The average EF_{OC}, ranged from 0.90±1.1 g kg^{-1} at high MCE to 52±18 g kg^{-1} at lower MCE values. Grasses, agricultural residues and cookstoves were examples for biomass categories with low EF_{OC}, with emission dominated by flaming combustion as reflected by relatively higher MCEs than other fuels. Conifers (40±33 g kg^{-1}) and peat (39±22 g kg^{-1}) had lower MCEs and showed the highest EF_{OC} for the studied biomass categories. EF_{OC} of conifers ($r = - 0.46$; $p = 0.05$), agricultural residues ($r = -0.42$; $p = 0.06$) and, grasses and other perennial plants (r

= -0.49; $p < 0.01$) were negatively correlated with MCE, as expected, with increasing contributions from smoldering-phase combustions (Figure 3.2b). However, EF_{OC} of other biomass categories did not correlate with corresponding MCE values. The range of EF_{OC} reported in literature is very large, even for same biomass category due to variation of fuel properties (e.g. moisture content), different burning conditions and various experimental procedures followed in different studies. As an example average EF_{OC} reported for conifers in previous laboratory studies range 3.5-170 g kg^{-1},[98-100, 141, 142] which is comparable to observed EF_{OC} for conifers during this study. Similarly, EF_{OC} reported for agricultural residues and grasses are on par with previous literature reported values. However, study average EF_{OC} (39±22 g kg^{-1}) for peat burning aerosol is considerably higher than that of literature reported EFs, 6 g kg^{-1} by Christian et al.;[21] 8-13 g kg^{-1} by Iinuma et al.;[100] 4-6 g kg^{-1} by Black et al.[144] and 12.4 g kg^{-1} by Jayarathne et al.[25] likely due higher $EF_{PM2.5}$ as discussed in section 3.1.

Cookstove EF_{OC} and EF_{EC} observed in this study ranged 0.4-5 g $kg^{-1}$and 0.5-24 g kg^{-1}, respectively (Table S3.1). For 3-stone and envirofit rocket cookstove types EF_{EC} is always higher than that of OC (Figure 3.4). High EC emissions are not unexpected due to flaming combustion as evident by high MCE (0.963-0.985) values. The EC and OC emission factors were higher for traditional 3-stone cookstoves than improved cookstoves for similar fuel types. But this difference was not prominent as observed for gaseous aromatic hydrocarbons, phenolic compounds and furans as shown by Stockwell et al.[94] Similarly, EF_{EC} and EF_{OC} depended on firewood type showing 15 times and 6 times high EF_{EC} and EF_{OC} for ocote than red oak or Douglas fir, respectively (Figure 3.4). Over all, cookstoves (5.9±9.1 g kg^{-1}) and grasses (2.3±2.2 g kg^{-1}) had the highest EF_{EC} which had

relatively higher MCE values than other burns. However, a significant correlation ($p > 0.37$) was not observed between MCE and EC for any of the fuel categories. Most of the EF_{EC} observed in this study is considerably higher than the previously reported values for similar fuel types.[25, 50, 98, 100, 141]

The average WSOC fraction of OC ranged from 24±2 % for peat to 71±10 % for wheat straw (Table 3.1). Noticeably lower fractions were observed for peat (21-34%) than the rest of the fuels (33-78 %). The lower WSOC fraction of peat burning aerosol is similar to recently reported values, 16±11 % by Jayarathne et al.[25] for Indonesian peatland fire emissions. This indicates the presence of hydrophobic organic compounds in peat fire emissions. The conifer WSOC fraction (45-52 %) observed in this study was higher than the values (29-37 %) reported by Iinuma et al.[100] WSOC can influence on aerosol hygroscopicity. Therefore, particles containing high fraction of WSOC can effectively activate a cloud droplet.

3.4.3 Composition of Organic Carbon

PM samples collected from black spruce (n=3), ponderosa pine (n=1), rice straw (n=2), sawgrass (n=1), wiregrass (n=1), peat (n=5) and cooking fires (n=9) were further speciated to quantify polycyclic aromatic compound (PAHs), hopanes, n-alkanes, anhydrosugars and sterols. On average, anhydrosugar fraction (19-46 %) dominated the OC fraction in conifers, agricultural residues and grasses while n-alkane fraction (21-32 %) dominated the peat PM OC (Figure 3.5). The higher n-alkane OC mass fraction is indicative to peat fire emissions likely due to the higher plant wax content in peat soil due to accumulation of those over the time of decomposition compared to other biomass

fuels.[25, 142, 148, 149] Cookstove emissions had a distinct variation based on the firewood type more than the cookstove technology. Anhydrosugars comprised to 7 % of red oak and Douglas fir OC mass while n-alkanes contributed to 3 % of millet OC mass. Surprisingly, both ocote burns resulted very high PAH mass fraction of OC (~5 %) relative to any other fuel types tested in the study. This is on par with the very high EF_{EC} observed for these two burns as PAHs are frequently associated with soot.[150, 151]

Anhydrosugars:

Levoglucosan (LG), mannosan (MN) and galactosan (GL) are quantified as anhydrosugars which are pyrolysis products of cellulose and hemicellulose in plant tissues.[152] Except two ocote burns, LG showed the highest individual EF among all the speciated organic compounds having EF_{LG} from ~40 mg kg^{-1} for EZstove-millet cookstove to ~40,000 mg kg^{-1} for ponderosa pine (Table 3.2 and Table S3.2). This wide variation of EF_{LG} is likely due to wide variation of EF_{OC} and variable content of cellulose in plant tissues.[153] Similarly, literature reported EF_{LG} values from previous laboratory and field studies also vary in the range of three orders of magnitude; thus the observed range during this study is comparable.[100, 154] The maximum EF_{LG} reported by Iinuma et al. (2007) is 4600 mg kg^{-1} for German peat which is an order of magnitude less EF_{LG} than the maximum value we observed in this study. However, LG mass fraction of OC is similar in both cases with 36 % in Iinuma et al. (2007) and 31 % in this study. Therefore, high EF_{LG} in this study was primarily due to high OC emissions. A strong correlation ($r = 0.81$; $p < 0.01$) was observed between EF_{OC} and EF_{LG}; thus emission of LG could consider as a function of OC emission. LG mass fraction of OC showed a distinct

variation among different fuel categories. On average, cookstoves (3.5±2.6 %) and peat (6.4±1.8 %) had the lowest LG mass fraction of OC; black spruce (18.1±0.4 %) and ponderosa pine (14 %) showed an intermediate mass fraction while sawgrass (27 %) , wiregrass (34 %) and rice straw (45 %) showed the highest LG mass fraction of OC (Table 3.2). This is likely due to differences of cellulose content in each fuel type.[153] The relative proportion of cellulose and hemicellulose in different plant species can give rise to distinct profiles of LG, MN and GL in biomass burning smoke. Thus, LG:MN ratio has been suggested as an potential indicator for identifying biomass burning emissions from different fuel types.[155, 156] Similarly, ponderosa pine (4.2), black spruce (7.7±1.6) and cookstoves (4.3) were characterized by relatively low LG:MN ratio, peat (23-27) and grasses (21-22) were characterized by intermediate LG:MN ratio and rice straw (47) was characterized by high LG:MN ratio (Table 3.2). These ratios are in an agreement with previously reported values in literature and could be helpful indicators to separate fresh biomass smoke of different fuel types.[155]

n-Alkanes:

n-Alkanes showed an odd carbon preference with maximum contribution either from C_{27}, C_{29} or C_{31} which is indicative to pyrolysis of plant waxes.[157] The carbon preference index (CPI = C_{odd}/C_{even}) was calculated for all the quantified n-alkanes and average CPI ranged from 1.3 to 2.6 (Table 3.2) which is similar to previously reported values for biomass burning emissions.[100, 142, 158] Relatively lower CPI values (1.2-1.5) were observed for peat than other fuels (1.5-2.6) except an ocote fire (burn # 115) which yielded a CPI of 1.3 (Table S3.2). Total n-alkane EFs were relatively lower for

cookstoves (6.3-157 mg kg^{-1}), grasses (212-479 mg kg^{-1}) and rice straw (406-653 mg kg^{-1}) than peat (325-1495 mg kg^{-1}) and conifers (877-2888 mg kg^{-1}). The higher EFs for peat and conifers are probably due to high content of plant wax per unit mass due to accumulation of those by decaying labile soft plant tissues or containing thick waxy epiticular layers or resin deposits in plant materials.[153] The n-alkane mass fraction of OC (1.4-32 %) observed in this study is slightly higher than the previously reported values (0.11-11 %) for similar fuel types.[100]

Other carbonaceous products:

Emission of sterols, PAHs and hopanes from biomass burning is generally less significant compared to anhydrosugars and n-alkanes due to their lower abundance, but frequently detected in biomass smoke.[154, 159]

Sterols:

Cholesterol, stigmasterol, β-sitosterol and campesterol were quantified as sterols. Among them cholesterol is associated with fauna while stigmasterol, sitosterol are markers for biomass smoke in general, and campesterol has been recognized as a specific tracer for grasses (*graminacea spp.*).[160] Cholesterol was consistently detected in cookstove emissions, but in very low quantities (<2 mg kg^{-1}). This is likely due to human contaminations due to handling of firewood.[161] On average, β-sitosterol were the most abundant sterol and higher EFs were observed for conifers than other fuel types (Table 3.2). Campesterol was detected only in rice straw and wiregrass emissions which both

belong to family *graminacea.* Thus, the specificity of campesterol for grass burn emissions is further confirmed.

PAHs:

The total EF of PAHs ranged from 5.9 mg kg^{-1} for cookstove – Douglas fir chips to 908 mg kg^{-1} for ponderosa pine and within the range of previously reported values for similar fuel types.[154, 159] On average, retene which is a tracer for softwood combustion was the most abundant PAH in conifers while pyrene and benzo(GHI)fluoranthene were the most abundant PAHs in other fuels.

Hopanes:

17α(H)-22,29,30-trisnorhopane, 17β(H)-21α (H)-30-norhopane and 17α(H)-21β(H)-hopane was identified using authentic standards and detected only in peat PM samples. Terpenoid and hopanoid hydrocarbon compounds that have the hopane-skeleton, which are derived by bacterial conversion of organic matter are ubiquitous in peat soil, but is not available in other studied fuel types.[162-167] Thus, presence of hopanes in peat PM is not surprising. The total EF for hopanes ranged from 32 mg kg^{-1} to 121 mg kg^{-1} (Table S3.2). Norhopane had the highest OC mass fraction followed by trisnorhopane and hopanes and a fairly consistent ratio of 0.2:0.7:0.1 was observed among trisnorhopane, norhopane and hopane for all the peat samples (Table 3.2). These observations are consistent with recent studies on *in-situ* peat emission characterization from Indonesian peatland fires.[25]

3.4.4 Composition and Emission Factors of Water-soluble Inorganic Ions

Although biomass burning PM is primarily dominated by carbonaceous materials, water-soluble inorganic ions also can contribute to a significant fraction. Inorganic ions comprise to a larger fraction of $PM_{2.5}$ emitted by agricultural residues (4.9-69 %) and, grasses and other perennial plants (6.0-23 %) relative to the other fuel categories (0.61-4.2 %) (Figure 3.1b). The higher inorganic mass fraction is associated with fuels, that have higher MCEs because inorganic ions effectively transfer to aerosol phase when combustion is more complete and combustion temperature is high.[168] Ion mass fraction of agricultural residues and grasses is dominated by K^+ and Cl^-, thus, KCl could be the primary inorganic compound in these PM. Similarly, K^+ showed a strong negative correlation with MCE for grasses and Cl^- showed a moderate negative correlation with MCE for both agricultural residues and grasses (Figure 3.2c-d) Next to K^+, NH_4^+ is the second abundant cation in agricultural residue samples and most likely they are in the form of NH_4Cl as Cl^- molar concentration is always higher than that of K^+ in agricultural residue burning PM. Sulfate was the second abundant anion in grasses and other perennial category, and most likely those are in the form of K_2SO_4 as excess K^+ molar concentration was observed in these PM relative to Cl^-, in contrast to agricultural residues. The observed high K^+, NH_4^+,Cl^- and SO_4^{2-} emissions are consistent with the reported high concentration of particulate phase potassium, ammonium, chloride and sulfate from field measurements of savanna fires in Africa and rice straw burning in Taiwan.[155, 169, 170] Apart from these 4 major ion species, F^- also comprises ~0.1% of PM mass. A comprehensive description of F^- emission is already published as a companion manuscript and will not discuss in detail here.[140] Na^+ and Ca^{2+} comprised another ~0.2%

of PM mass fraction while Mg^{2+} was not detected in any of the PM samples. This indicates the minimum resuspension of soil dust during the combustion process.

The average $EF_{total\ ion}$ varied in a larger range from 103 mg kg^{-1} for cookstoves to 17300 mg kg^{-1} for rice straw – China showing $PM_{2.5}$ mass fractions of 1.6 % and 62 %, respectively. The second highest $EF_{total\ ion}$ was 3450 mg kg^{-1} for hay (Table 3.3), but contributed only 13 % of total PM mass. The exceptionally high $EF_{total\ ion}$ in Chinese rice straw is likely due to accumulation of inorganic elements in rice plant, may be associated with higher usage of fertilizer or mineral-rich irrigation water. Considering individual burns, agricultural residues showed the highest $EF_{total\ ion}$ ranging 263-4800 mg kg^{-1} with average $PM_{2.5}$ mass fraction of 5-69 %. However, the extremely high EFs of Chinese rice straw, 21000 mg kg^{-1} and 29000 mg kg^{-1} were excluded from this range (Table S3.3). The observed $EF_{total\ ion}$ in this study for agricultural residues are in a very good agreement with EFs computed from previous FLAME-2 experiment.[98] Grasses and other perennial plants $EF_{total\ ion}$ ranged 86-3450 mg kg^{-1} and $PM_{2.5}$ mass fractions ranged 6-23 %. Overall, these values are higher than the EFs reported by Iinuma et al.[100] and May et al.,[141] but similar to EFs reported by McMeeking et al.[98] for savanna fuels. Conifers and peat showed the lowest water-soluble ion emission factors and $EFs_{total\ ion}$ ranged 243-2520 mg kg^{-1} and 181-798 mg kg^{-1}, respectively. Similarly, the $PM_{2.5}$ mass fraction of water-soluble ions were <4% for these fuel types. However, EFs observed in this study are higher than the EFs reported by Iinuma et al.,[100] McMeeking et al.[98] and Jayarathne et al.[25] for pine, spruce and peat.

3.4.5 Composition and Emission Factors of Metals

On average, metal oxide contributions to PM mass is ~1%. Al, Si and Fe were the most abundant metals in biomass burning emissions and study average of total metal EF is ~400 mg kg^{-1} (Table S3.4). Generally, higher EFs were observed for the agricultural residues, probably due to accumulation of those elements inside plant tissues from chemical sprays, fertilizers and irrigation water apply in the agricultural practices.

3.5 Conclusion

This work presents the chemical characterization of biomass burning $PM_{2.5}$ emitted from combustion of 5 different biomass categories; including conifers (black spruce, ponderosa pine), agricultural residues (millet, rice straw, wheat straw, sugar cane), grasses and other perennial plants (African grass, sawgrass, wiregrass, Hay, alfalfa, manzanita, chamise), peat (N.Carolina, Canada, Indonesia) and cookstoves (red oak, douglasfir, ocote, millet) during the fourth Fire Laboratory at Missoula experiment (FLAME-4). These biomass categories included both historically undersampled and well-studied fuels while adding new instrumentation and experimental methods to provide previously unavailable information on chemical properties of biomass burning emissions. This manuscript primarily focused on chemical characterization of PM and several companion papers have already been published on gas-phase characterizations.[94, 95, 139] and particulate fluoride emissions.[140]

The sampled $PM_{2.5}$ is chemically characterized and EFs were computed for $PM_{2.5}$ mass, OC, EC, WSOC, water-soluble inorganic ions, metals and organic species using various analytical techniques. Generally, EFs varied with fuel type and the geographic

location where it was harvested, burning condition (stack vs room) and MCE. The MCEs ranged from 0.683 for peat to 0.985 for cookstoves, from complete smoldering combustion to mixture of flaming and smoldering. Further, PM was collected from multiple fires from same fuel under different MCEs. Thus, were able to assess the differences in PM emission for a single fuel type under different combustion efficiencies and can be expected to enhance the accuracy of model emission estimates as pointed out by Yokelson et al.[135] The $EF_{PM2.5}$ and EF_{OC} depended on MCE having higher EFs towards lower MCEs. However, agricultural residues did not show a correlation with MCE, and thus, this relationship strongly depended on biomass types. EF_{ion} depend most on the fuel type rather than the MCE showing higher ion mass fraction of PM for agricultural residues and grasses relative to other fuel types.

Anhydrosugars dominated the OC mass fraction of conifers, agricultural residues and grasses while n-alkanes dominated the OC mass fraction of peat. The OC emission profile of cookstoves were depend on the fuel type rather than the cookstove technology showing major contributions from anhydrosugars for red oak, n-alkanes for millet and PAHs for ocote. The particularly high EF_{PAH} and EF_{EC} were characteristic to ocote relative to other tested firewood types. Based on personal communications with the firewood users and direct observations of the ocote fires during the experiment, it is a resinous wood burning with a heavy smoke, and on par with high PAH and EC emission factors. Considering the health risk associated with PAHs, human exposure studies are needed to evaluate the health risk associated with ocote emissions.

3.6 Supporting Information

Table S3.1: Emission factors of $PM_{2.5}$, EC, OC and WSOC mass fraction of OC for individual burns; Table S3.2: Emission factors of organic species for individual burns; Table S3.3: Emission factors of water-soluble inorganic ions for individual burns; Table S3.4: Emission factors of metals for individual burns.

3.7 Acknowledgments

We thank Allan L. Robinson, Sonia M. Kreidenweis, Paul J. DeMott and Ryan C. Sullivan for assistance organizing the FLAME-4 laboratory study and Shawn Urbanski at the USDA Forest Service Fire Sciences Laboratory in Missoula, Montana for support during the FLAME-IV study. We also thank Ted Christian, Dorothy L. Fibiger, Shunsuke Nakao and Austin Kammerer for assistance with filter sample collection and sample preparation. We also appreciate the contribution of Eric Miller, David Weise, Christine Wiedinmyer, Greg Askins, Savitri Garivait, Christian L'Orange, Benjamin Legendre, Brian Jenkins, Emily Lincoln, Navashni Govender and Kary Peterson for harvesting the fuels for this study. This work was supported by the National Science Foundation (ATM-0936321, AGS-1256042, ER-65296); NASA Earth Science Division (Award NNX12AH17); US Department of State-US Forest Service Partnership, and the University of Iowa.

Figure 3.1: Average a) $PM_{2.5}$ composition and b) water-soluble ion mass fraction of $PM_{2.5}$ for different fuel categories.

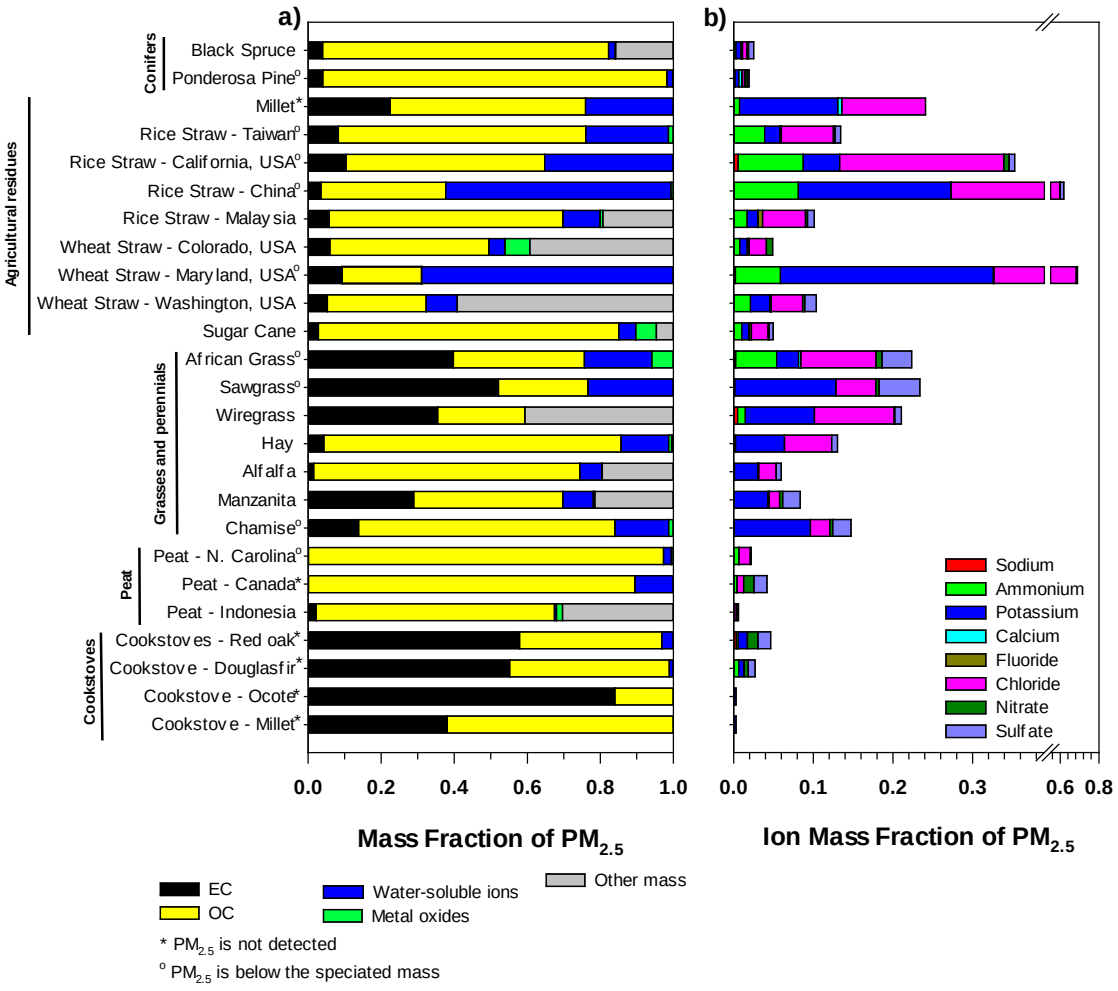

Figure 3.2: Fire-integrated $PM_{2.5}$ emission factors (EF) as a function of fire-integrated modified combustion efficiency (MCE) for a) $PM_{2.5}$ mass, b) OC, c) K^+ and d) Cl^- for individual sample data. Solid lines indicate the linear regression of EF onto MCE with Pearson's *r* and *p* values, color coded by biomass category. (Agricultural residues $EF_{PM2.5}$, EF_{OC}, EF_{K+} and EF_{Cl-} did not show a significant correlation with MCE, and conifers EF_{K+} did not show a significant correlation with MCE. Thus, not shown in the graphs).

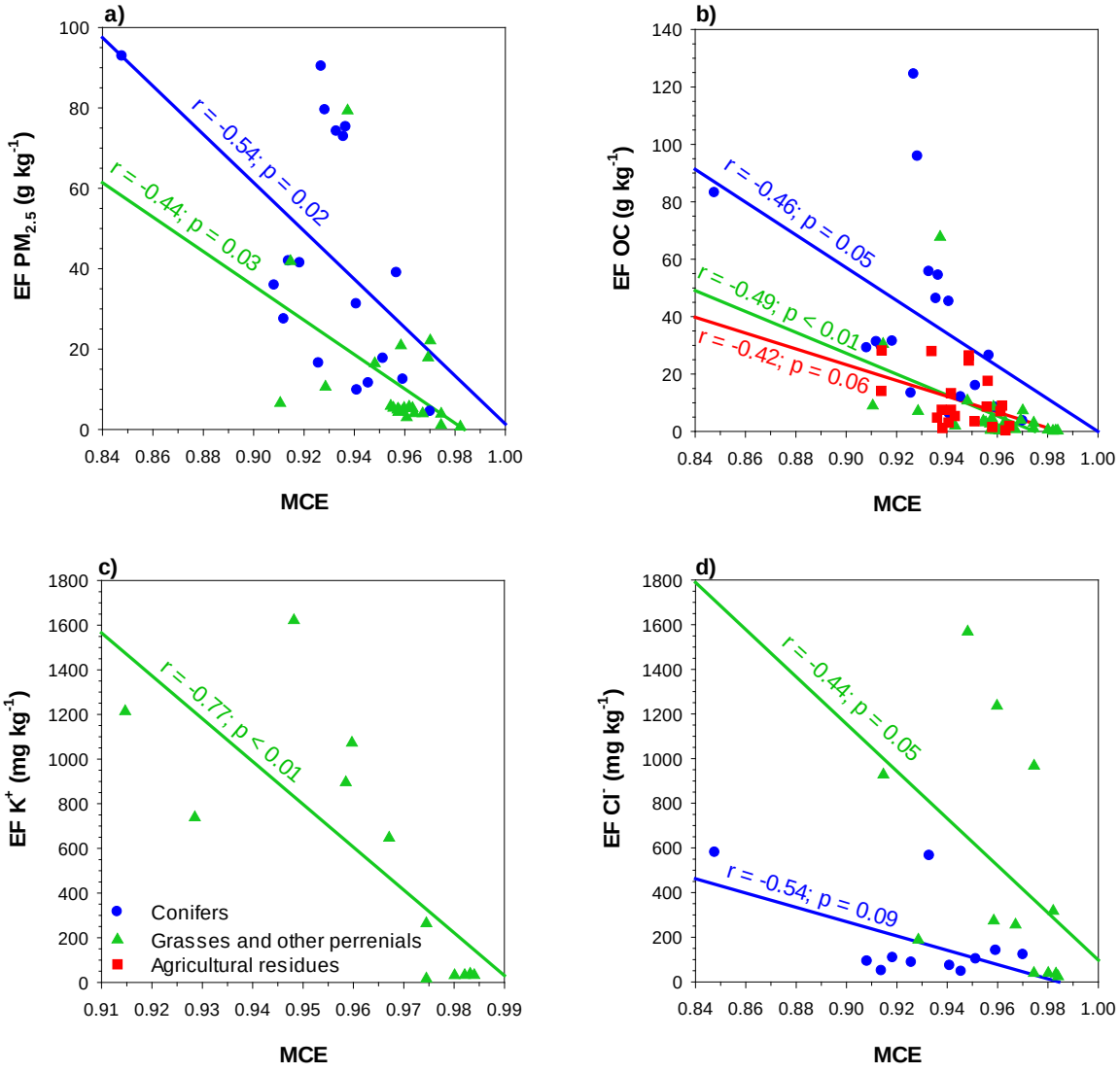

Figure 3.3: Backup filter OC loading as a function of front filter OC lading. Error bars represent propagated analytical uncertainty.

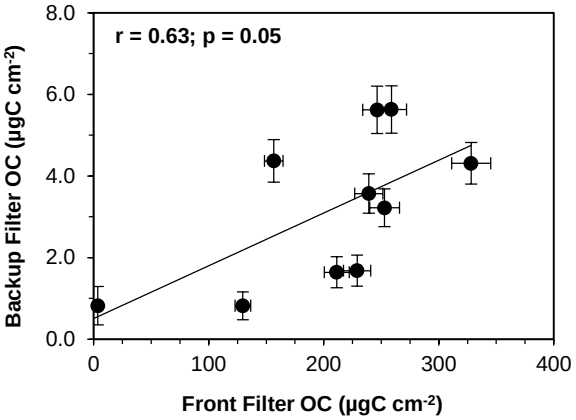

Figure 3.4: OC and EC emission factors for different cookstove types. Error bars represent propagated analytical uncertainty.

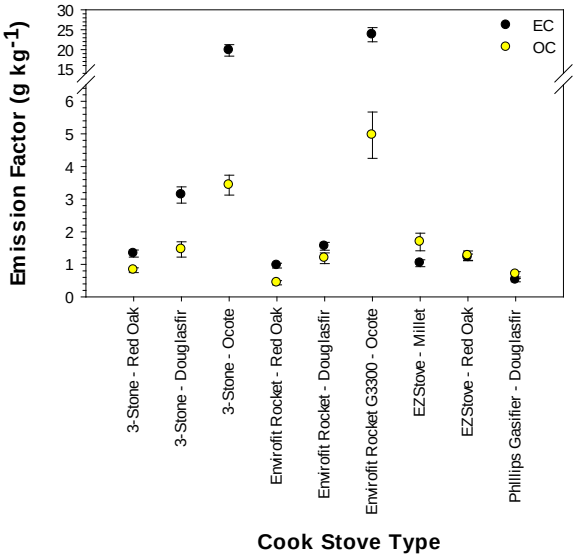

Figure 3.5: Organic carbon mass fraction of the speciated compound classes in select fuel samples. The individual emission factors are available in Table S3.2.

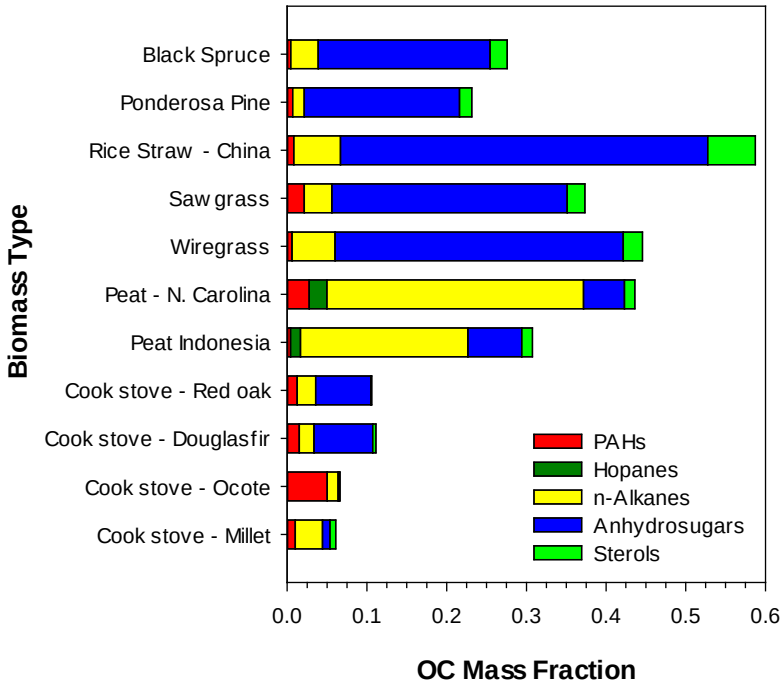

Table 3.1: Average emission factors of $PM_{2.5}$, EC, OC and WSOC mass fraction of OC for each biomass burning category (average ± 1 SD; standard deviation is given only for n ≥ 3). Individual sample EF data is available in Table S3.1.

Category	**Biomass Type - Location**	**Number of Samples**	**EF $PM_{2.5}$ (g kg^{-1})**	**EF EC (g kg^{-1})**	**EF OC (g kg^{-1})**	**WSOC Fraction of OC (%)**
Conifers	Black Spruce	8	41±29	1.7±0.8	32±21	52±6
	Ponderosa Pine	10	45±32	2.0±1.3	46±41	45±7
Agricultural residues	Millet	1	ND	0.5	1.2	NM
	Rice Straw - Taiwan	3	6.6±1.9	0.9±0.7	7.7±5.6	47±10
	Rice Straw – California, USA	1	8.9	1.4	7.1	NM
	Rice Straw - China	3	23±15	1.0±0.5	9.5±3.3	41±13
	Rice Straw - Malaysia	2	36	0.8	26	48
	Wheat Straw – Colorado, USA	5	17±13	1.0±0.9	7.3±6.4	71±10
	Wheat Straw – Maryland, USA	1	6.3	0.6	1.5	48
	Wheat Straw – Washington, USA	2	17	0.9	4.6	42
	Sugar Cane	2	34	0.97	28	48
Grasses and other perennial plants	African Grass	6	1.9±1.7	1.0±1.3	0.90±1.1	NM
	Sawgrass	9	4.6±0.8	2.7±2.3	1.3±1.1	NM
	Wiregrass	5	12±9	4.4±2.6	2.9±2.7	NM
	Hay	4	27±36	1.2±0.5	22±31	NM
	Alfalfa	1	42	0.7	31	NM
	Manzanita	1	21	6.1	8.5	NM
	Chamise	4	8±3	1.1±0.3	5±3	NM
Organic soil	Peat – N. Carolina	2	32	ND	34	30
	Peat – Canada	1	ND	ND	6.8	NM
	Peat – Indonesia	3	80±46	1.7±0.1	52±18	24±2
Cookstove	Cookstoves – Red oak	3	ND	1.2±0.2	0.84±0.4	NM
	Cookstoves - Douglasfir	3	ND	1.7±1.3	1.1±0.4	NM
	Cookstoves - Ocote	2	ND	22	4.2	NM
	Cookstoves - Millet	1	ND	1.0	1.7	NM

ND-not detected; NM-not measured

Table 3.2: Average emission factors of speciated organic compounds in mg kg^{-1} for selected fuel categories (average ± 1 SD; standard deviation is given only for $n \geq 3$). Individual sample EF data is available in Table S3.2.

	Conifers		Agri. residues	Grasses		Organic soil		Cookstove
	Black Spruce (n=3)	**Ponderosa Pine (n=1)**	**Rice Straw - China (n=2)**	**Sawgrass (n=1)**	**Wiregrass (n=1)**	**Peat - N. Carolina (n=2)**	**Peat - Indonesia (n=3)**	**Cookstoves (n=9)**
PAHs								
Phenanthrene	14±2	58	1.4	1.4	1.5	2.0	2.5±2.5	4.0±7.1
Anthracene	3.0±0.5	20	0.71	0.39	0.37	2.1	0.80±0.54	1.2±2.1
Fluoranthene	19±8	86	7.4	8.7	8.1	1.8	2.6±1.6	8±11
Pyrene	23±10	99	8.7	9.9	9.9	4.5	3.3±2.2	8±12
9-Methylanthracene	ND	7.2	ND	ND	ND	1.4	0.50±0.48	0.20±0.30
Benzo(GHI)fluoranthene	4.8±1.3	52	6.6	14.6	6.0	9.0	1.7±1.0	7±10
Cyclopenta(cd)pyrene	3.8±1.8	31	4.4	12	3.0	2.6	0.96±0.58	ND
Benz(a)anthracene	3.2±1.0	31	5.5	7.5	2.1	1.0	1.9±1.2	4.4±7.0
Chrysene	3.4±1.4	34	6.0	7.6	2.1	1.3	2.6±1.7	3.7±5.9
1-Methylchrysene	0.91±0.04	8.9	0.95	ND	ND	0.91	2.0±1.1	0.26±0.45
Retene	61±15	351	3.9	0.95	3.4	5.8	1.6±0.4	1.4±1.5
Benzo(b)fluoranthene	3.3±0.2	28	4.6	5.9	1.9	0.67	1.1±0.7	3.0±4.3
Benzo(k)fluoranthene	1.2±1.1	15	2.9	6.6	1.5	0.33	0.22±0.14	4.2±6.8
Benzo(j)fluoranthene	0.8±0.1	7.7	1.5	2.7	0.66	0.84	0.22±0.18	1.9±3.0
Benzo(e)pyrene	1.3±0.3	12	2.5	4.6	1.5	2.5	1.0±0.6	1.8±2.5
Benzo(a)pyrene	2.1±0.7	25	4.4	9.6	2.0	3.2	0.83±0.56	4.7±7.5
Perylene	0.22	3.4	0.48	1.5	0.27	0.80	0.49±0.22	1.0±1.4
Indeno(1,2,3-cd)pyrene	0.8±0.7	17	2.8	8.4	1.4	0.86	ND	3.5±5.5
Benzo(GHI)perylene	0.89±1.2	12	2.3	6.9	1.5	0.21	ND	2.4±3.6
Dibenz(ah)anthracene	1.1	3.3	0.73	0.82	0.31	1.1	ND	0.55±0.80
Picene	1.50±0.04	6.5	1.3	1.9	0.44	0.48	ND	1.1±1.6
Hopanes								
17α(H)-22,29,30-Trisnorhopane	ND	ND	ND	ND	ND	6.0	20±9	ND
17β(H)-21α(H)-30-Norhopane	ND	ND	ND	ND	ND	25	51±24	ND
17α(H)-21β(H)-Hopane	ND	ND	ND	ND	ND	4.6	10±8	ND
n-Alkanes								
Tetradecane	14±10	32	1.2	4.3	6.5	ND	ND	0.42±0.28
Pentadecane	15±2	125	4.7	13	10.	ND	ND	1.2±1.0
Hexadecane	7.30	ND	ND	ND	10.	28	ND	0.59±0.36
Heptadecane	58±60	147	8.0	3.4	10.	ND	ND	1.0±1.3
Octadecane	ND	ND	ND	ND	0.78	8.6	6.3	0.5±1.1
Nonadecane	50±29	45	13	4.9	8.0	9.5	26	1.5±2.8
Eicosane	14±9	25	0.85	2.0	5.3	37	31±33	1.2±2.2
Heneicosane	59±19	26	11	5.5	7.6	53	104±28	1.7±2.3
Docosane	41±31	101	3.2	6.7	19	27	86±40	1.4±1.6
Tricosane	83±66	133	17	14	14	59	95±9	2.1±2.0
Tetracosane	53±39	105	7.6	7.2	9.7	40	98±5	1.7±1.8
Pentacosane	128±41	173	43	19	26	54	104±6	3.3±3.5
Hexacosane	89±27	119	34	9.6	18	13	62±23	2.6±3.1
Heptacosane	144±63	251	50	23	43	69	137±5	4.7±4.3
Octacosane	99±59	85	39	13	24	74	120±4	3.2±3.9
Nonacosane	185±114	146	70	26	63	91	179±12	4.5±4.3
Triacontane	119±159	67	41	13	22	56	102±2	2.7±3.4
Hentriacontane	140±137	235	50	15	91	58	81±6	3.2±3.4
Dotriacontane	104±143	43	3	7.4	11	25	49±2	1.9±3.0
Tritriacontane	101±119	132	47	15	59	16	38±1	2.2±2.9
Tetratriacontane	33±23	99	41	1.0	6.2	11	23±2	1.1±1.3
Pentatriacontane	112±116	96	34	8.7	13	0.65	7.5±4.6	1.5±1.7
CPI (C_{odd}/C_{even})	*2.0±0.1*	*2.2*	*1.6*	*2.3*	*2.6*	*1.4*	*1.3±0.1*	*1.7±0.2*
Anhydrosugars								
Levoglucosan	16377±8640	38848	7848	3043	5702	188	799±299	89±79
Mannosan	2327±1563	9180	165	148	255	7.8	30±11	30±19
Galactosan	937±752	7062	13	122	189	6.6	13±7	18±12
LG mass fraction of OC (%)	*18.1±0.4*	*14*	*45*	*27*	*34*	*4.8*	*6.4±1.8*	*3.5±2.6*
LG:MN ratio	*7.7±1.6*	*4.2*	*47*	*21*	*22*	*23*	*27±6*	*4.3±0.7*
Sterols								
Cholesterol	ND	ND	5.7	ND	ND	ND	ND	0.84±0.74
Stigmasterol	95	ND	120	ND	26	ND	9.7	2.5±2.4
β-Sitosterol	1320±765	1988	273	ND	133	29	76±52	2.3±3.2
Campesterol	ND	ND	192	ND	56	ND	ND	ND

Table 3.3: Average emission factors of water-soluble ions for each biomass burning category. (average ± 1 SD; standard deviation is given only for n ≥ 3). Individual EFs are given in Table S3.3.

	Biomass Type	n	EF Na^+ (mg kg^{-1})	EF NH_4^+ (mg kg^{-1})	EF K^+ (mg kg^{-1})	EF Ca^{2+} (mg kg^{-1})	EF F^- (mg kg^{-1})	EF Cl^- (mg kg^{-1})	EF NO_3^- (mg kg^{-1})	EF SO_4^{2-} (mg kg^{-1})
Conifers	Black Spruce	4	15±16	111±124	268±295	36±40	33±47	232±222	68±62	263±330
	Ponderosa Pine	7	60±112	27±24	227±72	138±315	44±45	148±192	142±273	99±29
Agricultural residues	Millet	1	<6.7	17	284	11	<3.9	241	<6.4	<13
	Rice Straw - Taiwan	3	7.1	437±186	212±26	20±16	14±13	666±159	23±2	79±15
	Rice Straw - China	3	2.7±2.7	2268±1843	5348±4303	5.0±3.2	4.8±5.5	9077±7274	676	498±398
	Rice Straw - Malaysia	1	2.9	295	227	10	98	943	46	148
	Wheat Straw – Colorado, USA	3	11±5	125±17	157±58	34±17	7.5±3.7	363±137	132±105	<13
	Wheat Straw – Maryland, USA	1	17	392	1864	4.0	<1.3	2488	<16	37
	Wheat Straw – Washington, USA	2	7.1	353	410	26	11	660	49	243
	Sugar Cane	2	25	332	304	19	84	723	39	177
Grasses and other perennial plants	African Grass	6	8.3±7.0	128±220	69±96	6.6±9.0	1.3±0.8	237±375	18±11	93±126
	Sawgrass	1	4.7	4.1	647	<8.6	<3.4	256	21	261
	Wiregrass	1	63	119	1073	<24	<3.4	1236	9.9	103
	Hay	1	<2.8	67	1622	<13	<3.5	1569	<6.3	194
	Alfalfa	1	14	39	1213	<9.7	51	927	<7.5	251
	Manzanita	1	4.2	6.6	895	<17	28	274	80	461
	Chamise	1	<2.4	5.2	738	<31	<1.8	188	30	177
Organic soil	Peat – N. Carolina	2	21	219	<8.1	12	<3.6	498	<22	43
	Peat – Canada	1	480	34	<12	<8.4	<26	62	99	122
	Peat – Indonesia	3	12±4	92±49	<16	7.7±3.2	<5.6	226±118	60±10	90±34
Cookstove	Cookstoves	5	4.8	9.5±6.9	20±6	16.8	<32	20±14	31±11	<39

ND-not detected; NM-not measured

CHAPTER FOUR

EMISSON OF FINE PARTICULATE FLUORIDE FROM BIOMASS BURNING[2]

4.1 Abstract

The burning of biomasses releases fluorine to the atmosphere, representing a major and previously uncharacterized flux of this atmospheric pollutant. Emissions of fine particle ($PM_{2.5}$) water-soluble fluoride (F^-) from biomass burning were evaluated during the fourth Fire Laboratory at Missoula Experiment (FLAME-IV) using scanning electron microscopy energy dispersive X-ray spectroscopy (SEM-EDX) and ion chromatography with conductivity detection. F^- was detected in 100% of the $PM_{2.5}$ emissions from conifers (*n*=11), 94% of emissions from agricultural residues (*n*=16), and 36% of the grasses and other perennial plants (*n*=14). When F^- was quantified, it accounted for an average (± standard error) of 0.13 ± 0.02 % of $PM_{2.5}$. F^- was not detected in remaining samples (*n* = 15) collected from peat burning, shredded tire combustion, and cook-stove emissions. Emission factors (EF) of F^- emitted per kilogram of biomass burned correlated with emissions of $PM_{2.5}$ and combustion efficiency and also varied with the type of biomass burned and the geographic location where it was harvested. Based on recent evaluations of global biomass burning, we estimate that biomass burning releases 76 Gg F^- yr^{-1} to the atmosphere, with upper and lower bounds of 40 – 150 Gg F^- yr^{-1}. The estimated F^- flux from biomass burning is comparable to total fluorine emissions from coal combustion plus other anthropogenic sources. These data

[2] This chapter was previously published as Jayarathne, T.; Stockwell, C.; Yokelson, R.; Nakao, S.; Stone, E.; "Emissions of Fine Particle Fluoride from Biomass Burning." *Environmental Science and Technology*, 2014, 48, 12636-12644.

Author Contributions

E.S. and R.Y. designed research and planned the experiments; T.J. collected extracted and analyzed PM samples, processed data; T.J. and E.S. wrote the manuscript; C.S. provided MCE and EF_{CO} data; S.N. assisted sample collection. C.S., R.Y., and S.N. reviewed and commented on the manuscript.

demonstrate the biomass burning represents a major source of fluorine to the atmosphere in the form of fine particles, which have potential to undergo long-range transport.

4.2 Introduction

Fluorine is the 13th most abundant element on earth and is widely dispersed across the lithosphere, hydrosphere, atmosphere, and biosphere.[171] The vast majority of fluorine is present in the form of minerals, such as fluorapatite ($Ca_5(PO_4)_3F$), fluorite (CaF_2), cryolite (Na_3AlF_6), and clay.[172] Fluorine contents of soils are dependent on soil parent material; soils that are derived from sedimentary fluorite or phosphate deposits or those that have regular inputs of volcanic ash are enriched in fluorine.[173] F^- may also be adsorbed to compounds in soil particles that contain Fe, Al, and Ca, which form complexes with F^-.[172]

Fluorinated compounds in the atmosphere include inorganic gases (e.g. HF, SF_6, SiF_4, F_2, H_2SiF_4), organic compounds (fluorocarbons, perfluorocompounds, trifluoroacetic acid), and minerals (CaF_2, NaF, Na_2SiF_6, $NaAlF_4$).[174-178] It is estimated that mixing ratios of gaseous organic fluorine in the troposphere average ~1 ppb, while gaseous inorganic fluorine is 0.1 – 0.4 ppb.[175] Some fluorinated gaseous compounds have long atmospheric lifetimes and are transported to the stratosphere where they deplete ozone.[179, 180] Particle-phase fluorine, however, is not as well characterized in terms of its background levels, global distribution, and sources.[179, 180]

Fluorine-containing particles enter the atmosphere via natural sources including the resuspension of soil dust, marine aerosols, and volcanic eruptions.[181, 182] Anthropogenic activities, particularly industry, emit fluorinated compounds by (e.g.) aluminum smelting, brick manufacturing, and coal burning and raise the concentration of

atmospheric fluorine well above the natural levels in many areas.[175, 183, 184] Mechanisms of fluorine removal from the atmosphere depend on the chemical species in which it is present. Minerals are removed by dry deposition, while water-soluble gases (trifluroacetic acid and HF) are removed by precipitation. It has been shown that wet and dry deposition of atmospheric fluorine can elevate soil levels by 2 – 20 times their natural levels.[172, 177, 183, 185-187]

Decades of prior research have documented the accumulation of fluorine in plants when exposed to F^- in the form of air pollution or rainwater. F^- is absorbed by plants via roots and leaves, stored in plant tissues, and thereby enters the food chain.[177, 188] Plants naturally contain 2 – 20 µgF g^{-1} (dry weight),[188] yet plants adjacent to industrial areas and active volcanoes, have been observed to accumulate up to 4000 µgF g^{-1}.[189, 190] Such accumulation of F^- has been observed in numerous tropical plants, including *Acacia*, *Oxylobium*, *Gastrolobium* and *Palicourea*.[191] Upon exposure to F^- in excess of threshold levels, plants show signs of phytotoxicity, of which fluorosis, necrosis, and growth suppression are the most common symptoms.[185, 188, 190, 192, 193] The effects of F^- contamination vary by plant species, genotype, growth stage, and exposure.[177, 190] Barley, corn, sorghum, gladiolus, fruit trees, douglas fir, and pines are among the plants most susceptible to F^- contamination.[194]

Although F^- is an essential element in faunal skeletons, high concentrations are toxic. The harmless daily intake of F^- for adult is about 1 mg day^{-1}, while 5 mg day^{-1} can cause chronic F^-poisoning in the form of dental or skeletal fluorosis.[176, 195-197] Additionally, reproductive, developmental, renal, neurological, endocrine, gastrointestinal and carcinogenic effects may result from exposure to F^-.[176] While direct

human health effects from exposure to ambient levels of atmospheric F^- have not been reported, fluorosis has plagued animals that feed on F^--contaminated foliage.[176, 188, 198] As F^- accumulates in plants, the burning of biomass may re-release this contaminant to the atmosphere.[175, 179]

The focus of this study is the quantitative evaluation of F^- emitted by plants during combustion. To the best of our knowledge, quantitative data was not previously available in the literature describing the emissions of particulate F^- from biomass burning. The presence of F^- is confirmed by two complementary analytical methods and quantitative analysis is achieved by ion chromatography with conductivity detection. These data are used to evaluate the content of F^- in $PM_{2.5}$ emitted from burning a range of biomass types harvested from diverse locations. In turn, these data are used to estimate the contribution of F^- to the atmosphere in $PM_{2.5}$ by global biomass burning.

4.3 Experimental Methods

4.3.1 Fuel Harvesting and Storage

A wide range of fuels were examined during the fourth Fire Laboratory at Missoula Experiment (FLAME-IV) including conifers, agricultural residues, grasses, perennial plants, organic soil (peat), shredded tires, and cooking fires. Conifers included fresh boughs of ponderosa pine harvested north of Missoula, Montana and fresh boughs of black spruce harvested near Fairbanks, Alaska. Agricultural residues included rice straw from Taiwan, China and Malaysia, organic baled wheat straw collected near Ft. Collins, Colorado, conventional winter wheat stubble and chaff collected near Waitsburg, Washington, wheat straw from Maryland, and sugar cane stalks from Louisiana. The

grass and perennial plant category included stems of tall African grass harvested at three locations in Kruger National Park in South Africa, stems of sawgrass from the Savannah National Wildlife Refuge in South Carolina, Longleaf Pine wiregrass from the Carolina Sandhills National Wildlife Refuge, baled organic hay stems and organic alfalfa stems collected near Ft. Collins, Colorado, and whole manzanita plants and chamise from the San Jacinto Mountains in California. When harvesting plants, the leaves and woody portions were collected and were free of rocks and soil. The study also examined emissions from peat collected in North Carolina, Canada, and Indonesia and various cookstoves burning red oak, okote, and Douglas fir, and shredded automobile tires. Fuels were shipped overnight to the Fire Sciences Laboratory and stored either at room temperature indoors, or in a refrigerator for 2-20 days, before they were burned. A summary of the fuels analyzed in this study, burn conditions, and fuel moisture content is provided in the supporting information (Table S4.1). Additional details about fuel harvesting are available elsewhere.[95]

4.3.2 Combustion Facility and Burn Procedure

Biomass samples were burned at the USDA Forest Service's combustion facility at the Fire Science Laboratory (FSL) in Missoula, Montana during FLAME-IV. The FSL is equipped with a combustion chamber in an air-conditioned room (12.5 m × 12.5 m × 22 m) and a fuel bed located in the middle of the chamber. Fuels (ranging in mass from 0.1 – 4 kg) were burned over the course of 2-30 minutes under conditions (e.g. loading, geometry, etc.) designed to mimic natural field burning.[95] Most fires were ignited with resistively heated coils, while others were ignited with a propane torch and sometimes

small amounts of alcohol were added. During "stack burns" an inverted funnel located above the fuel bed carried the smoke through the exhaust stack at a constant flow rate (Figure 4.1). The $PM_{2.5}$ sampler was positioned on a platform 17 m up the stack with the sampler inlet located at the center of the stack.[101, 137, 199] For "room burns," the combustion chamber was sealed by closing the exhaust stack and a large circulation fan was used to distribute the smoke evenly throughout the room (typically requiring 15-20 minutes). In this configuration, the $PM_{2.5}$ sampler inlet was positioned at the North wall of the room. In "stack" and "room" configurations, the biomass smoke was diluted significantly with room air to bring the smoke to ambient temperature and allow gas-particle partitioning to equilibrate.

4.3.3 $PM_{2.5}$ Sample Collection

$PM_{2.5}$ samples were collected on 37 mm Teflon and quartz filters (Pall Life Sciences) in parallel using a custom-built $PM_{2.5}$ sampler. Sampled smoke was drawn through conductive tubing (TSI) into cyclones (URG) with a 2.5 μm size-cut. The Teflon and quartz filter channels were operated at constant flow rates of 30 and 42 liters per minute (LPM), respectively. Flow-rates were monitored using a computer controlled program every two seconds. Filter samples were collected at ambient temperature and pressure, which ranged (and averaged ± one standard deviation) 15.1 - 28.8 ^{o}C (22.3 ± 2.8 ^{o}C) and 890 – 914 mbar (901 ± 7 mbar), respectively. Field blanks were collected every 7 samples.

4.3.4 Determination of $PM_{2.5}$ Mass

Before and after sample collection Teflon filters were conditioned for 48 hours in a desiccator and weighed using an analytical microbalance (Mettler Toledo XP26) in a temperature (21.9 °C) and humidity (25±5 %) controlled room. $PM_{2.5}$ mass was calculated as the difference of pre-and post-sampling filter weights, which were determined in triplicate. The mass of collected $PM_{2.5}$ during each burn ranged from 0.002 – 5.23 mg and averaged 1.0 mg per filter. The uncertainty in the $PM_{2.5}$ mass measurement was propagated from the standard deviation of the pre- and post-sampling filter weights and the standard deviation of the field blank mass; the relative error in $PM_{2.5}$ mass concentrations was approximately 10%.

4.3.5 SEM-EDX Microanalysis

SEM-EDX spectroscopy was used to confirm the presence of fluorine in three biomass burning samples. A sub-sample of a quartz fiber filter was mounted on a SEM sampling stub using double-sided carbon tape. Morphology and $PM_{2.5}$ composition were examined using a scanning electron microscope (Hitachi S-3400N) coupled with an energy dispersive X-ray spectrometer (Bruker) at 15.0 kV accelerating voltage. EDX spectra were collected for the fluorine Kα line at 676.8 eV and were used to map elemental fluorine distributions in $PM_{2.5}$ samples.

4.3.6 Aqueous Extraction and Ion Chromatography

Prior to extraction, Teflon filters were cut in half using ceramic scissors and blades on a clean guided glass surface. The full and half-filter masses were measured on

an analytical balance (Mettler Toledo XS204) in order to accurately determine the fraction of filter extracted; results were scaled accordingly assuming uniform PM deposition. Half of the Teflon filter was uniformly wet with 100 µL of isopropyl alcohol and subsequently extracted into 15.0 mL ultra-pure water (Thermo, BARNSTED EasyPure-II; 18.2 MΩ resistivity) by shaking 12 hours at 125 rpm. For every 10 samples, 1 lab blank, 2 field blanks, and 1 spike recovery sample were prepared and analyzed. Extracts were filtered with 0.45 µm PTFE (Whatman) filters prior to analysis.

Aqueous extractions of filter samples were analyzed by ion exchange chromatography (Dionex-ICS5000). For anion analysis, a Dionex IonPac^{TM} AS22 anion column was used. The mobile phase consisted of 4.5 mM sodium carbonate (Na_2CO_3) and 1.4 mM sodium bicarbonate ($NaHCO_3$) at a flow rate of 1.2 mL min^{-1}. For cation analysis, a Dionex IonPac^{TM} CS12A cation column was used. The mobile phase consisted of 20 mM methane sulfonic acid and flowed at 0.5 mL min^{-1}. A conductivity detector (Thermo) was used for detection and was preceded by a self-regenerating suppressor (ASRS^{TM} 300 for anions and CSRS^{TM} 300 for cations).

Anions and cations were identified against authentic standards (Dionex) and quantified with seven point calibration curves. For F^-, the calibration curve ranged from 0.010 – 1.00 mg L^{-1} ($R^2 \geq 0.999$) and the instrument detection limit (IDL), method detection limit (MDL), and average spike recovery were 2.2 µg L^{-1}, 5.0 µg L^{-1}, and 98 ± 1 % (n=7), respectively. Figures of merit for other anions and cations are provided in chapter two, experimental methods (Table 2.2). The observed F^- and alkaline earth metal concentrations were more than three orders of magnitude below the solubility limits of CaF_2 and MgF_2. The F^- concentration in the biomass smoke (µg m^{-3}) was calculated

from the measured F^- concentration (ppb), aqueous extract volume, fraction of the filter area extracted, and sampled air volume. The analytical uncertainty of the F^- concentration was propagated using the MDL and 10 % of the measurement value.

To confirm the presence of F^- and evaluate potential matrix effects in quantitation, eight extracts with F^- concentrations varying from 10 - 80 ppb were analyzed by the multi-point method of standard addition. Each extract was split into 5 portions, and a known amount of F^- was added to increase the F^- concentration three to five fold. All sample portions were then re-analyzed and the F^- concentration determined using standard addition calibration curves.

4.3.7 Emission Factor and MCE Calculation

The mixing ratios of CO, CO_2, and 18 other gases were measured by an open-path Fourier transform infrared (OP-FTIR) spectrometer.[137] Fire-integrated carbon monoxide (CO) emission factors (EF_{CO}) in mass of CO per kg of dry fuel burned were calculated by Stockwell et al.[95] following the carbon mass balance approach.[200-202] Fire-integrated emission factors of $PM_{2.5}$ and F^- ($EF_{PM2.5}$ and EF_F) were calculated using CO as a reference species. In Equation 4.1, the EF of component X was calculated as the product of the ratio of the mass of component X (M_X) to CO (M_{CO}) and the EF_{CO}.

$$EF_X = \frac{M_X}{M_{CO}} \times EF_{CO} \quad (4.1)$$

The uncertainty of EF_X was propagated from the analytical uncertainties of EF_{CO} (estimated at 5%), M_{CO} which is accurate to 1-2 % when compared to NIST-traceable standards,[203] and M_X described previously. This mass balance approach is rigorous, but

underestimates the CO, PM, and particle species EF by 1-2% because not all C-containing species can be measured with current instrumentation.[93] Fire-integrated modified combustion efficiency (MCE) was calculated as $MCE = \Delta CO_2/(\Delta CO + \Delta CO_2)$.[137] A high MCE value signifies a relatively complete combustion (i.e. flaming) and a low MCE value designates a less complete combustion (i.e. smoldering).[137]

4.4 Results and Discussion

4.4.1 Identification and Quantification of Fluoride

The SEM image and EDX elemental map of fluorine for $PM_{2.5}$ emitted from burning black spruce showed a high Kα emission signal for fluorine relative to the field blank (Figure 4.2). It can be seen that the black spruce $PM_{2.5}$ sample contained a relatively even distribution of fluorine across the filter. No fluorine agglomeration or crystalline structures was observed. It is expected that F^- is present in the form of a salt and is associated with major cations emitted by biomass burning (e.g. potassium or ammonium); however no patterns of fluorine associating with a particular element were observed in SEM-EDX images. These results show a random distribution of fluorine in biomass burning emissions, unlike the ordered crystalline structures involving chloride, fluoride, calcium, and magnesium observed by Hall et al. (1972) in some African plants.[191] It is also possible the fluorine is present in the form of organofluorine compounds, such as monofluoroacetate, which is biosynthesized by more than two dozen plant species.[194]

Fluorine was observed and also further quantified as F^- with ion-exchange chromatography and conductivity detection. The chromatographic retention time for F^- in a standard solution on the IC system was 3.13 minutes and all F^- signals were observed within 3.13±0.05 minutes (±1 standard deviation, *n* = 237). Upon addition of F^- to biomass burning extracts in the standard addition experiments, a consistent growth in the F^- peak was observed with increasing concentrations of the added F^- standard, further confirming its identity. The correlation plot of the F^- concentration calculated from the external calibration curve and the standard addition calibration curve is given in the supporting information (Figure 4.3). A tight correlation (R^2 = 0.994) and proximity of results to the 1:1 line confirmed the absence of interference or matrix effects in F^- quantitation.

4.4.2 Frequency of Fluoride Detection and Quantitation

The frequency at which F^- was detected and quantified in various biomass burning samples is summarized in Table 4.1 with individual sample data is provided in the supporting information (Table S4.1). All $PM_{2.5}$ samples collected from black spruce (*n* = 4), ponderosa pine (*n* = 7), rice straw (*n* = 7), and sugar cane (*n* = 2) combustion contained quantifiable amounts of F^-. Additionally, F^- was detected in all wheat straw samples (*n* = 6), but was below the quantitation limit in one sample from each harvest location (Colorado, Washington, and Maryland). For grasses and other perennial plants (*n* = 13), F^- was detected in only 38% of samples and quantified in 31%. The remaining $PM_{2.5}$ emission samples from peat (n = 6), shredded tires (n = 2), and cook-stoves (*n* = 7) did not contain detectable amounts of F^-. The detection of F^- in some, but not all samples

within a fuel type (e.g. Colorado wheat straw and African grass) is attributed in part to differences in the amount of $PM_{2.5}$ collected; heavily-loaded $PM_{2.5}$ samples were more likely to contain measureable amounts of F^- compared to filters with low $PM_{2.5}$ loadings.

4.4.3 Fluoride Contribution to $PM_{2.5}$

When F^- was quantified, its percentage by mass of the $PM_{2.5}$ varied by plant species, geographic location, and combustion conditions. The percent contribution of F^- to $PM_{2.5}$ is summarized in Table 4.1 by fuel type and location, with individual sample data presented in the supporting information (Table S4.1). Within the category of conifers, F^- accounted for an average (± standard error) of 0.10 ± 0.01 % of $PM_{2.5}$ (by mass). Results from black spruce and ponderosa pine ranged from 0.06 to 0.14 % (averaging 0.09 %) and 0.09 to 0.15 % (averaging 0.11%), respectively, and were not statistically different from one another at the 95% confidence interval (p = 0.498). For these two conifer species, the highest F^- contributions to $PM_{2.5}$ were observed for samples with the lowest MCE values (and vice versa), which indicated that $PM_{2.5}$ is enriched in F^- under incomplete combustion conditions.

Agricultural residues showed a large degree of variability in F^- across plant types and geographic location. F^- contributions to $PM_{2.5}$ for individual samples ranged from a minimum of 0.01% for Colorado wheat straw to a maximum of 0.44% for Louisiana sugar cane (Table S4.1), with an average of 0.15 ± 0.04 %. The greater degree of variability is expected to result in part from differences in plant genotype, growth stage, and maturity of leaves.[177, 204] The comparison of F^- contribution to $PM_{2.5}$ across rice straw from Taiwan (0.18 %), China (0.06 %), and Malaysia (0.28 %) reveals the importance of

geographic location and environmental exposure, which affect the chemical composition of the underlying soil, rainwater and/or irrigation water, and the use of fertilizers and/or pesticides. Prior studies have documented the enrichment of fluorine in plants in close proximity to atmospheric sources of fluorine (e.g. industry or volcanoes). To understand the relationship between fuel fluorine content and F^- emissions, measurements of total fluorine in the fuel are needed, but were not possible in this study. Similar to conifers, agricultural residue emissions of $PM_{2.5}$ were also enriched in F^- when MCE values were low, further demonstrating the important role of combustion conditions in the relative amount of F^- in $PM_{2.5}$. Statistical analysis indicated that the F^- contributions to $PM_{2.5}$ were not significantly different across the biomass types of conifers, agricultural residues, grasses, and perennial plants. Overall, the average F^- contribution to $PM_{2.5}$ mass was 0.13 ± 0.02 %.

The comparison of the F^- content in $PM_{2.5}$ to other anions and cations provides information about the presence of inorganic salts in biomass burning emissions and the relative importance of F^- among them. The major anions observed in this study include chloride and sulfate and major cations include potassium and ammonium (Table 4.1), which agreed with prior studies of biomass burning.[98, 205] The molar equivalents of anionic and cationic charge were 38 % different on average, with excesses of both cations and anions. This imbalance suggests the presence of unmeasured contributors to charge (e.g. Fe^{2+}, H^+, formate, acetate). The individual anion contributions to the measured molar anionic charge were 12 % F^-, 65 % Cl^-, 5.5 % NO_3^-, 17 % SO_4^{2-}, and < 0.1 % bromide. Individual cation contributions to the total measured cationic charge were 3.7 % Na^+, 39 % NH_4^+, 57 % K^+, and 0.6 % Ca^{2+}. For these relative abundances of cations, it is

expected that F^- predominantly forms inorganic salts with potassium (KF) and ammonium (NH_4F). The low abundances of sodium and calcium, combined with no detection of magnesium, and suggests the presence of sodium fluoride (NaF), calcium fluoride (CaF_2), and magnesium fluoride (MgF_2) are unlikely.

4.4.4 Fluoride Emission Factors

$EF_{PM2.5}$ and EF_F express the mass of $PM_{2.5}$ or F^- emitted by combusting a unit mass of fuel and have units of g kg^{-1} and mg kg^{-1}, respectively. Mean EF by fuel category and type are provided in Table 4.1, with data from individual burn experiments provided in the supplementary information (Table S4.1). EF_F varied over several orders of magnitude in individual burns (0.7 – 136 mg kg^{-1}) with a study average (± standard error) of 38 ± 10 mg kg^{-1}. Variation in EF_F was observed with respect to burn conditions (namely MCE) and fuel characteristics (i.e. type and geographic location). Figure 4.4 shows the direct relationship between emissions of $PM_{2.5}$ and F^- for individual samples. Linear regressions for agricultural residues and grasses yielded y-intercepts that were not statistically significant, and were therefore forced through the origin. Strong correlations between $EF_{PM2.5}$ and EF_F for conifers ($r = 0.991$, $p < 0.001$) and grasses ($r = 0.997$, $p = 0.003$) indicate that factors that influence total PM emissions from these fuels influenced F^- emissions as well. A weaker, but also significant, correlation between $EF_{PM2.5}$ and EF_F was observed for agricultural residues ($r = 0.707$, $p = 0.010$), which is likely related to different environmental exposures of agricultural residues to fluorine and differing abilities of the studied plant species to accumulate fluorine.

$EF_{PM2.5}$ and EF_F depend the MCE of the burn (Figure 4.5). Flaming combustion has MCE near 0.99 with nearly all burned carbon oxidized to CO_2, while smoldering flames become enriched in CO and fine particles with MCE approaching 0.8.[98, 137, 143] Most fires, including those studied here, have intermediate MCE values with a mix of flaming and smoldering.[137] Prior studies have shown that as MCE decreases below its maximum possible value of one, emissions of $PM_{2.5}$ increase.[98, 143] A significant negative correlation was observed between $EF_{PM2.5}$ and MCE (Figure 4.5A) for conifers (Pearson's r = -0.82, p = 0.002) and grasses (r = -0.986, p = 0.01). The negative correlation for agricultural residues not statistically significant (r = -0.51, p = 0.5). Likewise, a significant negative correlation was observed between EF_F and MCE values (Figure 4.5B) for conifers (-0.80, p = 0.003) and grasses (r = -0.97, p = 0.03), but was not significant for agricultural residues (r = 0.44, p = 0.2). The dependence of EF_F on MCE implies that fluorine in biomass may be lost to the ash, particle, or gas phase during combustion. Volatile components of biomasses, such as N or P, are lost to the gas phase in proportion to the weight of biomass, whereas nonvolatile components, such as Ca, can accumulate in the ash.[168] The relationship between EF_F and MCE suggests that at high combustion efficiency, fluorine is transmitted to the ash or gas phase. Future studies should target quantifying both ash-F and gaseous emissions of fluorine from biomass burning.

For agricultural residues, EF_F shows a greater dependence on plant type and geographic location. For samples with intermediate MCE values ranging from 0.93 - 0.96 (which controls somewhat for variability in combustion efficiency), Malaysian rice straw had the greatest EF_F at 98 mg kg^{-1}, followed by sugar cane at 51.0 mg kg^{-1}. The

lowest EF_F were observed for rice straw from China (0.7-11 mg kg^{-1}) and Taiwan (3.5-9.1 mg kg^{-1}) and wheat straw from Colorado and Washington (4.9-10.6 mg kg^{-1}). These data suggest plant type and environmental exposure to fluorine, which affect the fuel fluorine content[177, 204] are important determinants in EF_F."

4.4.5 Atmospheric Implications

Biomass burning is a significant source of $PM_{2.5}$ to the atmosphere, and we have shown that it also represents a significant source of F^- to the atmosphere. While the selection of fuels analyzed in the FLAME-IV study do not include all biomass types, they represent a broad mixture of fuels types sampled from North America, Asia, and Africa, and constitute a starting point for estimating the amount of F^- released to the atmosphere by biomass burning. As shown in equation 4.2, the annual flux of fine particle F^- to the atmosphere (f_F) for a biomass burning category (i) was calculated as the product of the annual flux of $PM_{2.5}$ ($f_{PM2.5}$) and the mass fraction of F^- in $PM_{2.5}$ (p_F).

$$f_F = \sum_{i=1}^{j} f_{PM2.5,i}\, p_{F,i} \quad \text{(Equation 4.2)}$$

Annual f_F F^- fluxes were summed over j biomass categories. Annual $PM_{2.5}$ fluxes ($f_{PM2.5}$) were compiled by Andreae and Merlet (2001)[84] and totaled 58.3 Tg yr^{-1}.[84] These global $PM_{2.5}$ fluxes are consistent with a more recent compilation of global biomass consumption[93] and are estimated to be accurate within a factor of two.[206] The study average p_F value (Table 4.1, all samples) was used, because the fluoride mass fraction was not significantly different across different fuel types. This estimation method assumes that the fuels examined in this study are globally representative with respect to p_F. Moreover, this calculation applies only to $PM_{2.5}$ F^- and does not capture gaseous

fluorine emissions, $PM_{2.5}$ species beyond water-soluble F^-, or PM_{10} fluorine from dust entrained in biomass burning plumes.

Our best-estimate of the annual emissions of fine particle F^- by biomass category is 76 Gg F^- yr^{-1}, with individual sector contributions are estimated to be with individual sector contributions from savanna and grassland (21 Gg yr^{-1}), tropical forest (15 Gg yr^{-1}), extratropical forests (11 Gg yr^{-1}), biofuel burning (25 Gg yr^{-1}), charcoal burning (0.4 Gg yr^{-1}), agricultural residues (2.7 Gg yr^{-1}). When considering a factor of two uncertainty in $f_{PM2.5}$, the upper and lower bounds of this flux are estimated to be 40 – 150 Gg F^- yr^{-1}.

Biomass burning is significant source of F^- in comparison to the anthropogenic sources of gaseous and particulate anthropogenic fluorine summarized in Table 4.2, including aluminum smelters and reduction plants (7-12 Gg yr^{-1}),[204] glass manufacturing (3 Gg yr^{-1}),[207] steel manufacturing (0.1 Gg yr^{-1}, gaseous F only),[204] phosphate processing (28 Gg yr^{-1}),[204, 208] and coal combustion (12-102 Gg yr^{-1}).[204] Volcanic releases of fluorine (700 – 8,600 Gg yr^{-1})[209, 210] significantly outweigh biomass burning and other characterized sources on a global scale. Additional contributors to atmospheric fluoride are sea spray (20 Gg yr^{-1})[209] and wind-blown dust (5.4 Gg yr^{-1}) for the United States only;[194] dust emissions from major source regions are not characterized with respect to fluoride, so that this flux is underestimated. Dust and sea spray emit coarse particles (> $PM_{2.5}$), which often deposit near the emission source, whereas combustion-related sources, such as biomass burning, have smaller particle diameters and longer atmospheric lifetimes, such that they can be transported greater distances in the atmosphere. Thus, biomass burning not only contributes significantly to the atmospheric flux of fluoride; it also has potential to redistribute it across the biosphere.

The observation of F^- emissions directly from biomass burning helps to explain prior ambient observations of F^- in the environment. Ice core studies in Greenland revealed six periods of F^- deposition in 1908, 1912, 1914, 1947, 1970, and 1980, of which the five latter periods were attributed to volcanic eruptions, while the event in 1908 was not.[179] In addition to F^-, the 1908 ice core contained elevated amounts of ammonium and organic acids, which led these authors to identify the origin as high northern latitude forest fires[179, 211]; this result is consistent with our findings of F^- emissions from conifer trees that are prominent in boreal forests. Kundu *et al*., (2010) observed the covariance of F^-, levoglucosan (a tracer for biomass burning),[160] and water-soluble potassium in $PM_{2.5}$ impacted by biomass burning in Rondonia, Brazil.[212] Similarly, Lewandowska *et al*., (2013) observed a several-fold increase in F^- in PM_{10} when an air mass impacted by biomass burning was transported to their study site in Gdynia, Poland.[213] These prior observations document high temporal variation in ambient F^- levels and the significant impact of biomass burning events. Thus, F^- can be useful as a qualitative indicator of the presence of biomass burning emissions, especially from fluorine-impacted biomasses when industrial background levels are stable. For F^- to be used as a more quantitative tracer of biomass burning, EF_F or ratios from the biomass type burned or region would be required and ambient background levels of F^- would need to be stable.

4.5 Supporting Information

Table S4.1: Fuel description, modified combustion efficiency (MCE), fluoride contribution to $PM_{2.5}$ (with analytical uncertainty), fluoride emission factor and $PM_{2.5}$ emission factor (with analytical uncertainty) for individual biomass burns.

4.6 Acknowledgments

We thank Allan L. Robinson, Sonia M. Kreidenweis, Paul J. DeMott and Ryan C. Sullivan for assistance organizing the FLAME-IV laboratory study and Shawn Urbanski at the USDA Forest Service Fire Sciences Laboratory in Missoula, Montana for support during the FLAME-IV study. We also thank Ted Christian, Dorothy L. Fibiger and Austin Kammerer for assistance with filter sample collection and sample preparation and Nishani Gankanda for assistance with graphic design. We also appreciate the contribution of Eric Miller, David Weise, Christine Wiedinmyer, Greg Askins, Guenter Engling, Savitri Garivait, Christian L'Orange, Benjamin Legendre, Brian Jenkins, Emily Lincoln, Navashni Govender and Kary Peterson for harvesting the fuels for this study. This work was supported by the National Science Foundation (ATM-0936321, AGS-1256042, ER-65296); NASA Earth Science Division (Award NNX12AH17); US Department of State-US Forest Service Partnership, and the University of Iowa.

Figure 4.1: A schematic of the USDA's Fire Sciences Laboratory in Missoula, Montana as used for stack burns.

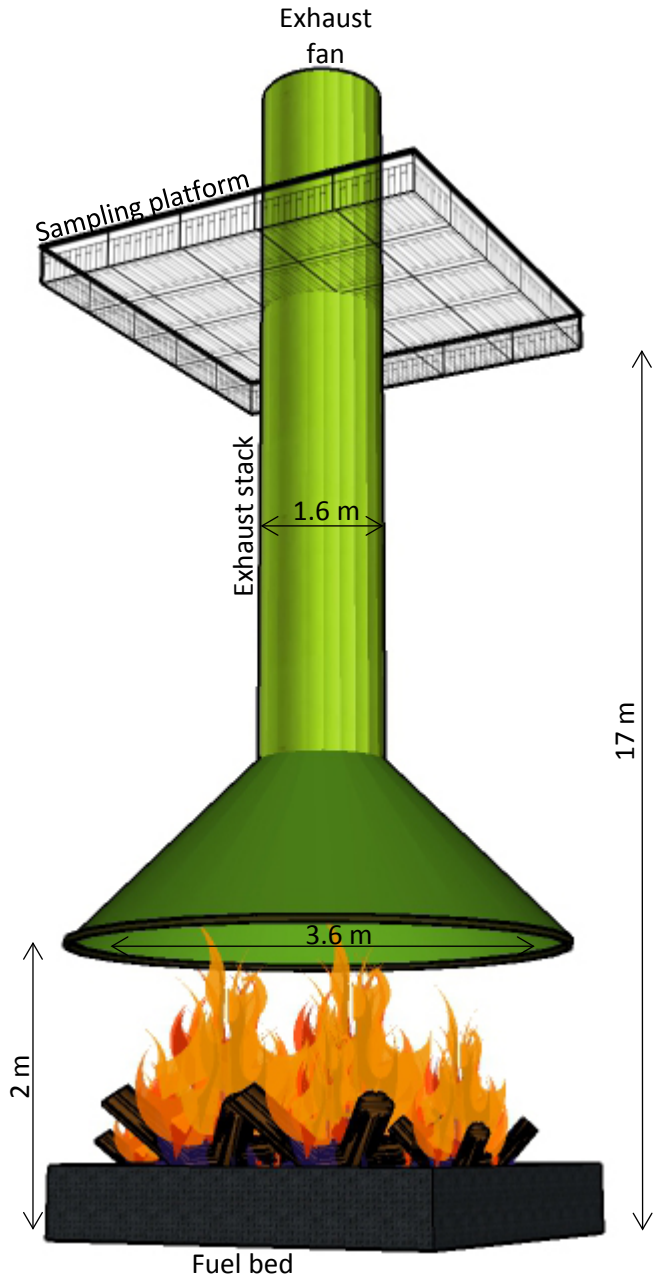

Figure 4.2: SEM images and fluorine elemental maps for (a) field blank filter (b) $PM_{2.5}$ sampled filter for black spruce burn.

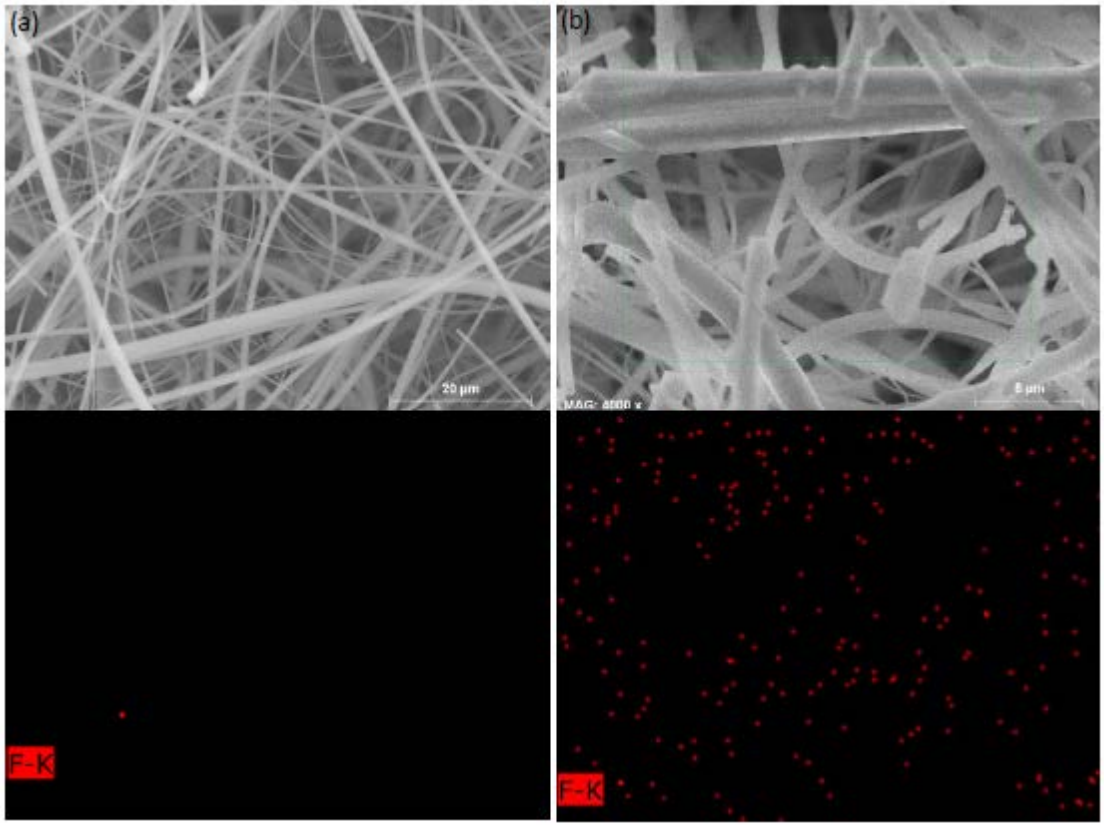

Figure 4.3: Comparison of water-soluble fluoride concentrations measured against an external calibration curve and by the method of standard addition. Error bars represent the propagated analytical uncertainty.

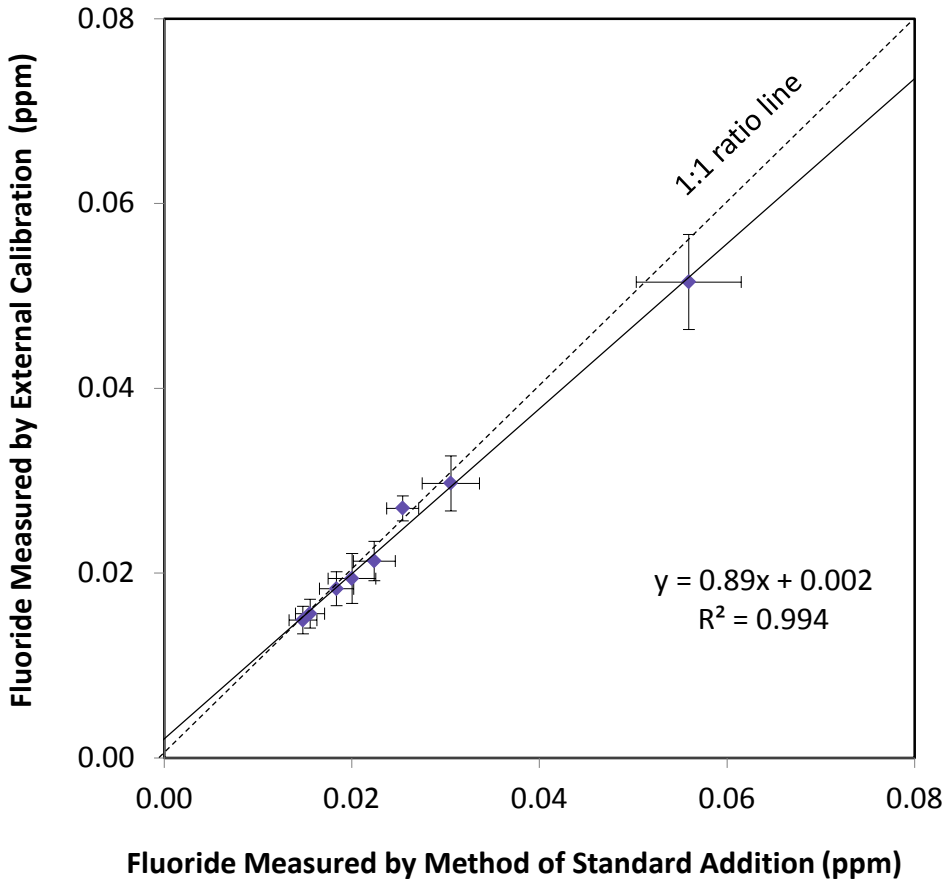

Figure 4.4: Linear regression for $EF_{PM2.5}$ and EF_F versus MCE for individual samples with Pearson's *r*, color coded by biomass category.

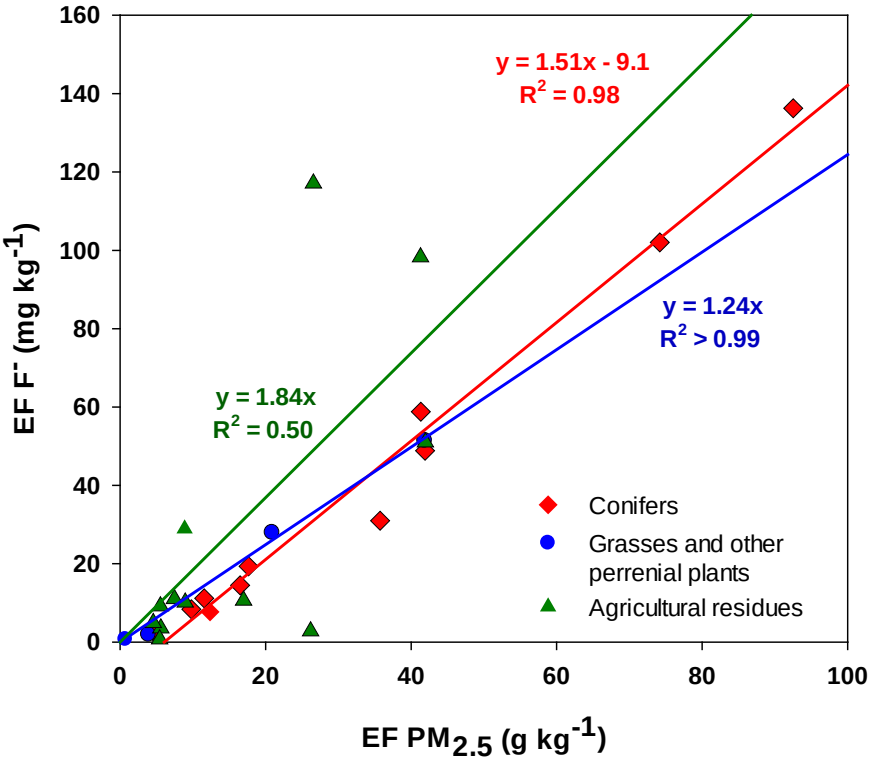

Figure 4.5: Dependence of $EF_{PM2.5}$ (A) and EF_F (B) on modified combustion efficiency (MCE) for individual sample data with Pearson's *r*, color coded by biomass category.

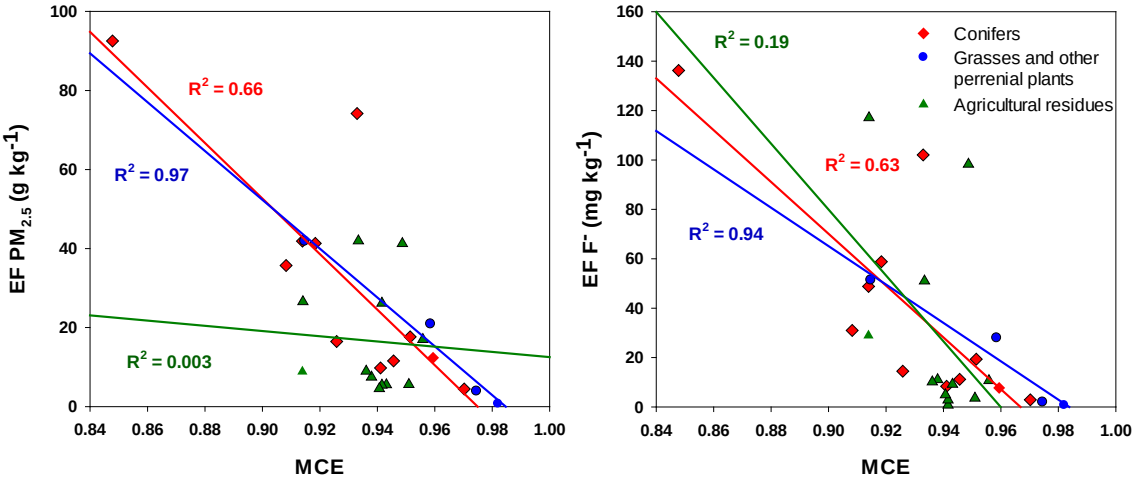

Table 4.1: Summary of fuels, location of harvest, number of burn experiments (n), frequency of fluoride detection (FOD_F), frequency of fluoride quantitation (FOQ_F), mean (± standard error) fluoride and $PM_{2.5}$ emission factors, and percent contribution of measured inorganic ions to $PM_{2.5}$ mass by fuel category and type. EF and percent composition data apply only to fuels in which fluoride was detected.

Fuel Category and Type	Location	*n*	FOD_F (%)	FOQ_F (%)	EF_F (mg kg^{-1})	$EF_{PM2.5}$ (g kg^{-1})	Fluoride (%)	Chloride (%)	Nitrate (%)	Sulfate (%)	Ammonium (%)	Sodium (%)	Potassium (%)	Calcium (%)
Conifers		**11**	**100**	**100**	**40 ± 13**	**33 ± 9**	**0.10 ± 0.01**							
Black Spruce	Alaska, USA	4	100	100	33 ± 24	27 ± 16	0.09	1.25	0.34	0.64	0.35	ND	1.22	ND
Ponderosa Pine	Montana, USA	7	100	100	44 ± 17	36 ± 11	0.11	0.42	0.24	0.51	0.08	ND	1.20	ND
Agricultural residues		**16**[b]	**94**	**75**	**29 ± 11**	**16 ± 4**	**0.15 ± 0.04**							
Rice Straw	Taiwan	3	100	100	14 ± 8	6.7 ± 1.1	0.18	10.9	0.42	11.6	7.90	12.3	3.40	ND
	China	3	100	100	4.8 ± 3.1	13 ± 6	0.06	32.5	0.22	1.78	8.06	ND	19.1	0.01
	Malaysia	1	100	100	98 ± 15[c]	37 ± 2[c]	0.28	2.70	0.13	0.43	0.85	ND	0.65	0.03
Sugar Cane	Louisiana, USA	2	100	100	84 ± 33	34 ± 8	0.28	1.87	0.16	0.42	0.83	ND	0.76	ND
Wheat Straw	Colorado, USA	3	100	67	7.5 ± 2.1	6.4 ± 1.8	0.11	5.14	0.64	ND	2.01	ND	2.07	ND
	Washington, USA	2	50	50	11 ± 1[c]	17 ± 1[c]	0.06	7.48	0.29	1.44	2.08	ND	3.96	ND
Grasses and perennial plants		**13**[d]	**38**	**31**	**59 ± 49**	**48 ± 40**	**0.10 ± 0.02**							
African Grass	South Africa	6	50	33	1.3 ± 0.4	2.3 ± 0.9	0.08	27.2	0.50	2.76	3.91	0.19	3.63	0.91
Alfalfa	Colorado, USA	1	100	100	51 ± 4[c]	42 ± 2[c]	0.12	2.22	ND	0.60	0.09	ND	2.90	ND
Manzanita	California, USA	1	100	100	28 ± 2[c]	21 ± 1[c]	0.13	1.31	0.38	2.20	0.03	ND	4.28	ND
All samples		**55**[e]	**56**	**49**	**32 ± 7**	**23 ± 4**	**0.13 ± 0.02**							

a) ND = not detected, b) in addition to the 14 samples listed, fluoride was not detected in emissions from wheat straw from Maryland or millet from Ghana, c) analytical uncertainty, d) in addition to the 8 samples listed, fluoride was not detected in emissions from giant sawgrass, sawgrass, or wiregrass from South Carolina, hay from Colorado, or chamise from California, e) in addition to the samples listed, fluoride was also not detected in emissions from peat (n = 6), shredded tires (n = 2), or cookstoves (n = 7).

Table 4.2: Summary of sources of gaseous and particulate fluorine and their annual fluxes to the atmosphere.

Fluoride Source	Gaseous F Species	Particulate F Species	Estimated Annual Flux (Gg yr^{-1})
Volcanic activities[210]	HF, SiF_4	Volcanic ash	700 – 8,600[a]
Sea spray[209]	NA	Soluble F^-	20[b]
Wind-blown dust[194]	NA	Mineral F (CaF_2, $Ca_5(PO_4)_3F$)	5.4[c]
Manufacturing of bricks and tiles[187]	HF, SiF_4	F^- containing dust	NA
Aluminum smelters / reduction plants[204]	HF	$NaAlF_4$	7 -12[d]
Glass manufacturing[207]	HF, SiF_4, BF_4	NaF, Na_3AlF_6	3[d]
Coal burning[204]	$HF_{(g)}$	fly-ash	12 – 102[d]
Steel manufacturing[204]	HF, SiF_4	NA	0.1[a]
Phosphate processing[204, 208]	$HF_{(g)}$ $SiF_{4(g)}$	Fluorapatite dust ($Ca_{10}(PO_4)_6F_2$)	28[d]
Biomass burning (this study)	NM	Soluble F^-	40 - 150[b]

NA-data not available; NM-not measured; a) estimated gaseous emission; b) particulate emission; c) United States only, d) total (gaseous and particulate) emission.

CHAPTER FIVE

CHEMICAL CHARACTERIZATION OF FINE PARICULATE MATTER EMITTED BY PEAT FIRES IN CENTRAL KALIMANTAN, INDONESIA, DURING THE 2015 EL NIÑO[3]

5.1 Abstract

Fine particulate matter ($PM_{2.5}$) was collected from authentic *in-situ* peat smoke during the 2015 El Niño peat fire episode in Central Kalimantan, Indonesia. Twenty-one PM samples were collected from 18 peat fire plumes that were primarily smoldering with MCE values of 0.725-0.833. PM emissions were determined and chemically characterized for elemental carbon (EC), organic carbon (OC), water-soluble OC, water-soluble ions, metals and organic species. Fuel-based $PM_{2.5}$ mass emission factors (EF) ranged from 6.0 - 29.6 g kg^{-1} with an average of 17.3±6.0 g kg^{-1}. EC was detected only in 15 plumes and comprises ~1% of PM mass. Together, OC (72 %), EC (1 %), water-soluble ions (1 %) and metal oxides (0.1 %) comprised 74±11 % of gravimetrically measured PM mass. Assuming that the remaining mass is associated with carbon in forming organic matter (OM; i.e. elements O, H, N, P) an OM to OC conversion factor of 1.26 was estimated by linear regression. Overall, chemical speciation revealed the following characteristics of peat burning emissions: high OC mass fractions (72 %), primarily water-insoluble OC (84±11 %C), low EC mass fractions (1 %), vanillic to syringic acid ratios of 1.9, and relatively high n-alkane contributions to OC (6.2 %C).

[3] This chapter is in preparation to publish as Jayarathne, T.; Stockwell, C.; Gilbert, A.; Daugherty, K.; Cochrane, M.; Ryan, K.; Putra, E.; Saharjo, B.; Nurhayati, A.; Albar, I.; Yokelson, R.; Stone, E.; "Chemical Characterization of Fine Particulate Matter Emitted by Peat Fires in Central Kalimantan, Indonesia During the 2015 El Niño.", *Atmospheric Chemistry and Physics.*
Author Contributions
R.Y., M.C., K.R., E.P. and B.S. designed research; E.S. and R.Y. planned the experiments; T.J. collected extracted and analyzed PM samples, processed data and wrote the chapter; C.S. provided MCE and EF_{CO} data; A.G. analyzed organic species; K.D. analyzed WSOC; A.N. and I.A. assisted in field work.

The EF developed herein are used to estimate that 3.2 - 11 Tg of $PM_{2.5}$ emitted to atmosphere during 2015 El Niño peatland fire event. Combined with gas-phase measurements of CO_2, CO, CH_4 and VOC from Stockwell et al. (2016), it is determined that OC and EC account for 2.1 % and 0.04 % of total carbon emissions, respectively. These *in-situ* EFs can be used to improve representation of emissions from Indonesian peat burning in emission inventories.

5.2 Introduction

In recent decades, peatland fires in Southeast Asia, especially the Indonesian provinces of Sumatra, Kalimantan, and Papua as well as Malaysian Borneo have become more frequent in occurrence.[90, 129, 214] The 2015 El Niño-driven peatland fire episode that occurred September – October 2015 was more extensive than in normal years and reported as the next-strongest peatland fire after 1997.[215-217] The 2015 fires burned over 2.6 million hectares of tropical forests and peatlands, and released ~0.2 Pg C of carbon to the atmosphere.[217] However, these values are well below the 1997 records of 4.6 million hectares of burned area and ~1.7 Pg C of carbon released to the atmosphere due to early monsoons and more effective fire control strategies in 2015.[217-219] The direct effects of 2015 peatland fire smoke affected neighboring Singapore, Malaysia, Thailand and Philippines with an estimated economic loss of >16 billion USD to their GDPs due to declines in productions and services during the event, and long-term impacts to human health and the environment.[219, 220] Negative health effects due to inhalation of peat smoke were widely reported during this catastrophe.[216] In Palangkaraya, the capital of Central Kalimantan PM_{10} levels reached up to 3741μg m^{-3}, nearly two orders of magnitude

higher than the world health organization (WHO) guideline for 24 hour PM exposure,[48, 49]. It has estimated that more than 40 million people suffered from continuous exposure to peat smoke over these two months and significant increase of premature deaths due to respiratory and cardiovascular diseases.[216] Despite the substantial environmental, socioeconomic and health impacts, the peatland fire emissions are still under-studied with respect to their chemical and physical properties. Thus, a mobile lab was deployed during 2015 fire episode in Palangkaraya, Central Kalimantan, in order to obtain *in-situ* ground based measurements of trace gases and aerosols directly from authentic peatland fire smoke. Samples were collected from 35 different peat plumes from six different sites and chemically speciated for ~90 gas phase species and ~70 particulate phase species. This paper focused only on particular phase species, and comprehensive description of gas phase species is given in Stockwell et al., (2016).

Peatlands are globally distributed over ~400 Mha land area and hold ~ 550 MgC ha^{-1} of carbon per 1 m depth and can extent up to 20 m. It has been estimated a total of ~5.4×10^{14} kgC carbon storage in peatlands and consider as a significant storage (44-71%) of terrestrial carbon pool.[221, 222] Majority of the peatlands are in the cold boreal belt under ice or maintained as wetlands or conserved areas, thus have evaded human interventions. However, tropical peatlands particularly in Malaysian and Indonesian lowlands are frequently converted to agricultural cropping, commercial forests or pasture by draining the peatlands.[221] During 1996-1999 Indonesian government excavated more than 4000 km of drainage channels over 1 Mha of peatland to cultivate rice under the former Mega Rice Project (MRP).[129] After the project was abandoned in 1999, deforested and degraded peatlands were covered with secondary vegetation.[129] In recent decades, Indonesian

peatland fires have occurred more frequently, intensively and extensively. Degraded peatlands are at high risk of uncontrolled fire, because dry peat is highly combustible and secondary vegetation is more fire-prone than the original forest.[129, 214, 218] Fires first occur in aboveground vegetation, then enter into carbon-rich soil and smolder underground until the peatland is flooded by next monsoon.[129] The burned lands does not easily regenerate into its primary conditions; instead, it is converted into grasslands with patchy secondary vegetation that are prone to repeat fires.[219]

Peat is a type of soft soil with high content of organic matter (>65%) with cellulose, hemicellulose, lignin, cutine, humic acid and fulvic acid being the major organic compound classes.[167, 223, 224] Peat is predominantly made out of degraded plant tissues and categories to three major types, fibric, hemic and sapric based on their degree of decomposition. Fabric peat is the least degraded type with higher fiber content and sapric peat is the most degraded peat type with an amorphous structure, while hemic peat has intermediate properties.[225] Thus, peat soils carry biomarkers indicative of floral origin and those could potentially use to identify peatland fire emissions. Levoglucosan, mannosan, syringaldehyde, vanillin, syringic acid, vanillic acid and n-alkanes are such biomass burning tracers suggested in previous studies by analyzing the ambient air impacted by peat smoke.[156, 226, 227] Some organic compounds (e.g. PAHs) are highly enriched in peat smoke compared to raw peat biomass, showing over 100 times greater concentration in smoke than soil indicating they formed during combustion.[144]

Prior studies of peat burning emissions involved either laboratory experiments or collecting ambient aerosols at receptor sites impacted by peat smoke. Many of these studies primarily focused on chemically characterizing gaseous emissions.[21, 94, 95, 99, 100,

[139, 141, 144, 145, 228-231] while fewer focused on the PM fraction.[100, 144, 156, 226] Peat fire emissions were not considered in emission inventories published by Andreae and Merlet.[84] Akagi et al. published more updated emission inventories in 2011 and have included peatland fires as a source of biomass burning emissions. Peat fire $PM_{2.5}$ emission factors reported in literature deviated on a large scale and ranged 5.9-79 g kg^{-1} and uncertainty of black carbon (BC) and organic carbon (OC) was >50% of the EF value.[93, 144, 145] Thus, the global estimates of peat fire $PM_{2.5}$, OC and BC emissions are associated with large uncertainties. The likely reason for this variation is different laboratory conditions maintain during the experiments as emissions alter on different burning conditions. In addition, the dissection of peat soil during sampling; handling, transport and storage of peat can significantly alter its physical properties and subsequent combustion. Thus, *in-situ* sampling of peat fire emissions under natural burning conditions is needed to accurately represent peat fire emissions in global peat fire emission estimates, human exposure studies and, climate and air quality models.[90, 93, 218]

The objectives of this manuscript are to characterize *in-situ* peat PM emissions from different peat burning sites in Indonesia during 2015 El Niño period, compute PM emission factors and develop source profiles for peat burning aerosol, and compare the PM emission factors from literature with our *in-situ* measurements. This work is complementary to that of Stockwell et al. (2016) on the peat burning emissions of more than 90 gaseous species, brown carbon (BrC), and black carbon (BC), and mass absorption coefficients for the bulk OC due to BrC. Combined together, EFs for more than 150 gaseous and particulate species were determined and allow us to evaluate the

magnitude particulate carbon relative to gaseous carbon emitted, and estimate total particulate emissions from the 2015 El Niño peat fires.

5.3 Experimental Details

5.3.1 Site Description

A comprehensive description of sampling sites is given in Stockwell et al., (2016). In brief, $PM_{2.5}$ samples were collected from 18 separate plumes from 6 different peatland areas in Central Kalimantan, Indonesia from 1-7 November during 2015 El Niño. The sites were carefully selected to represent different peat types (fibric, hemic, or sapric) and cover a range of burning depths ranging from 18 – 62 cm, averaging (±standard deviation) 34±12 cm. The sampled sites were located where the maximum fire activity is typically reported, in moderately to heavily disturbed areas by road or canal building and/or previous fires. The aboveground vegetation was nonexistent or limited to ferns or patchy secondary vegetation and were not burning in most cases. The samples were directly collected from visible plumes and sampling was immediately stopped in the occasional events of flaming combustion of aboveground vegetation in the vicinity in order to sample pure emissions from the smoldering peat.

Each plume was identified by an English letter (E-Z to AA) and complete description of the plumes including peat type, burning depth and surface fuel is given in Table S1 Stockwell et al. (2016). Duplicate samples were collected from plumes E, F and W, and number of PM samples increased to 21. However, plume Y showed a different emission profile likely due to co-burning of foliage litter as these were sampled from shallow peat burning sites. Thus, plume Y was excluded from average calculations but individual values are reported in Table S5.1 and corresponding figures.

5.3.2 Sample Collection

A comprehensive description of sample collection is given in Stockwell et al., (2016). In brief, $PM_{2.5}$ was collected using a custom-built, two-channel PM sampler. The inlet was positioned at a point where the plume of smoke cooled to ambient temperature, to allow for gas-particle partitioning to equilibrate prior to sample collection. The sample inlet was not fixed to a point and always followed the plume path in occasions of change in plume directions due to wind. The PM was collected on pre-cleaned 47 mm quartz fiber filters (QFF) and pre-weighed Teflon filters (PALL, Life Sciences, Port Washington, NY) preceded by two 2.5 µm sharp-cut cyclones (URG). The filtered air was then passed to the land-based Fourier transform infrared (LA-FTIR) spectrometer multipass cell for the measurement of gas phase species as described by Stockwell et al. (2016). Sampled filters were stored in dark and frozen (-20 °C) and were shipped frozen to the University of Iowa for chemical analysis.

Field blanks were collected for every fifth sample. For some samples a second (backup) QFF filter was placed in series behind the first (front) QFF filter in order to assess the positive sampling artifacts from carbonaceous gas adsorption. Filter samples were collected from upwind of the plumes for ~20 minutes (similar to smoke sampling duration) in order to account for background $PM_{2.5}$.

5.3.3 $PM_{2.5}$ Mass, Elemental Carbon and Organic Carbon Measurement

A comprehensive description of PM mass, elemental carbon (EC) and organic carbon (OC) measurement is given in Stockwell et al., (2016). In brief, PM mass was

calculated as the difference of pre-and post-sampling filter weights of Teflon filters after conditioned for 48 hours in a desiccator. The relative error in the PM mass measurements was propagated from the standard deviation of the triplicate measurements of pre-and post-sampling filter weights, the standard deviation of background PM masses, and 10 % of the PM mass concentration, which is a conservative estimate of the analytical uncertainty associated with the mass measurement. Ambient background $PM_{2.5}$ concentrations were very similar across all the sites and on average the ambient $PM_{2.5}$ contributed only 0.60 % of the sampled $PM_{2.5}$ mass, indicating that ambient PM contribution is very small compared to PM concentration in the peat smoke. Nevertheless, the average background concentration was subtracted from the sample concentrations in order to obtain emissions only from pure peat fire emissions.

EC and OC were measured by thermal optical analysis following the NIOSH 5040 method using 1.00 cm^2 punches of quartz fiber filters (Sunset Laboratories, Forest Grove, OR) [110]. The uncertainty in OC measurements was propagated from the standard deviation of the background filters, the standard deviation of the back-up filters, and 10 % of the OC concentration, a conservative estimate of the method precision in replicate measurements [110]. The uncertainty of EC measurements was propagated from the instrumental uncertainty (0.05 μg cm^{-2}), 5 % of the measured EC, and 5 % of pyrolyzed carbon, which refers to organic carbon that charred during analysis.

5.3.4 Water-soluble Organic Carbon

A 1.053 cm^2 sub-sample of QFF filter was analyzed for water soluble organic carbon (WSOC) using a total organic carbon analyzer (GE, Sievers 5310 C). WSOC was

extracted into 15.0 mL of >18.2 MΩ resistivity ultra-pure water (Thermo, Barnstead Easypure II) using acid washed (10% nitric acid) and pre-baked (550 °C for 5.5 hours) glassware. Inorganic carbon was removed with an inorganic carbon remover (GE, Sievers ICR). WSOC was measured in triplicates and quantified using a standard calibration curves prepared from potassium hydrogen phthalate (Ultra Scientific). The WSOC concentration in the sampled plumes was calculated using the extraction volume, total filter area and sampled air volume. The uncertainty of the WSOC measurement was propagated using the standard deviation of the triplicate measurements, standard deviation of the background filters and 10 % of the WSOC concentration. The fraction of water insoluble organic carbon (WIOC) was calculated by subtracting the WSOC concentration from total OC concentration. The error of WIOC concentration was propagated from individual uncertainties of OC and WSOC.

5.3.5 Water-soluble Inorganic Ions

Water-soluble inorganic ions were quantified in aqueous extracts of Teflon filters by ion exchange chromatography coupled with conductivity detection as described in detail elsewhere.[140] In brief, half of the Teflon filter was uniformly wet with 50 µL of isopropyl alcohol and subsequently extracted into 15.0 mL ultra-pure water (>18.2 MΩ resistivity) by shaking 12 hours at 125 rpm. For cation analysis, a Dionex IonPac CS12A column was used with the mobile phase of 20 mM methane sulfonic acid at 0.5 mL min^{-1} flow rate. Dionex IonPac AS22 anion column with the mobile phase of 4.5 mM sodium carbonate (Na_2CO_3) and 1.4 mM sodium bicarbonate ($NaHCO_3$) at a flow rate of 1.2 mL min^{-1} was used for anion separation. A conductivity detector (Thermo) was used for

detection and was preceded by a self-regenerating suppressor, CERS-500 and AERS-500 for cations and anions, respectively.

5.3.6 Total Metals

Teflon filters were cut in half using ceramic blades and then digested in mixture of 2:1 concentrated nitric and hydrochloric acid (TraceMetal Grade, Fisher Chemical) using a MARS 6 microwave assisted digestion system (CEM Corporation, Matthews, NC) at 200 °C for 13 minutes following US EPA Method 3052.[121] Extracts were filtered (0.45 µm PTFE) and analyzed for metals using a Thermo X-Series II quadrupole ICP-MS instrument (Thermo Fisher Scientific Inc., Waltham, MA, USA).[122] The instrument was calibrated against IV-ICPMS-71A ICP-MS standard (Inorganic Ventures) at concentrations ranging from 0.1 - 50 ppb. The metal concentration in the extract is converted to metal oxide concentration in the sampled plumes (µg m^{-3}) using extraction volume, total filter area, sampled air volume, metal to metal oxide ratio and natural metal isotope abundance.[232] The uncertainty of the measurement was propagated using the standard deviation of the background filters and 10% of the metal concentration.

5.3.7 Organic Species

Organic species were quantified in organic extracts of QFF by gas chromatography mass spectrometry (GC-MS) as described in detail elsewhere.[123] In brief, quartz fiber filters were sub-sampled to obtain ~200 µg C prior to organic species characterization. These sub-samples were spiked with deuterated internal standards which were used in quantification: pyrene-D_{10}, benz(a)anthracene-D_{12}, cholestane-D_4,

pentadecane-$D_{32,}$ eicosane-D_{42}, tetracosane-D_{50}, triacontane-D_{62}, dotriacontane-D_{66}, hexatriacontane-D_{74} , levoglucosan-$^{13}C_6$ and cholesterol-D_6. Each sub-sample was then stepwise extracted in 2×20 mL aliquots of hexane followed by 2×20 mL aliquots of acetone by ultra-sonication (60 sonics min^{-1}, 5510-Branson) for 15 minutes. The solvent extracts were subsequently concentrated to a final volume of ~100 µL using Turbovap (Caliper Life Sciences, Turbo Vap LV Evaporator) and minivap (Thermo Scientific, Reacti-Vap™ Evaporator) upon high-purity nitrogen (PRAXAIR Inc.). These extracted samples were stored at -20 °C until the chemical analysis.

Organic species in filter extracts were quantified using gas chromatography coupled to mass spectrometry (Agilent Technologies GC-MS 7890A) equipped with an Agilent DB-5 column (30 m × 0.25 mm × 0.25 µm) with electron ionization (EI) source using a temperature range from 60 to 300 °C. Helium was utilized as the carrier gas, and the 3 µL aliquots of the extracts were injected in splitless mode. More oxygenated polar compounds were analyzed following trimethylsilyl (TMS) derivatization.[124] Briefly, 10 µL of the extract was blown down to complete dryness and reconstituted in 10 µL of pyridine (Burdick & Jackson, Anhydrous). A 20 µL of the silylation agent N,O-bis-(trimethylsilyl)trifluoroacetamide (Fluka Analytical, 99%) was added to the mixture, and was heated for 3 hours at 70 °C to complete the silylation reaction. The silylated samples were immediately analyzed for polar compounds.

Responses of analytes were normalized to the corresponding isotopically-labeled internal standard and five-point linear calibration curves (with correlation coefficients, $R^2 \geq 0.995$) were utilized for the quantification of organic species. Compounds that were not in the standards were measured by assessing the response curve from the compound that

is most analogous in structure and retention time. The analyte concentration in the extract was converted to ambient concentrations (μg m^{-3}) using extraction volume, the total filter area and sampled air volume. The analytical uncertainties for the measured species were propagated from the standard deviation of the background filters and 20% of the measured concentration, which is a conservative estimate of the analytical uncertainty associated with the instrumental reproducibility.

5.3.8 Emission Factor Calculation

The mixing ratios of CO_2, CO, CH_4 and ~90 other gases were quantified by a field-deployed open-path Fourier transform infrared (OP-FTIR) spectrometer combined with whole air sampling (WAS) and gas chromatography.[49] The carbon mass balance approach was used to determine fuel-based emission factors (EF) for gases, in units of mass of analyte per kilogram of fuel burned (g kg^{-1}).[49] Carbon monoxide was used as the reference species to calculate the EF of particulate species. In this purpose, carbon monoxide mass drawn through the filter (M_{CO}) that was measured in series by FTIR, the mass of the analyte (M_X) and emission factor of carbon monoxide (EF_{CO}) was used to calculate the emission factors of the desired analyte (EF_X) (e.g. PM mass, EC, OC, etc.) using equation 5.1.

$$EF_X = \frac{M_X}{M_{CO}} \times EF_{CO} \quad (5.1)$$

Uncertainty in EF_X was propagated from the relative uncertainty of EF_{CO}, conservatively estimated as 5 % of the value and the analytical uncertainty of the considered analyte.

5.3.9 Modified Combustion Efficiency

The Modified combustion efficiency (MCE) was calculated as $MCE = \Delta CO_2/(\Delta CO + \Delta CO_2)$ and was used as an indicator of flaming combustion (MCE > 0.9) and smoldering combustion (~0.75-0.84).[137] Notably, the filter-integrated MCE values reported herein correspond to the duration of filter sample collection and could differ slightly from those reported by Stockwell et al. (2016) that included grab samples.

5.4 Results and Discussion

5.4.1 Emission of $PM_{2.5}$

$PM_{2.5}$ mass EFs for *in-situ* Indonesian peat burning ranged 6.04 – 29.6 g kg^{-1} for 20 sampled plumes, averaging 17.3 g kg^{-1} (Figure 5.1). The relative standard deviation (RSD) of the replicate measurements of EF $PM_{2.5}$ in this study was ±6.0 g kg^{-1} or 35 %, indicating the reproducibility of the $PM_{2.5}$ EFs across samples while RSDs reported in literature varied 45-114 %.[144, 145, 229] Literature reported values for peat $PM_{2.5}$ emission factors by previous laboratory studies are given in Table 5.1. The average EFs reported by Black et al.[144] (7.1±5.6 g kg^{-1} and 5.9±6.7 g kg^{-1}) are in the lower range of EFs observed in this study, perhaps due to oven drying the samples before combustion. As evident by the relatively higher MCE values observed by Black et al., (0.80 – 0.88) compared to this study (0.73 – 0.83), it is presumed to have lower $PM_{2.5}$ EFs as higher MCEs correlate with lower PM emissions.[140, 233] However, our average EF value is lower than the EF values reported by other laboratory studies, 46±21 g kg^{-1} by Geron and Hays;[145] 33-44 g kg^{-1} (for PM_{10}) by Iinuma et al.;[100] 42 g kg^{-1} by Chen et al.;[99] 35 g kg^{-1} by May et al.[141] and 30±20 g kg^{-1} by McMahon et al.[229] In general, the previously

reported, higher $PM_{2.5}$ emission factors for peat burning corresponded to higher carbon and moisture content, and for the plumes sampled from initial stages of a fire.[144, 145, 229] Thus, these higher $PM_{2.5}$ EFs could be due to higher organic content in peat soil, higher soil moisture content and sampling from early stage of fires. Further, alterations to the bulk density by sampling, transporting and handling of peat soils; differences associated with igniting the peat sample (e.g. heated coil vs propane touch) and sustainability of fire during the time of sample collection could also affect the EF $PM_{2.5}$. In contrast, the EFs computed during this study correspond to natural conditions of peat (e.g. moisture content, bulk density) and were not handled, transported or processed disturbing the peat soil micro-properties, and directly sampled from sustained peat fires with different maturities.

5.4.2 Chemical Composition of $PM_{2.5}$

OC accounted for the major fraction of PM mass (72±12 %) while EC was detected only in 15 plumes and on average comprised ~1 % of PM mass. Water-soluble ions and metal oxides also comprised to a minor fraction of PM mass and accounted ~1 % and ~0.1 %, respectively (Table 5.2).

5.4.3 Emission of OC and EC

OC EFs were ranged 1.76 – 26.9 g kg^{-1}, averaging at 12.4±5.4 g kg^{-1} (Figure 5.1). The observed OC mass fraction of PM (72±12 %) is in a good agreement with literature reported values 73-89 % by Black et al.[144] and 94% by Chen et al.[99] for laboratory peat studies of $PM_{2.5}$.

On average, only a minor fraction of OC was water soluble (16±11 %) and the majority (84±11 %) was water insoluble (Table 5.2), indicating that the majority of OC is composed of hydrophobic hydrocarbon-like organic compounds. Fresh peat burning emissions, thus contain a substantial fraction of water-insoluble species that decrease aerosol hygroscopicity and CCN activity.[234] However, unsaturated hydrocarbons (e.g. alkenes) can be gradually oxidized by ozone to alkanoic acids, which in turn increase the hygroscopicity and CCN activity of the aged peat smoke at receptor sites.[234-236]

The EF_{EC} ranged 0.09 – 0.44 g kg^{-1}, averaging at 0.24±0.10 g kg^{-1} (Table 5.2). The lower EC values are consistent with purely smoldering MCE values of 0.725 - 0.833 as discussed by Stockwell et al. (2016). However, optically measured EF_{BC} by PAX (0.006±0.002 g kg^{-1}) is noticeably lower than that of filter based EF_{EC} likely due to sampling of char particles by filters.[49] However, both EC and BC EFs are very small compared to EF_{OC}. The OC:EC ratio in our study ranged 27-129, averaging at 67±26. This is in the upper end of the range of OC:EC ratio: 1.3-78 reported for biomass burning aerosol.[93, 100, 142, 233] However, average OC:EC ratio from this study is substantially higher than the ratios reported for peat fires, 31 by Akagi et al., [93] 13-14 by Iinuma et al.[100] and lower than the ratios 151 by Christian et al.,[21] 87-115 by Black et al.[144]. The PAX results showed that light absorption at 405 nm wave length is ~50 times greater than at 870 nm, which the latter wavelength (870 nm) is indicative of BC. Thus, the light absorption by peat smoke is largely due to BrC and indicated high BrC:BC ratio (52) that is similar of OC:EC.[49] The bright yellow color of the PM collected filters (Figure 5.2) is also an indication of the relatively high OC:EC ratio in which blackish filters are characteristic for higher EC emissions.

The sum of OC, EC, water-soluble ion and metal oxide masses comprises 74±11 % of gravimetrically measured PM mass. The remaining mass is expected to be primarily from elements associated with carbon in forming organic matter (e.g. O, H, N, P). Thus, it was estimated that remaining mass together with OC mass is from organic matter (OM). A linear regression analysis was performed between estimated OM mass and measured OC mass and a strong correlation (R^2 = 0.93) was observed between these two variables indicating their dependent co-variance (Figure 5.3). The slope of the regression line gives the best fit of the co-variance and 1.26±0.04 was estimated as the conversion factor of OC to OM for fresh peat burning aerosols. This OC to OM factor is in the range of values typically observed for gasoline combustion (1.1-1.3)[237, 238] and below those used for biomass burning (1.4-1.8).[26]

5.4.4 MCE

The calculated MCEs were indicative of smoldering combustions with values ranging 0.725-0.833 (average = 0.78±0.04).[137] Burn depth and MCE were negatively correlated (r = -0.738; p = 0.001; Figure 5.4) consistent with higher emission of $CO_{(g)}$ relative to $CO_{2(g)}$ for deep peat combustions, probably due to less oxygen supply. Neither MCE nor burn depth were correlated with PM mass, EC or OC emission factors (p > 0.23). Thus, did not affect PM emissions.

5.4.5 Organic Species

A subset of samples, representing at least 1 sample per sample collection site was analyzed for anhydrosugars, lignin decomposition compounds, alkanes, hopanes, PAHs

and sterols. On average, the quantified organic compounds accounted ~9 % of the total OC mass on carbon basis with major contribution from alkanes (6.2 %), followed by anhydrosugars (2.1 %), lignin decomposition products (0.36 %), hopanes (0.12 %), sterols (0.06 %) and PAHs (0.03%) (Figure 5.5). However, plume Y that was obtained from shallow peat burning sites and pant roots were observed in the burn pit had a different emission profile with a larger contribution from anhydrosugars (16 %) compared to lignin decomposition products (2.8 %) and alkanes (1.6 %). Because of the likelihood of co-burning of foliage litter and plant roots as evident by higher emissions of anhydrosugar and lignin decomposition products relative to other PM samples, plume Y was excluded from average calculations in order to compute more representative EFs for peat burning.

Alkanes:

The homologous series of n-alkanes with carbon numbers in the range of C_{14} to C_{40} along with norpristane, pristane, phytane and squalene were quantified in PM samples. The total n-alkane emissions ranged 456-3834 mg kg^{-1} (Table S5.1). The OC mass fraction of n-alkane was substantially higher than the values reported for other types of biomass burning aerosol in which n-alkane OC mass fraction is typically <1 %.[100, 142] The high n-alkane OC mass fraction is likely due to the higher lipid content by accumulating plant waxes (e.g. cutin, suberin) in peat soil over the time of decomposition compared to other biomass fuels.[142, 148, 149]

Peat emissions consistently showed a C_{31} carbon maximum (C_{max}) (Table S5.1). Higher n-alkane EFs were observed for C_{20-33} relative to C_{14-19} and C_{34-40} and had an odd

carbon preference (Figure 5.6) which is indicative of biogenic material, particularly plant waxes.[154, 157, 159, 239] Similarly, Abas et al.[240] and Fujii et al.[130, 226] reported maximum concentrations of C_{20-33} n-alkanes in ambient PM influenced by peatland fire emissions. The carbon preference index (CPI) was calculated using concentrations of C_{24-32} n-alkanes using the method described by Fujii et al.[227] and ranged 1.22-1.60, averaging 1.42±0.10. Peat burning emissions' CPI is distinct from values reported for foliage, softwood and hardwood combustion emissions (1.6-6.2).[142, 241] Comparable CPI values, 1.5 for Indonesian peat, 1.8 for German peat,[100] 1.4 and 1.5 for North Carolina peat[231] has reported previously for laboratory peat combustion studies. Thus, CPI values ranging 1.2-1.6 along with higher n-alkane mass fraction of OC are characteristic features of peat fire emissions.

Anhydrosugars:

Anhydrosugar EF ranged 157-2041 mg kg^{-1} and contributed 48±41 mg gOC^{-1} of OC mass. The dominant anhydrosugar was levoglucosan (46±40 mg gOC^{-1}), followed by mannosan (0.93±0.76 mg gOC^{-1}) and galactosan (0.14±1.13 mg gOC^{-1}) (Figure 5.7, Table 5.2). Levoglucosan was the largest contributor to the identified organic mass for any individual compound (Table S5.1). However, a significant correlation was not observed ($p = 0.4$) between OC and levoglucosan EFs as observed for grass, softwood and hardwood combustion emissions.[242] This is likely due to diverse cellulose content in different peat soils.[242] Potassium has been used as an indicator of biomass burning, both on its own and in concert with Levoglucosan.[152, 242-244] From peat burning, extremely low

potassium emissions were observed, at concentrations too low for it to be a useful indicator species.

The relative ratios of levoglucosan, mannosan and galactosan may be used to distinguish between biomass combustion emissions.[245] Fujii et al.[227] reported levoglucosan:mannosan ratio to be 14-22 for the ambient aerosols that were impacted by Indonesian peat fires. In this study, a moderate correlation (R^2=0.54) was observed between levoglucosan and mannosan and based on the slope of the regression line levoglucosan:mannosan ratio was estimated as 31 (Figure 5.8a). However, the regression statistics were biased by the EFs of plume W-2, and R^2 value decreased down to 0.11 upon excluding that data point (Figure 5.8b) indicating a no-correlation. This is likely due to variable content of cellulose and hemicellulose in different peat soils.[242] Therefore, a representative value for levoglucosan:mannosan ratio could not be determined.

Lignin decomposition compounds:

Syringaldehyde (S), vanillin (V), syringic acid (SA) and vanillic acid (VA) derived from lignin pyrolysis was quantified as lignin decomposition products. EF of this compound class ranged 15-154 mg kg^{-1} with an average EF of 80±50 mg kg^{-1} (Figure 5.9, Table S5.1). VA to SA ratio has been suggested as an indicator for peat fire emissions previously in which ambient aerosols affected by Indonesian peat fires showed VA:SA ratio of 1.7±0.36 while the unaffected aerosols had a ratio of 0.59±0.27.[227] We also observed a good correlation (R^2=0.65; p=0.004) between VA and SA emission factors. Based on linear regression analysis, 1.9±0.2 was determined as the ratio of VA:SA for freshly emitted peat smoke (Figure 5.10). Because of its consistency, VA:SA ratio is

recommended as an indicator of peat smoke. Correlations among aldehydes (V and S) were not significant, possibly due to V partitioning to the gas phase, as indicated by its detection on backup filters while others species (S, VA and SA) were detected only on front filters.

PAHs, Hopanes and sterols:

PAH emission factors were ranged 1.7-17 mg kg^{-1} and were consistent with previously reported EF values, 6-25 mg kg^{-1} for laboratory peat burning studies.[100, 144] PAH composition was dominated by pyrene, chrysene, methylfluoranthene, fluoranthene and retene that accounted for ~56 % of the measured PAH emissions (Table 5.2). Several biomass burning studies have reported retene, a biomarker of softwood combustion as the most abundant PAH in wood smoke,[142, 239, 246] whereas it contributed only 8 % of the total PAH in this study. Benz(a)anthracene, benzo(a)pyrene, benzo(b)fluoranthene, benzo(k)fluoranthene, chrysene and dibenz(a,h)anthracen, the PAHs that were categories as probable human carcinogens by US Environmental Protection Agency[247] were detected in peat burning aerosols and together these PAHs accounted for 39 % of total quantified PAH emission. The toxic equivalency factor was estimated for quantified PAHs to estimate the overall human health hazard level.[248] The estimated B[a]P equivalent toxicity value ranged 0.05-0.39 B[a]P eqs, mg kg^{-1}, averaging at 0.13±0.10 B[a]P eqs, mg kg^{-1} and comparable to previously reported toxicity values for peat smoke, 0.12-0.16 by Black et al.[144] The total PAH concentration in undiluted peat smoke ranged 0.3-18 µg m^{-3} and was similar to PAH concentrations reported for exhaust smoke of

coke-oven (25 μg m^{-3}), aluminum smelting (15 μg m^{-3}), diesel engines (5 μg m^{-3}) and gasoline engines (3 μg m^{-3}).[53, 54]

To the best of our knowledge hopanes have not being previously quantified in peat fire emissions. 17α(H)-22,29,30-trisnorhopane, 17β(H)-21α (H)-30-norhopane and 17α(H)-21β(H)-hopane was identified using authentic standards and quantified in pure peat smoke for the first time. The total EF for hopanes ranged 11-37 mg kg^{-1}, averaging at 17±8 mg kg^{-1} (Table S5.1). Terpenoid and hopanoid hydrocarbon compounds that have the hopane-skeleton are ubiquitous in peat soil.[162-167] Thus, presence of hopanes in peat smoke is not unexpected. Norhopane had the highest OC mass fraction followed by trisnorhopane and hopane (Table 5.2). A fairly consistent ratio of 0.25:0.60:0.15 was observed among trisnorhopane, norhopane and hopane irrespective of the sampling site and burning depth indicating the formation of hopanes are independent of burning conditions (Figure 5.11). The observed hopanes ratio is clearly distinct from that of diesel (0.04:48:48)[238] and noncatalyst gasoline (0.10:0.42:0.48)[237] engine emissions. However, it is comparable to the hopane ratio of lignite (0.23:0.66:0.11) and sub-bituminous (0.29:0.49:0.22) coal smoke.[249] It indicates similarities of terpenoid and hopanoid hydrocarbon in peat soil and coal deposits as those are younger in geological timescale than crude oil.

Stigmasterol, β-sitosterol and campesterol were detected in peat smoke and accounted 0.14-1.7 mg gOC^{-1} of OC mass fraction (Table S5.1). Sterols have been identified in peat soils with a major contribution from β-sitosterol.[165, 166] Similarly, β-sitosterol is the predominant sterol in PM (Table 5.2) indicating the emission of soil constituents to atmosphere as PM during smoldering.

5.4.6 Water-soluble Inorganic Ions

Water-soluble ions accounted only 1.1 % of the PM mass and total quantified ion EF ranged 45 – 490 mg kg^{-1}, averaging 201±144 mg kg^{-1}. Ammonium and chloride were detected in all the samples with average EFs of 92±61 mg kg^{-1} and 75±52 mg kg^{-1}, respectively. Frequency of detection (FOD) for sulfate, nitrate and fluoride was 83 %, 61 % and 56 % and EFs were ranged 2-133 mg kg^{-1}, 0.2-6.8 mg kg^{-1} and 0.4-45.9 mg kg^{-1}, respectively. PM mass fractions of ammonium vs sulfate ($r = 0.95$, $p<0.001$) and ammonium vs chloride ($r = 0.89$, $p<0.001$) was strongly correlated indicating inorganic fraction of peat PM is dominated by $(NH_4)_2SO_4$ and NH_4Cl. The EFs of gaseous NH_3, NO and HONO were 31 times, 105 times and 71 times higher than that of NH_4^+ and NO_3^-, respectively indicating a dominance of gas phase species.[49] Atmospheric oxidation of these gases could increase the concentration of nitrate and ammonium ions,[7, 8] and as a result the concentration of these secondary inorganic products could be further increased in aged peat smoke at receptor sites.

5.4.7 Metals

Metal oxides accounted only 0.1 % of the PM mass and total quantified metal EF ranged 7 – 24 μg kg^{-1}, averaging at 13±5 μg kg^{-1} (Table 5.2, Table S5.1). Metal fraction was dominated by Al, Ti, V, Mn, Ni, Sr and Ba which are commonly found in peat soil.[224] The lower EFs of metal indicate the minimum influence of re-suspended soil dust to PM. Further, peat combustion was occurring under very low temperatures at complete smoldering conditions at which metal elemental transfer is not feasible to aerosol phase.[250]

5.5 Emission Estimates from 2015 Indonesian Peat Fires

The emissions from Indonesian peat fires during 2015 El Niño was estimated using mean EFs calculated in this study for an estimated burned area of 8.5×10^5 ha[251] to an average burning depth of 34±12 cm calculated during this study,[49] and peat bulk density 0.120±0.005 g cm^{-3}.[252] The uncertainty of the estimated value is propagated using standard deviation of the mean EFs, burn depth and peat bulk density. The total $PM_{2.5}$ released to the atmosphere from this fire event was estimated to be 3.2 - 11 Tg, averaging 6.0±5.5 Tg with major contribution from OC (4.3 Tg) followed by EC (0.08 Tg) and water-soluble ions (0.07 Tg) (Table 5.3). Combined our OC and EC emission factors with gas-phase EFs of CO_2, CO, CH_4 and other carbon containing gases from Stockwell et al. (2016), it is estimated a total carbon emission of 205±77 TgC to the atmosphere, of which 73 % as CO_2 (149±71 TgC), 21 % as CO (44±30 TgC), 2.7 % as other carbon containing gases (5.5±1.3 TgC), 1.2 % as CH_4 (2.5±2.6 TgC), 2.1 % as OC (4.3±4.3 TgC) and 0.04 % as EC (0.083±0.081 TgC). Our carbon emission estimates are in a good agreement with Huijnen et al.[217] that estimated total C emission of 227±67 TgC for this fire event. However, this is ~8 times lower than the carbon emission estimated for 1997 Indonesian peat fires (810-2570 TgC) which burned total area of 4.6×10^6 ha to a depth of 50 cm.[218]

5.6 Conclusion

$PM_{2.5}$ was collected from authentic *in-situ* peat smoke during the 2015 El Niño peat fire episode in Central Kalimantan, Indonesia and was chemically characterized for PM mass, EC, OC, water-soluble ions, metals and organic species. Fuel based $EF_{PM2.5}$

ranged 6.0 - 29.6 g kg^{-1} and it was estimated 3.2 - 11 Tg of $PM_{2.5}$ released to the atmosphere during 2015 El Niño peat fire episode. OC accounted for the major fraction of PM mass while EC, water-soluble ions and metal oxides comprised only a minor fraction of PM mass. Combined our OC and EC emission factors with gas-phase EFs of CO_2, CO, CH_4 and other carbon containing gases from Stockwell et al. (2016), it is estimated a total carbon emission of 205±77 TgC to the atmosphere. It was determined that OC and EC comprise to 2.1 % and 0.04 % of total carbon emissions, respectively. Overall, chemical speciation of OC revealed the following characteristics of peat burning emissions: high OC mass fractions (72 %), primarily water-insoluble OC (84±11 %C), low EC mass fractions (1 %), vanillic to syringic acid ratios of 1.9, and relatively high n-alkane contributions to OC (6.2 %C) which could use as indicators of peat fire PM. This chemical profile could use in source apportionment molding to identify contribution from peat smoke when ambient aerosol at a receptor site is impacted by peatland fire emissions. High concentration of PAHs was detected in peat smoke. Thus, people who live near Indonesian peat burning sites were facing a significant health risk due to continuous inhalation of undiluted peat smoke over the entire fire episode.[53, 253] To the best of our knowledge a comprehensive study on human exposure of peat fire PM has not being conducted. Thus, calculated PAH toxicity factors could use for human exposure studies and health assessments.

The quantitative emission factors developed in this study is more representative to natural peat burning conditions and may be used to update regional/global emission inventories which are currently based on EFs computed from laboratory studies. The most recent emission inventory compiled by Akagi et al. (2011) does not report an EF

value for $PM_{2.5}$ for peatland fire emissions. Further, the EF_{OC} reported in Akagi et al. (2011) is 50 % lower than the average EF_{OC}, and EF_{BC} is ~30 times higher than the average EF_{BC} observed in this study. Thus, using our EFs in atmospheric and climate models can compute more representative emission estimates for peatland fires. Further, more studies should be carried out in downwind to evaluate the effects of atmospheric dilution and atmospheric photochemical reactions to the chemical composition of peat fire PM.

5.7 Supporting Information

Table S5.1: Emission factors of $PM_{2.5}$ mass, OC, EC, water-soluble ions, metals and organic species in individual samples.

5.8 Acknowledgments

This research was primarily supported by NASA Grant NNX13AP46G to SDSU and UM. The research was also supported by NASA grant NNX14AP45G to UM. We also acknowledge T. Anne Cleary International Dissertation Research Fellowship awarded by Graduate College, University of Iowa and Center for Global and Reginal Environmental Research (CGRER) graduate student travel award for field research. We also thank Dr. David Peate, Iowa Trace Element Analysis Laboratory for the assistance given during metal analysis. We also grateful to Laura Graham, Grahame Applegate and BOS field team for their excellent support during the sample collection.

Figure 5.1: Emission factors of $PM_{2.5}$ mass, EC, OC, water-soluble ions and metal oxides. Error bars represent propagated analytical uncertainty.

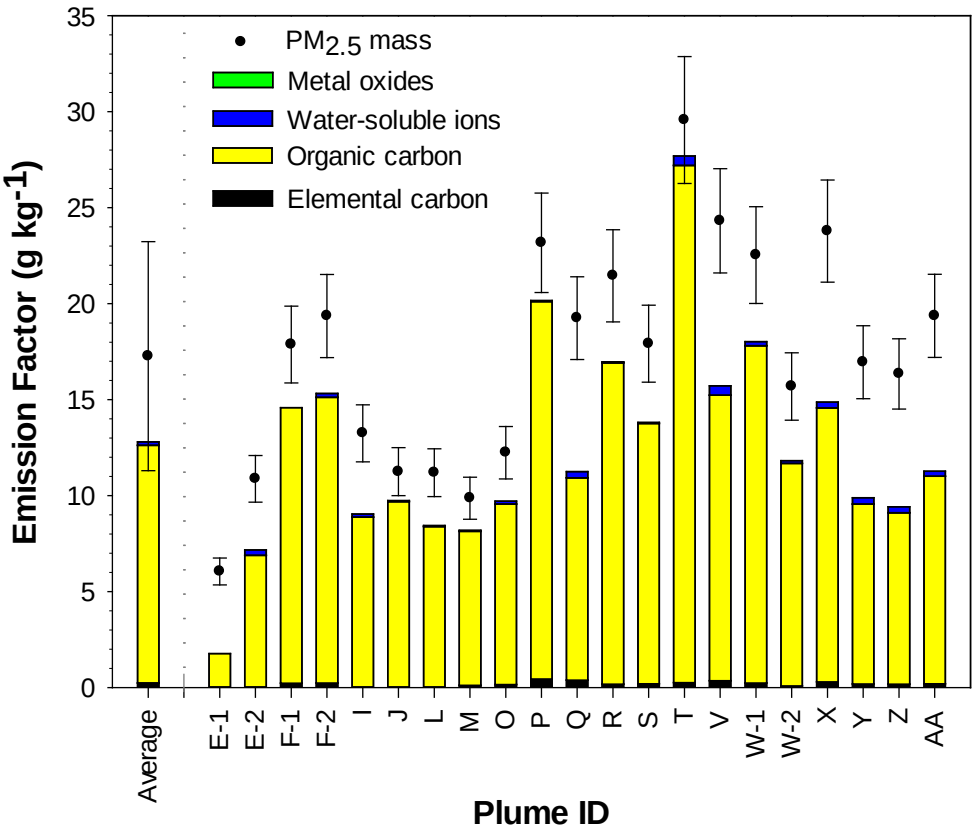

Figure 5.2: Picture of PM collected filters.

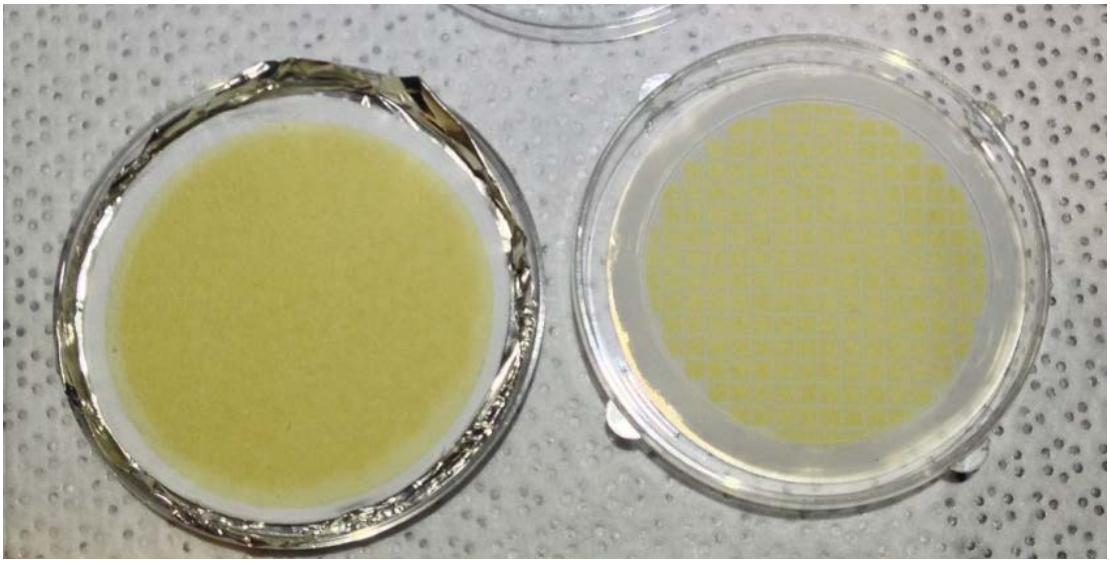

Figure 5.3: Linear regression of the measured organic carbon concentration with the unmeasured $PM_{2.5}$ mass, which is an approximation of organic matter if other major species are quantified. Error bars represent propagated analytical uncertainty.

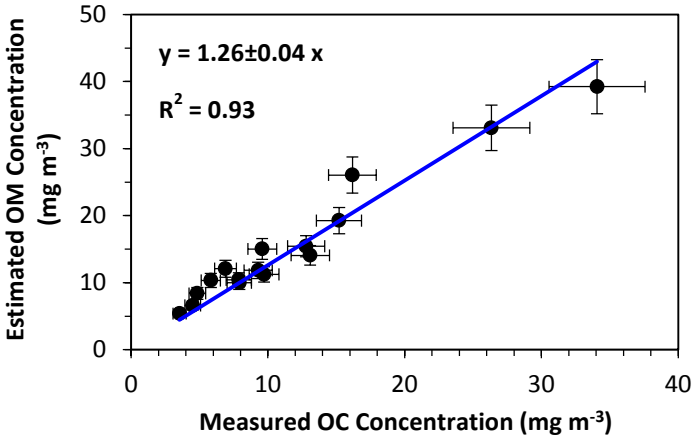

Figure 5.4: The relationship between the burn depth and MCE.

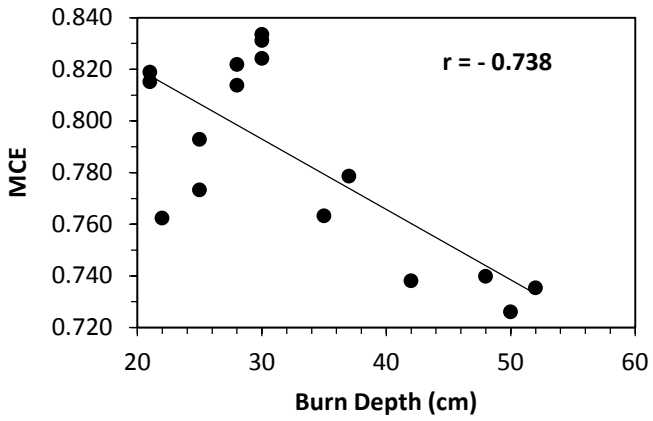

Figure 5.5: Organic carbon mass fraction of the speciated compound classes in select peat burning emission samples.

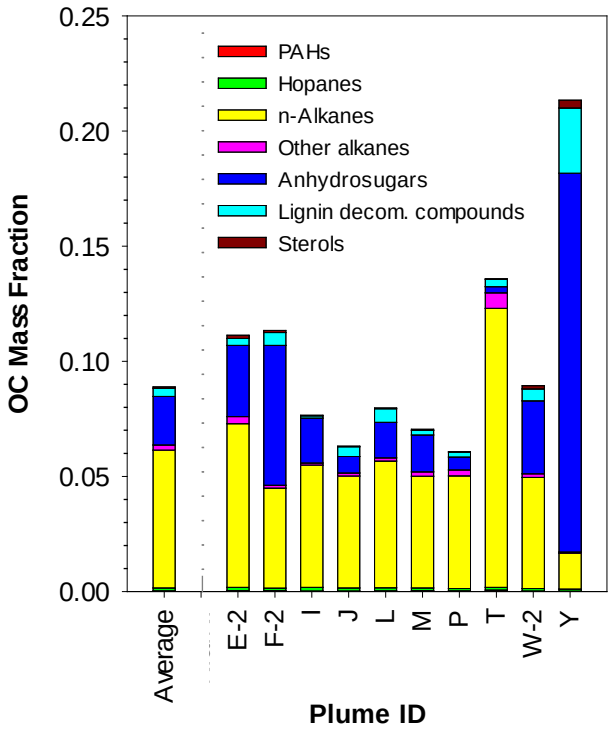

Figure 5.6: Molecular distribution of n-alkanes. The horizontal lines (black) in the box represent the 25th, 50th and 75th percentiles and mean values are indicated by the blue lines.

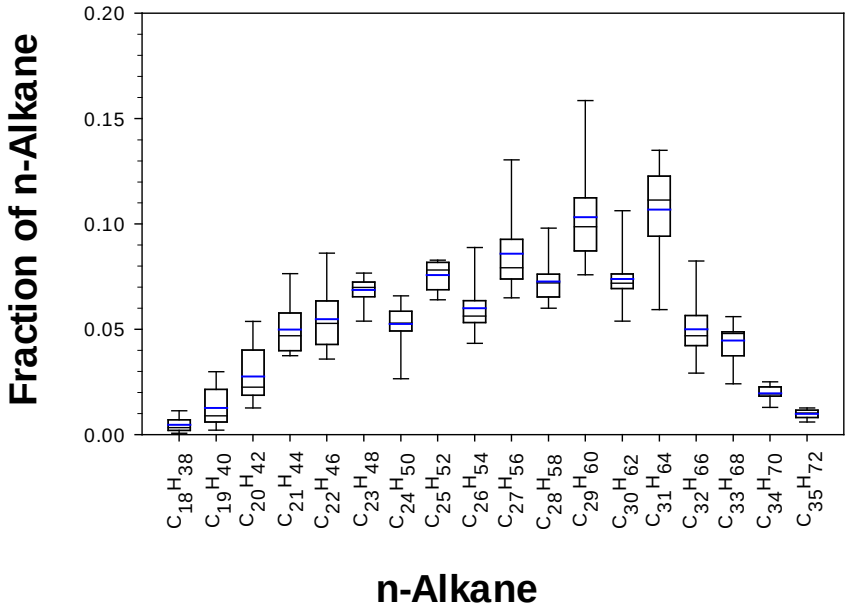

Figure 5.7: Organic carbon mass fractions of select anhydrosugars. On average, the galactosan mass fraction was 0.14 mg gOC^{-1} (maximum = 0.77 mg gOC^{-1}); due to its low concentrations, it was not included in the plot.

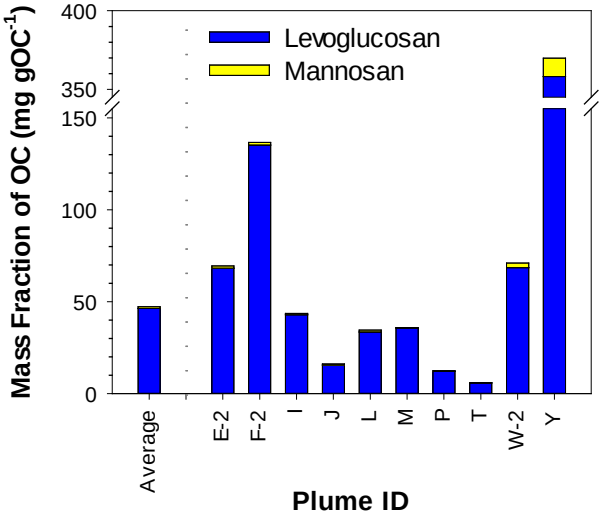

Figure 5.8: a) The emission ratio of levoglucosan and mannosan for all the plumes and b) the emission ratio of levoglucosan and mannosan for other plumes excluding plume W-2.

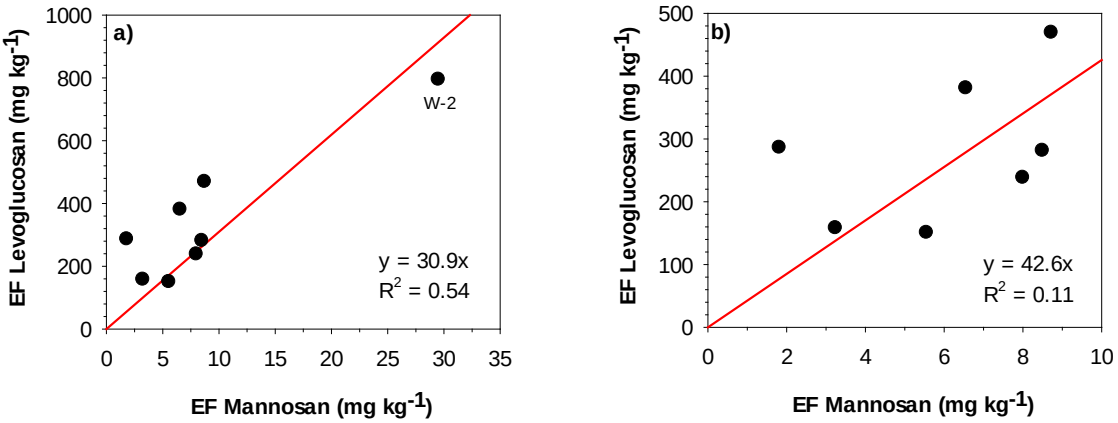

Figure 5.9: Organic carbon mass fraction of lignin decomposition products.

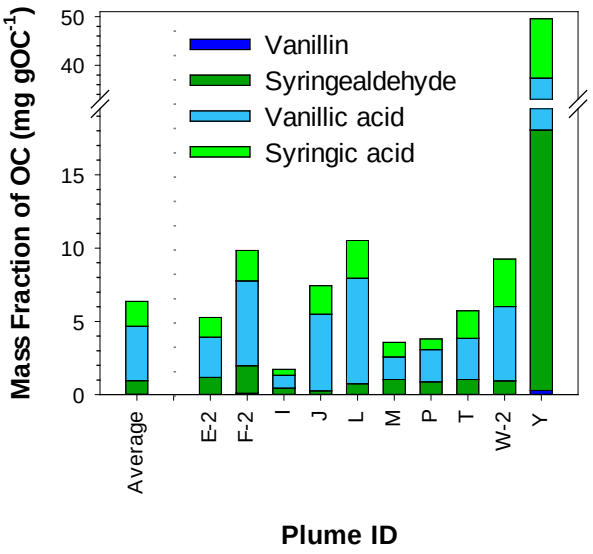

Figure 5.10: Emission ratios of vanillic acid to syringic acid. Error bars represent propagated analytical uncertainty.

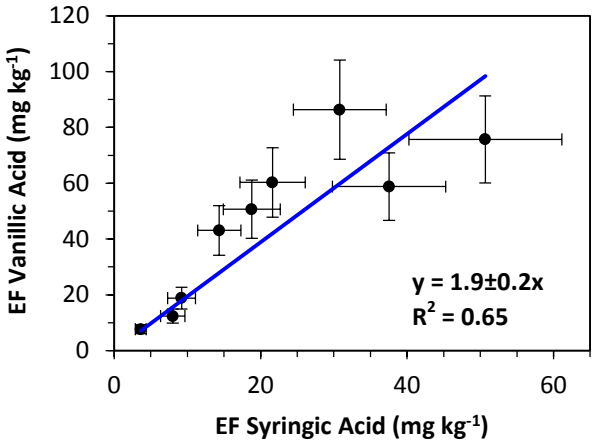

Figure 5.11: Organic carbon mass fraction of hopanes.

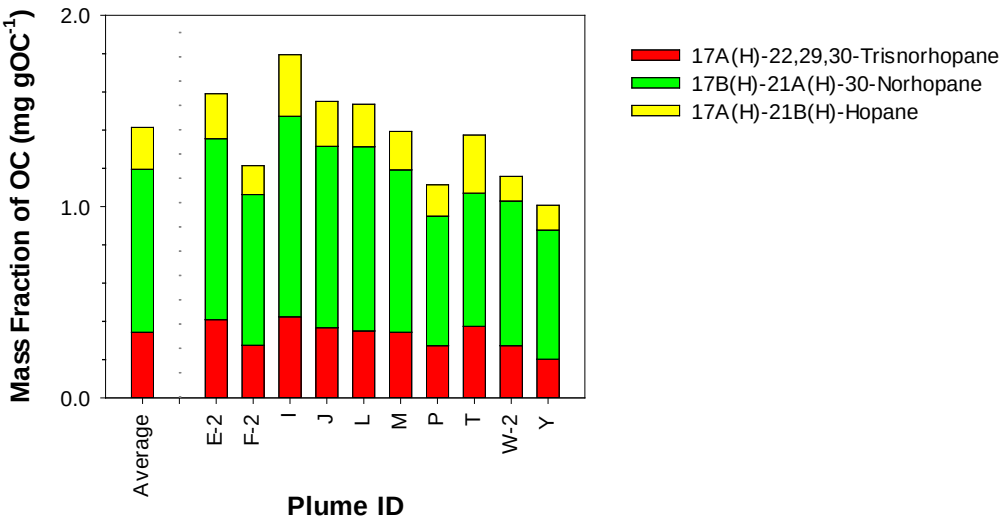

Table 5.1: Comparison of *in-situ* peat emission data computed during this study with previous laboratory measurements.

Location of peat collection	No. of samples	EF $PM_{2.5}$ mass (g kg^{-1})	% Contribution to $PM_{2.5}$ mass		WSOC % of OC	Reference
			OC	EC		
Indonesian peat	21	17	72	1.2	16	This study
German peat	1	44[a]	29	2.2	52	Iinuma et al.[100]
Indonesian peat	1	33[a]	24	1.7	39	Iinuma et al.[100]
N Carolina peat	-	7.1	89	0.73	-	Black et al.[144]
N Carolina peat	-	5.9	73	1.4	-	Black et al.[144]
Alaskan Tundra core	-	42[b]	94	2.6	-	Chen et al.[99]
Florida sawgrass peat	6	30	-	-	-	McMahon et al.[229]
Indonesian peat	1	6.1[c]	-	-	-	Christian et al.[21]
N Carolina peat	17	46	-	-	-	Geron and Hays[145]
Indonesian peat	-	35[d]	-	-	-	May et al.[141]

a-PM_{10}; b-TSP; c-only sum of OC and EC; d-PM_1

Table 5.2: Average emission factors for $PM_{2.5}$, EC, OC, water-soluble ions, metals (as mass fraction of $PM_{2.5}$), and organic species normalized to organic carbon mass. Individual EF data is given in Table S5.1.

Species	Study Average	Standard Deviation
EF $PM_{2.5}$ mass (g kg^{-1})	17.3	6.0
EC (as mass fraction of $PM_{2.5}$; g $gPM_{2.5}^{-1}$)	0.0120	0.0038
OC (as mass fraction of $PM_{2.5}$; g $gPM_{2.5}^{-1}$)	0.70	0.15
Water-soluble OC fraction	0.16	0.11
Water-insoluble OC fraction	0.84	0.11
Water-soluble ions (as mass fraction of $PM_{2.5}$; mg $gPM_{2.5}^{-1}$)		
Sodium	0.054	0.065
Ammonium	5.1	3.0
Potassium	0.26	0.43
Fluoride	0.66	0.63
Chloride	4.2	2.4
Nitrate	0.16	0.13
Sulfate	1.41	1.42
Metals (as mass fraction of $PM_{2.5}$; µg $gPM_{2.5}^{-1}$)		
Al	0.113	0.059
Ti	0.083	0.056
V	0.048	0.021
Mn	0.058	0.031
Ni	0.019	0.011
Sr	0.059	0.030
Ba	0.40	0.19
Organic species (as mass fraction of organic carbon; mg gOC^{-1})		
PAHs		
Anthracene	0.0062	0.0036
Fluoranthene	0.036	0.017
Pyrene	0.056	0.031
Methylfluoranthene	0.043	0.021
Cyclopenta(cd)pyrene	0.004514	0.000081
Benz(a)anthracene	0.023	0.013
Chrysene	0.054	0.021
1-Methylchrysene	0.019	0.010
Retene	0.031	0.028
Benzo(b)fluoranthene	0.023	0.013
Benzo(k)fluoranthene	0.0036	0.0028
Benzo(j)fluoranthene	0.0031	0.0023
Benzo(e)pyrene	0.029	0.016
Benzo(a)pyrene	0.0081	0.0066
Perylene	0.0041	0.0034
Benzo(GHI)perylene	0.016	0.011
Dibenz(ah)anthracene	0.0098	0.0085
Picene	0.0139	0.0051
Hopanes		
17α(H)-22,29,30-Trisnorhopane	0.344	0.058
17β(H)-21α (H)-30-Norhopane	0.85	0.13
17α(H)-21β(H)-Hopane	0.218	0.066
n-Alkanes		
Octadecane	0.39	0.46
Nonadecane	1.1	1.3
Eicosane	2.2	2.2

Table 5.2 - continued

Heneicosane	3.8	2.8
Docosane	4.3	3.2
Tricosane	4.8	2.1
Tetracosane	4.1	2.2
Pentacosane	5.4	2.4
Hexacosane	4.1	2.1
Heptacosane	5.5	2.2
Octacosane	4.8	2.0
Nonacosane	6.5	1.9
Triacontane	4.7	1.4
Hentriacontane	6.7	1.4
Dotriacontane	3.03	0.52
Tritriacontane	2.83	0.54
Tetratriacontane	1.25	0.23
Pentatriacontane	0.66	0.15
Heptatriacontane	0.82	0.26
Octriacontane	2.5	1.3
Nonatriacontane	0.98	0.47
Other Alkanes		
Norpristane	0.35	0.47
Pristane	1.0	1.2
Squalane	1.31	0.74
Anhydrosugars		
Levoglucosan	46	40
Mannosan	0.93	0.76
Galactosan	0.14	0.13
Lignin Decomposition Products		
Vanillin	0.030	0.044
Syringealdehyde	0.93	0.46
Vanillic acid	3.7	2.2
Syringic acid	1.69	0.91
Sterols		
Stigmasterol	0.22	0.11
β-Sitosterol	0.53	0.34
Campesterol	0.29	0.20

Table 5.3: Estimated emissions from Indonesian peat fires during 2015 El Niño, based on a burned area of 8.5×10^5 ha (Whitburn et al., 2016), an average burning depth of 34±12 cm (Stockwell et al, 2016), and peat bulk density 0.120±0.005 g cm^{-3} (Konecny et al., 2016). The uncertainty of the estimated value is propagated using standard deviation of the mean EFs, burn depth and peat bulk density.

Species	Total Estimated Emission	
	C based (Tg C)	Species based (Tg)
$PM_{2.5}$	-	6.0±5.5
C containing compounds		
OC	4.3±4.3	-
EC	0.083±0.081	-
$CO_{2(g)}$[a]	149±71	547±259
$CO_{(g)}$[a]	44±30	102±69
$CH_{4(g)}$[a]	2.5±2.6	3.3±3.5
Other C containing trace gases[a]	5.5±1.3	9.3±2.6
Total C	205±77	-
Water-soluble ions		
NH_4^+	-	0.032±0.039
Cl^-	-	0.026±0.032
NO_3^-	-	0.0010±0.0013
SO_4^{2-}	-	0.0096±0.0151
Other atmospheric gases		
$NH_{3(g)}$[a]	-	1.00±0.91
$HCl_{(g)}$[a]	-	0.012±0.014
$NO_{(g)}$[a]	-	0.11±0.17
$HONO_{(g)}$[a]	-	0.073±0.061

a-EFs are based on Stockwell et al., (2016)

CHAPTER SIX

ENRICHMENT OF SACCHARIDES AND DIVALENT CATIONS IN SEA SPRAY AEROSOL DURING TWO PHYTOPLANKTON BLOOMS[4]

6.1 Abstract

Sea spray aerosol (SSA) is a globally important source of particulate matter. A mesocosm study was performed to determine the relative enrichment of saccharides and inorganic ions in nascent fine ($PM_{2.5}$) and coarse ($PM_{10-2.5}$) SSA and sea surface microlayer (SSML) relative to bulk seawater. Saccharides comprise a significant fraction of organic matter in fine and coarse SSA (11% and 27%, respectively). Relative to sodium, individual saccharides were enriched 14-1314 times in fine SSA, 3-138 times in coarse SSA, but only up to 1.0-16.2 times in SSML. Enrichments in SSML were attributed to rising bubbles that scavenge surface-active species from seawater, while further enrichment into fine SSA likely derives from bubble films. Mean enrichment factors for major ions demonstrated significant enrichment in fine SSA for potassium (1.3), magnesium (1.4), and calcium (1.7), likely due to their interactions with organic matter. Consequently, fine SSA develops a significantly different salt profile from that of seawater. Maximum enrichments of saccharides and ions coincided with the second of

[4] This chapter was previously published as Jayarathne, T.; Sultana, C.; Lee, C.; Malfatti, F,; Cox, J.; Pendergraft, M.; Moore, K.; Azam, F.; Tivanski, A.; Cappa, C.; Bertram, T.; Grassian, V.; Prather, K.; Stone, E. "Enrichment of Saccharides and Divalent Cations in Sea Spray Aerosol During Two Phytoplankton Blooms." *Environmental Science & Technology* 50.21 (2016): 11511-11520.
Author Contributions
E.S. and T.J. designed research; E.S., A.T., C.C., T.B., K.P., F.A. and V.G. planned the experiment; C.S. and C.L. set up the experiment; C.S., K.M. and F.M. provided chlorophyll and bacteria data; J.C. and M.P. collected seawater and SSML samples; T.J. collected SSA samples, extracted and analyzed samples, processed data and wrote the manuscript. C.S., C.L., F.M., J.C., M.P., K.M., F.A., A.T., C.C., T.B., V.G., K.P. and E.S. reviewed and commented on the manuscript.

two phytoplankton blooms, signifying the influence of ocean biology on selective mass transfer across the ocean-air interface.

6.2 Introduction

The ocean represents a major source of primary aerosol emissions, emitting an estimated 2-100 × 10^{15} g of sea spray aerosol (SSA) per year.[58, 61, 254, 255 256] By scattering light, SSA attenuate solar radiation, and by serving as cloud condensation nuclei (CCN) and ice nuclei (IN) they affect cloud formation, cloud albedo, and precipitation cycles.[65] These physical properties of SSA are affected by particle size and chemical composition.[32, 69] Thus, a detailed understanding of size-dependent SSA composition as a function of ocean biogeochemistry is required to advance the understanding and improve predictions of SSA influences on air quality and climate.[58, 61, 63, 70]

SSA is produced when bubbles burst at the ocean surface. Bubbles at the surface may burst instantly (<1 s) or persist for extended period of time (10-100 s).[257] Breaking of the bubble film releases film drops, and the collapse of the bubble ejects a jet drop.[256] The SSA produced ranges in diameter from few nanometers to several microns; film drops are smaller in size (generally <1 μm) than jet drops (generally >1 μm).[64, 256] At the ocean surface, there is a thin film (20 – 400 μm) termed the sea surface microlayer (SSML) that is chemically distinct from seawater due to its higher organic matter content.[258, 259] The SSML may be disturbed by crashing waves or wind, but quickly reforms within seconds.[260, 261]

The relative ratio of organic matter to sea salt in SSA is higher than that of seawater, with the greatest organic-to-salt enrichment occurring in sub-micron sized particles.[22, 60, 73, 262-265] The mechanism proposed for this enrichment is the scavenging of

surface-active organic matter by rising bubbles and bursting of bubble films that are enriched in organic matter.[74-80] The organic carbon fraction of SSA increases with decreasing particle size.[22, 35, 73, 262, 266] Sub-micron SSA (0.56 – 1 μm) contains more water-insoluble and aliphatic-rich organic matter while super-micron SSA (1.8 – 3.2 μm) is more water-soluble and oxygen-rich.[267] Contributing to this organic matter are intact marine microorganisms (e.g. phytoplankton, bacteria and virus), their products (e.g. bacteria vesicles) and detritus,[79, 268-270] proteinaceous material,[79, 271] transparent exopolymers,[271] polysaccharides,[79, 272] fatty acids,[273] alkanes,[273] organic anionic surfactants,[105] and sterols.[274] There is mounting evidence that phytoplankton, bacteria, and viruses in the marine microbial loop modify the composition of SSA by altering the pool of organic material in the ocean.[267, 275, 276]

Carbohydrates (a.k.a. saccharides) are omnipresent in the marine environment, comprising up to 20% of dissolved organic carbon (DOC) in seawater.[277] Carbohydrates in marine samples could be in the form of free-monosaccharides (e.g. free glucose) or oligo/polysaccharides (e.g. glucan). Carbohydrates serve as substrates for energy storage and structural materials of marine microbes.[278] Glucose, galactose, mannose, xylose and fructose are monomers of energy and structure-related polysaccharides in phytoplankton, while fucose, arabinose and rhamnose-containing polysaccharides are synthesized by stressed phytoplankton and are associated with bacterial activities.[75, 76, 279-281] Due to the surface active nature of polysaccharides, they have been identified as a class of organic matter that is likely enriched at the air-water interface and SSA.[60, 77, 81, 272, 282]

Enrichment factors (EF) provide a means of quantitatively evaluating enrichment, as the ratio of the concentrations of species *x* relative to sodium (Na^+) in phase *i* (SSML and SSA) and seawater:

$$EF_{x(i)} = \frac{[x]_i/[Na^+]_i}{[x]_{seawater}/[Na^+]_{seawater}} \quad (6.1)$$

EF greater than 1 indicates enrichment of species *x* relative to Na^+ in phase *i*, while EF less than 1 indicates depletion. Saccharide enrichment has been demonstrated for total hydrolysable saccharides in total suspended particles (TSP), with EF in the range of 22-70 for laboratory bubble bursting studies.[272] The enrichment of saccharides in SSML has also been shown to vary seasonally and with phytoplankton blooms,[272, 282] suggesting that enrichment of saccharides in SSA depends on the biological condition of the seawater. Prior to this study, the enrichment of individual saccharides with respect to size-resolved SSA and its dependence on ocean biology had not been evaluated.

The enrichment of organic matter in SSA can influence metal ions (e.g. Ca^{2+}, Mg^{2+}, K^+) through complexation.[59, 76, 79, 283-286] The interaction of organic molecules and inorganic ions in SSA has been demonstrated through single-particle mapping, which shows, for example, potassium associated with carbon and hydroxyl groups.[79, 80] Hexadecanoic acid, the most prominent fatty acid in SSA,[105] binds preferentially to calcium, magnesium and potassium over sodium, leading to their accumulation at the air-water interface.[287, 288] Enrichment of Ca^{2+}, Mg^{2+}, K^+ and trace metals at the air-water interface has also been documented in field studies.[289-291] However, field measurements of SSA are challenged by due to the ubiquity of inorganic ions in the atmosphere and their potential to arise from terrestrial sources (e.g. mineral dust) or atmospheric

processes.[59, 73, 292-294] Attributing the enrichment of these inorganic ions in SSA to its production, requires isolating SSA from confounding sources.[59, 286, 295]

In this study, nascent SSA particles were generated from simulated wave breaking in a large wave-flume. The wave-flume setup is comparable to natural wave breaking and is expected to yield a particle size distribution similar to natural marine aerosols.[64] The system was isolated from background aerosol and gas-phase pollutants, allowing for the characterization of nascent SSA without influence from other sources.[267] The central objectives of this study include evaluating 1) the enrichment of organic carbon (OC), saccharides, and inorganic ions in nascent SSA, 2) the extent to which the selective transfer across the air-water interface leads to chemical differences in SSA from bulk seawater, and 3) the influence of the microbial loop on these phenomena. To this end, OC, saccharides, and inorganic ions were quantified in parallel samples of seawater, SSML, fine and coarse SSA during the Investigation into Marine Particle Chemistry and Transfer Science (IMPACTS) experiment in 2014 that spanned two consecutive phytoplankton blooms. To the best of our knowledge, this is the first report of enrichment factors for saccharides that can be specifically attributed to selective transfer across the air-water interface.

6.3 Experimental Procedures

6.3.1 IMPACTS Experiment

The IMPACTS experiment was conducted at the Scripps Institution of Oceanography, University of California, San Diego and is described in detail elsewhere.[267] In brief, a wave-flume was pre-cleaned, filled with coastal ocean water (day

1) and SSA was generated by wave breaking. The growth of phytoplankton was promoted by addition of nutrients (f/2 algae growth medium, sodium metasilicate, sodium phosphate) and exposure to artificial photosynthetically-active light. While all species in the mesocosm were present in coastal seawater introduced to the wave flume, the laboratory conditions likely favored certain species, giving rise to microbe populations and distributions that are expected to differ from the marine environment. The biological activity of the mesocosm was monitored by *in vivo* chlorophyll (chl) and heterotrophic bacteria levels as described elsewhere.[267] The wave-flume was covered with a lid to isolate the air inside from the ambient environment. Cleaned, particle free air that was filtered by activated charcoal, potassium permanganate and HEPA filters to remove volatile organic compounds, nitrogen and sulfur oxides, and aerosol particles was introduced to the headspace of the wave-flume.[64] Prior to sample collection, particle counts were monitored (<10 cm^{-3}) to ensure that the wave flume was free of background air. Nascent SSA was sampled 1 m downstream the breaking wave.

6.3.2 Sample Collection

Seawater samples were collected 20-25 cm below the surface in the flume using a Teflon tube and stored in pre-cleaned polypropylene bottles. SSML was collected using the glass plate method[259] and was stored in pre-cleaned glass vials. SSA in fine ($PM_{2.5}$) and coarse ($PM_{10-2.5}$) size fractions was collected on pre-cleaned 37 mm quartz fiber filters (QFF) and pre-weighed Teflon filters (Pall, Life Sciences) using a dichotomous aerosol sampler (Andersen Instruments, series 241) equipped with a PM_{10} cutoff impactor inlet (Anderson Instruments, Model 246b). SSA particles were collected daily for 3-6

hours at ambient temperature and relative humidity (RH; 67-76%) without drying. Collection of wet aerosol would increase their aerodynamic diameter upon particle sizing by a factor of 1.2-1.6 compared to dry particles.[32] Field blanks were collected for every 5 samples. All samples were stored frozen (-20 °C) in the dark until chemical analysis.

6.3.3 Sample Characterization and Analysis

Determination of SSA particle mass: SSA mass was determined as the difference between pre- and post-sampling weights of Teflon filters upon which SSA was collected. Filters were first conditioned for 48 hours in a desiccator and then weighed by an analytical microbalance (Mettler, Toledo XP26) in a temperature 129 (72.4±0.8 ^{0}C) and RH (33±5 %) controlled environment.

Organic carbon (OC) in SSA particles: The OC and elemental carbon (EC) content of SSA was quantified by a 1.00 cm^2 sub-sample of QFF using a thermal optical analyzer (Sunset Laboratories) following the ACE-Asia protocol.[111] EC was not detected.

Analysis of water soluble inorganic ions: Seawater and SSML samples were filtered through a 0.45 µm PTFE filter and were analyzed by ion-exchange chromatography coupled with conductivity detection (Dionex, ICS-5000) as described elsewhere.[140] For SSA samples, Teflon filters were pre-wet with 200 µL of acetone and extracted into 6.00 mL of ultra-pure water by shaking (125 rpm) for 10 minutes and ultra-sonication (60 sonics min^{-1}, 5510-Branson) for 30 minutes. The extract was filtered (0.45 µm PTFE) prior to analysis.

Analysis of free-monosaccharides and oligo/polysaccharides: Filtered seawater, SSML and aqueous SSA extract were directly analyzed by high performance anion exchange chromatography (HPAEC; Dionex-ICS 5000) with pulsed amperometry for free-monosaccharides. A second sample aliquot was hydrolyzed with 0.1 M trifluoroacetic acid at 100 ^{0}C for 12 hours and subsequently analyzed for total saccharides.[112] The oligo/polysaccharide fraction was calculated as the difference between the total and free-saccharides. Saccharides were separated on a Dionex CarboPac^{TM} PA20 (3 × 150 mm) carbohydrate column, preceded by a guard column and Dionex AminoTrap^{TM} trap column with isocratic 27.5 mM sodium hydroxide at a flow rate of 0.480 mL min^{-1}. In between samples, 200 mM sodium hydroxide was passed through the column for 15 minutes to reequilibrate the stationary phase. Saccharides were identified by their retention times against 15 standards (xylitol, mannitol, arabinose, glucose, xylose, fructose (Sigma-Aldrich), erythritol, arabitol, trehalose, fucose, (Alfa-Aesar), rhamnose, mannose, ribose (Acros Organics), galactose, sucrose (Fisher)). Seven-point calibration curves ranging from 10 nM to 10 µM were used for quantification.

Statistical analysis: Significant deviations of EF from 1 were assessed at the 95% confidence interval by the Wilcoxon signed rank test. To evaluate significant differences in EF factors across phases, the Mann-Whitney test at the 95% confidence interval was used. Spearman's rank-order correlation coefficients (r_s) were used to compare saccharide levels across phases.[296] Statistical analyses were performed in Minitab-17 statistical software.

6.4 Results and Discussion

6.4.1 Biological Activity and Dissolved Organic Carbon in Seawater

During the IMPACTS mesocosm experiment, two phytoplankton blooms occurred in succession as indicated by sustained increases in *in vivo* chl concentrations above the initial level of 0.64 µg L^{-1} (Figure 6.1a). Phytoplankton bloom 1 began 10 days after the start of the mesocosm experiment and lasted for 6 days, reaching peak *in vivo* chl levels of 2.7 µg L^{-1} on day 13. Bloom 2 occurred on days 20 – 27 of the experiment, reaching a peak *in vivo* chl concentration of 5.7 µg L^{-1} on day 25. Maximum heterotrophic bacteria counts were lower in bloom 1 (2.1×10^6 mL^{-1} on day 13) compared to bloom 2 (7.8×10^6 mL^{-1} on day 25). Particulate organic carbon (POC), defined as particles > 0.45 µm, concentrations peaked at 185 ± 4 µM C on day 12 and 163 ± 6 µM C on day 26 compared to an initial level of 121 µM C (Figure 6.1b). The elevated levels of POC along with higher *in vivo* chl levels likely resulted from healthy phytoplankton (during the initial bloom phase), phytoplankton detritus (during the decay of the bloom), organic colloids >0.45 µm (cut-off for DOC), marine gels and transparent exopolymer particles (TEP).[35, 76, 297] DOC of the initial seawater was 138±4 µM C and steadily increased to a maximum DOC level on day 25 of 173±1 µM C. The 25% increase in DOC from its initial level is attributed to the release of organic substances by physiologically old cells, rapid bacterial breakdown of cellular material, and bacterial extra-cellular secretions.[76, 297, 298] However, no significant correlations were observed between biological markers (chl and bacteria) and chemical measurements (POC, DOC, saccharides, salts). This is likely due in part to the lag between phytoplankton blooms and organic matter enrichment observed in prior mesocosm experiments.[275]

The succession of bacteria following a phytoplankton bloom reflects tight bacteria-phytoplankton coupling that is responsible for controlling levels of DOC in the ocean.[298] The *in vivo* chl levels observed in wave-flume bulk seawater was comparable to natural chl levels of phytoplankton blooms (~1-30 μg L^{-1}) reported in prior field studies of coastal and open ocean environments.[35] Meanwhile, the observed bacterial counts are comparable to the values reported in field studies (10^5-10^7 cells mL^{-1}).[298] The observed seawater carbon levels were within the range of values reported over the coastal ocean during phytoplankton blooms for both DOC (50-300 μM C)[279] and POC (30-3000 μM C).[75] As demonstrated by these data, the observed levels of biological activity during IMPACTS and their temporal variation are similar to conditions and processes occurring in the ocean.

6.4.2 Composition of SSA Particles

Because the absolute SSA concentrations depended on aerosol residence times in the wave flume and the headspace velocity varied during the experiment, the discussion of results focuses on relative concentrations (e.g. mass fractions) of SSA components. Fine SSA particles were composed of sodium (averaging 18%), chloride (33%), sulfate (5.5%), magnesium (2.5%), calcium (0.9%), and organic carbon (8%, ranging 5-15%) (Figure 6.2a). Coarse SSA particles were comprised of sodium (22%), chloride (41%), sulfate (6.3%) magnesium (2.8%), calcium (0.9%), and OC (1.2%, ranging 0.6-1.9%) (Figure 6.2b). The uncharacterized mass fraction of fine and coarse SSA particles was 31% and 25%, respectively, and includes particle-bound water (as particles were not dried before collection), elements associated with carbon in forming organic matter (e.g.

O, H, N, P), and trace elements (e.g. Fe, Al, Si). The fractional contributions of salt and OC to the total SSA particle mass were relatively consistent throughout the mesocosm experiment, with little sensitivity to chl or bacteria levels (Figure 6.3). The steady OC mass fractions in SSA over a wide range of chl levels is consistent with observations of Quinn *et al*. (2014) that reported consistent OC/Na^+ ratios for sub-micron SSA in high and low chlorophyll regions.[35]

6.4.3 Enrichment of Organic Carbon in SSA Particles

OC was significantly enriched in SSA relative to sodium, with mean (± 95% CI) EF_{OC} values for fine and coarse particles of 669 ± 143 and 85 ± 15, respectively (Table 6.1), indicative of the selective transfer of OC to SSA over salt. EF_{OC} is approximately an order of magnitude higher for fine particles relative to coarse particles, demonstrating a greater enrichment in smaller size particles. Similar EF_{OC} values and its increase with decreasing particle size have been previously reported for both laboratory and field studies.[60] Like the OC mass fraction, EF_{OC} varied little during the mesocosm experiment (Figure 6.5a), indicating that EF_{OC} values for fine and coarse size fractions are not sensitive to the biological state of the seawater. Co-located measurements by high-resolution aerosol mass spectrometry, however, demonstrated that for 1 μm sized particles, the relative intensity of the organic matter-to-PM mass signal was sensitive to biological activity during bloom 1, but not bloom 2.[267] Together, these data indicate that OC enrichment may vary for sub-micron sized particles during a phytoplankton bloom with low bacteria levels, but that this enrichment becomes undetectable when mixed with particles 1-2.5 μm that dominate mass-based measurements of fine particles. Thus, the

fine particle size cut (<2.5 μm) used in this experiment will include both film and jet drops, which would mask the extent of OC enrichment in film drops.

6.4.4 Saccharide Dynamics and Enrichment During the Mesocosm

Saccharide concentrations in seawater and SSML:

Glucose was the most abundant saccharide in both seawater (26 – 94 nM) and SSML (75 -181 nM). Glucose was predominantly in the form of oligo- and polysaccharides, and was only detected in its free form in seawater and SSML after the beginning of bloom 1 (from day 10). Galactose, mannose, xylose, fructose, arabinose, rhamnose and ribose were detected in seawater and SSML only in their oligo- and polysaccharide forms (Table 6.2). Free glucose levels peaked in both seawater (32.2 nM) and SSML (38.9 nM) on day 13 coinciding with *in vivo* chl in bloom 1 (Figure 6.1c-d). Within one day, glucose rapidly declined (by ~60%) in both seawater (11.8 nM) and SSML (12.7 nM), reaching a minima on day 18. Its concentration increased thereafter into bloom 2. Rapid changes of free glucose concentrations is likely due to production of labile glucans by phytoplankton (as a means of energy storage) and their rapid consumption by heterotrophic bacteria.[279, 280]

Saccharide concentration and dynamics in SSA:

Saccharides in SSA were detected only after hydrolysis, but not in their free forms. This indicates that in SSA carbohydrate formed oligo/polysaccharides; however, the molecular assembly and speciation of oligo/polysaccharides is not known, as these features were lost upon hydrolysis. In fine SSA, glucose, galactose, mannose, xylose,

fructose, arabinose, rhamnose and ribose contributed 4 – 20 % of OC mass. Glucose, galactose, arabinose, rhamnose, and fucose were also detected in coarse SSA, in which total saccharide concentrations contributed 15 – 44 % of OC (Figure 6.4, Table 6.2). On average, the measured saccharides accounted for 11±5 % of fine and 27±10 % of coarse SSA OC (Figure 6.2c-d). However, the analytical methods employed include neither charged saccharides (uronic acids, sulfate-sugars and amino-sugars) nor carbohydrates that did not hydrolyze under the mild hydrolysis conditions employed. Therefore, total saccharide concentrations are likely 2 – 10 % higher than the values reported herein.[76, 77, 113, 120]

OC mass fractions of glucose, galactose, mannose, xylose and fructose in fine SSA were elevated with *in vivo* chl levels in seawater (Figure 6.1e and Figure 6.4). With the exception of galactose, saccharide mass fractions were lower in bloom 1 than in bloom 2, with the latter having higher levels of heterotrophic bacteria. The higher galactose fraction in bloom 1 may be due to the presence of phytoplankton species that specifically elevate galactose levels, such as dinoflagellates.[280, 299] Glucose, mannose, xylose and fructose in fine SSA OC were correlated ($r_s > 0.73$, $p < 0.03$), indicating their common origin from oligo/polysaccharides. These sugars comprise labile energy-related saccharides that undergo rapid changes in concentration in seawater, SSML, and SSA.

Higher OC mass fractions of arabinose, rhamnose (fine SSA) and fucose (coarse SSA) were observed in the latter part of the experiment (Figure 6.4). Polysaccharides containing arabinose, rhamnose, and fucose are synthesized by stressed diatoms under nutrient deficiency.[279] While some diatom cells have been shown to survive nutrient deficiency and remain inactive until nutrients become available, others die and leave

behind organic detritus that can be further cleaved by bacteria to release these saccharides.[300] In addition, arabinose, rhamnose and fucose are associated with bacterial extracellular release.[75, 279-281, 301, 302] The peak of these chemical species during bloom 2 is likely reflective of the combination of declining phytoplankton and high bacterial levels. Also during bloom 2, high bacterial levels may have given rise to elevated mass fractions of ribose, the saccharide moiety of ribonucleic acid.[76, 303, 304]

Saccharide profiles in fine and coarse SSA:

Glucose, galactose, mannose, xylose, fructose, arabinose, rhamnose and ribose were detected in fine SSA with 65% of the average saccharide mass being from glucose and galactose. Most of these saccharides are associated with substrates used for energy storage (e.g. glucan) in marine organisms and primarily exist as dissolved organic matter (DOM).[120, 280, 299] Glucose and galactose were also detected in coarse SSA, with significant added contributions from arabinose, rhamnose and fucose (26% of total saccharide). The higher abundance of these structural saccharides[299] are reflective of cell wall material, TEP,[76] and particulate organic matter (POM).[77, 81] Qualitatively, fine SSA contains saccharides characteristic of DOM, while coarse SSA contains more saccharides that are characteristic of POM.

The different saccharide profiles of fine and coarse SSA are expected to result from the exclusion of POM from SSA particles that are relatively smaller in size. As bubbles age POM likely drains back to the base of the bubble prior to bursting, leaving behind a films of surface-active DOM that generates film drops upon bursting.[258, 276] As the inner bubble cavity retracts and produces a larger jet drops, POM may become

entrained.[258, 276] Burrows *et al.* (2016) demonstrated that water-soluble saccharides can sorb to surfactants and may co-occur on bubble films and be simultaneously transferred to SSA.[305] In support of this proposed mechanism are co-located data from IMPACTS, particularly work by Cochran *et al.*[105] that reported more surface active species (e.g. short chain fatty acids) in fine SSA and Patterson *et al.*[268] that reported the incorporation of biological structures and POM into larger SSA particles. Future studies into the dissolved versus particulate nature of these saccharides can aid in clarifying this mechanism.

Enrichment of saccharides:

Saccharides were enriched in SSML and SSA over seawater. Average EF values in SSML ranged from 1.2 – 5.5 (Table 6.1) and are in agreement with previously reported values of 1.5 by Compiano *et al.*,[75] 3.5 - 12.1 by Gao *et al.*,[272] and 0.7 - 1.2 by van Pinxteren *et al.*[282] Greater enrichments were observed for coarse (with EF ranging 32-52) and fine (with EF ranging 30-321) SSA particles (Table 6.1). Coarse mode EF are in good agreement with the EFs (TSP), 22-70 estimated by Gao *et al.*[272] Enrichment of saccharides at the SSML is due to bubble-scavenged, surface-active polysaccharides.[77, 81] The higher enrichments of saccharides in SSA compared to SSML, reflect an additional chemical fractionation in SSA formation. SSML is a heterogeneous medium, with higher OM levels at the air-water interface.[259] Fine SSA particles exhibited the greatest EF and were generated in part by film drops by the bursting of bubble caps that are enriched in highly-surface active organic matter and are depleted in sodium relative to other cations. Coarse SSA largely generated by jet drops incorporates less-enriched portions of the SSML, giving rise to EF values less than fine SSA, but greater than SSML. The glass

plate method generally captures bulk SSML to 20-150 μm depth and unable to fractionate the different layers of it.[259] Future research on SSA enrichment relative to the SSML should employ SSML sampling methods specific to the air-water interface to more accurately represent where SSA is generated. Likewise, additional SSA size fraction is needed to better distinguish between film and jet drops.

The variation in EF for saccharides during the mesocosm experiment (Figure 6.5 b-g) demonstrates that saccharide enrichment is a dynamic process that changes with the biological state of the seawater. All the saccharides in SSA reported the highest enrichment either on day 22 (xylose, fructose) or on day 25 (glucose, galactose, mannose, arabinose) during bloom 2 with higher chl and bacteria levels. Saccharide EF had a similar temporal variation as saccharide mass fraction of OC in SSA (Figure 6.4), which indicates that maximum saccharide enrichment coincided with their greatest mass contributions to OC.

6.4.5 Enrichment of Major Cations in SSML and SSA

Salts are highly abundant in seawater, SSML and SSA. Median Na^+ and Cl^- concentrations in the seawater were 483 mM and 568 mM, respectively, in good agreement with prior studies by Barker and Zeitlin,[289] Holland,[306] Keene *et al.*,[73] and Sarmiento and Gruber[297] (Table 6.3).

Mg^{2+}, Ca^{2+}, and K^+ were enriched in SSML and SSA relative to Na^+, with EF values significantly higher than unity ($p \leq 0.005$). In SSML, EF averaged 1.24 ± 0.14 for Ca^{2+}, 1.21 ± 0.13 for K^+, and 1.20 ± 0.13 for Mg^{2+}. In fine and coarse SSA, Ca^{2+} was the most enriched cation, followed by Mg^{2+} and K^+ (Table 6.1). In SSA, Ca^{2+} and Mg^{2+}

always exhibited enrichment (EF > 1), while EF for K^+ was more variable (ranging 0.79 – 2.24) and below 1 on days 12, 13, 15, and 17. EF for Mg^{2+} and Ca^{2+} in SSA were significantly higher than SSML ($p < 0.05$), indicating a selective enrichment of these divalent cations in SSA. While fine and coarse SSA were both enriched in these cations, they were not significantly different from one another.

The observed selectivity in cation transfer ($Ca^{2+} > Mg^{2+} > K^+$) follows the same trend of cation binding affinities to fatty acids (e.g. palmitic acid) and anionic surfactants (e.g. dodecyl sulfate).[287, 288, 307] Natural organic films of lipids, fatty acids, polysaccharides and proteins reside at bubble surfaces due to surface activity of those molecules.[60, 79, 105, 271-274] They also can complex Ca^{2+}, Mg^{2+} and K^+ via chelation and selectively transport them to SSA in the process of bubble bursting.[76, 79] It has been shown that divalent cations ($Ca^{2+} > Mg^{2+}$) facilitate the aggregation of extracellular polymeric substances due to their strong binding capability with phenolic –OH, aromatic C=C and polysaccharide C-O groups.[291] The role of organic species in affecting enrichment of Ca^{2+}, Mg^{2+} and K^+ in SSA is supported by the temporal consistency in the cation EF with those of saccharides (Figure 6.5). In the presence of organic complexing agents, cations are selectively transferred to SSA in a way that reflects their binding affinity to surface active species.

Enrichment of Ca^+ and K^+ in SSA due to bubble bursting was first demonstrated by Oppo *et al*. (1999), who attributed cation enrichment in sub-micron SSA to their interactions with surfactants at the air-water interface and super-micron enrichment to cation interactions with bacteria.[286] More recently, Ca^{2+} enrichment was demonstrated in a laboratory study of SSA without adding organic matter to the seawater matrix,

suggesting surfactants are not required for enrichment and carbonate or bicarbonate may be responsible.[295] Prior field studies likewise report calcium enrichment in marine aerosol, but suggested it was due to wind-blown mineral dust, calcareous shell debris or fragments of calcareous phytoplankton rather than SSA production.[73, 79, 294] Results from this study further confirm the enrichment of Ca^{2+}, Mg^{2+} and K^{+} in SSA due to SSA production mechanisms. For the first time we demonstrate that ocean biological conditions affects ion enrichment, with maximum enrichments of cations in SSML and SSA occurring during periods of elevated phytoplankton and bacteria levels.

6.4.6 Enrichment of Major Anions in SSA

Nitrate was the most enriched anion in SSA, with EF of 7 ± 1 and 2.2 ± 0.4 for fine and coarse SSA particles, respectively. The EF varied widely during the experiment (1.2 – 12.0) with the greatest enrichment occurring on day 23 during bloom 2 (Figure 6.5i). The actual mechanism of nitrate enrichment is not known, but may be carried to SSA by charged organic compounds (e. g., amino saccharides, amino acids, proteins).[308] Like nitrate, sulfate was significantly ($p<0.001$) enriched in SSA, with mean EF of 1.19 ± 0.06 and 1.14 ± 0.07 for fine and coarse SSA particles, respectively. Sulfate enrichment varied across a narrower range (0.79 – 1.42) and exhibited depletion (EF < 1) on days 18, 22, and 25 and $EF_{sulfate}$ was higher in bloom 1 than bloom 2. Sulfate was not enriched in the SSML, indicating that the enrichment is unique to SSA. The exact mechanism for sulfate enrichment in SSA is also not known, but it may be transported as a charge-compensating anion by organic or inorganic cations. Meanwhile, chloride was not significantly enriched or depleted in SSML or SSA (Table 6.1, Figure 6.5k), with EF

values not significantly deviating ($p > 0.06$) from unity. To the best of our knowledge, these are the first quantitative data demonstrating anion enrichment in SSA.

6.4.7 Implications of Ion Enrichment

The parallel analysis of seawater, SSML, and SSA has revealed differences in the ion composition of each phase (Table 6.3), such that salt composition in SSA should not be assumed to be that of seawater. Due to the enrichment of divalent cations relative to Na^+, the estimation of sea salt mass in SSA using Na^+ concentrations and Na^+-to-salt ratios of seawater is biased low. In this dataset, the measured salt components exceeded the estimated salt mass by an average of 6%. This underestimation was most significant for enriched species in fine SSA: K^+ (18%), Mg^{2+} (28%), Ca^{2+} (35%), NO_3^- (83%) and SO_4^{2-} (15%). As demonstrated by these calculations, the sea salt estimation method can underestimate total salt concentrations in SSA and substantially underestimate concentrations of individual ions. Using of Cl^- instead of Na^+ in estimation method is not recommended, due to its depletion from marine aerosols due to secondary processing.[309-311]

Excess sulfate in SSA, termed non-sea-salt-sulfate (NSS), has been attributed to secondary sulfate production via atmospheric reactions.[294] Our observation of sulfate enrichment in nascent SSA particles indicates that the marine environment contributes to NSS in addition to secondary sulfate formation. Such a marine source would underestimate sea-salt sulfate and overestimate secondary sulfate (as NSS) in prior studies. However, the extent of this bias is expected to depend on SSA-size and seawater

conditions. Further research on the mechanism of sulfate enrichment and the extent to which it occurs in ambient environments is needed.

6.5 Acknowledgements

This material is based upon work supported by the National Science Foundation through the Centers of Chemical Innovation Program under grant CHE1305427. We would like to thank Grace Irumva, Hosiana Abewe, Zehra Khan, and Josh Kettler for their assistance with sample collection and/or analysis.

Figure 6.1: Temporal variation of a) *in vivo* chlorophyll, heterotrophic bacteria in the seawater, b) POC and DOC concentration in seawater and concentration, and OC mass fraction of glucose in c) seawater, d) SSML, e) fine and f) coarse SSA.

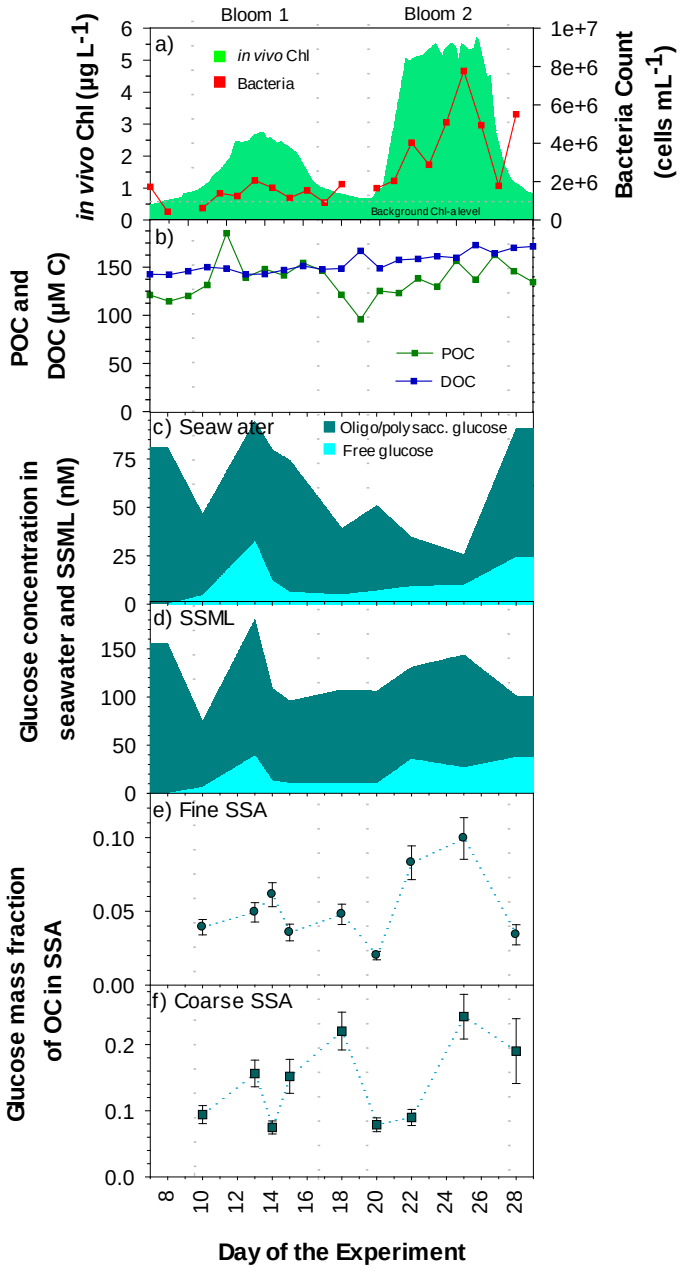

Figure 6.2: Mass distribution of inorganic ions and organic carbon to a) fine and b) coarse SSA mass. Contribution of total (free and oligo/polysaccharide bound) saccharides to organic carbon mass for c) fine and d) coarse SSA particles.

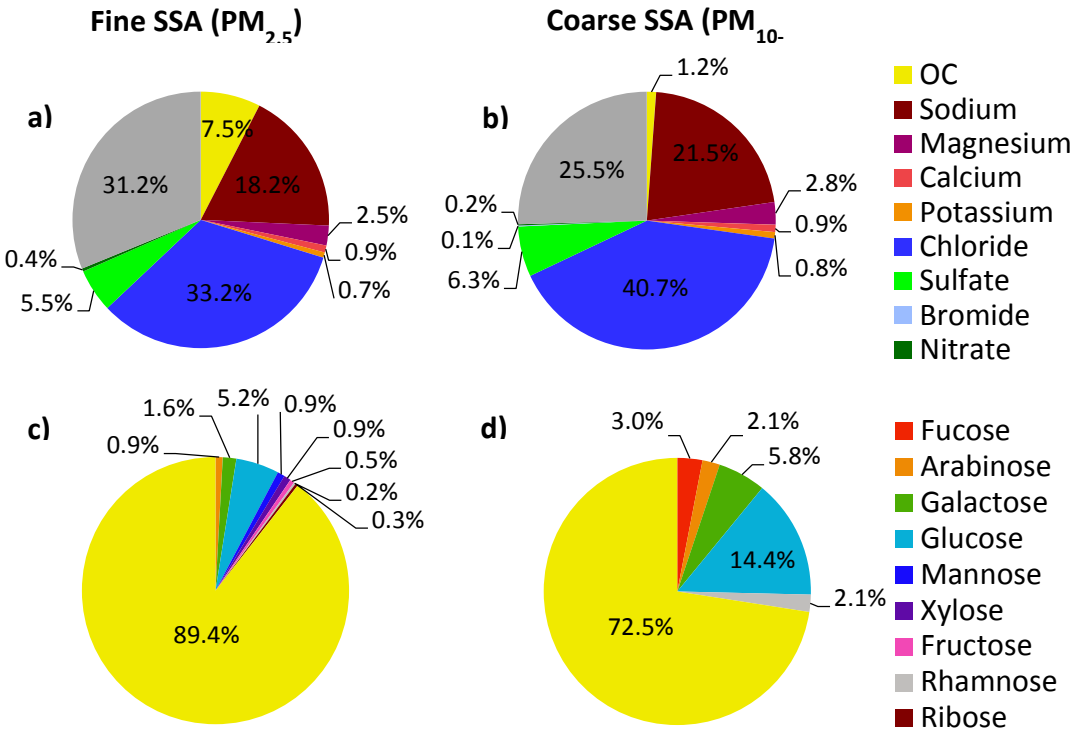

Figure 6.3: PM mass composition of a) fine and b) coarse SSA.

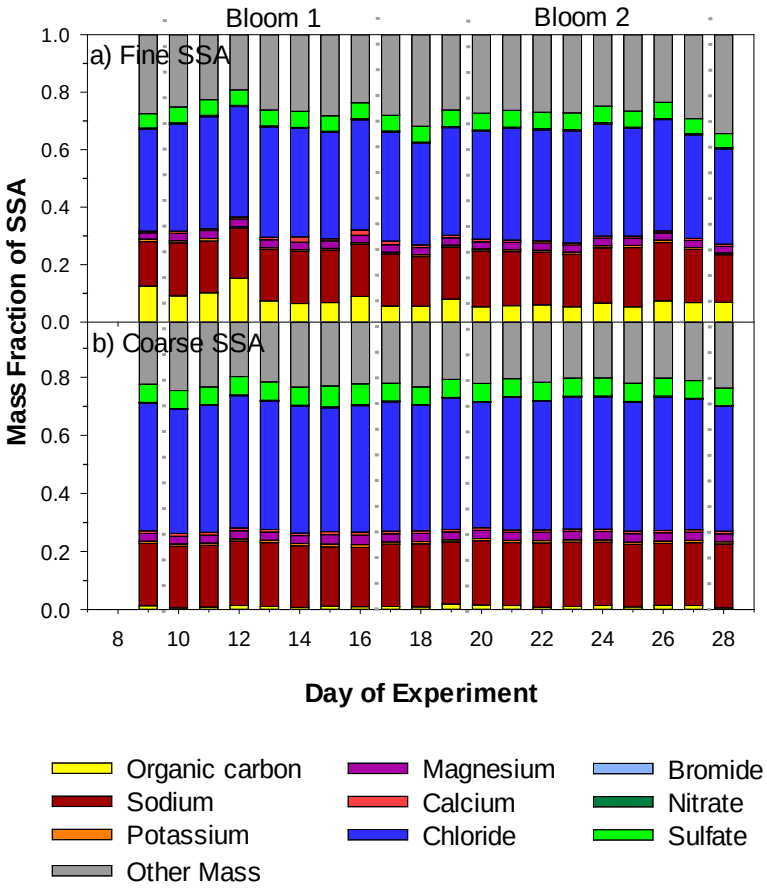

Figure 6.4: Total (free and oligo/polysaccharide bound) saccharide mass fraction of OC in a) fine and b) coarse SSA.

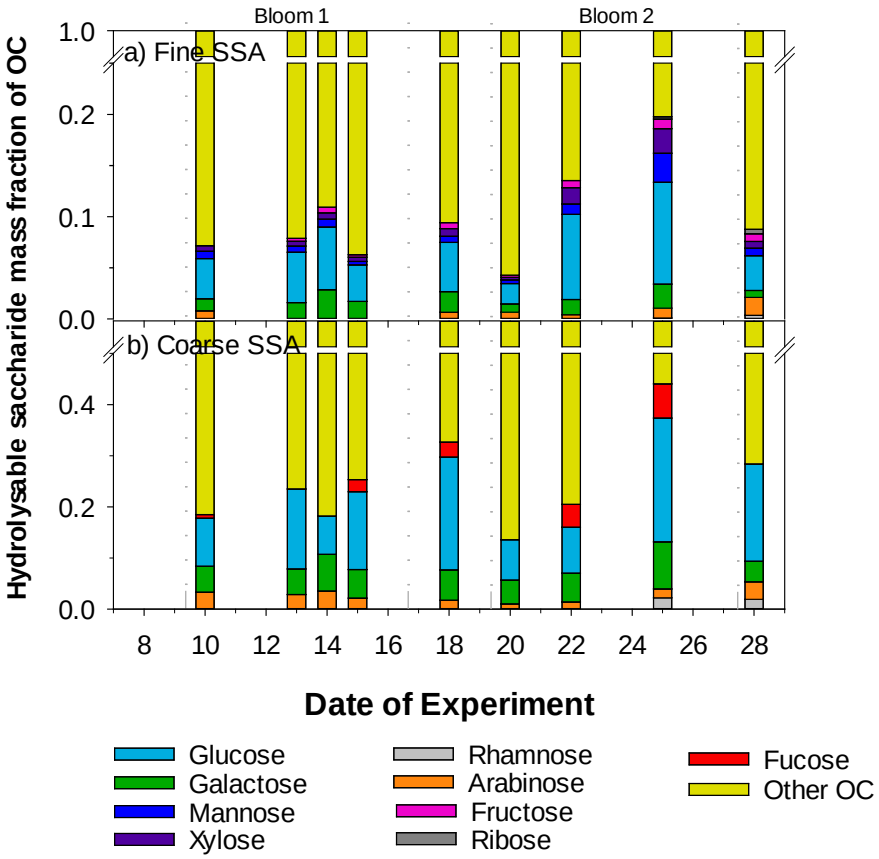

Figure 6.5: Time series of a) organic carbon, b-f) total (free and oligo/polysaccharide bound) saccharide and h-m) inorganic ion enrichment factors in SSML, fine and coarse SSA during the IMPACTS experiment.

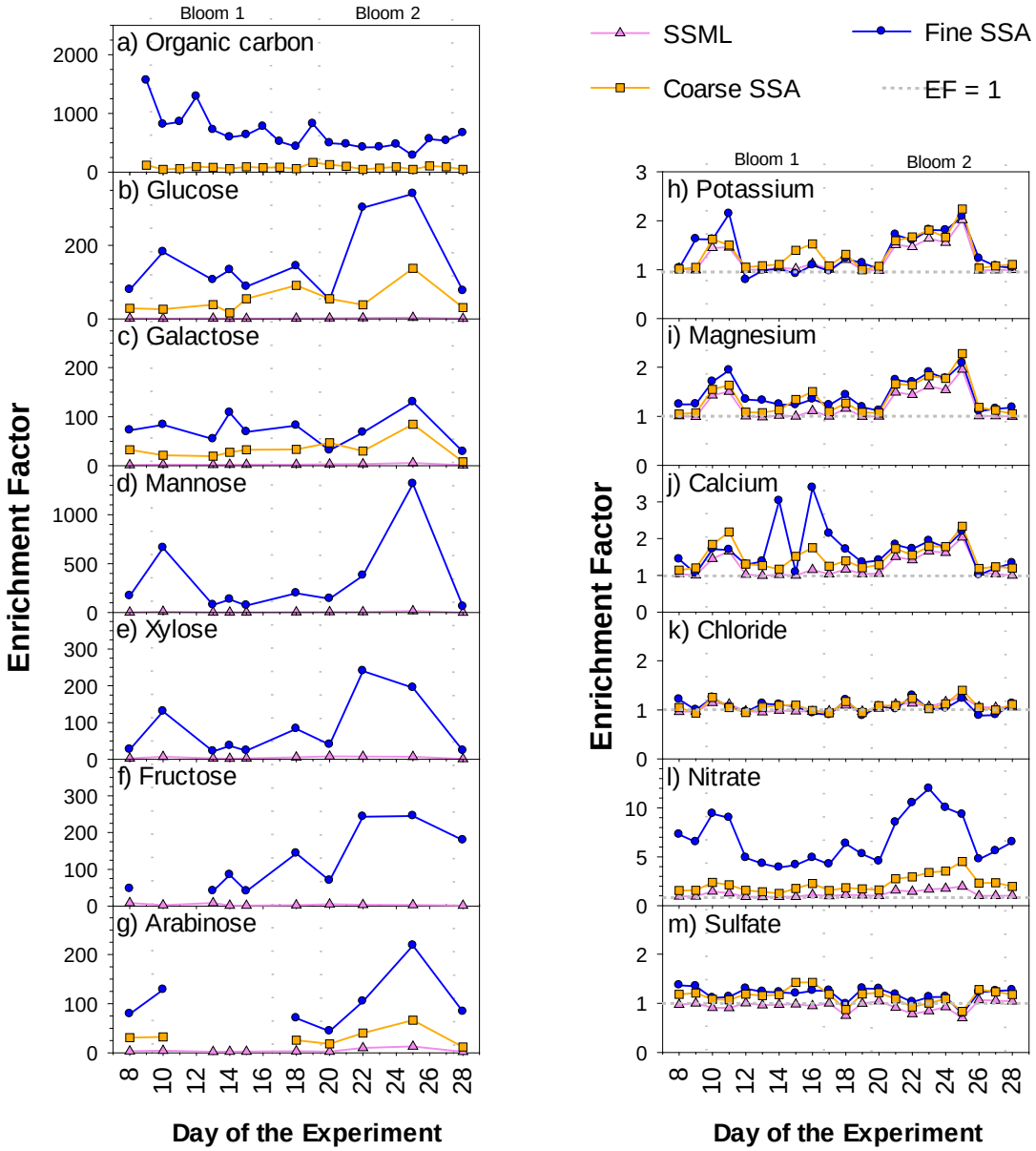

Table 6.1: The range and mean enrichment factors (EF ± 95% CI) for a) organic carbon, b) total (free and oligo/polysaccharide bound) saccharides and c) select water-soluble ions in SSA particles collected over the course of two consecutive phytoplankton blooms during IMPACTS 2014. Sodium was used as the reference species and by definition has an EF of 1.

Analyte	EF for SSML		EF for Fine SSA		EF for Coarse SSA	
	Range	Mean	Range	Mean	Range	Mean
a) Organic carbon	NA	NA	282 - 1564	669 ± 143	47 - 167	85 ± 15
b) Saccharides						
Glucose	1.1 - 3.7	1.9 ± 0.6	53 - 340	151 ± 70	17 - 138	52 ± 26
Galactose	1.5 - 5.7	2.8 ± 0.9	28 - 130	73 ± 22	8 - 85	34 ± 15
Mannose	1.1 - 16.2	5 ± 3	60 - 1314	321 ± 282	NA	NA
Xylose	1.4 - 8.4	5 ± 2	22 - 240	82 ± 57	NA	NA
Fructose	1.3 - 8.3	4 ± 2	40 - 245	122 ± 65	NA	NA
Arabinose	2.2 - 13.0	5 ± 3	44 - 218	104 ± 53	12 - 66	32 ± 16
Rhamnose	1.0 - 1.6	1.2 ± 0.4	14 - 34	NA*	3 - 21	NA*
Ribose	1.1 - 2.6	1.8 ± 0.4	15 - 50	30 ± 46	NA	NA
c) Inorganic ions						
Potassium	0.99 - 2.02	1.2 ± 0.1	0.79 - 2.14	1.3 ± 0.2	1.00 - 2.24	1.3 ± 0.2
Magnesium	0.98 - 1.96	1.2 ± 0.1	1.10 - 2.08	1.4 ± 0.1	1.05 - 2.28	1.4 ± 0.2
Calcium	1.00 - 2.04	1.2 ± 0.1	1.02 - 3.38	1.7 ± 0.3	1.15 - 2.34	1.5 ± 0.2
Chloride	0.95 - 1.26	1.05 ± 0.04	0.88 - 1.29	1.06 ± 0.06	0.94 - 1.26	1.05 ± 0.05
Nitrate	0.89 - 1.98	1.2 ± 0.1	3.90 - 12.0	7 ± 1	1.25 - 4.52	2.2 ± 0.4
Sulfate	0.70 - 1.07	0.94 ± 0.05	0.79 - 1.36	1.19 ± 0.06	0.83 - 1.42	1.14 ± 0.07

NA – Not available; *n = 2

Table 6.2: Frequency of detection (FOD), range and mean concentration (± standard error) of total (free and oligo/polysaccharide bound) saccharides in seawater, SSML, fine and coarse SSA over the IMPACTS experiment (n=10).

Analyte	Seawater			SSML			Fine SSA			Coarse SSA		
	FOD (%)	Concentration (nM)		FOD (%)	Concentration (nM)		FOD (%)	Concentration (nmol m^{-3})		FOD (%)	Concentration (nmol m^{-3})	
		Range	Mean ± SE		Range	Mean ± SE		Range	Mean ± SE		Range	Mean ± SE
Glucose	100	26 - 94	62 ± 8	100	75 - 181	120 ± 10	100	0.35 – 1.5	0.9 ± 0.1	100	0.94 – 2.9	1.6 ± 0.2
Galactose	100	16 - 75	41 ± 6	100	88 - 136	114 ± 5	100	0.11 – 0.54	0.29 ± 0.04	100	0.26 – 0.92	0.69 ± 0.06
Xylose	100	8.1 - 57	24 ± 5	100	70 - 119	89 ± 5	100	0.04 – 0.44	0.16 ± 0.04	0	ND	ND
Mannose	100	1.9 - 24	8 ± 2	100	18 - 46	28 ± 2	100	0.06 – 0.44	0.15 ± 0.03	0	ND	ND
Fructose	100	3.3 - 15	8 ± 1	100	12 - 128	31 ± 11	90	0.02 – 0.14	0.08 ± 0.01	0	ND	ND
Arabinose	100	3.8 - 42	20 ± 4	100	52 - 99	69 ± 4	70	0.09 – 0.33	0.17 ± 0.03	70	0.18 – 0.46	0.29 ± 0.04
Rhamnose	50	7.5 - 23	15 ± 3	90	5.4 - 14	10 ± 1	20	0.02 – 0.06	0.04 ± 0.02	20	0.14 – 0.25	0.19 ± 0.06
Ribose	100	11 - 35	20 ± 2	100	31 - 49	39 ± 2	30	0.04 – 0.08	0.06 ± 0.01	0	ND	ND
Fucose	0	ND	ND	0	ND	ND	0	ND	ND	60	0.09 – 0.74	0.38 ± 0.09

ND – not detected

Table 6.3: Summary statistics of salt concentration observed during IMPACTS 2014 and prior studies (uncertainties are associated with last significant digit and represent standard error (n=21)).

Compartment	Statistic	Sodium Concentration	Molar Ratio to Sodium							Reference
			Magnesium	Potassium	Calcium	Chloride	Sulfate	Bromide	Nitrate	
Seawater	Minimum	338 mM	0.056	0.010	0.010	0.95	0.054	0.0008	0.007	
	Maximum	504 mM	0.112	0.020	0.020	1.23	0.083	0.0018	0.0018	
	Median	483 mM	0.110	0.020	0.019	1.15	0.059	0.0015	0.0014	
	Mean	456 ± 10 mM	0.097(±4)	0.0174(±8)	0.0170(±7)	1.14(±2)	0.062(±2)	0.00139(±6)	0.00131(±7)	
SSML	Minimum	503 mM	0.1101	0.0197	0.0196	1.147	0.0563	0.00148	0.00134	IMPACTS (This study)
	Maximum	521 mM	0.1128	0.0205	0.0208	1.209	0.0588	0.00169	0.00156	
	Median	510 mM	0.1113	0.0201	0.0201	1.195	0.0581	0.00155	0.00147	
	Mean	511 ± 1 mM	0.1113(±2)	0.02008(±6)	0.02015(±6)	1.190(±3)	0.0579(±1)	0.00157(±1)	0.00146(±1)	
Fine SSA	Mean	370 ± 22 nmol m^{-3}	0.134(±2)	0.0219(±8)	0.028(±2)	1.21(±3)	0.0732(±8)	ND	0.0082(±4)	
Coarse SSA	Mean	1866 ± 104 nmol m^{-3}	0.125(±2)	0.0221(±4)	0.0244(±6)	1.22(±2)	0.070(±1)	0.00155(±3)	0.00266(±7)	
Seawater		468 mM	0.114	0.022	0.022	1.16	0.060	-	-	Holland (1978)
Seawater		474 mM	0.111	0.023	0.022	1.13	0.061	0.0017	-	Keene et al. (2007)
Seawater		481 mM	0.112	0.022	0.022	1.16	-	0.0018	-	Sarmiento and Gruber (2013)
Seawater		462 mM	0.117	0.021	0.022	-	-	-	-	Barker and Zeitlin (1972)
SSML		476 mM	0.115	0.022	0.023	-	-	-	-	Barker and Zeitlin (1972)
Nascent SSA (TSP)		881 nmol m^{-3}	0.107	0.020	0.025	1.14	0.058	0.0018	-	Keene et al. (2007)

ND – not detected

CHAPTER SEVEN

ENRICHMENT OF SACCHARIDES AT AIR-WATER INTERFACE: A QUANTITATIVE COMPARISON OF SEA SURFACE MICROLAYER AND FOAM[5]

7.1 Abstract

Organic matter accumulates at the ocean surface. Herein, we provide the first quantitative assessment of the enrichment of dissolved saccharides in persistent whitecap foam and compare this enrichment to the sea surface microlayer (SSML) during a nine day mesocosm experiment involving a phytoplankton bloom. Free monosaccharides were quantified directly, total saccharides were determined following mild acid hydrolysis, and the oligo/polysaccharide component was determined as the difference of total and monosaccharides. Total saccharides contributed a significant fraction of dissolved organic carbon (DOC), accounting for 13% of DOC in seawater, 27% in SSML and 31% in foam. Median enrichment factors (EF), the ratio of the concentrations of saccharides relative to sodium in SSML or foam to that of seawater ranged from 1.7-6.4 and 2.1-12.1 in SSML and foam, respectively. Based on median EFs, xylitol, mannitol, glucose, galactose, mannose, xylose, fucose, rhamnose and ribose were more enriched in foam layer than SSML. The greatest EFs for saccharides coincided with high chlorophyll levels, indicating changing surface enrichment with phytoplankton blooms. Higher enrichments of organic matter in sea foam over the SSML indicate that surface active

[5] This chapter is in preparation to publish as Jayarathne, T.; Cappa, C.; Bertram, T.; Grassian, V.; Prather, K. and Stone, E., "Enrichment of Saccharides and Metals at Air-Water Interface: A Quantitative Comparison of Sea Surface Microlayer and Foam", *Environmental Science and Technology Letters*.
Author Contributions
T.J. and E.S. designed research; E.S., C.C., T.B., K.P., and V.G. planned the experiment; T.J. collected samples, extracted and analyzed, processed data and wrote the chapter.

organic compounds become increasingly enriched on persistent bubble film surfaces. These findings help to explain how marine organic matter becomes highly enriched in sea spray aerosol that is generated by bursting bubbles at the ocean surface.

7.2 Introduction

Seawater, in addition to salt, contains complex matrix organic compounds, with saccharides (a.k.a carbohydrates), proteins, and lipids being the predominant compound classes.[78, 312-314] Saccharides, in particular, are present in a variety of chemical forms, including sugar alcohols (e.g., arabitol, mannitol), free monosaccharides (e.g., glucose, galactose), oligo/polysaccharides (e.g., glucan, transparent exopolysaccharides or TEP) or saccharides complexed with other molecules such as lipids and protein (e.g., lipopolysaccharides, glycoproteins).[76, 113, 282] These saccharides serve as substrates for energy storage and the formation of structural materials (e.g. cell wall) of marine micro-organisms.[76, 277, 278, 315] They have been estimated to contribute up to 40 % of dissolved organic carbon (DOC) in the ocean with levels dependent on biological activity.[120, 277, 299, 316] During a phytoplankton bloom, the molecular composition of saccharides is altered by phytoplankton and bacteria.[279] Glucose and fructose are the monomers of major energy-related polysaccharides in phytoplankton (e.g. glucan, fructan) and are released in large quantities following the peak of the bloom due to phytoplankton lysis.[75, 279, 317] Galactose, mannose, xylose, fucose, rhamnose and arabinose comprise less labile, structural-related polysaccharides that are released by bacterial breakdown of phytoplankton cellular materials. Meanwhile, fucose, arabinose and rhamnose containing polysaccharides are synthesized by stressed phytoplankton under nutrient deficiency, and elevated levels of

these carbohydrate monomers are observed during phytoplankton bloom decay.[75, 279, 280] In addition, rhamnose and arabinose containing polysaccharides are associated with bacterial secretions and found to be elevated in areas where higher bacterial activity in the ocean.[279, 281] Hence, the changes in the concentrations and molecular distributions of saccharides are suggested to provide insights to biochemical processes controlling DOC in the ocean.[279]

Breaking waves entrain air in sub-surface seawater. As tiny bubbles rise to the ocean surface, they scavenge surface-active materials in marine DOC (e.g. lipopolysaccharides), leading to their accumulation at the ocean surface.[77, 81, 258, 259] In general, bubbles that reach to the surface may either burst instantly (<1 s) or persist for extended period of time (10-100 s), producing persistent layer of whitecap foam. Elevated levels of either DOC or surface active material in seawater increases bubble lifetime, leading to more persistent bubbles.[64, 257, 318] As bubbles age, bubble films drastically decrease in thickness (1 μm to 100 nm) as less surface-active materials drain to the base of the bubble creating a highly organic enriched bubble film.[257, 258] The drainage creates a thin (20 – 400 μm), chemically distinct film at ocean surface referred to as the sea surface microlayer (SSML).[258, 259]

This extent of the accumulation of material at the ocean surface is often quantitatively evaluated by enrichment factors (EF). EF for species *x* (saccharides) relative to sodium (Na^+) in phase *i* (either SSML and foam) over seawater were calculated by Equation 7.1.

$$EF_{x(i)} = \frac{[x]_i / [Na^+]_i}{[x]_{seawater} / [Na^+]_{seawater}} \quad \text{(Equation 7.1)}$$

EF greater than 1 indicates enrichment of species *x* relative to sodium in phase *i*, while EF less than 1 indicates depletion. Prior studies have demonstrated enrichment of DOC, organic and inorganic species in SSML.[75, 272, 282] In particular, DOC in SSML reported to be enriched 0.8 – 1.6 times than that of seawater.[319, 320] Further, enrichment of total saccharides has been observed in SSML with EFs ranging from 0.7 to 12.1 across field and laboratory studies, indicating a selective enrichment of saccharides over bulk DOC.[28, 75, 272, 282]

To the best of our knowledge, enrichments of saccharides have not been quantitatively evaluated for persistent bubble films. Meanwhile, it has been suggested that extremely high organic enrichment ($10^2 – 10^3$) in sea spray aerosol (SSA) may result from organic matter being selectively enriched on bubble film surfaces prior to bursting.[80, 258] In the presence of sea foam, Collins et al. (2014) demonstrated a preferential enrichment of organic matter in SSA. However, chemical speciation of SSA with quantitative measurements of foam composition has yet to be studied. Further, fine SSA (with particle diameters< 2.5 μm) has been demonstrated to be more enriched in saccharides than coarse SSA (with particle diameters 2.5-10 μm), which is proposed to result from fine SSA generation by the bursting of bubble films, called film drops, that have the greatest carbohydrate enrichment.[28] Further, it was reported that dissolved and particulate saccharides selectively transfer to smaller and larger SSA particles, respectively. It was suggested that the different SSA generation mechanism control this process; however, the exact selectivity mechanism is not understood.[28] As the air-water interface is involved in SSA production, it is essential to understand its chemical

composition in order to predict the chemical composition of SSA and its potential to influence on atmospheric processes and climate.

The central objective of this study is the quantitative assessment of saccharide enrichment in SSML and sea foam layer over a full phytoplankton bloom cycle. In this way, we compare the enrichment of species at the sea surface across SSML and foam and evaluate the role of marine microbiology on this enrichment. Real microbial processes that mimic primary production in the ocean was involved in this experiment and thus accurately represent biological and chemical transformations that occur in the ocean. A Marine Aerosol Reference Tank (MART) was used for foam production providing an accurate mimic for wave breaking, air entrainment, and bubble generation that occurs in the real marine environment.[256] This study provides insight to the enrichment of saccharides in sea foam compared to SSML that is relevant to the formation of SSA at the air-water interface.

7.3 Experimental Methods

7.3.1 Sample Collection and Preparation

A mesocosm was created in a MART following the method described by Lee et al., (2015) during the Investigation into Marine Particle Chemistry and Transfer Science (IMPACTS) laboratory study. The biological activity of the MART was monitored immediately before the sample collection by chlorophyll-a (chl-a) levels using a Wetlabs ECO BBFL2 sensor and Turner AquaFluor handheld unit as described by Wang et al., (2015).

Seawater samples were collected from 15-20 cm below the air-water interface of the MART using a disposable plastic pipette and SSML samples were collected from the air-water interface following membrane filter method for 9 consecutive days.[259] Foam samples were collected from day 3-9 using an auto- pipette by rastering the pipette tip over the foam layer (Figure 7.1). The foam was generated by plunging the MART by impacting a water sheet on the water surface to mimic the plunging jet of water from a breaking wave crest.[64, 256] The MART was plunged for 5 minutes and accumulated foam was immediately collected. Several plugging cycles (10-15 cycles) were carried out to collect enough volume of foam for the chemical analysis. All samples were stored in polypropylene bottles in dark and frozen (-20 ^{0}C). Prior to chemical analysis, samples were filtered (450 nm PTFE filters, Whatman) to isolate DOC, operationally defined as solutes and colloids smaller than 450 nm. A subset of seawater, SSML and foam samples (Day 1-3, 5, 7, 9) were subjected to ultrafiltration for fractionation of material <3 kDa and <100 kDa using Amicon centrifugal ultracel membrane filters (Sigma-Aldrich). These cutoff diameters are referred to globular proteins and in general ~1 kDa refers to a globular protein with ~1 nm in diameter.[321-323]

7.3.2 Saccharide, DOC and Major Inorganic Ion Analysis

Instrumental analysis of saccharides was performed using high performance anion exchange chromatography (HPAEC) (Dionex-ICS 5000) along with pulsed amperometric detection (PAD) following the conditions described by Jayarathne et al., (2016).[28] Samples were analyzed in four ways: 1) directly analysis to quantify free monosaccharides, 2) hydrolysis using trifluoroacetic acid (0.1 M) at 100 °C for 12 hours

for total saccharides, 3) 3 kDa ultrafiltration and then hydrolysis, and 4) 100 kDa ultrafiltration and then hydrolysis. This allowed for saccharides to be quantified in four size bins: free monosaccharides, low molecular weight (LMW) oligo- and polysaccharides less than 3 kDa, high molecular weight (HMW) polysaccharides ranging 3-100 kDa, and colloidal polysaccharides ranging 100 kDa-450 nm. Analytical uncertainties were propagated from the method detection limits and 10 % of the saccharide concentration.

DOC was analyzed using Sievers 5310C Laboratory Total Organic Carbon Analyzer (GE Instruments) and inorganic ion concentration was analyzed by ion-exchange chromatography coupled with conductivity detection as described in detail elsewhere.[140] The enrichment of saccharide relative to Na^+ in SSML and foam with respect to seawater was calculated using equation 7.1.

7.4 Results and Discussion

7.4.1 Biological Activity of the Seawater

The initial chl-a concentration of the seawater was 3.1 μg L^{-1} (day 0) indicating a mild phytoplankton bloom was occurring in the coastal ocean.[35, 275] Addition of nutrients and exposure to natural sunlight triggered the growth of phytoplankton, increasing to a maximum chl-a level of 45.4 μg L^{-1} on day 2 (Figure 7.2). Natural levels of chl-a in the open and coastal ocean have been observed in the range of 0.03 μg L^{-1} to 50 μg L^{-1}.[35, 324] Chl-a levels rapidly declined to a minimum of 0.24 μg L^{-1} on day 5. Potential reasons for this decline include nutrient deficiency, growth of heterotrophic bacteria and viruses, and mechanical breakdown of phytoplankton due to plunging of the MART.[275, 325] After day

5, chl-a levels steadily increased up to 3.1 μg L^{-1} by the end of experiment on day 9. The growth of phytoplankton after day 5 was likely promoted by nutrients re-released to the seawater by crashing the phytoplankton bloom, a process that is commonly observed in the ocean.[279, 325, 326] The ratio of the sum of fucose and rhamnose concentrations to the sum of arabinose and xylose concentrations in seawater was used as an indicator for the bacterial activity in the tank (Figure 7.2). Typically, ratios <1 indicate the presence of less-labile organic matter which is indicative of higher bacterial concentration.[120, 327, 328] In this experiment, this ratio decreased below 1 (0.69) on day 4, with a consistent decrease to 0.50 on day 9 indicating the sustained growth of marine bacteria after the phytoplankton bloom.[120, 327]

7.4.2 Contribution of Saccharides to DOC

The total quantified saccharide concentration (<450 nm) in seawater ranged 0.9 – 5.1 μM and averaged 3±1 μM. These concentration levels agree well with previously reported saccharide concentrations in seawater.[120, 329] The total saccharide concentration in SSML ranged 1.4 – 51 μM, averaging 18±15 μM. In foam, saccharide concentrations ranged 11 – 32 μM and averaged 22±7 μM. Total measured saccharides comprised a considerable fraction of DOC in seawater (13%), SSML (27%) and foam (31%).

7.4.3 Sugar Alcohols

Concentrations of three sugar alcohols—xylitol, arabitol and mannitol—varied from below method detection limits to 674±67 nM for mannitol on day 9 in SSML (Table S7.1). Sugar alcohol contributions to quantified total saccharides were small, contributing

an average of 2.1±0.8% in seawater, 2.5±1.9% in SSML and 2.4±0.5% in foam with a maximum contribution of 5.8% on day 9 in SSML. From this, we conclude that xylitol, arabitol and mannitol have minor contributions to the total saccharide pool in the ocean. The sugar alcohol concentration significantly increased at the latter part of the mesocosm suggesting a probable bacterial origin (Figure 7.3a-c).[330, 331] Sugar alcohols were primarily (>43%) in the form of free monosaccharides (Figure 7.4a), likely due to direct release of free alditols by bacteria from lignocellulosic material breakdown. [332] Further, the relative distribution of sugar alcohols in different size fractions were rather similar in all the compartments indicating a non-selective transfer of sugar alcohols to the ocean surface (Figure 7.4a).

7.4.4 Energy-related Saccharides

Energy-related saccharides were elevated during the phytoplankton bloom, declined with bloom crashing and consistently increased thereafter (Figure 7.3d-e). The high, energy-related saccharide concentrations during the phytoplankton bloom progression were likely due to the synthesis of energy storage products (e.g., glucans, fructans) and their release to surrounding water upon cell lysis.[75, 77, 279] Bacteria rapidly utilize these liable polysaccharides as energy substrates, leading to their sharp decline in concentration after bloom crashed.[333] In this process, either in-situ enzymatic hydrolysis or extra-cellular hydrolysis by bacterial enzymes could release free monosaccharides, producing free glucose and fructose[317] as observed on day 3 following the peak of the phytoplankton bloom. The steady increase of total saccharide from day 4 was probably related to breakdown of more stable structural saccharides (e.g., cellulose, hemicellulose)

by bacterial hydrolysis.[278, 334] The energy-related saccharides were dominated (34 - 65%) by LMW fraction (Figure 7.4b) and a prominent variation of saccharide distribution across different compartments was not observed. However, colloidal fraction considerably increased (27 – 36%) in SSML and foam probably due to enrichment of cellular materials at air-water interface.

7.4.5 Structure-related Saccharides

Concentrations of structure-related saccharides differed from the previously discussed energy-related saccharides in that they were not elevated during the phytoplankton bloom and instead steadily increased throughout the experiment (Figure 7.3f-k). This is likely due to gradual bacterial degradation of more stable cellular materials, such as marine POC or high molecular weight DOC.[278, 281, 301, 317, 333] The saccharide composition in the ocean was observed to shift towards stable polysaccharides at the end of a mesocosm as a result of preferential bacterial uptake of low molecular weight algal exopolymers during the initial stage, followed by feeding on less labile components.[335, 336] In this process bacteria reduce detrital organic matter to soluble foams and convert algal exopolysaccharides to bacterial polysaccharides as evident by elevated levels of structural and bacterial-related saccharides at the end of the experiment.[77] Galactose has some characteristics of energy-related saccharides such as elevated concentrations during phytoplankton bloom and release of free galactose monosaccharide after bloom crashing. This is probably due to use of galactan, the polysaccharide form of galactose as an energy storage material by some phytoplankton species.[280, 299] Ribose also showed a distinct variation pattern over the experiment (Figure 7.3l) relative to other

structure-related saccharides. The lysis of phytoplankton nucleotides during the phytoplankton bloom and the lysis of bacterium nucleotides at the latter part of the bloom is likely the source of ribose oligo/polysaccharides.[323, 337] Unlike sugar alcohols and energy-related saccharides structure-related saccharides showed a distinct distribution pattern in different compartments. The LMW fraction dominated (44 – 59%) the seawater saccharide pool while HMW fraction dominated the SSML and foam (45 – 88%) saccharide pool (Figure 7.4c). This is attributed to selective transfer of higher molecular weight oligo/polysaccharides towards ocean surface likely due to scavenging on rising bubbles due their high surface activity and coagulate at sea surface to form higher molecular weight saccharides. Further, smaller surface active oligo/polysaccharides can coagulate to form higher molecular weight polysaccharides and those could rise to the ocean surface due to positive buoyancy.[323, 338]

7.4.6 Enrichment of Saccharides in Foam and SSML over Seawater

Total saccharides (<450 nm) were significantly enriched ($p<0.05$) in SSML and foam with individual median EFs ranging from 1.7-6.4 and 2.1-12, respectively (Figure 7.5). This enrichment provides evidence for scavenging the saccharides on bubble surfaces and their accumulation at ocean surface where SSA is generated. Median EF for xylitol, mannitol, glucose, galactose, mannose, xylose, fucose, rhamnose and ribose demonstrated greater enrichment in foam compared to SSML. The relatively higher EFs in foam layer provide the first quantitative evidence of further enrichment of saccharides on bubble films compared to SSML. This is attributed to thinning the bubble film by draining the seawater constituents keeping the surface active materials on the bubble

film.[64, 77, 81, 257] This phenomenon could lead further enrichment on the bubble film with bubble ageing and could result an extremely enriched bubble film at the time of bursting generating highly organic enriched SSA.

The enrichment process was dynamic with the greatest EF occurring on days 2-4 with peak chl-a levels (Figure 7.6) indicating higher accumulation of saccharides in SSML and foam during the active bloom period. This observation demonstrates that the saccharide enrichment at ocean surface is influenced by biological activity of the seawater.

The size of the saccharide played a significant role in enrichment process. Low molecular weight oligo/polysaccharides were the major enriched species for sugar alcohols (Figure 7.7a-b) and showed 2-15 times greater EFs than their EFs for total dissolved (<450 nm) saccharides. The enrichment of energy-related saccharides was dominated by colloidal polysaccharides (Figure 7.7c-d). This is likely due to bulky glucan and fructan polysaccharides which are found to be effectively transported to the ocean surface by scavenging on bubble surfaces.[271, 330, 339] Further, these bulky colloids could easily drain back to the SSML during the bubble ageing, thus, higher EFs could observe in SSML than foam (Figure 7.6d-e). High molecular weight saccharides dominated the enrichment of structure-related saccharides (Figure 7.7e-f) showing 2-4 times higher enrichment than total dissolved saccharides. This enrichment was more prominent in foam than SSML. This is likely due to higher surface activity of these saccharides than other saccharide types. Interestingly, low molecular weight oligo/polysaccharides were depleted in both SSML and foam for structure-related saccharides. This indicates that low molecular weight oligo/polysaccharides are

effectively transformed to high molecular weight polysaccharides at the ocean surface. The actual reason for this transformation is not known; possibly it may due to higher photo-chemical reaction rates at air-water interface due to high light intensity and oxygen supply.

Interestingly, free monosaccharide fraction of glucose, galactose, fructose, xylitol, arabitol and mannitol were significantly enriched in SSML and foam with EFs ranging from 3-18 despite their complete solubility in water. This suggest a preferential movement of these water soluble saccharides towards the ocean surface and provide experimental evidences to support the theoretical concept of the model OCEANFILM-2 that describes co-adsorption of water soluble saccharides on organic surfactants and their enrichment at air-water interface.[340] In addition, the enrichment of free monosaccharides at the ocean surface may also result from, active movements of bacteria towards surface active oligo/polysaccharides that are enriched and resides at ocean surface and faster enzymatic hydrolysis rates at the air-water interface due to favorable conditions (e.g. higher temperature and dissolved oxygen).[75, 317]

7.5 Conclusions

Here we provide the first quantitative enrichment of saccharides on bubble film surfaces where SSA is actually generated. We observed higher saccharide enrichment in foam layer than SSML and further ageing of bubbles could result an extremely organic enriched SSA. Structure-related saccharides coagulate to form higher molecular weight saccharides are selectively enriched in ocean surface. Thus, structure-related saccharides are expected to be selectively transfer to larger SSA and unlikely to find in sub-micron

size particles. The quantitative results obtained from this study support the theoretical concept of free monosaccharide enrichment in ocean surface[258, 340] and field observations of different saccharide transfer pathways to fine and coarse SSA.[28]

7.6 Supporting Information

Table S7.1: Concentration of saccharides in different size fractions.

7.7 Acknowledgement

For their contributions to IMPACTS, we thank Prof. Kimberly Prather Research Group members, Christopher Lee, Camille Sultana, Josh Cox, Matthew Pendergraft, Grace Irumva and Hosiana Abewe at the University of California-San Diego. We thank Zehra Khan and Josh Kettler at the University of Iowa for assistance with sample preparation. This work was funded by the National Science Foundation through the Center of Chemical Innovation Program under grant CHE 1305427.

Figure 7.1: a) A picture showing the marine aerosol reference tank (MART) used for the experiment and b) a picture showing the whitecap foam generated on the water surface.

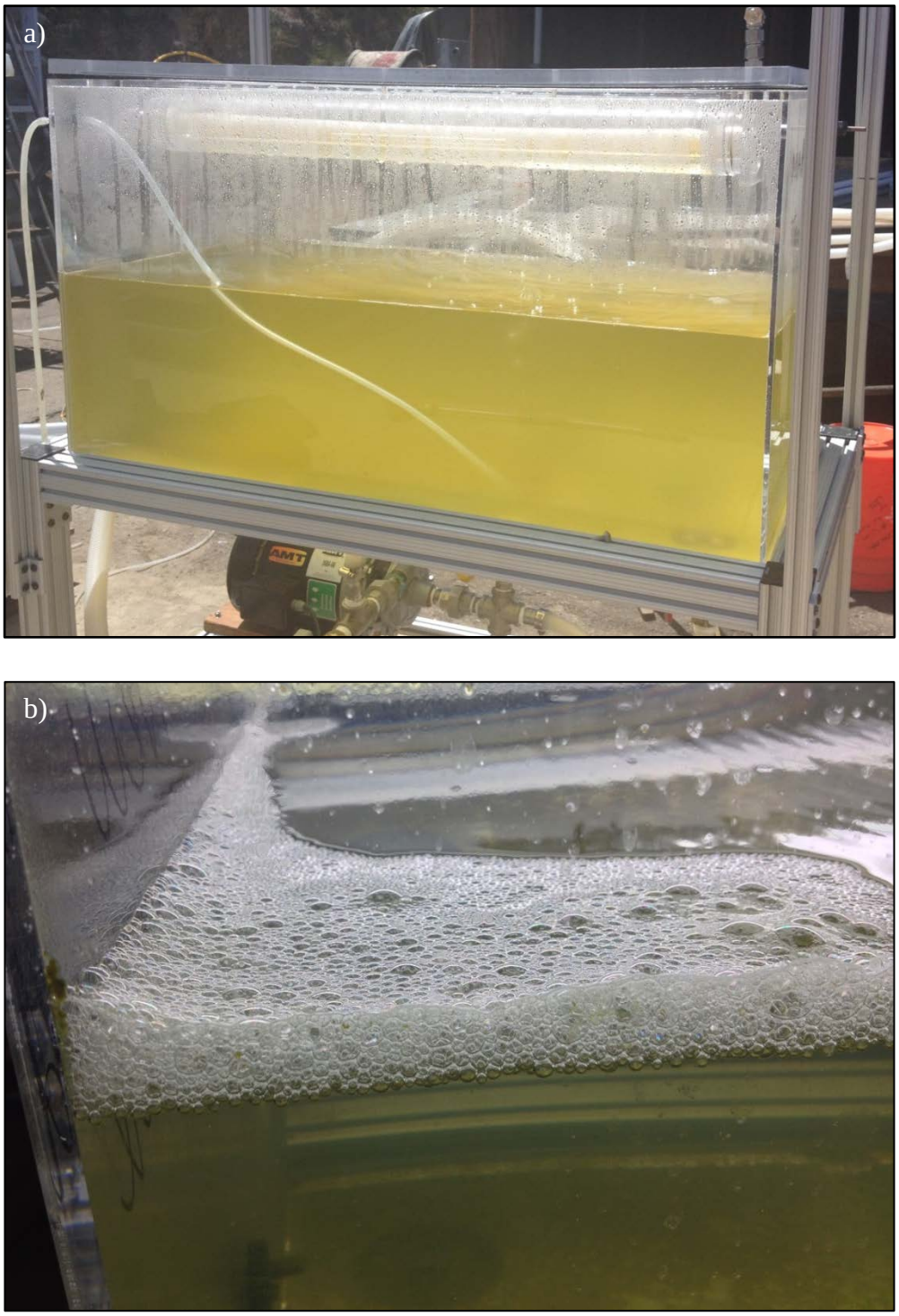

Figure 7.2: Chlorophyll-a concentration and ratio of fucose and rhamnose to arabinose and xylose concentrations in seawater. Chlorophyll-a concentration peaked on day 2 and came to a minimum on day 5. Saccharide ratio decreased below 1 from day 4 indicating higher bacterial activity from day 4-9.

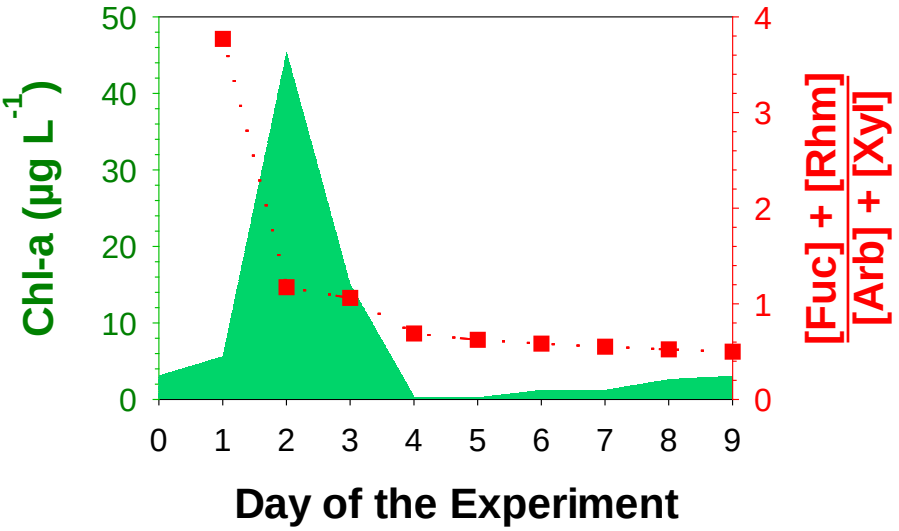

Figure 7.3: Variation of sugar alcohol (a-c), energy-related saccharide (d-e) and structure-related saccharide (f-l) concentrations during the mesocosm experiment.

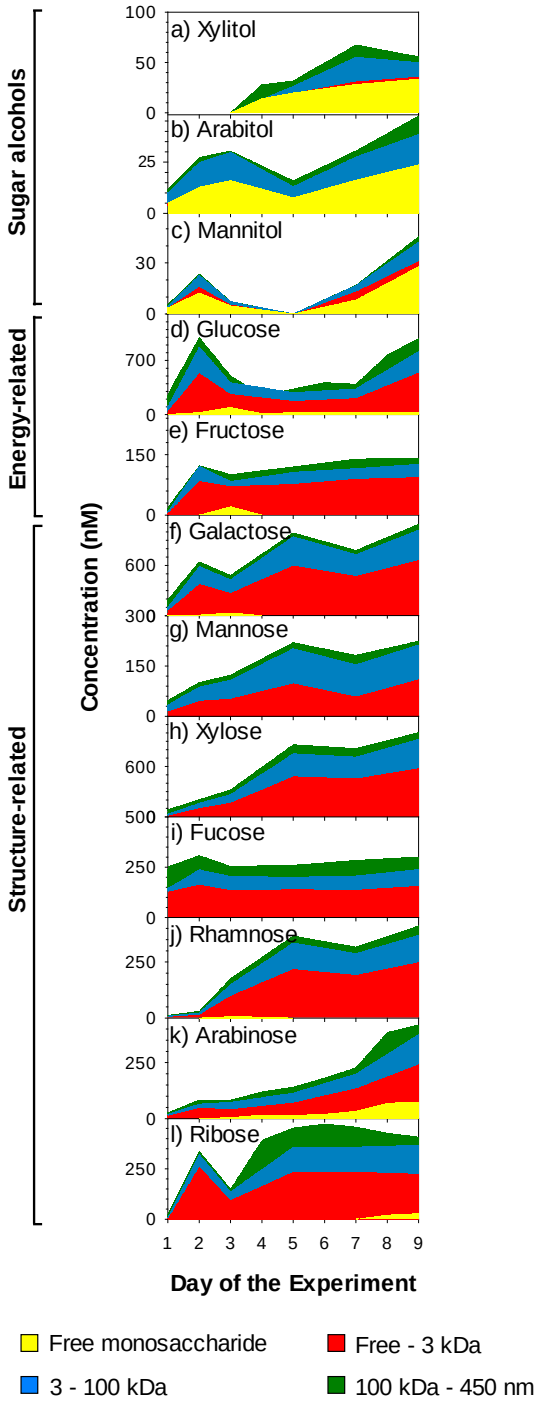

Figure 7.4: Relative composition of sugar alcohols (a), energy-related saccharides (b) and structure-related saccharides (c) in different size fractions.

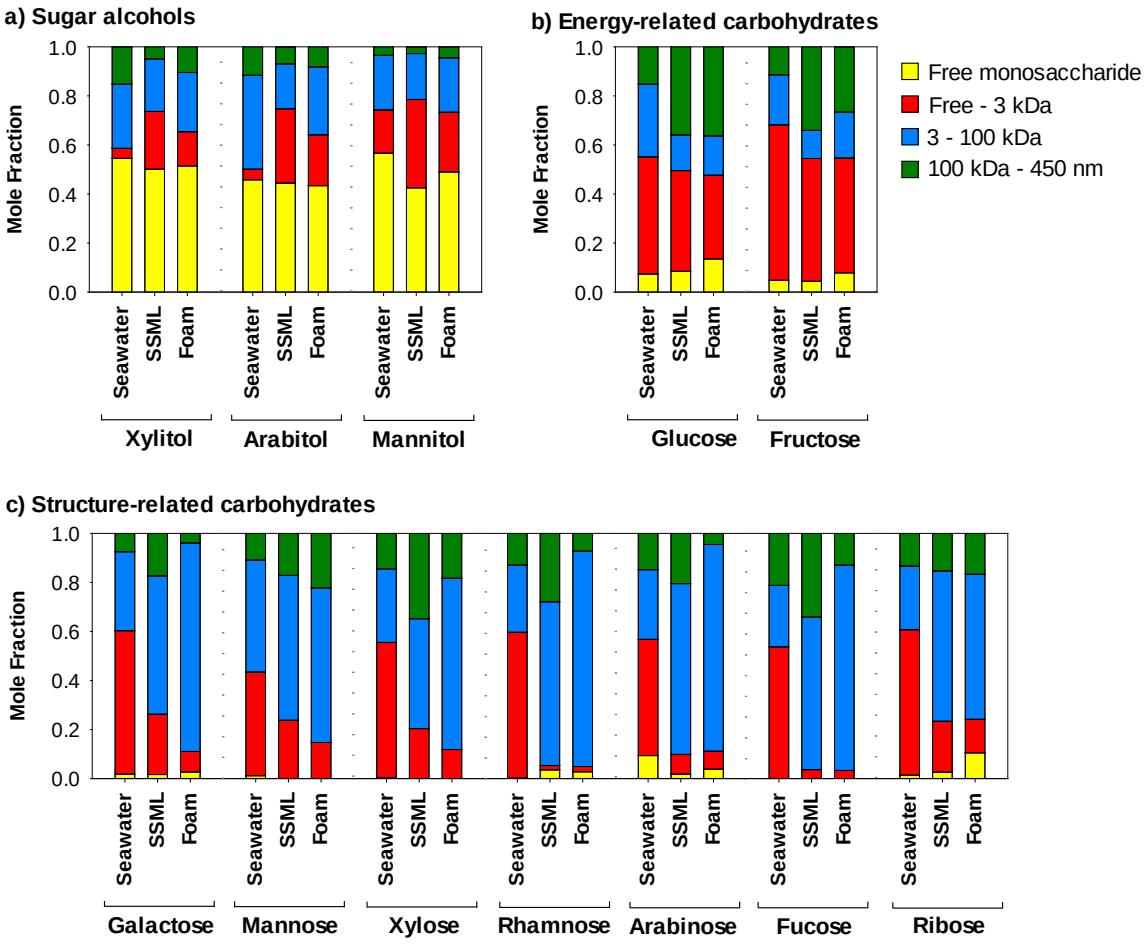

Figure 7.5: Boxplot graphs showing (a) EF of total saccharides (<450 nm) in SSML (n=9) and foam (n=7). (The two end caps indicate the data range, box indicate the first quartile, median and third quartile, respectively). All the carbohydrates were significantly enriched in SSML and foam.

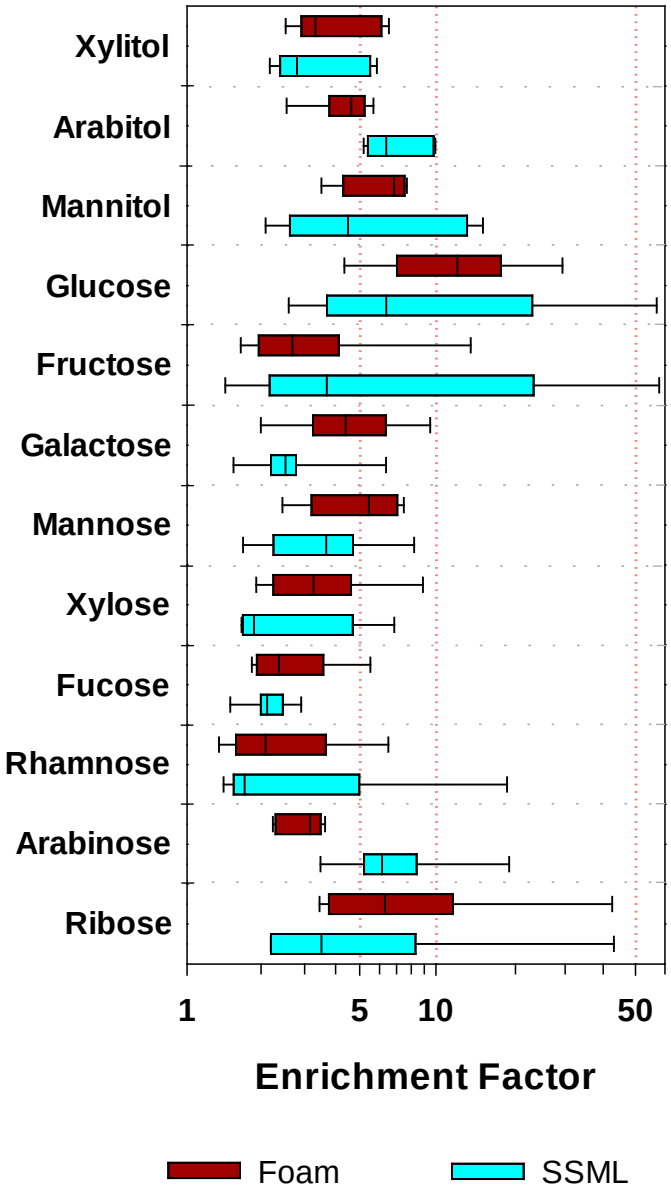

Figure 7.6: Daily variation of total saccharide (<450 nm) enrichment factors.

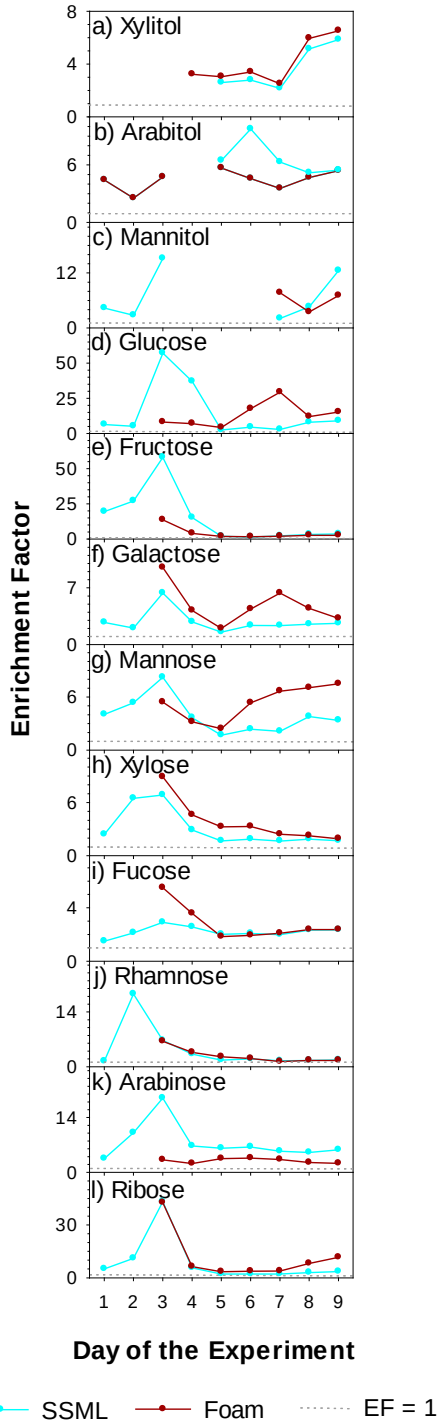

Figure 7.7: Enrichment of different saccharide fractions of (a-b) xylitol, (c-d) glucose and (e-f) fucose in SSML and foam. Error bars represent propagated analytical uncertainty.

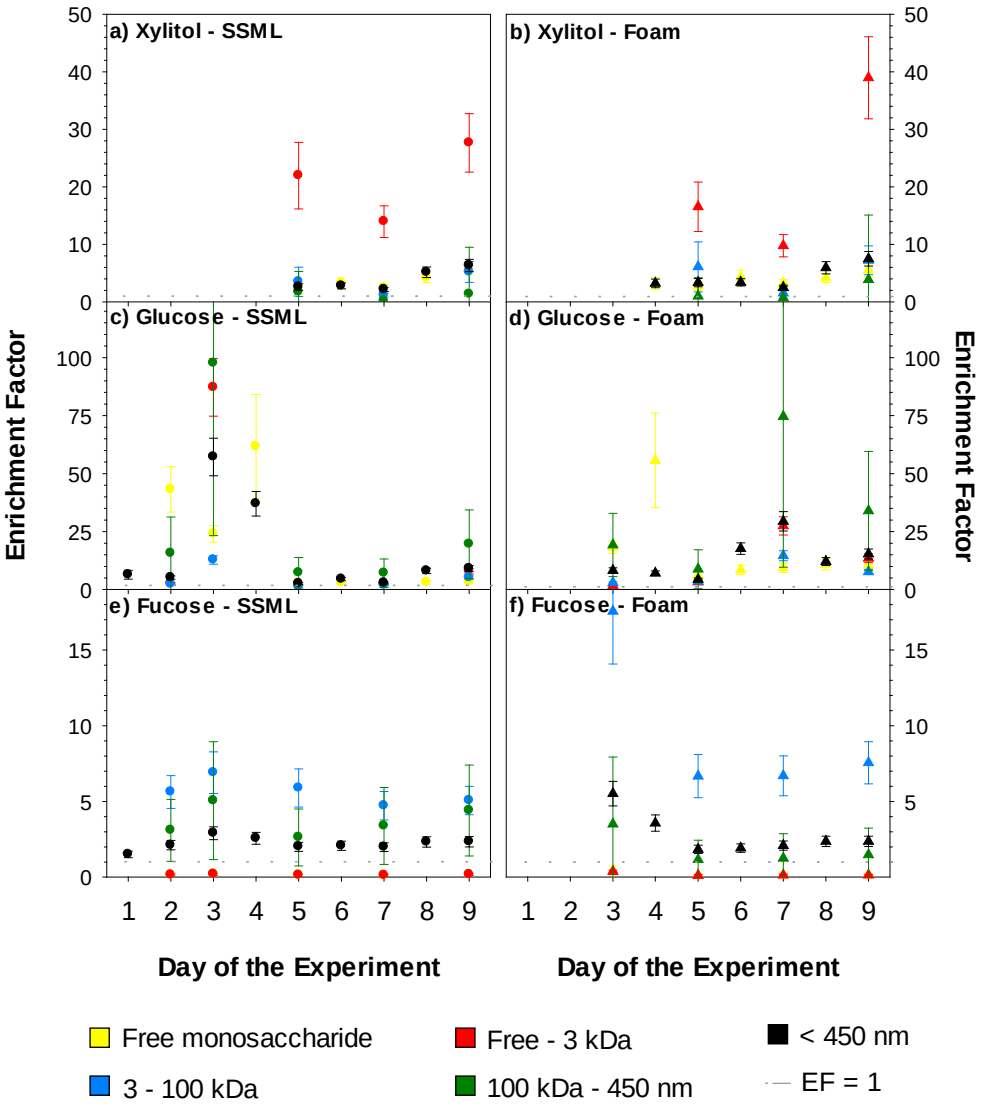

CHAPTER EIGHT

CONCLUSIONS AND FUTURE DIRECTIONS

8.1 Conclusions

The focus of the research presented in this dissertation is chemical characterization of atmospheric aerosols. Atmospheric aerosols impact the Earths' radiative balance, climate, biogeochemical cycles and human health.[2] Biomass burning and sea spray aerosols are two of the most important natural sources of primary atmospheric aerosols with significant influence on aerosol properties. Although it is widely accepted that the role of the biomass burning and sea spray aerosols in atmospheric chemistry and climate is crucial, the chemical composition and total atmospheric flux is not fully understood yet.[26, 60, 341] Therefore, the research projects reported in this thesis were designed to improve the understanding of the chemical composition of biomass burning and sea spray aerosols, and to compute more representative emission factors for biomass burning emissions.

Biomass burning is the main source of primary fine carbonaceous particles in the atmosphere as well the second largest source of trace gases.[93] Despite its large role in atmospheric chemistry, many important unknowns limit our understanding of smoke impacts on the environment and human health. A number of studies indicate that large amounts of unidentified, gases and particles are present in biomass smoke and those are vary by fuel type and with burning conditions.[93] To fill this gap, aerosol samples were collected during the FLAME-4 field campaign (2012) in order to investigate the chemical composition of aerosols emitted by different biomass types under different burning conditions. Fuel-based emission factors (mass of pollutant per kilogram fuel burned) of

organic and inorganic species in biomass smoke were calculated to build-up emission profiles for different fuel types. Chapter 3 presented the chemical composition and EFs of the $PM_{2.5}$ emitted from biomass combustion, representing five different fuel categories including conifers, agricultural residues, grasses and other perennials, peat and cookstoves. The EFs were computed for $PM_{2.5}$ mass, OC, EC, WSOC, water-soluble inorganic ions, metals and organic species using various analytical techniques. Generally, EFs varied with fuel type and the geographic location where it was harvested, burning condition (stack vs room) and MCE indicating the influence of those factors on PM emissions. Our measurements spanned a variety of fuel types collected from different geographical locations and a large range of MCEs. These chemical profiles have provided better parameterizations of direct radiative forcing by using EC and OC to estimate single-scattering albedo (SA) and absorption Ångström exponent (AAE).[342 86, 89, 102]

Emissions of fine particle water-soluble fluoride (F^-) from biomass burning were evaluated and research findings were discussed in Chapter 4. When F^- was quantified, it accounted for an average (± standard error) of 0.13 ± 0.02 % of $PM_{2.5}$. Based on recent evaluations of global biomass burning, we estimate that biomass burning releases 76 Gg F^- yr^{-1} to the atmosphere, with lower and upper bounds of 40 – 150 Gg F^- yr^{-1}. The estimated F^- flux from biomass burning is comparable to total fluorine emissions from coal combustion plus other anthropogenic sources (Figure 8.1). These data demonstrate the biomass burning represents a major source of fluorine to the atmosphere in the form of fine particles, which have potential to undergo long-range transport.

Chapter 5 focused on the chemical characterization of $PM_{2.5}$ collected from authentic *in-situ* peat smoke during the 2015 El Niño peat fire episode in Central Kalimantan, Indonesia. Overall, chemical speciation revealed the following characteristics of peat burning emissions: high OC mass fractions (72 %), very low EC mass fractions (1 %), vanillic to syringic acid ratios of 1.9 (compared to other biomass burning emissions that are <1), relatively high n-alkane contributions to OC (6.2 %). These characteristics distinguish peat burning aerosols from other combustion emissions. The EFs were converted to emission estimates using burned area, burn depth and peat bulk density, and it was estimated that 3.2 - 11 Tg of $PM_{2.5}$ emitted to atmosphere during 2015 El Niño peat fires. Combined with gas-phase measurements of CO_2, CO, CH_4 and VOC from Stockwell et al. (2016), it is determined that OC and EC comprise to 2.1 % and 0.04 % of total carbon emissions, respectively. This is the first comprehensive *in-situ* field measurement of peat fire PM emissions that are expected to provide better representation of peatland fires.

The EFs reported herein can be integrated with databases that provide estimates of global biomass consumption to produce total global biomass burning emission estimates using atmospheric models. The first comprehensive global emission inventories were published by Andreae and Merlet in 2001 compiling all the EF data available at that time. They categorized biomass burning into 6 different categories; savanna and grassland, tropical forest, extratropical forest, biofuel, charcoal and agricultural residues and was primarily focused on gaseous emissions. The next effort of updating the emission inventories was led by Akagi et al. in 2011 using the EFs computed until 2010. Akagi et al. added biomass burning categories for peatland fires, chaparral burning, cooking fires,

dung burning and garbage burning in addition to previous, and included more gas and particle phase species relative to Andreae and Merlet (2001). New data presented in this thesis will improve the representativeness of EF used in regional and global emissions inventories, particularly for peatland fire emissions as currently used EFs for peat fires based on a lab study of a single sample. Further, we showed that certain biomass species, especially peat and ocote produce high amounts of PAHs than other fuels. Thus, people who live near the peat burning sites and who regularly use these types of firewood face significant health risks.

The second half of this thesis focused on aerosols generated from ocean wave breaking. The ocean represents a major source of primary aerosol emissions, emitting an estimated 2-100 × 10^{15} g of sea spray aerosol (SSA) per year.[58, 61, 254, 255 256] Traditionally, SSA was thought to be completely salt. But recent research findings discovered that SSA is a complex mixture of both organics and inorganics, and organic fraction can dominate the aerosol mass fraction in ultrafine particles.[22] Carbohydrates (a.k.a. saccharides) are omnipresent in seawater and due to the surface active nature of polysaccharides, they have been identified as a class of organic matter that is likely enriched at the air-water interface and sea spray aerosol.[60] The mechanism proposed for this enrichment is the scavenging by rising bubbles and the rise of organic colloids through positive buoyancy, leading to the accumulation of organic matter at SSML where SSA is formed.[81] However, quantitative data for carbohydrate composition or its enrichment at air-water interface and SSA were previously not available. In Chapter 6, we have shown that saccharides comprise a significant fraction of organic matter in fine and coarse SSA (11% and 27%, respectively), with oligo/polysaccharides the major form of saccharides. Relative to

sodium, individual saccharides were enriched 14-1314 times in fine SSA, 3-138 times in coarse SSA, but only up to 1.0-16.2 times in SSML. Enrichments in SSML were attributed to rising bubbles that scavenge surface-active species from seawater, while further enrichment into SSA likely derives from bubble films. Fine SSA particles exhibited the greatest EF and were generated in part by film drops by the bursting of bubble caps that are enriched in highly-surface active organic matter (Figure 8.2). Coarse SSA largely generated by jet drops incorporate less-enriched portions of the SSML, giving rise to EF values less than fine SSA, but greater than SSML. Thus, bubble film plays a significant role in the enrichment process. To the best of our knowledge, enrichments of organic matter have not been quantitatively evaluated previously for persistent bubble films or sea foam. Chapter 7 provides the first quantitative enrichment of saccharides on bubble film surfaces and we showed higher saccharide enrichment in foam layer than SSML confirming the high enrichment of saccharides that formed via rupturing the bubble film. Further, ultra-filtration of saccharides to different size fractions showed that structure-related saccharides (e.g. galactose, fucose, rhamnose, arabinose, xylose) tend to coagulate and form higher molecular weight saccharides, and are selectively transferred to ocean surface. Most likely divalent cations facilitate this coagulation process acting as binding agents as evident by higher concentration of Ca^{2+}, Mg^{2+} in SSML and foam than seawater. The quantitative results obtained from this study support the theoretical concepts of saccharide transfer via ocean-air interface and to interpret the field observations of organic matter enrichment in SSA.

Our sea spray aerosol studies showed that organic matter, saccharides and inorganic ions are selectively enriched in SSA. Further, higher enrichments were

observed during phytoplankton bloom periods indicating the influence of ocean biology in this selective transfer. Therefore, the composition of SSA is dynamic and should not assume to be the same as seawater. Thus, complex parameterizations based on actual chemical composition of SSA, considering the effects of enrichment should be incorporated in future atmospheric and climate model estimations. Further, these improved chemical profiles of SSA should use to inform laboratory proxies to assess SSA physical properties such as hygroscopicity, CCN and IN activity.

It has been shown that 45 % of the variance of aerosol radiative forcing arises from uncertainties in natural emissions mainly from volcanic SO_2, marine DMS, biogenic VOCs, biomass burning and seaspray.[343] My graduate work was focused on two of these sources, and my research findings enhanced the current knowledge in chemical composition of biomass burning and sea spray aerosols. The use of new chemical profiles in atmospheric, climate and source apportionment models will reduce the associated uncertainties and will facilitate towards more accurate model predictions.

8.2 Future Directions

The research findings presented in this dissertation, opens-up new avenues to continue future work to improve further understanding of biomass burning emissions. The computed EFs and emission profiles in these studies correspond to fresh biomass burning PM that was sampled few meters away from the emission source. The PM was always collected after smoke was cooled to ambient temperature, to allow for gas-particle partitioning to be equilibrate. However, the PM resident time in ambient air is only seconds to minutes by the time of collection. Thus, biomass burning PM was neither

diluted nor exposed enough to sunlight, other atmospheric aerosols (e.g. mineral dust) and gasses. Chamber experiments have shown that $EF_{PM2.5}$ could be reduced >50 % at ×100 dilution for wood smoke. This reduction was primarily due to changes in partitioning of semivolatile organic compounds, which at undiluted conditions semivolatile species largely occur in the particle phase while under diluted conditions semivolatile species shifts towards the gas phase in order to maintain phase equilibrium.[344] In contrast, gas phase and semivolatile species in the smoke can undergo photochemical reactions by varies oxidants in the atmosphere such as hydroxyl, ozone and nitrate increasing their ability to partition in to particle phase. Further, smoke can also condense on to existing atmospheric particles such as mineral dust increasing the particle concentration in the emission plume.[345] Thus, atmospheric dilution can decrease the $EF_{PM2.5}$ while atmospheric residence time can increase the $EF_{PM2.5}$. Since PM sampling techniques involved in our experiments were stationary, the described changes that take place over the spatial and temporal scales were not accounted in EF calculations. Therefore, understanding this gap will further reduce the uncertainties associated with $EF_{PM2.5}$. To this end several PM samples should be simultaneously collected at regular distances (e.g. 2 m, 10 m, 100 m, 1 km, 10 km) from the downwind of the emission source. Filter loading may be an issue due to dilution, and high volume samplers can be used to overcome this issue. Using an air craft to sample along the flow path of the smoke is another option to collect samples. As CO concentration is relatively constant in ambient air, it can use as a reference species to assess the atmospheric dilution. As we have capabilities to quantify ~150 gas and particle phase species we can evaluate the relative concentration of the same species in different samples. The

concentrations can convert to EFs following the mass balance approach. The EFs computed for different samples could be compared to understand their changes due to increased dilution and atmospheric residence time. Possibly a mathematical relationship could be developed to use as a correction for atmospheric dilution and secondary processing to minimize those effects on EF calculations.

The next step in understanding the transfer of saccharides to SSA is to evaluate its phase state. Our research to date suggests that energy-related saccharides are efficiently transferred to fine SSA and structure-related saccharides in to coarse SSA. The different saccharide profiles of fine and coarse SSA are expected to result from the exclusion of particulate organic matter associated structure-related saccharides from SSA particles that are relatively smaller in size. Particulate organic matter is heavier than dissolved organic matter, and likely drains from the bubble surface prior to bursting. Thus, POM hardly transfer to film drops that generate via rupturing the upper bubble cap.[28] However, further studies are needed to fully understand the transfer of different saccharide types in to different size fractions of SSA. In this purpose SSA samples should be collected into different size fractions using a cascade impactor during a mesocosm experiment. Along with SSA, bulk seawater, SSML and foam samples should be collected. The liquid samples and SSA extracts then should be filtered using an ultra-filtration setup as a means of fractioning dissolved, colloidal, and particulate species with size cuts of 0.7 µm, 0.45 µm, 0.1 µm, 100 KDa, and 3 KDa (Table 8.1).[76, 114] Then the each fraction should be hydrolyzed and analyze for saccharides. The saccharide profile of different SSA sizes then could be compared with the saccharide composition of different organic matter classes in order to accurately understand the saccharide transfer pathways via ocean-air

interface. This will provide the insights of organic matter composition in different size fractions of SSA. Similarly, different organic compounds have different physical properties such as surface activity. Therefore, the physical characteristics of the organic molecules can be taken into account to understand the hygroscopicity, cloud condensation and ice nucleation properties of individual SSA particles.

Enzymes play a significant role in cleaving large organic matter (e.g. lipopolysaccharides) in to smaller organic compounds.[76] Thus, effect of enzymes in saccharide enrichment should be assessed using laboratory model studies. For this purpose, larger organic molecules like LPS, dextrin, pectin and alginic acid should be spiked in to artificial seawater with a smaller amount of their cleaving enzymes (lipase, amylase and protease). Aerosols should be generated by artificial aerosol generation techniques at regular intervals and sampled SSA should be analyzed along with bulk seawater for saccharides to examine the effects of enzyme activity on saccharide transfer. This will further enhance our current knowledge in the effects of microbial loop in the transfer of organic species to SSA from seawater.

Figure 8.1: Particulate fluoride emission from biomass burning.

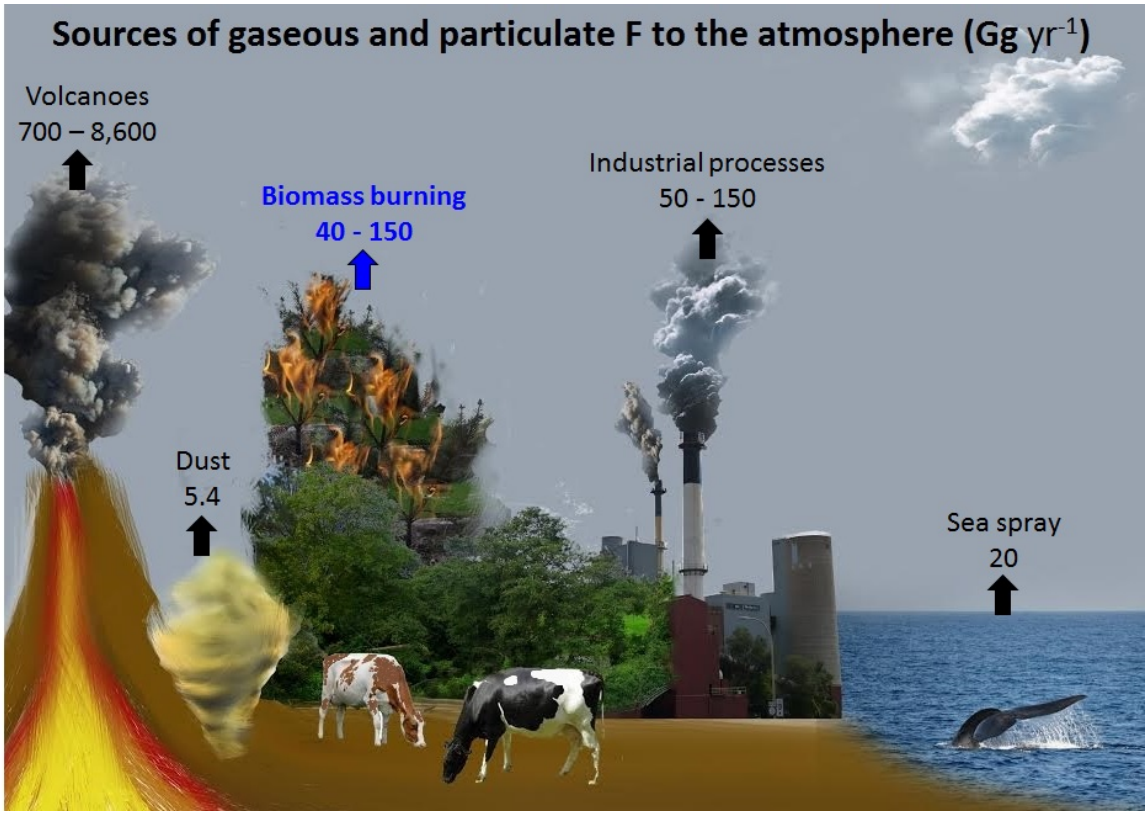

Figure 8.2: Enrichment of saccharides in SSA.

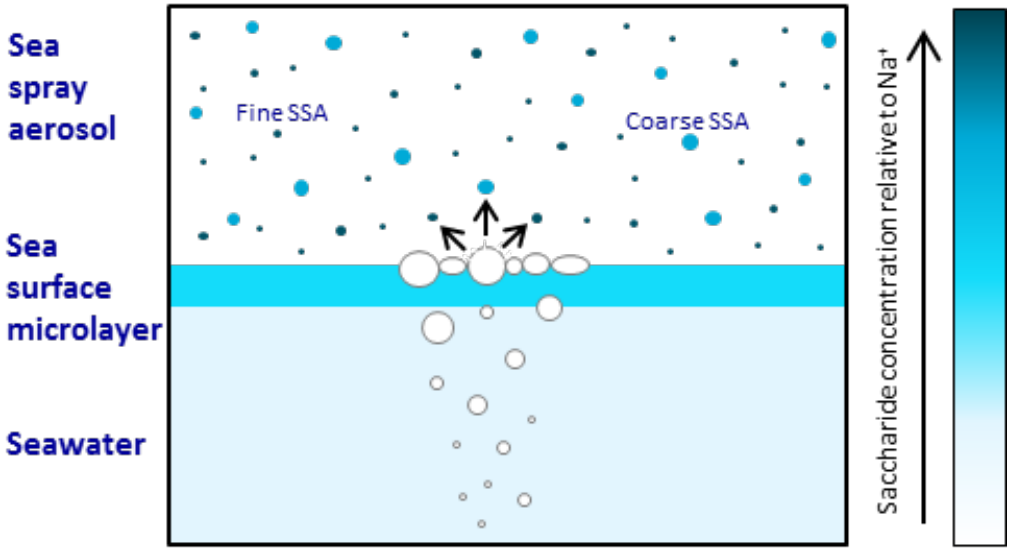

Table 8.1: Ultrafiltration filter cut sizes and corresponding classes of organic matter.

Filter Cut size	Organic matter category	Examples
No filtering	particulate, colloidal, dissolved	Micro-organism (e.g. diatoms, bacteria), structural materials (e.g. cell wall), POM, TEP and all the organic compounds/classes listed below
0.7 µm	particulate, colloidal, dissolved	Nano & micro-hydrogels, organic aggregates, POM, DOM and all the organic compounds/classes listed below
0.45 µm	particulate, colloidal, dissolved	Nano & micro-hydrogels, organic aggregates, POM, DOM and all the organic compounds/classes listed below
0.1 µm	colloidal, dissolved	DOM, gelation & annealing compounds and all the organic compounds/classes listed below
100 KDa	dissolved	Free fibrils, high molecular weight organic compounds and all the organic compounds/classes listed below
3 KDa	solutes	Free polymers, low molecular weight organic compounds

REFERENCES

1. Pöschl, U., Atmospheric Aerosols: Composition, Transformation, Climate and Health Effects. *Angew. Chem. Int. Ed.* **2005,** *44*, (46), 7520-7540.
2. Seinfeld, J. H.; Pandis, S. N., *Atmospheric Chemistry and Physics, From Air Pollution to Climate Change*. John Wiley & Sons, New York: 1998; Vol. 1326.
3. Prospero, J.; Charlson, R.; Mohnen, V.; Jaenicke, R.; Delany, A.; Moyers, J.; Zoller, W.; Rahn, K., The Atmospheric Aerosol System: An Overview. *Rev. Geophys.* **1983,** *21*, (7), 1607-1629.
4. Malm, W. C.; Schichtel, B. A.; Pitchford, M. L.; Ashbaugh, L. L.; Eldred, R. A., Spatial and Monthly Trends in Speciated Fine Particle Concentration in the United States. *J. Geophys. Res. Atmos.* **2004,** *109*, (D3).
5. Kundu, S.; Stone, E. A., Composition and Sources of Fine Particulate Matter Across Urban and Rural Sites in the Midwestern United States. *Env. Sci. Process. Impact* **2014,** *16*, (6), 1360-1370.
6. Prather, K. A.; Hatch, C. D.; Grassian, V. H., Analysis of Atmospheric Aerosols. *Annu. Rev. Anal. Chem.* **2008,** *1*, 485-514.
7. Gankanda, A.; Coddens, E. M.; Zhang, Y.; Cwiertny, D. M.; Grassian, V. H., Sulfate Formation Catalyzed by Coal Fly Ash, Mineral Dust and Iron(iii) Oxide: Variable Influence of Temperature and Light. *Env. Sci. Process. Impact* **2016,** *18*, (12), 1484-1491.
8. Gankanda, A.; Grassian, V. H., Nitrate Photochemistry in NaY Zeolite: Product Formation and Product Stability under Different Environmental Conditions. *J. Phys. Chem. A* **2013,** *117*, (10), 2205-2212.
9. Gankanda, A.; Cwiertny, D. M.; Grassian, V. H., Role of Atmospheric CO_2 and H_2O Adsorption on ZnO and CuO Nanoparticle Aging: Formation of New Surface Phases and the Impact on Nanoparticle Dissolution. *J. Phys. Chem. C* **2016,** *120*, (34), 19195-19203.
10. Gankanda, A.; Grassian, V. H., Nitrate Photochemistry on Laboratory Proxies of Mineral Dust Aerosol: Wavelength Dependence and Action Spectra. *J. Phys. Chem. C* **2014,** *118*, (50), 29117-29125.
11. Tang, M.; Larish, W. A.; Fang, Y.; Gankanda, A.; Grassian, V. H., Heterogeneous Reactions of Acetic Acid with Oxide Surfaces: Effects of Mineralogy and Relative Humidity. *J. Phys. Chem. A* **2016,** *120*, (28), 5609-5616.
12. Usher, C. R.; Michel, A. E.; Grassian, V. H., Reactions on Mineral Dust. *Chem. Rev.* **2003,** *103*, (12), 4883-4940.
13. Lim, S.; Lee, M.; Lee, G.; Kim, S.; Yoon, S.; Kang, K., Ionic and Carbonaceous Compositions of PM_{10}, $PM_{2.5}$ and $PM_{1.0}$ at Gosan ABC Superstation and Their Ratios as Source Signature. *Atmos. Chem. Phys* **2012,** *12*, 2007-2024.
14. Pandis, S. N.; Harley, R. A.; Cass, G. R.; Seinfeld, J. H., Secondary Organic Aerosol Formation and Transport. *Atmos. Environ. Part A* **1992,** *26*, (13), 2269-2282.
15. Katzman, T. L.; Rutter, A. P.; Schauer, J. J.; Lough, G. C.; Kolb, C. J.; Van Klooster, S., $PM_{2.5}$ and $PM_{10\text{-}2.5}$ Compositions During Wintertime Episodes of Elevated PM Concentrations across the Midwestern USA. *Aerosol Air Qual. Res* **2010,** *10*, 140-153.

16. Stanier, C.; Singh, A.; Adamski, W.; Baek, J.; Caughey, M.; Carmichael, G.; Edgerton, E.; Kenski, D.; Koerber, M.; Oleson, J., Overview of the LADCO Winter Nitrate Study: Hourly Ammonia, Nitric Acid and PM 2.5 Composition at an Urban and Rural Site Pair During PM 2.5 Episodes in the US Great Lakes Region. *Atmos. Chem. Phys.* **2012,** *12*, (22), 11037-11056.
17. Jayarathne, T.; Rathnayake, C. M.; Stone, E. A., Local Source Impacts on Primary and Secondary Aerosols in the Midwestern United States. *Atmos. Environ.* **2016,** *130*, 74-83.
18. Rathnayake, C. M.; Metwali, N.; Jayarathne, T.; Kettler, J.; Huang, Y.; Thorne, P. S.; O'Shaughnessy, P. T.; Stone, E. A., Influence of Rain on the Abundance of Bioaerosols in Fine and Coarse Particles. *Atmos. Chem. Phys.* **2017,** *17*, (3), 2459-2475.
19. Turpin, B. J.; Huntzicker, J. J., Identification of Secondary Organic Aerosol Episodes and Quantitation of Primary and Secondary Organic Aerosol Concentrations During SCAQS. *Atmos. Environ.* **1995,** *29*, (23), 3527-3544.
20. Bond, T. C.; Bhardwaj, E.; Dong, R.; Jogani, R.; Jung, S.; Roden, C.; Streets, D. G.; Trautmann, N. M., Historical Emissions of Black and Organic Carbon Aerosol from Energy-related Combustion, 1850-2000. *Global Biogeochem. Cycles* **2007,** *21*, (2), GB2018.
21. Christian, T. J.; Kleiss, B.; Yokelson, R. J.; Holzinger, R.; Crutzen, P.; Hao, W. M.; Saharjo, B.; Ward, D. E., Comprehensive Laboratory Measurements of Biomass-burning Emissions: 1. Emissions from Indonesian, African, and Other Fuels. *J. Geophys. Res. Atmos.* **2003,** *108*, (D23).
22. O'Dowd, C. D.; Facchini, M. C.; Cavalli, F.; Ceburnis, D.; Mircea, M.; Decesari, S.; Fuzzi, S.; Yoon, Y. J.; Putaud, J.-P., Biogenically Driven Organic Contribution to Marine Aerosol. *Nature* **2004,** *431*, (7009), 676-680.
23. Chow, J. C.; Chen, L. W. A.; Watson, J. G.; Lowenthal, D. H.; Magliano, K. A.; Turkiewicz, K.; Lehrman, D. E., $PM_{2.5}$ Chemical Composition and Spatiotemporal Variability During the California Regional PM_{10}/$PM_{2.5}$ Air Quality Study (CRPAQS). *J. Geophys. Res.* **2006,** *111*, (D10), D10S04.
24. Lee, T.; Yu, X.-Y.; Kreidenweis, S. M.; Malm, W. C.; Collett, J. L., Semi-continuous Measurement of $PM_{2.5}$ Ionic Composition at Several Rural Locations in the United States. *Atmos. Environ.* **2008,** *42*, (27), 6655-6669.
25. Jayarathne, T.; Stockwell, C. E.; Gilbert, A. A.; Daugherty, K.; Cochrane, M. A.; Ryan, K. C.; Putra, E. I.; Saharjo, B. H.; Nurhayati, A. D.; Albar, I., *et al.*, Chemical characterization of fine particulate matter emitted by peat fires in Central Kalimantan, Indonesia, during the 2015 El Niño. *Atmos. Chem. Phys.* ***in preparation***.
26. Reid, J.; Koppmann, R.; Eck, T.; Eleuterio, D., A Review of Biomass Burning Emissions Part II: Intensive Physical Properties of Biomass Burning Particles. *Atmos. Chem. Phys.* **2005,** *5*, (3), 799-825.
27. Rathnayake, C. M.; Metwali, N.; Baker, Z.; Jayarathne, T.; Kostle, P. A.; Thorne, P. S.; O'Shaughnessy, P. T.; Stone, E. A., Urban Enhancement of PM_{10} Bioaerosol Tracers Relative to Background Locations in the Midwestern United States. *J. Geophys. Res. Atmos.* **2016,** *121*, (9), 5071-5089.

28. Jayarathne, T.; Sultana, C. M.; Lee, C.; Malfatti, F.; Cox, J. L.; Pendergraft, M. A.; Moore, K. A.; Azam, F.; Tivanski, A. V.; Cappa, C. D., *et al.*, Enrichment of Saccharides and Divalent Cations in Sea Spray Aerosol During Two Phytoplankton Blooms. *Environ. Sci. Technol.* **2016,** *50*, (21), 11511-11520.
29. Andreae, M. O.; Crutzen, P. J., Atmospheric Aerosols: Biogeochemical Sources and Role in Atmospheric Chemistry. *Science* **1997,** *276*, (5315), 1052-1058.
30. Laskina, O., Physicochemical Properties of Mineral Dust and Sea Spray Aerosols. *PhD (Doctor of Philosophy) thesis, University of Iowa* **2015**.
31. Mahowald, N.; Ward, D. S.; Kloster, S.; Flanner, M. G.; Heald, C. L.; Heavens, N. G.; Hess, P. G.; Lamarque, J.-F.; Chuang, P. Y., Aerosol Impacts on Climate and Biogeochemistry. *Annu. Rev. Environ. Resour.* **2011,** *36*, (1), 45.
32. Laskina, O.; Morris, H. S.; Grandquist, J. R.; Qin, Z.; Stone, E. A.; Tivanski, A. V.; Grassian, V. H., Size Matters in the Water Uptake and Hygroscopic Growth of Atmospherically Relevant Multicomponent Aerosol Particles. *J. Phys. Chem. A* **2015,** *119*, (19), 4489–4497.
33. DeMott, P. J.; Prenni, A. J.; Liu, X.; Kreidenweis, S. M.; Petters, M. D.; Twohy, C. H.; Richardson, M.; Eidhammer, T.; Rogers, D., Predicting Global Atmospheric Ice Nuclei Distributions and Their Impacts on Climate. *PNAS* **2010,** *107*, (25), 11217-11222.
34. McFiggans, G.; Artaxo, P.; Baltensperger, U.; Coe, H.; Facchini, M. C.; Feingold, G.; Fuzzi, S.; Gysel, M.; Laaksonen, A.; Lohmann, U., The Effect of Physical and Chemical Aerosol Properties on Warm Cloud Droplet Activation. *Atmos. Chem. Phys.* **2006,** *6*, (9), 2593-2649.
35. Quinn, P. K.; Bates, T. S.; Schulz, K. S.; Coffman, D.; Frossard, A.; Russell, L.; Keene, W.; Kieber, D., Contribution of Sea Surface Carbon Pool to Organic Matter Enrichment in Sea Spray Aerosol. *Nat. Geosci.* **2014,** *7*, (3), 228-232.
36. Levin, E.; McMeeking, G.; DeMott, P.; McCluskey, C.; Carrico, C.; Nakao, S.; Jayarathne, T.; Stone, E.; Stockwell, C.; Yokelson, R., Ice-nucleating Particle Emissions from Biomass Combustion and the Potential Importance of Soot Aerosol. *J. Geophys. Res. Atmos.* **2016,** *121*, (10), 5888-5903.
37. Sun, J.; Ariya, P. A., Atmospheric Organic and Bio-aerosols as Cloud Condensation Nuclei (CCN): A Review. *Atmos. Environ.* **2006,** *40*, (5), 795-820.
38. Haywood, J.; Boucher, O., Estimates of the Direct and Indirect Radiative Forcing due to Tropospheric Aerosols: A Review. *Rev. Geophys.* **2000,** *38*, (4), 513-543.
39. Jacobson, M. Z., Global Direct Radiative Forcing due to Multicomponent Anthropogenic and Natural Aerosols. *J. Geophys. Res.* **2001,** *106*, (D2), 1551-1568.
40. Jacobson, M. Z., Strong Radiative Heating Due to the Mixing State of Black Carbon in Atmospheric Aerosols. *Nature* **2001,** *409*, (6821), 695-697.
41. Pope III, C. A., Respiratory Hospital Admissions Associated with PM10 Pollution in Utah, Salt Lake, and Cache Valleys. *Arch. Environ. Health* **1991,** *46*, (2), 90-97.
42. Bell, M. L.; Davis, D. L., Reassessment of the Lethal London Fog of 1952: Novel Indicators of Acute and Chronic Consequences of Acute Exposure to Air Pollution. *Environ. Health Perspect.* **2001,** *109*, (Suppl 3), 389.
43. Brunekreef, B.; Holgate, S. T., Air Pollution and Health. *The lancet* **2002,** *360*, (9341), 1233-1242.

44. Pope III, C. A.; Thun, M. J.; Namboodiri, M. M.; Dockery, D. W.; Evans, J. S.; Speizer, F. E.; Heath Jr, C. W., Particulate Air Pollution as a Predictor of Mortality in a Prospective Study of US Adults. *Am. J. Respir. Crit. Care Med.* **1995,** *151*, (3), 669-674.
45. Dominici, F.; Peng, R. D.; Bell, M. L.; Pham, L.; McDermott, A.; Zeger, S. L.; Samet, J. M., Fine Particulate Air Pollution and Hospital Admission for Cardiovascular and Respiratory Diseases. *Jama* **2006,** *295*, (10), 1127-1134.
46. Le Tertre, A.; Medina, S.; Samoli, E.; Forsberg, B.; Michelozzi, P.; Boumghar, A.; Vonk, J.; Bellini, A.; Atkinson, R.; Ayres, J., Short-term Effects of Particulate Air Pollution on Cardiovascular Diseases in Eight European Cities. *J Epidemiol Community Health* **2002,** *56*, (10), 773-779.
47. Anderson, H. R.; Limb, E. S.; Bland, J. M.; De Leon, A. P.; Strachan, D. P.; Bower, J. S., Health Effects of an Air Pollution Episode in London, December 1991. *Thorax* **1995,** *50*, (11), 1188-1193.
48. WHO, Air Quality Guidelines for Particulate Matter, Ozone, Nitrogen Dioxide and Sulfur Dioxide. *World Health Organization, Global Update 2005, Summary of Risk Assessment* **2005**.
49. Stockwell, C. E.; Jayarathne, T.; Cochrane, M. A.; Ryan, K. C.; Putra, E. I.; Saharjo, B. H.; Nurhayati, A. D.; Albar, I.; Blake, D. R.; Simpson, I. J., Field Measurements of Trace Gases and Aerosols Emitted by Peat Fires in Central Kalimantan, Indonesia, During the 2015 El Niño. *Atmos. Chem. Phys.* **2016,** *16*, (18), 11711-11732.
50. Jayarathne, T.; Stockwell, C. E.; Bhave, P. V.; Praveen, P. S.; Rathnayake, C. M.; Islam, R. M.; K, P. A.; Adhikari, S.; Maharjan, R.; Goetz, J. D., *et al.*, Nepal Ambient Monitoring and Source Testing Experiment (NAMaSTE): Emissions of Particulate Matter from Wood and Dung Cooking Fires, Garbage and Crop Residue Burning, Brick kilns, and Other Sources. *Atmos. Chem. Phys.* ***in preparation***.
51. Kelly, F. J., Oxidative Stress: Its Role in Air Pollution and Adverse Health Effects. *Occup. Environ. Med.* **2003,** *60*, (8), 612-616.
52. Sørensen, M.; Autrup, H.; Møller, P.; Hertel, O.; Jensen, S. S.; Vinzents, P.; Knudsen, L. E.; Loft, S., Linking Exposure to Environmental Pollutants with Biological Effects. *Mutat Res Rev Mutat Res.* **2003,** *544*, (2), 255-271.
53. Armstrong, B.; Hutchinson, E.; Unwin, J.; Fletcher, T., Lung Cancer Risk after Exposure to Polycyclic Aromatic Hydrocarbons: A Review and Meta-analysis. *Environ. Health Perspect.* **2004**, 970-978.
54. Khalili, N. R.; Scheff, P. A.; Holsen, T. M., PAH Source Fingerprints for Coke Ovens, Diesel and, Gasoline Engines, Highway Tunnels, and Wood Combustion Emissions. *Atmos. Environ.* **1995,** *29*, (4), 533-542.
55. Fethke, N. B.; Peters, T. M.; Leonard, S.; Metwali, M.; Mudunkotuwa, I. A., Reduction of Biomechanical and Welding Fume Exposures in Stud Welding. *Ann Occup Hyg.* **2016,** *60*, (3), 387-401.
56. Downard, J.; Singh, A.; Bullard, R.; Jayarathne, T.; Rathnayake, C. M.; Simmons, D. L.; Wels, B. R.; Spak, S. N.; Peters, T.; Beardsley, D., Uncontrolled Combustion of Shredded Tires in a Landfill–Part 1: Characterization of Gaseous and Particulate Emissions. *Atmos. Environ.* **2015,** *104*, 195-204.
57. Eakins, B.; Sharman, G. In *Volumes of the World's Oceans From ETOPO1*, NOAA National Geophysical Data Center, Boulder, CO, 2010.

58. O'Dowd, C. D.; de Leeuw, G., Marine Aerosol Production: A Review of the Current Knowledge. *Phil. Trans. R. Soc. A* **2007,** *365*, (1856), 1753-1774.
59. Duce, R. A.; Hoffman, E. J., Chemical Fractionation at the Air-Sea Interface. *Annu. Rev. Earth Planet. Sci.* **1976,** *4*, 187.
60. Quinn, P. K.; Collins, D. B.; Grassian, V. H.; Prather, K. A.; Bates, T. S., Chemistry and Related Properties of Freshly Emitted Sea Spray Aerosol. *Chem. Rev.* **2015,** *115*, (10), 4383-4399.
61. de Leeuw, G.; Andreas, E. L.; Anguelova, M. D.; Fairall, C.; Lewis, E. R.; O'Dowd, C.; Schulz, M.; Schwartz, S. E., Production Flux of Sea Spray Aerosol. *Rev. Geophys.* **2011,** *49*, (2), 1-39.
62. Spiel, D. E., On the Births of Film Drops From Bubbles Bursting on Seawater Surfaces. *J. Geophys. Res. Oceans.* **1998,** *103*, (C11), 24907-24918.
63. Lewis, E. R.; Schwartz, S. E., *Sea Salt Aerosol Production: Mechanisms, Methods, Measurements, and Models-A Critical Review*. American Geophysical Union: 2004; p 777-780.
64. Collins, D.; Zhao, D.; Ruppel, M.; Laskina, O.; Grandquist, J.; Modini, R.; Stokes, M.; Russell, L.; Bertram, T.; Grassian, V., Direct Aerosol Chemical Composition Measurements to Evaluate the Physicochemical Differences Between Controlled Sea Spray Aerosol Generation Schemes. *Atmos. Meas. Tech.* **2014,** *7*, (11), 3667-3683.
65. Andreae, M.; Rosenfeld, D., Aerosol Cloud Precipitation Interactions. - Part 1. The Nature and Sources of Cloud-active Aerosols. *Earth-Sci. Rev.* **2008,** *89*, (1), 13-41.
66. McCluskey, C. S.; Hill, T. C.; Malfatti, F.; Sultana, C. M.; Lee, C.; Santander, M. V.; Beall, C. M.; Moore, K. A.; Cornwell, G. C.; Collins, D. B., *et al.*, A Dynamic Link between Ice Nucleating Particles Released in Nascent Sea Spray Aerosol and Oceanic Biological Activity during Two Mesocosm Experiments. *J. Atmos. Sci.* **2017,** *74*, (1), 151-166.
67. Jaeglé, L.; Quinn, P. K.; Bates, T. S.; Alexander, B.; Lin, J. T., Global Distribution of Sea Salt Aerosols: New Constraints from In-situ and Remote Sensing Observations. *Atmos. Chem. Phys.* **2011,** *11*, (7), 3137-3157.
68. O'Dowd, C. D.; Langmann, B.; Varghese, S.; Scannell, C.; Ceburnis, D.; Facchini, M. C., A Combined Organic-inorganic Sea Spray Source Function. *Geophys. Res. Lett.* **2008,** *35*, (1), 1-5.
69. Schill, S. R.; Collins, D. B.; Lee, C.; Morris, H. S.; Novak, G. A.; Prather, K. A.; Quinn, P. K.; Sultana, C. M.; Tivanski, A. V.; Zimmermann, K., The Impact of Aerosol Particle Mixing State on the Hygroscopicity of Sea Spray Aerosol. *ACS Cent. Sci.* **2015,** *1*, (3), 132-141.
70. Calvo, A.; Alves, C.; Castro, A.; Pont, V.; Vicente, A.; Fraile, R., Research on Aerosol Sources and Chemical Composition: Past, Current and Emerging Issues. *Atmos. Res.* **2013,** *120-121*, 1-28.
71. Woodcock, A. H., Note Concerning Human Respiratory Irritation Associated with High Concentrations of Plankton and Mass Mortality of Marine Organisms. *J Mar Res* **1948,** *7*, (1), 56-62.
72. Cochran, R. E.; Jayarathne, T.; Stone, E. A.; Grassian, V. H., Selectivity Across the Interface: A Test of Surface Activity in the Composition of Organic Enriched Aerosols from Bubble Bursting. *J. Phys. Chem. Lett.* **2016,** *7*, 1692-1696.

73. Keene, W. C.; Maring, H.; Maben, J. R.; Kieber, D. J.; Pszenny, A. A.; Dahl, E. E.; Izaguirre, M. A.; Davis, A. J.; Long, M. S.; Zhou, X., Chemical and Physical Characteristics of Nascent Aerosols Produced by Bursting Bubbles at a Model Air-Sea Interface. *J. Geophys. Res. Atmos.* **2007,** *112*, (D21), 1-16.
74. Azetsu-Scott, K.; Passow, U., Ascending Marine Particles: Significance of Transparent Exopolymer Particles (TEP) in the Upper Ocean. *Limnol. Oceanogr.* **2004,** *49*, (3), 741-748.
75. Compiano, A.-M.; Romano, J.-C.; Garabetian, F.; Laborde, P.; de la Giraudièrea, I., Monosaccharide Composition of Particulate Hydrolysable Sugar Fraction in Surface Microlayers from Brackish and Marine Waters. *Mar. Chem.* **1993,** *42*, (3), 237-251.
76. Verdugo, P.; Alldredge, A. L.; Azam, F.; Kirchman, D. L.; Passow, U.; Santschi, P. H., The Oceanic Gel Phase: A Bridge in the DOM–POM Continuum. *Mar. Chem.* **2004,** *92*, (1), 67-85.
77. Mopper, K.; Zhou, J.; Ramana, K. S.; Passow, U.; Dam, H. G.; Drapeau, D. T., The Role of Surface-active Carbohydrates in the Flocculation of a Diatom Bloom in a Mesocosm. *Deep Sea Res. Part 2* **1995,** *42*, (1), 47-73.
78. Garabetian, F.; Romano, J.-C.; Paul, R.; Sigoillot, J.-C., Organic Matter Composition and Pollutant Enrichment of Sea Surface Microlayer Inside and Outside Slicks. *Mar. Environ. Res.* **1993,** *35*, (4), 323-339.
79. Hawkins, L. N.; Russell, L. M., Polysaccharides, Proteins, and Phytoplankton Fragments: Four Chemically Distinct Types of Marine Primary Organic Aerosol Classified by Single Particle Spectromicroscopy. *Adv. Meteorol.* **2010,** *2010*, 1-14.
80. Russell, L. M.; Hawkins, L. N.; Frossard, A. A.; Quinn, P. K.; Bates, T. S., Carbohydrate-like Composition of Submicron Atmospheric Particles and Their Production from Ocean Bubble Bursting. *PNAS* **2010,** *107*, (15), 6652-6657.
81. Zhou, J.; Mopper, K.; Passow, U., The Role of Surface-active Carbohydrates in the Formation of Transparent Exopolymer Particles by Bubble Adsorption of Seawater. *Limnol. Oceanogr.* **1998,** *43*, (8), 1860-1871.
82. Brain, C. K.; Sillent, A., Evidence from the Swartkrans Cave for the Earliest Use of Fire. *Nature* **1988,** *336*, (6198), 464-466.
83. Doren, R. F.; Whiteaker, L. D.; Larosa, A. M., Evaluation of Fire as a Management Tool for Controlling Schinus terebinthifolius as Secondary Successional Growth on Abandoned Agricultural Land. *Environ. Manage.* **1991,** *15*, (1), 121-129.
84. Andreae, M. O.; Merlet, P., Emission of Trace Gases and Aerosols from Biomass Burning. *Global Biogeochem. Cycles* **2001,** *15*, (4), 955-966.
85. Bond, T. C.; Streets, D. G.; Yarber, K. F.; Nelson, S. M.; Woo, J. H.; Klimont, Z., A Technology-based Global Inventory of Black and Organic Carbon Emissions from Combustion. *J. Geophys. Res. Atmos.* **2004,** *109*, (D14).
86. Liu, S.; Aiken, A. C.; Arata, C.; Dubey, M. K.; Stockwell, C. E.; Yokelson, R. J.; Stone, E. A.; Jayarathne, T.; Robinson, A. L.; DeMott, P. J., Aerosol Single Scattering Albedo Dependence on Biomass Combustion Efficiency: Laboratory and Field Studies. *Geophys. Res. Lett.* **2014,** *41*, (2), 742-748.

87. Rappold, A. G.; Stone, S. L.; Cascio, W. E.; Neas, L. M.; Kilaru, V. J.; Carraway, M. S.; Szykman, J. J.; Ising, A.; Cleve, W. E.; Meredith, J. T., Peat Bog Wildfire Smoke Exposure in Rural North Carolina is Associated with Cardiopulmonary Emergency Department Visits Assessed Through Syndromic Surveillance. *Environ. Health Perspect.* **2011,** *119*, (10), 1415.
88. Kim, Y. H.; Tong, H.; Daniels, M.; Boykin, E.; Krantz, Q. T.; McGee, J.; Hays, M.; Kovalcik, K.; Dye, J. A.; Gilmour, M. I., Cardiopulmonary Toxicity of Peat Wildfire Particulate Matter and the Predictive Utility of Precision Cut Lung Slices. *Part. Fibre. Toxicol.* **2014,** *11*, (1), 1.
89. Pokhrel, R. P.; Wagner, N. L.; Langridge, J. M.; Lack, D. A.; Jayarathne, T.; Stone, E. A.; Stockwell, C. E.; Yokelson, R. J.; Murphy, S. M., Parameterization of Single-scattering Albedo (SSA) and Absorption Ångström Exponent (AAE) with EC/OC for Aerosol Emissions from Biomass Burning. *Atmos. Chem. Phys.* **2016,** *16*, (15), 9549-9561.
90. Van der Werf, G. R.; Randerson, J. T.; Giglio, L.; Collatz, G.; Mu, M.; Kasibhatla, P. S.; Morton, D. C.; DeFries, R.; Jin, Y. v.; van Leeuwen, T. T., Global Fire Emissions and the Contribution of Deforestation, Savanna, Forest, Agricultural, and Peat Fires (1997–2009). *Atmos. Chem. Phys.* **2010,** *10*, (23), 11707-11735.
91. Robinson, J. M., Fire from Space: Global Fire Evaluation Using Infrared Remote Sensing. *Int. J. Remote. Sens.* **1991,** *12*, (1), 3-24.
92. Bowman, D. M.; Balch, J. K.; Artaxo, P.; Bond, W. J.; Carlson, J. M.; Cochrane, M. A.; D'Antonio, C. M.; DeFries, R. S.; Doyle, J. C.; Harrison, S. P., Fire in the Earth System. *Science* **2009,** *324*, (5926), 481-484.
93. Akagi, S.; Yokelson, R. J.; Wiedinmyer, C.; Alvarado, M.; Reid, J.; Karl, T.; Crounse, J.; Wennberg, P., Emission Factors for Open and Domestic Biomass Burning for Use in Atmospheric Models. *Atmos. Chem. Phys.* **2011,** *11*, (9), 4039-4072.
94. Stockwell, C.; Veres, P.; Williams, J.; Yokelson, R., Characterization of Biomass Burning Emissions from Cooking Fires, Peat, Crop Residue, and Other Fuels with High-resolution Proton-transfer-reaction Time-of-flight Mass Spectrometry. *Atmos. Chem. Phys.* **2015,** *15*, (2), 845-865.
95. Stockwell, C.; Yokelson, R.; Kreidenweis, S.; Robinson, A.; DeMott, P.; Sullivan, R.; Reardon, J.; Ryan, K.; Griffith, D.; Stevens, L., Trace Gas Emissions from Combustion of Peat, Crop Residue, Domestic Biofuels, Grasses, and Other Fuels: Configuration and Fourier transform infrared (FTIR) Component of the Fourth Fire Lab at Missoula Experiment (FLAME-4). *Atmos. Chem. Phys.* **2014**, 9727.
96. Stockwell, C. E.; Christian, T. J.; Goetz, J. D.; Jayarathne, T.; Bhave, P. V.; Praveen, P. S.; Adhikari, S.; Maharjan, R.; DeCarlo, P. F.; Stone, E. A., Nepal Ambient Monitoring and Source Testing Experiment (NAMaSTE): Emissions of Trace Gases and Light-absorbing Carbon from Wood and Dung Cooking Fires, Garbage and Crop Residue Burning, Brick Kilns, and Other Sources. *Atmos. Chem. Phys.* **2016,** *16*, (17), 11043-11081.
97. Levin, E.; McMeeking, G.; Carrico, C.; Mack, L.; Kreidenweis, S.; Wold, C.; Moosmüller, H.; Arnott, W.; Hao, W.; Collett, J., Biomass Burning Smoke Aerosol Properties Measured During Fire Laboratory at Missoula Experiments (FLAME). *J. Geophys. Res. Atmos.* **2010,** *115*, (D18).

98. McMeeking, G. R.; Kreidenweis, S. M.; Baker, S.; Carrico, C. M.; Chow, J. C.; Collett, J. L.; Hao, W. M.; Holden, A. S.; Kirchstetter, T. W.; Malm, W. C., Emissions of Trace Gases and Aerosols During the Open Combustion of Biomass in the Laboratory. *J. Geophys. Res. Atmos.* **2009,** *114*, (D19).
99. Chen, L.-W. A.; Moosmüller, H.; Arnott, W. P.; Chow, J. C.; Watson, J. G.; Susott, R. A.; Babbitt, R. E.; Wold, C. E.; Lincoln, E. N.; Hao, W. M., Emissions from Laboratory Combustion of Wildland Fuels: Emission Factors and Source Profiles. *Environ. Sci. Technol.* **2007,** *41*, (12), 4317-4325.
100. Iinuma, Y.; Brüggemann, E.; Gnauk, T.; Müller, K.; Andreae, M.; Helas, G.; Parmar, R.; Herrmann, H., Source Characterization of Biomass Burning Particles: The Combustion of Selected European Conifers, African Hardwood, Savanna Grass, and German and Indonesian Peat. *J. Geophys. Res. Atmos.* **2007,** *112*, (D8).
101. Christian, T. J.; Kleiss, B.; Yokelson, R. J.; Holzinger, R.; Crutzen, P. J.; Hao, W. M.; Shirai, T.; Blake, D. R., Comprehensive Laboratory Measurements of Biomass-burning Emissions: 2. First Intercomparison of open-path FTIR, PTR-MS, and GC-MS/FID/ECD. *J. Geophys. Res. Atmos.* **2004,** *109*, (D2).
102. Pokhrel, R. P.; Beamesderfer, E. R.; Wagner, N. L.; Langridge, J. M.; Lack, D. A., Relative Importance of Black Carbon, Brown Carbon and Absorption Enhancement from Clear Coatings in Biomass Burning Emissions. *Atmos. Chem. Phys. Discuss.* **2016**.
103. Cochran, R. E.; Laskina, O.; Trueblood, J.; Estillore, A. D.; Morris, H. S.; Jayarathne, T.; Sultana, C. M.; Lee, C.; Lin, P.; Laskin, J., *et al.*, Molecular Characterization of Sea Spray Particles: Influence of Ocean Biology on Particle Composition and Interaction with Water. *Chem - in press doi:10.1016/j.chempr.2017.03.007* **2017**.
104. Adams, E. M.; Verreault, D.; Jayarathne, T.; Cochran, R. E.; Stone, E. A.; Allen, H. C., Surface Organization of a DPPC Monolayer on Concentrated $SrCl_2$ and $ZnCl_2$ solutions. *PCCP* **2016,** *18*, (47), 32345-32357.
105. Cochran, R. E.; Laskina, O.; Jayarathne, T.; Laskin, A.; Laskin, J.; Lin, P.; Sultana, C.; Lee, C.; Moore, K. A.; Cappa, C. D., Analysis of Organic Anionic Surfactants in Fine and Coarse Fractions of Freshly Emitted Sea Spray Aerosol. *Environ. Sci. Technol.* **2016,** *50*, (5), 2477-2486.
106. Hettiyadura, A. P. S.; Jayarathne, T.; Baumann, K.; Goldstein, A. H.; de Gouw, J. A.; Koss, A.; Keutsch, F. N.; Skog, K.; Stone, E. A., Qualitative and Quantitative Analysis of Atmospheric Organosulfates in Centreville, Alabama. *Atmos. Chem. Phys.* **2017,** *17*, (2), 1343-1359.
107. Finlayson-Pitts, B. J.; Pitts Jr, J. N., *Chemistry of the Upper and Lower Atmosphere: Theory, Experiments, and Applications*. Academic press: 2000.
108. AWMA, *Air and Waste Management Association, Air Pollution Engineering Manual*. Van Nostrand, Reinhold, New York, NY: 1992.
109. Chow, J. C., Measurement Methods to Determine Compliance with Ambient Air Quality Standards for Suspended Particles. *J. Air Waste Manage. Assoc.* **1995,** *45*, (5), 320-382.
110. NIOSH, Diesel Particulate Matter (as Elemental Carbon), Method 5040. NIOSH Manual of Analytical Methods. **2003**.

111. Schauer, J. J.; Mader, B.; Deminter, J.; Heidemann, G.; Bae, M.; Seinfeld, J. H.; Flagan, R.; Cary, R.; Smith, D.; Huebert, B., ACE-Asia Intercomparison of a Thermal-optical Method for the Determination of Particle-phase Organic and Elemental Carbon. *Environ. Sci. Technol.* **2003,** *37*, (5), 993-1001.
112. Panagiotopoulos, C.; Sempéré, R., Analytical Methods for the Determination of Sugars in Marine Samples: A Historical Perspective and Future Directions. *Limnol. Oceanogr-Meth.* **2005,** *3*, (10), 419-454.
113. Borch, N. H.; Kirchman, D. L., Concentration and Composition of Dissolved Combined Neutral Sugars (polysaccharides) in Seawater Determined by HPLC-PAD. *Mar. Chem.* **1997,** *57*, (1), 85-95.
114. Engel, A.; Händel, N., A Novel Protocol for Determining the Concentration and Composition of Sugars in Particulate and in High Molecular Weight Dissolved Organic Matter (HMW-DOM) in Seawater. *Mar. Chem.* **2011,** *127*, (1), 180-191.
115. Rocklin, R. D.; Clarke, A. P.; Weitzhandler, M., Improved Long-term Reproducibility for Pulsed Amperometric Detection of Carbohydrates via a New Quadruple-potential Waveform. *Anal. Chem.* **1998,** *70*, (8), 1496-1501.
116. Lee, Y. C., High-performance Anion-exchange Chromatography for Carbohydrate Analysis. *Anal. Biochem.* **1990,** *189*, (2), 151-162.
117. Miller, J. M., *Chromatography: Concepts and Contrasts*. Second edition ed.; John Wiley & Sons: 2005.
118. Rodrigues, A.; Lu, Z.; Loureiro, J.; Carta, G., Peak Resolution in Linear Chromatography: Effects of Intraparticle Convection. *J. Chromatogr. A* **1993,** *653*, (2), 189-198.
119. Kerhervé, P.; Charrière, B.; Gadel, F., Determination of Marine Monosaccharides by High-pH Anion-exchange Chromatography with Pulsed Amperometric Detection. *J. Chromatogr. A* **1995,** *718*, (2), 283-289.
120. Engbrodt, R.; Kattner, G., On the Biogeochemistry of Dissolved Carbohydrates in the Greenland Sea (Arctic). *Org. Geochem.* **2005,** *36*, (6), 937-948.
121. USEPA, Method 3052: Microwave Assisted Acid Digestion of Siliceous and Organically Based Matrices. *Test Methods for Evaluating Solid Waste* **1995**.
122. Peate, D. W.; Breddam, K.; Baker, J. A.; Kurz, M. D.; Barker, A. K.; Prestvik, T.; Grassineau, N.; Skovgaard, A. C., Compositional Characteristics and Spatial Distribution of Enriched Icelandic Mantle Components. *J. Petrol.* **2010**, egq025.
123. Al-Naiema, I.; Estillore, A. D.; Mudunkotuwa, I. A.; Grassian, V. H.; Stone, E. A., Impacts of Co-firing Biomass on Emissions of Particulate Matter to the Atmosphere. *Fuel* **2015,** *162*, 111-120.
124. Stone, E. A.; Nguyen, T. T.; Pradhan, B. B.; Dangol, P. M., Assessment of Biogenic Secondary Organic Aerosol in the Himalayas. *Envir. Chem.* **2012,** *9*, (3), 263-272.
125. RTI International, Standard Operating Procedure for the X-ray Fluorescence Analysis of Particulate Matter Deposits on Teflon filters. Prepared by Environmental and Industrial Measurements Division, RTI International, Research, Triangle Park, North Carolina. **2009**.
126. Kuo, C.-P.; Liao, H.-T.; Chou, C. C.-K.; Wu, C.-F., Source Apportionment of Particulate Matter and Selected Volatile Organic Compounds with Multiple Time Resolution Data. *Sci. Total Environ.* **2014,** *472*, 880-887.

127. Crutzen, P. J.; Andreae, M. O., Biomass Burning in the Tropics: Impact on Atmospheric Chemistry and Biogeochemical Cycles. *Science* **1990,** *250*, (4988), 1669-1679.
128. Bird, M.; Cali, J., A Million-year Record of Fire in sub-Saharan Africa. *Nature* **1998,** *394*, (6695), 767-769.
129. Page, S.; Hoscilo, A.; Langner, A.; Tansey, K.; Siegert, F.; Limin, S.; Rieley, J., Tropical Peatland Fires in Southeast Asia. In *Tropical Fire Ecology*, Springer: 2009; pp 263-287.
130. Fujii, Y.; Tohno, S.; Amil, N.; Latif, M. T.; Oda, M.; Matsumoto, J.; Mizohata, A., Annual Variations of Carbonaceous PM 2.5 in Malaysia: Influence by Indonesian Peatland Fires. *Atmos. Chem. Phys.* **2015,** *15*, (23), 13319-13329.
131. McMeeking, G. R.; Kreidenweis, S. M.; Lunden, M.; Carrillo, J.; Carrico, C. M.; Lee, T.; Herckes, P.; Engling, G.; Day, D. E.; Hand, J., Smoke-impacted Regional Haze in California during the Summer of 2002. *Agr. Forest. Meteorol.* **2006,** *137*, (1), 25-42.
132. Ito, A.; Penner, J. E., Historical Emissions of Carbonaceous Aerosols from Biomass and Fossil Fuel Burning for the Period 1870–2000. *Global Biogeochem. Cycles* **2005,** *19*, (2).
133. Andreae, M. O., Biomass Burning: Its History, Use, and Distribution and Its Impact. In Global Biomass Burning: Atmospheric, Climatic, and Biospheric Implications [JS Levine (Ed.)]. Cambridge, MA, MIT Press: 1991.
134. Christian, T. J.; Yokelson, R. J.; Carvalho, J. A.; Griffith, D. W.; Alvarado, E. C.; Santos, J. C.; Neto, T. G. S.; Veras, C. A. G.; Hao, W. M., The Tropical Forest and Fire Emissions Experiment: Trace Gases Emitted by Smoldering Logs and Dung from Deforestation and Pasture Fires in Brazil. *J. Geophys. Res. Atmos.* **2007,** *112*, (D18).
135. Yokelson, R. J.; Christian, T. J.; Karl, T. G.; Guenther, A., The Tropical Forest and Fire Emissions Experiment: Laboratory Fire Measurements and Synthesis of Campaign Data. *Atmos. Chem. Phys.* **2008,** *8*, (13), 3509-3527.
136. Crutzen, P. J.; Heidt, L. E.; Krasnec, J. P.; Pollock, W. H.; Seiler, W., Biomass Burning as a Source of Atmospheric Gases CO, H_2, N_2O, NO, CH_3Cl and COS. *Nature* **1979,** *282*, 253-256.
137. Yokelson, R. J.; Griffith, D. W. T.; Ward, D. E., Open-path Fourier Transform Infrared Studies of Large-scale Laboratory Biomass Fires. *J. Geophys. Res. Atmos.* **1996,** *101*, (D15), 21067-21080.
138. Wiedinmyer, C.; Akagi, S.; Yokelson, R. J.; Emmons, L.; Al-Saadi, J.; Orlando, J.; Soja, A., The Fire INventory from NCAR (FINN): A High Resolution Global Model to Estimate the Emissions from Open Burning. *Geosci. Model Dev.* **2011,** *4*, (3), 625.
139. Hatch, L. E.; Luo, W.; Pankow, J. F.; Yokelson, R. J.; Stockwell, C. E.; Barsanti, K., Identification and Quantification of Gaseous Organic Compounds Emitted from Biomass Burning using Two-dimensional Gas Chromatography–time-of-flight Mass Spectrometry. *Atmos. Chem. Phys.* **2015,** *15*, (4), 1865-1899.
140. Jayarathne, T.; Stockwell, C. E.; Yokelson, R. J.; Nakao, S.; Stone, E. A., Emissions of Fine Particle Fluoride from Biomass Burning. *Environ. Sci. Technol.* **2014,** *48*, (21), 12636-12644.

141. May, A.; McMeeking, G.; Lee, T.; Taylor, J.; Craven, J.; Burling, I.; Sullivan, A.; Akagi, S.; Collett, J.; Flynn, M., Aerosol Emissions from Prescribed Fires in the United States: A Synthesis of Laboratory and Aircraft Measurements. *J. Geophys. Res. Atmos.* **2014,** *119*, (20).
142. Hays, M. D.; Geron, C. D.; Linna, K. J.; Smith, N. D.; Schauer, J. J., Speciation of Gas-phase and Fine Particle Emissions from Burning of Foliar Fuels. *Environ. Sci. Technol.* **2002,** *36*, (11), 2281-2295.
143. Yokelson, R. J.; Karl, T.; Artaxo, P.; Blake, D. R.; Christian, T. J.; Griffith, D. W. T.; Guenther, A.; Hao, W. M., The Tropical Forest and Fire Emissions Experiment: Overview and Airborne Fire Emission Factor Measurements. *Atmos. Chem. Phys.* **2007,** *7*, (19), 5175-5196.
144. Black, R. R.; Aurell, J.; Holder, A.; George, I. J.; Gullett, B. K.; Hays, M. D.; Geron, C. D.; Tabor, D., Characterization of Gas and Particle Emissions from Laboratory Burns of Peat. *Atmos. Environ.* **2016,** *132*, 49-57.
145. Geron, C.; Hays, M., Air Emissions from Organic Soil Burning on the Coastal Plain of North Carolina. *Atmos. Environ.* **2013,** *64*, 192-199.
146. Cheng, Y.; He, K.; Duan, F.; Zheng, M.; Ma, Y.; Tan, J., Positive Sampling Artifact of Carbonaceous Aerosols and its Influence on the Thermal-optical Split of OC/EC. *Atmos. Chem. Phys.* **2009,** *9*, (18), 7243-7256.
147. Turpin, B. J.; Huntzicker, J. J.; Hering, S. V., Investigation of Organic Aerosol Sampling Artifacts in the Los Angeles Basin. *Atmos. Environ.* **1994,** *28*, (19), 3061-3071.
148. Ficken, K.; Barber, K.; Eglinton, G., Lipid Biomarker, δ 13 C and Plant Macrofossil Stratigraphy of a Scottish Montane Peat Bog Over the Last Two Millennia. *Org. Geochem.* **1998,** *28*, (3), 217-237.
149. Schauer, J. J.; Kleeman, M. J.; Cass, G. R.; Simoneit, B. R., Measurement of Emissions from Air Pollution Sources. 3. C1-C29 Organic Compounds from Fireplace Combustion of Wood. *Environ. Sci. Technol.* **2001,** *35*, (9), 1716-1728.
150. Ravindra, K.; Sokhi, R.; Van Grieken, R., Atmospheric Polycyclic Aromatic Hydrocarbons: Source Attribution, Emission Factors and Regulation. *Atmos. Environ.* **2008,** *42*, (13), 2895-2921.
151. Richter, H.; Howard, J. B., Formation of Polycyclic Aromatic Hydrocarbons and their Growth to Soot - A Review of Chemical Reaction Pathways. *Prog. Energy Combust. Sci.* **2000,** *26*, (4), 565-608.
152. Simoneit, B. R.; Schauer, J. J.; Nolte, C.; Oros, D. R.; Elias, V. O.; Fraser, M.; Rogge, W.; Cass, G. R., Levoglucosan, a Tracer for Cellulose in Biomass Burning and Atmospheric Particles. *Atmos. Environ.* **1999,** *33*, (2), 173-182.
153. Pettersen, R. C., The Chemical Composition of Wood. In ACS Publications, Washington, D.C.: 1984; pp 57-126.
154. Oros, D. R.; Simoneit, B. R., Identification and Emission Factors of Molecular Tracers in Organic Aerosols from Biomass Burning Part 1. Temperate Climate Conifers. *Appl. Geochem.* **2001,** *16*, (13), 1513-1544.
155. Engling, G.; Lee, J. J.; Tsai, Y.-W.; Lung, S.-C. C.; Chou, C. C.-K.; Chan, C.-Y., Size-resolved Anhydrosugar Composition in Smoke Aerosol from Controlled Field Burning of Rice Straw. *Aerosol Sci. Technol.* **2009,** *43*, (7), 662-672.

156. Fujii, Y.; Iriana, W.; Oda, M.; Puriwigati, A.; Tohno, S.; Lestari, P.; Mizohata, A.; Huboyo, H. S., Characteristics of Carbonaceous Aerosols Emitted from Peatland Fire in Riau, Sumatra, Indonesia. *Atmos. Environ.* **2014,** *87*, 164-169.
157. Baker, E. In *Chemistry and Morphology of Plant Epicuticular Waxes*, Linnean Society symposium series, 1982; 1982.
158. Wang, Z.; Bi, X.; Sheng, G.; Fu, J., Characterization of Organic Compounds and Molecular Tracers from Biomass Burning Smoke in South China I: Broad-leaf Trees and Shrubs. *Atmos. Environ.* **2009,** *43*, (19), 3096-3102.
159. Oros, D. R.; Simoneit, B. R., Identification and Emission Factors of Molecular Tracers in Organic Aerosols from Biomass Burning Part 2. Deciduous Trees. *Appl. Geochem.* **2001,** *16*, (13), 1545-1565.
160. Simoneit, B. R. T., Biomass Burning - A Review of Organic Tracers for Smoke from Incomplete Combustion. *Appl. Geochem.* **2002,** *17*, (3), 129-162.
161. Takemura, T.; Wertz, P.; Sato, K., Free Fatty Acids and Sterols in Human Eccrine Sweat. *Br. J. Dermatol.* **1989,** *120*, (1), 43-47.
162. Ries-Kautt, M.; Albrecht, P., Hopane-derived Triterpenoids in Soils. *Chem. Geol.* **1989,** *76*, (1), 143-151.
163. Venkatesan, M.; Ruth, E.; Kaplan, I., Terpenoid Hydrocarbons in Hula Peat: Structure and Origins. *Geochim. Cosmochim. Acta* **1986,** *50*, (6), 1133-1139.
164. Quirk, M.; Wardroper, A.; Wheatley, R.; Maxwell, J., Extended Hopanoids in Peat Environments. *Chem. Geol.* **1984,** *42*, (1), 25-43.
165. López-Días, V.; Borrego, Á.; Blanco, C.; Arboleya, M.; López-Sáez, J. A.; López-Merino, L., Biomarkers in a Peat Deposit in Northern Spain (Huelga de Bayas, Asturias) as Proxy for Climate Variation. *J. Chromatogr. A* **2010,** *1217*, (21), 3538-3546.
166. Del Rio, J.; Gonzalez-Vila, F.; Martin, F., Variation in the Content and Distribution of Biomarkers in Two Closely Situated Peat and Lignite Deposits. *Org. Geochem.* **1992,** *18*, (1), 67-78.
167. Dehmer, J., Petrological and Organic Geochemical Investigation of Recent Peats with Known Environments of Deposition. *Int. J. Coal Geol.* **1995,** *28*, (2), 111-138.
168. Raison, R. J.; Khanna, P. K.; Woods, P. V., Mechanisms of Element Transfer to the Atmosphere During Vegetation Fires. *Can. J. For. Res.* **1985,** *15*, (1), 132-140.
169. Formenti, P.; Elbert, W.; Maenhaut, W.; Haywood, J.; Osborne, S.; Andreae, M., Inorganic and Carbonaceous Aerosols During the Southern African Regional Science Initiative (SAFARI 2000) Experiment: Chemical Characteristics, Physical Properties, and Emission Data for Smoke from African Biomass Burning. *J. Geophys. Res. Atmos.* **2003,** *108*, (D13).
170. Andreae, M.; Andreae, T.; Annegarn, H.; Beer, F.; Cachier, H.; Elbert, W.; Harris, G.; Maenhaut, W.; Salma, I.; Swap, R., Airborne Studies of Emissions from Savanna Fires in Southern Africa. 2. Aerosol Chemical Composition. *J. Geophys. Res.* **1998,** *103*, (D24), 32119-32128.
171. Mason, B. H.; Moore, C. B., *Principles of Geochemistry*. John Wiley: 1987; p 350-351.
172. Pickering, W. F., The Mobility of Soluble Fluoride in Soils. *Environ. Pollut. B* **1985,** *9*, (4), 281-308.

173. Oskarsson, N., The Interaction between Volcanic Gases and Tephra: Fluorine Adhering to Tephra of the 1970 Hekla Eruption. *J. Volcanol. Geoth. Res.* **1980,** *8*, (2), 251-266.
174. Tsai, W. T., An overview of environmental hazards and exposure risk of hydrofluorocarbons (HFCs). *Chemosphere* **2005,** *61*, (11), 1539-1547.
175. Cicerone, R. J., Halogens in the Atmosphere. *Rev. Geophys.* **1981,** *19*, (1), 123-139.
176. Ozsvath, D. L., Fluoride and Environmental Health: A Review. *Rev. Environ. Sci. Bio* **2009,** *8*, (1), 59-79.
177. Vike, E.; Habjorg, A., Variation in Fluoride Content and Leaf Injury on Plants Associated with Three Aluminium Smelters in Norway. *Sci. Total Environ.* **1995,** *163*, (1), 25-34.
178. Shoeib, M.; Harner, T.; Ikonomou, M.; Kannan, K., Indoor and Outdoor Air Concentrations and Phase Partitioning of Perfluoroalkyl Sulfonamides and Polybrominated Diphenyl Ethers. *Environ. Sci. Technol.* **2004,** *38*, (5), 1313-1320.
179. De Angelis, M.; Legrand, M., Origins and Variations of Fluoride in Greenland Precipitation. *J. Geophys. Res. Atmos.* **1994,** *99*, (D1), 1157-1172.
180. Ravishankara, A. R.; Solomon, S.; Turnipseed, A. A.; Warren, R. F., Atmospheric Lifetimes of Long-lived Halogenated Species. *Science* **1993,** *259*, (5092), 194-199.
181. Carpenter, R., Factors Controlling the Marine Geochemistry of Fluorine. *Geochim. Cosmochim. Acta* **1969,** *33*, (10), 1153-1167.
182. Barnard, W. R.; Nordstrom, D. K., Flouride in Precipitation - II. Implications for the Geochemical Cycling of Fluorine. *Atmos. Environ.* **1982,** *16*, (1), 105-111.
183. Polomski, J.; Fluhler, H.; Blaser, P., Accumulation of Airborne Fluoride in Soils. *J. Environ. Qual.* **1982,** *11*, (3), 457-461.
184. Okita, T.; Kaneda, K.; Yanaka, T.; Sugai, R., Determination of Gaseous and Particulate Chloride and Fluoride in the Atmosphere. *Atmos. Environ.* **1974,** *8*, (9), 927-936.
185. Gritsan, N. P.; Miller, G. W.; Schumatkov, G. G., Correlation Among Heavy Metals and Fluoride in Soil, Air and Plants in Relation to Environmental Damage. *Fluoride* **1994,** *28*, (4), 180-188.
186. Wu, D.; Zheng, B.; Tang, X.; Li, S.; Wang, B.; Wang, M., Fluorine in Chinese Coals. *Fluoride* **2004,** *37*, 125-132.
187. Xie, Z. M.; Wu, W. H.; Xu, J. M., Study on Fluoride Emission from Soils at high Temperature Related to Brick-making Process. *Chemosphere* **2003,** *50*, (6), 763-769.
188. Cronin, S. J.; Manoharan, V.; Hedley, M. J.; Loganathan, P., Fluoride: A Review of its Fate, Bioavailability, and Risks of Fluorosis in Grazed-pasture Systems in New Zealand. *New Zeal. J. Agr. Res.* **2000,** *43*, (3), 295-321.
189. Fung, K. F.; Zhang, Z. Q.; Wong, J. W. C.; Wong, M. H., Fluoride Contents in Tea and Soil from Tea Plantations and the Release of Fluoride into tea Liquor During Infusion. *Environ. Pollut.* **1999,** *104*, (2), 197-205.
190. Jacobson, J. S.; Weinstein, L. H.; McCune, D. C.; Hitchcock, A. E., The Accumulation of Fluorine by Plants. *J Air Pollut Control Assoc.* **1966,** *16*, (8), 412-417.
191. Hall, R. J., The Distribution of Organic Fluorine in Some Toxic Tropical Plants. *New Phytol.* **1972,** *71*, (5), 855-871.

192. Walton, K. C., Environmental Fluoride and Fluorosis in Mammals. *Mammal Rev.* **1988,** *18*, (2), 77-90.
193. Vikoren, T.; Stuve, G., Fluoride Exposure in Cervids Inhabiting Areas Adjacent to Aluminum Smelters in Norway, II. Fluorosis. *J. Wildlife. Dis.* **1996,** *32*, (2), 181-189.
194. Weinstein, L. H., Fluoride and Plant Life. *J. Occup. Env. Med.* **1977,** *19*, (1), 49-78.
195. Aoba, T.; Fejerskov, O., Dental Fluorosis: Chemistry and Biology. *Crit Rev Oral Biol Med.* **2002,** *13*, (2), 155-170.
196. Freni, S. C., Exposure to High Fluoride Concentrations in Drinking Water is Associated with Decreased Birth Rates. *J. Toxicol. Environ. Health* **1994,** *42*, (1), 109-121.
197. Whitford, G. M., The Physiological and Toxicological Characteristics of Fluoride. *J. Dent. Res.* **1990,** *69*, 539-49; discussion 556-7.
198. Franzaring, J.; Hrenn, H.; Schumm, C.; Klumpp, A.; Fangmeier, A., Environmental Monitoring of Fluoride Emissions Using Precipitation, Dust, Plant and Soil Samples. *Environ. Pollut.* **2006,** *144*, (1), 158-165.
199. Burling, I.; Yokelson, R. J.; Akagi, S.; Urbanski, S.; Wold, C. E.; Griffith, D. W.; Johnson, T. J.; Reardon, J.; Weise, D., Airborne and Ground-based Measurements of the Trace Gases and Particles Emitted by Prescribed Fires in the United States. *Atmos. Chem. Phys.* **2011,** *11*, (23), 12197-12216.
200. Ward, D. E.; Radke, L. F., *Emissions measurements from vegetation fires: A comparative evaluation of methods and results*. John Wiley: New York, 1993.
201. Burling, I. R.; Yokelson, R. J.; Griffith, D. W. T.; Johnson, T. J.; Veres, P.; Roberts, J. M.; Warneke, C.; Urbanski, S. P.; Reardon, J.; Weise, D. R., Laboratory Measurements of Trace Gas Emissions from Biomass Burning of Fuel Types From the Southeastern and Southwestern United States. *Atmos. Chem. Phys.* **2010,** *10*, (22), 11115-11130.
202. Yokelson, R. J.; Goode, J. G.; Ward, D. E.; Susott, R. A.; Babbitt, R. E.; Wade, D. D.; Bertschi, I.; Griffith, D. W.; Hao, W. M., Emissions of Formaldehyde, Acetic Acid, Methanol, and Other Trace Gases from Biomass Fires in North Carolina Measured by Airborne Fourier Transform Infrared Spectroscopy. *J. Geophys. Res. Atmos.* **1999,** *104*, (D23), 30109-30125.
203. Akagi, S.; Yokelson, R. J.; Burling, I.; Meinardi, S.; Simpson, I.; Blake, D. R.; McMeeking, G.; Sullivan, A.; Lee, T.; Kreidenweis, S., Measurements of Reactive Trace Gases and Variable O_3 Formation Rates in some South Carolina Biomass Burning Plumes. *Atmos. Chem. Phys.* **2013,** *13*, (3), 1141-1165.
204. Weinstein, L. H., *Fluorides in the Environment: Effects on Plants and Animals*. CABI: 2004.
205. Silva, P. J.; Liu, D.-Y.; Noble, C. A.; Prather, K. A., Size and Chemical Characterization of Individual Particles Resulting from Biomass Burning of Local Southern California Species. *Environ. Sci. Technol.* **1999,** *33*, (18), 3068-3076.
206. Wiedinmyer, C.; Akagi, S. K.; Yokelson, R. J.; Emmons, L. K.; Al-Saadi, J. A.; Orlando, J. J.; Soja, A. J., The Fire INventory from NCAR (FINN): a high resolution global model to estimate the emissions from open burning. *Geosci. Model Dev.* **2011,** *4*, (3), 625-641.

207. Schorr, J. R.; T., H. D.; Brockway, M. C.; Sticksel, P. R.; Niesez, D. E., In *Source Assessment: Pressed and Blown Glass Manufacturing Plants (EPA-600/2-77-005)*, Research Triangle Park, North Carolina., 1977.
208. Villalba, G.; Liu, Y.; Schroder, H.; Ayres, R. U., Global Phosphorus Flows in the Industrial Economy from a Production Perspective. *J. Ind. Ecol.* **2008,** *12*, (4), 557-569.
209. Cadle, R. D., A Comparison of Volcanic with Other Fluxes of Atmospheric Trace Gas Constituents. *Rev. Geophys.* **1980,** *18*, (4), 746-752.
210. Halmer, M. M.; Schmincke, H. U.; Graf, H. F., The Annual Volcanic Gas Input into the Atmosphere, in Particular into the Stratosphere: A Global Data Set for the Past 100 Years. *J. Volcanol. Geoth. Res.* **2002,** *115*, (3), 511-528.
211. Legrand, M.; De Angelis, M.; Staffelbach, T.; Neftel, A.; Stauffer, B., Large Perturbations of Ammonium and Organic Acids Content in the Summit - Greenland Ice Core. Fingerprint from Forest Fires? *Geophys. Res. Lett.* **1992,** *19*, (5), 473-475.
212. Kundu, S.; Kawamura, K.; Andreae, T. W.; Hoffer, A.; Andreae, M. O., Diurnal Variation in the Water-soluble Inorganic Ions, Organic Carbon and Isotopic Compositions of Total Carbon and Nitrogen in Biomass Burning Aerosols from the LBA-SMOCC Campaign in Rononia, Brazil. *J. Aerosol. Sci.* **2010,** *41*, (1), 118-133.
213. Lewandowska, A.; Falkowska, L.; Jozwik, J., Factors Determining the Fluctuation of Fluoride Concentrations in PM10 Aerosols in the Urbanized Coastal Area of the Baltic Sea (Gdynia, Poland). *Environ Sci Pollut Res.* **2013,** *20*, 6109-6118.
214. Langner, A.; Siegert, F., Spatiotemporal Fire Occurrence in Borneo over a Period of 10 Years. *Global Change Biol.* **2009,** *15*, (1), 48-62.
215. Parker, R. J.; Boesch, H.; Wooster, M. J.; Moore, D. P.; Webb, A. J.; Gaveau, D.; Murdiyarso, D., Atmospheric CH_4 and CO_2 Enhancements and Biomass Burning Emission Ratios Derived from Satellite Observations of the 2015 Indonesian Fire Plumes. *Atmos. Chem. Phys.* **2016,** *16*, (15), 10111-10131.
216. Koplitz, S. N.; Mickley, L. J.; Marlier, M. E.; Buonocore, J. J.; Kim, P. S.; Liu, T.; Sulprizio, M. P.; DeFries, R. S.; Jacob, D. J.; Schwartz, J., Public Health Impacts of the Severe Haze in Equatorial Asia in September–October 2015: Demonstration of a New Framework for Informing Fire Management Strategies to Reduce Downwind Smoke Exposure. *Environ. Res. Lett.* **2016,** *11*, (9), 094023.
217. Huijnen, V.; Wooster, M.; Kaiser, J.; Gaveau, D.; Flemming, J.; Parrington, M.; Inness, A.; Murdiyarso, D.; Main, B.; van Weele, M., Fire Carbon Emissions Over Maritime Southeast Asia in 2015 Largest Since 1997. *Sci. Rep.* **2016,** *6*, 26886.
218. Page, S. E.; Siegert, F.; Rieley, J. O.; Boehm, H.-D. V.; Jaya, A.; Limin, S., The Amount of Carbon Released from Peat and Forest Fires in Indonesia During 1997. *Nature* **2002,** *420*, (6911), 61-65.
219. Chisholm, R. A.; Wijedasa, L. S.; Swinfield, T., The Need for Long-term Remedies for Indonesia's Forest Fires. *Conserv. Biol.* **2016,** *30*, (1), 5-6.
220. Glover, D.; Jessup, T., *Indonesia's Fires and Haze: The Cost of Catastrophe*. IDRC: 2006.
221. Maltby, E.; Immirzi, P., Carbon Dynamics in Peatlands and Other Wetland Soils Regional and Global Perspectives. *Chemosphere* **1993,** *27*, (6), 999-1023.
222. Yu, Z.; Loisel, J.; Brosseau, D. P.; Beilman, D. W.; Hunt, S. J., Global Peatland Dynamics Since the Last Glacial Maximum. *Geophys. Res. Lett.* **2010,** *37*, (13).

223. Zulkifley, M. T. M.; Ng, T. F.; Abdullah, W. H.; Raj, J. K.; Shuib, M. K.; Ghani, A. A.; Ashraf, M. A., Geochemical Characteristics of a Tropical Lowland Peat Dome in the Kota Samarahan-Asajaya Area, West Sarawak, Malaysia. *Environ. Earth Sci.* **2015,** *73*, (4), 1443-1458.
224. Dizman, M.; Tutar, A.; Horuz, A., The Characterization of the Arifiye Peat. *J. Chem. Soc. Pak.* **2015,** *37*, (1), 131-138.
225. Huat, B. B.; Kazemian, S.; Prasad, A.; Barghchi, M., State of an Art Review of Peat: General Perspective. *Int. J. Phys. Sci.* **2011,** *6*, (8), 1988-1996.
226. Fujii, Y.; Kawamoto, H.; Tohno, S.; Oda, M.; Iriana, W.; Lestari, P., Characteristics of Carbonaceous Aerosols Emitted from Peatland Fire in Riau, Sumatra, Indonesia (2): Identification of Organic Compounds. *Atmos. Environ.* **2015,** *110*, 1-7.
227. Fujii, Y.; Tohno, S.; Amil, N.; Latif, M. T.; Oda, M.; Matsumoto, J.; Mizohata, A., Annual Variations of Carbonaceous $PM_{2.5}$ in Malaysia: Influence by Indonesian Peatland Fires. *Atmos. Chem. Phys.* **2015,** *15*, (23), 13319-13329.
228. Benner, W. H., *Photochemical Reactions of Forest Fire Combustion Products*. 1977.
229. McMahon, C. K.; Wade, D. D.; Tsoukalas, S. N., Combustion Characteristics and Emissions from Burning Organic Soils. **1980**.
230. Ward, D., Factors Influencing the Emissions of Gases and Particulate Matter from Biomass Burning. In *Fire in the Tropical Biota*, Springer: 1990; pp 418-436.
231. George, I. J.; Black, R. R.; Geron, C. D.; Aurell, J.; Hays, M. D.; Preston, W. T.; Gullett, B. K., Volatile and Semivolatile Organic Compounds in Laboratory Peat Fire Emissions. *Atmos. Environ.* **2016,** *132*, 163-170.
232. Rosman, K.; Taylor, P., Report of the IUPAC Subcommittee for Isotopic Abundance Measurements. *Pure Appl. Chem* **1999,** *71*, 1593-1607.
233. McMeeking, G. R.; Kreidenweis, S. M.; Baker, S.; Carrico, C. M.; Chow, J. C.; Collett, J. L.; Hao, W. M.; Holden, A. S.; Kirchstetter, T. W.; Malm, W. C., Emissions of Trace Gases and Aerosols During the Open Combustion of Biomass in the Laboratory. *J. Geophys. Res. Atmos.* **2009,** *114*, (D19).
234. Dusek, U.; Frank, G.; Helas, G.; Iinuma, Y.; Zeromskiene, K.; Gwaze, P.; Hennig, T.; Massling, A.; Schmid, O.; Herrmann, H., "Missing" Cloud Condensation Nuclei in Peat Smoke. *Geophys. Res. Lett.* **2005,** *32*, (11).
235. Mauzerall, D. L.; Logan, J. A.; Jacob, D. J.; Anderson, B. E.; Blake, D. R.; Bradshaw, J. D.; Heikes, B.; Sachse, G. W.; Singh, H.; Talbot, B., Photochemistry in Biomass Burning Plumes and Implications for Tropospheric Ozone over the Tropical South Atlantic. *J. Geophys. Res. Atmos.* **1998,** *103*, (D7), 8401-8423.
236. Duncan, B.; Bey, I.; Chin, M.; Mickley, L.; Fairlie, T.; Martin, R.; Matsueda, H., Indonesian Wildfires of 1997: Impact on Tropospheric Chemistry. *J. Geophys. Res. Atmos.* **2003,** *108*, (D15).
237. Schauer, J. J.; Kleeman, M. J.; Cass, G. R.; Simoneit, B. R., Measurement of Emissions from Air Pollution Sources. 5. C_1-C_{32} Organic Compounds from Gasoline-powered Motor Vehicles. *Environ. Sci. Technol.* **2002,** *36*, (6), 1169-1180.
238. Schauer, J. J.; Kleeman, M. J.; Cass, G. R.; Simoneit, B. R., Measurement of Emissions from Air Pollution Sources. 2. C_1 through C_{30} Organic Compounds from Medium Duty Diesel Trucks. *Environ. Sci. Technol.* **1999,** *33*, (10), 1578-1587.

239. Fine, P. M.; Cass, G. R.; Simoneit, B. R., Chemical Characterization of Fine Particle Emissions from the Fireplace Combustion of Woods Grown in the Southern United States. *Environ. Sci. Technol.* **2002,** *36*, (7), 1442-1451.
240. bin Abas, M. R.; Oros, D. R.; Simoneit, B. R., Biomass Burning as the Main Source of Organic Aerosol Particulate Matter in Malaysia During Haze Episodes. *Chemosphere* **2004,** *55*, (8), 1089-1095.
241. Yamamoto, S.; Kawamura, K.; Seki, O.; Kariya, T.; Lee, M., Influence of Aerosol Source Regions and Transport Pathway on δD of Terrestrial Biomarkers in Atmospheric Aerosols from the East China Sea. *Geochim. Cosmochim. Acta* **2013,** *106*, 164-176.
242. Sullivan, A.; Holden, A.; Patterson, L.; McMeeking, G.; Kreidenweis, S.; Malm, W.; Hao, W.; Wold, C.; Collett, J., A method for Smoke Marker Measurements and its Potential Application for Determining the Contribution of Biomass Burning from Wildfires and Prescribed Fires to Ambient $PM_{2.5}$ Organic Carbon. *J. Geophys. Res. Atmos.* **2008,** *113*, (D22).
243. Chuang, M.-T.; Chou, C. C.-K.; Sopajaree, K.; Lin, N.-H.; Wang, J.-L.; Sheu, G.-R.; Chang, Y.-J.; Lee, C.-T., Characterization of Aerosol Chemical Properties from Near-source Biomass Burning in the Northern Indochina During 7-SEAS/Dongsha Experiment. *Atmos. Environ.* **2013,** *78*, 72-81.
244. Gao, S.; Hegg, D. A.; Hobbs, P. V.; Kirchstetter, T. W.; Magi, B. I.; Sadilek, M., Water-soluble Organic Components in Aerosols Associated with Savanna Fires in Southern Africa: Identification, Evolution, and Distribution. *J. Geophys. Res. Atmos.* **2003,** *108*, (D13).
245. Engling, G.; He, J.; Betha, R.; Balasubramanian, R., Assessing the Regional Impact of Indonesian Biomass Burning Emissions Based on Organic Molecular Tracers and Chemical Mass Balance Modeling. *Atmos. Chem. Phys.* **2014,** *14*, (15), 8043-8054.
246. Schauer, J. J.; Cass, G. R., Source Apportionment of Wintertime Gas-phase and Particle-phase Air Pollutants using Organic Compounds as Tracers. *Environ. Sci. Technol.* **2000,** *34*, (9), 1821-1832.
247. USEPA, Polycyclic Aromatic Hydrocarbons (PAHs)-EPA Fact Sheet. Washington, DC: National Center for Environmental Assessment, Officeof Research and Development. *Environmental Protection Agency* **2008**.
248. Nisbet, I. C.; LaGoy, P. K., Toxic Equivalency Factors (TEFs) for Polycyclic Aromatic Hydrocarbons (PAHs). *Regul. Toxicol. Pharm.* **1992,** *16*, (3), 290-300.
249. Oros, D.; Simoneit, B., Identification and Emission Rates of Molecular Tracers in Coal Smoke Particulate Matter. *Fuel* **2000,** *79*, (5), 515-536.
250. Raison, R.; Khanna, P.; Woods, P., Mechanisms of Element Transfer to the Atmosphere During Vegetation Fires. *Can. J. For. Res.* **1985,** *15*, (1), 132-140.
251. Whitburn, S.; Van Damme, M.; Clarisse, L.; Turquety, S.; Clerbaux, C.; Coheur, P. F., Doubling of Annual Ammonia Emissions from the Peat Fires in Indonesia During the 2015 El Niño. *Geophys. Res. Lett.* **2016,** *43*, (20).
252. Konecny, K.; Ballhorn, U.; Navratil, P.; Jubanski, J.; Page, S. E.; Tansey, K.; Hooijer, A.; Vernimmen, R.; Siegert, F., Variable Carbon Losses from Recurrent Fires in Drained Tropical Peatlands. *Global Change Biol.* **2016,** *22*, (4), 1469-1480.

253. Kim, K.-H.; Jahan, S. A.; Kabir, E.; Brown, R. J., A Review of Airborne Polycyclic Aromatic Hydrocarbons (PAHs) and their Human Health Effects. *Environ. Int.* **2013,** *60*, 71-80.
254. Erickson, D. J.; Duce, R. A., On the Global Flux of Atmospheric Sea Salt. *J. Geophys. Res. Oceans.* **1988,** *93*, (C11), 14079-14088.
255. Andreae, M. O., *Climatic Effects of Changing Atmospheric Aerosol Levels*. Elsevier: 1995; Vol. 16, p 347-398.
256. Stokes, M.; Deane, G.; Prather, K.; Bertram, T.; Ruppel, M.; Ryder, O.; Brady, J.; Zhao, D., A Marine Aerosol Reference Tank System as a Breaking Wave Analogue for the Production of Foam and Sea Spray Aerosols. *Atmos. Meas. Tech.* **2013,** *6*, (4), 1085-1094.
257. Modini, R. L.; Russell, L. M.; Deane, G. B.; Stokes, M. D., Effect of Soluble Surfactant on Bubble Persistence and Bubble-produced Aerosol Particles. *J. Geophys. Res. Atmos.* **2013,** *118*, (3), 1388-1400.
258. Burrows, S.; Ogunro, O.; Frossard, A.; Russell, L.; Rasch, P.; Elliott, S., A Physically Based Framework for Modeling the Organic Fractionation of Sea Spray Aerosol from Bubble Film Langmuir Equilibria. *Atmos. Chem. Phys.* **2014,** *14*, (24), 13,601-13,629.
259. Cunliffe, M.; Engel, A.; Frka, S.; Gašparović, B.; Guitart, C.; Murrell, J. C.; Salter, M.; Stolle, C.; Upstill-Goddard, R.; Wurl, O., Sea Surface Microlayers: A Unified Physicochemical and Biological Perspective of the Air–Ocean Interface. *Prog. Oceanogr.* **2013,** *109*, 104-116.
260. Van Vleet, E. S.; Williams, P. M., Surface Potential and Film Pressure Measurements in Seawater Systems. *Limnol. Oceanogr.* **1983,** *28*, (3), 401-414.
261. Wurl, O.; Wurl, E.; Miller, L.; Johnson, K.; Vagle, S., Formation and Global Distribution of Sea-surface Microlayers. *Biogeosciences* **2011,** *8*, (1), 121-135.
262. Facchini, M. C.; Rinaldi, M.; Decesari, S.; Carbone, C.; Finessi, E.; Mircea, M.; Fuzzi, S.; Ceburnis, D.; Flanagan, R.; Nilsson, E. D., Primary Submicron Marine Aerosol Dominated by Insoluble Organic Colloids and Aggregates. *Geophys. Res. Lett.* **2008,** *35*, (17), 1-5.
263. Cavalli, F.; Facchini, M.; Decesari, S.; Mircea, M.; Emblico, L.; Fuzzi, S.; Ceburnis, D.; Yoon, Y.; O'Dowd, C.; Putaud, J. P., Advances in Characterization of Size-resolved Organic Matter in Marine Aerosol Over the North Atlantic. *J. Geophys. Res. Atmos.* **2004,** *109*, (D24215), 1-14.
264. Yoon, Y.; Ceburnis, D.; Cavalli, F.; Jourdan, O.; Putaud, J.; Facchini, M.; Decesari, S.; Fuzzi, S.; Sellegri, K.; Jennings, S., Seasonal Characteristics of the Physicochemical Properties of North Atlantic Marine Atmospheric Aerosols. *J. Geophys. Res. Atmos.* **2007,** *112*, (D4), 1-14.
265. Ovadnevaite, J.; O'Dowd, C.; Dall'Osto, M.; Ceburnis, D.; Worsnop, D. R.; Berresheim, H., Detecting High Contributions of Primary Organic Matter to Marine Aerosol: A Case Study. *Geophys. Res. Lett.* **2011,** *38*, (2), 1-5.
266. Prather, K. A.; Bertram, T. H.; Grassian, V. H.; Deane, G. B.; Stokes, M. D.; DeMott, P. J.; Aluwihare, L. I.; Palenik, B. P.; Azam, F.; Seinfeld, J. H., Bringing the Ocean into the Laboratory to Probe the Chemical Complexity of Sea Spray Aerosol. *PNAS* **2013,** *110*, (19), 7550-7555.

267. Wang, X.; Sultana, C. M.; Trueblood, J.; Hill, T. C.; Malfatti, F.; Lee, C.; Laskina, O.; Moore, K. A.; Beall, C. M.; McCluskey, C. S., Microbial Control of Sea Spray Aerosol Composition: A Tale of Two Blooms. *ACS Cent. Sci.* **2015,** *1*, (3), 124-131.
268. Patterson, J. P.; Collins, D. B.; Michaud, J. M.; Axson, J. L.; Sultana, C. M.; Moser, T.; Dommer, A. C.; Conner, J.; Grassian, V. H.; Stokes, M. D., Sea Spray Aerosol Structure and Composition Using Cryogenic Transmission Electron Microscopy. *ACS Cent. Sci.* **2016,** *2*, (1), 40-47.
269. Aller, J. Y.; Kuznetsova, M. R.; Jahns, C. J.; Kemp, P. F., The Sea Surface Microlayer as a Source of Viral and Bacterial Enrichment in Marine Aerosols. *J. Aerosol. Sci.* **2005,** *36*, (5), 801-812.
270. Leck, C.; Bigg, E. K., Biogenic Particles in the Surface Microlayer and Overlaying Atmosphere in the Central Arctic Ocean During Summer. *Tellus B* **2005,** *57*, (4), 305-316.
271. Kuznetsova, M.; Lee, C.; Aller, J., Characterization of the Proteinaceous Matter in Marine Aerosols. *Mar. Chem.* **2005,** *96*, (3), 359-377.
272. Gao, Q.; Leck, C.; Rauschenberg, C.; Matrai, P. A., On the Chemical Dynamics of Extracellular Polysaccharides in the High Arctic Surface Microlayer. *Ocean Sci.* **2012,** *8*, (4), 401-418.
273. Marty, J.; Saliot, A.; Buat-Ménard, P.; Chesselet, R.; Hunter, K., Relationship Between the Lipid Compositions of Marine Aerosols, the Sea Surface Microlayer, and Subsurface Water. *J. Geophys. Res. Oceans.* **1979,** *84*, (C9), 5707-5716.
274. Barbier, M.; Tusseau, D.; Marty, J.; Saliot, A., Sterols in Aerosols, Surface Microlayer and Subsurface Water in the Northeastern Tropical Atlantic. *Oceanol. Acta* **1981,** *4*, (1), 77-84.
275. Lee, C.; Sultana, C. M.; Collins, D. B.; Santander, M. V.; Axson, J. L.; Malfatti, F.; Cornwell, G. C.; Grandquist, J. R.; Deane, G. B.; Stokes, M. D., Advancing Model Systems for Fundamental Laboratory Studies of Sea Spray Aerosol Using the Microbial Loop. *J. Phys. Chem. A* **2015,** *119*, (33), 8860-8870.
276. Frossard, A. A.; Russell, L. M.; Burrows, S. M.; Elliott, S. M.; Bates, T. S.; Quinn, P. K., Sources and Composition of Submicron Organic Mass in Marine Aerosol Particles. *J. Geophys. Res. Atmos.* **2014,** *119*, (22).
277. Pakulski, J. D.; Benner, R., An Improved Method for the Hydrolysis and MBTH Analysis of Dissolved and Particulate Carbohydrates in Seawater. *Mar. Chem.* **1992,** *40*, (3), 143-160.
278. Haug, A.; Myklestad, S., Polysaccharides of Marine Diatoms with Special Reference to Chaetoceros Species. *Mar. Biol.* **1976,** *34*, (3), 217-222.
279. Ittekkot, V., Variations of Dissolved Organic Matter During a Plankton Bloom: Qualitative Aspects, Based on Sugar and Amino Acid Analyses. *Mar. Chem.* **1982,** *11*, (2), 143-158.
280. Ittekkot, V.; Degens, E. T.; Brockmann, U., Monosaccharide Composition of Acid-hydrolyzable Carbohydrates in Particulate Matter During a Plankton Bloom1. *Limnol. Oceanogr.* **1982,** *27*, (4), 770-776.
281. Liebezeit, G.; Bolter, M.; Brown, I.; Dawson, R., Dissolved Free Amino-acids and Carbohydrates at Pycnocline Boundaries in the Sargasso Sea and Related Microbial Activity. *Oceanol. Acta* **1980,** *3*, (3), 357-362.

282. van Pinxteren, M.; Müller, C.; Iinuma, Y.; Stolle, C.; Herrmann, H., Chemical Characterization of Dissolved Organic Compounds from Coastal Sea Surface Microlayers (Baltic Sea, Germany). *Environ. Sci. Technol.* **2012,** *46*, (19), 10455-10462.
283. Casillas-Ituarte, N. N.; Callahan, K. M.; Tang, C. Y.; Chen, X.; Roeselová, M.; Tobias, D. J.; Allen, H. C., Surface Organization of Aqueous MgCl2 and Application to Atmospheric Marine Aerosol Chemistry. *PNAS* **2010,** *107*, (15), 6616-6621.
284. Russell, S. C., Microorganism Characterization by Single Particle Mass Spectrometry. *Mass Spectrom. Rev.* **2009,** *28*, (2), 376-387.
285. Guasco, T. L.; Cuadra-Rodriguez, L. A.; Pedler, B. E.; Ault, A. P.; Collins, D. B.; Zhao, D.; Kim, M. J.; Ruppel, M. J.; Wilson, S. C.; Pomeroy, R. S., Transition Metal Associations with Primary Biological Particles in Sea Spray Aerosol Generated in a Wave Channel. *Environ. Sci. Technol.* **2013,** *48*, (2), 1324-1333.
286. Oppo, C.; Bellandi, S.; Degli Innocenti, N.; Stortini, A.; Loglio, G.; Schiavuta, E.; Cini, R., Surfactant Components of Marine Organic Matter as Agents for Biogeochemical Fractionation and Pollutant Transport via Marine Aerosols. *Mar. Chem.* **1999,** *63*, (3), 235-253.
287. Adams, E. M.; Allen, H. C., Palmitic Acid on Salt Subphases and in Mixed Monolayers of Cerebrosides: Application to Atmospheric Aerosol Chemistry. *Atmosphere* **2013,** *4*, (4), 315-336.
288. Tang, C. Y.; Allen, H. C., Ionic Binding of Na+ versus K+ to the Carboxylic Acid Headgroup of Palmitic Acid Monolayers Studied by Vibrational Sum Frequency Generation Spectroscopy. *J. Phys. Chem. A* **2009,** *113*, (26), 7383-7393.
289. Barker, D. R.; Zeitlin, H., Metal-ion Concentrations in Sea-surface Microlayer and Size-separated Atmospheric Aerosol Samples in Hawaii. *J. Geophys. Res.* **1972,** *77*, (27), 5076-5086.
290. Piotrowicz, S. R.; Ray, B. J.; Hoffman, G. L.; Duce, R. A., Trace Metal Enrichment in the Sea-Surface Microlayer. *J. Geophys. Res.* **1972,** *77*, (27), 5243-5254.
291. Xu, H.; Lv, H.; Liu, X.; Wang, P.; Jiang, H.-L., Electrolyte Cations Binding with Extracellular Polymeric Substances Enhanced Microcystis Aggregation: Implication for Microcystis Bloom Formation in Eutrophic Freshwater Lakes. *Environ. Sci. Technol.* **2016**.
292. Bates, T.; Quinn, P.; Frossard, A.; Russell, L.; Hakala, J.; Petäjä, T.; Kulmala, M.; Covert, D.; Cappa, C.; Li, S., Measurements of Ocean Derived Aerosol Off the Coast of California. *J. Geophys. Res. Atmos.* **2012,** *117*, (D21), 1-13.
293. Keene, W. C.; Pszenny, A. A.; Galloway, J. N.; Hawley, M. E., Sea-salt Corrections and Interpretation of Constituent Ratios in Marine Precipitation. *J. Geophys. Res. Atmos.* **1986,** *91*, (D6), 6647-6658.
294. Sievering, H.; Cainey, J.; Harvey, M.; McGregor, J.; Nichol, S.; Quinn, P., Aerosol Non-sea-salt Sulfate in the Remote Marine Boundary Layer under Clear-sky and Normal Cloudiness Conditions: Ocean-derived Biogenic Alkalinity Enhances Sea-salt Sulfate Production by Ozone Oxidation. *J. Geophys. Res. Atmos.* **2004,** *109*, (D19), 1-12.
295. Salter, M. E.; Hamacher-Barth, E.; Leck, C.; Werner, J.; Johnson, C. M.; Riipinen, I.; Nilsson, E. D.; Zieger, P., Calcium Enrichment in Sea Spray Aerosol Particles. *Geophys. Res. Lett.* **2016,** *43*, (15), 8277-8285.

296. Mukaka, M., A Guide to Appropriate use of Correlation Coefficient in Medical Research. *Malawi Med. J.* **2012,** *24*, (3), 69-71.
297. Sarmiento, J. L.; Gruber, N., *Ocean Biogeochemical Dynamics*. Princeton University Press: 2013; p 102-352.
298. Azam, F.; Fenchel, T.; Field, J. G.; Gray, J. S.; Meyer-Reil, L. A.; Thingstad, F., The Ecological Role of Water-column Microbes in the Sea. *Mar. Ecol. Prog. Ser.* **1983,** *10*, (3), 257-263.
299. Biersmith, A.; Benner, R., Carbohydrates in Phytoplankton and Freshly Produced Dissolved Organic Matter. *Mar. Chem.* **1998,** *63*, (1), 131-144.
300. Hollibaugh, J., Metabolic Adaptation in Natural Bacterial Populations Supplemented with Selected Amino Acids. *Estuar. Coast. Mar. Sci.* **1979,** *9*, (2), 215-230.
301. Coombs, J.; Volcani, B., Studies on the Biochemistry and Fine Structure of Silica Shell Formation in Diatoms. *Planta* **1968,** *80*, (3), 264-279.
302. dela Giraudiere, I.; Laborde, P.; Romano, J.-C., HPLC Determination of Chlorophylls and Breakdown Products in Surface Microlayers. *Mar. Chem.* **1989,** *26*, (3), 189-204.
303. Bordovskiy, O., Sources of Organic Matter in Marine Basins. *Mar. Geol.* **1965,** *3*, (1), 5-31.
304. Bordovskiy, O., Accumulation of Organic Matter in Bottom Sediments. *Mar. Geol.* **1965,** *3*, (1), 33-82.
305. Burrows, S. M.; Gobrogge, E.; Fu, L.; Link, K.; Elliott, S. M.; Wang, H.; Walker, R., OCEANFILMS-2: Representing Coadsorption of Saccharides in Marine Films and Potential Impacts on Modeled Marine Aerosol Chemistry. *Geophys. Res. Lett.* **2016,** *43*, (15), 8306-8313.
306. Holland, H. D., *The Chemistry of the Atmosphere and Oceans*. Wiley, New York: 1978; p 153-183.
307. Shaloski, M. A.; Sobyra, T. B.; Nathanson, G. M., DCl Transport through Dodecyl Sulfate Films on Salty Glycerol: Effects of Seawater Ions on Gas Entry. *J. Phys. Chem. A* **2015,** *119*, (50), 12357-12366.
308. Nelson, D. L.; Lehninger, A. L.; Cox, M. M., *Lehninger Principles of Biochemistry*. Macmillan: 2008.
309. Pio, C. A.; Lopes, D. A., Chlorine Loss from Marine Aerosol in a Coastal Atmosphere. *J. Geophys. Res. Atmos.* **1998,** *103*, (D19), 25263-25272.
310. Laskin, A.; Wang, H.; Robertson, W. H.; Cowin, J. P.; Ezell, M. J.; Finlayson-Pitts, B. J., A New Approach to Determining Gas-particle Reaction Probabilities and Application to the Heterogeneous Reaction of Deliquesced Sodium Chloride Particles with Gas-phase Hydroxyl Radicals. *J. Phys. Chem. A* **2006,** *110*, (36), 10619-10627.
311. Laskin, A.; Moffet, R. C.; Gilles, M. K.; Fast, J. D.; Zaveri, R. A.; Wang, B.; Nigge, P.; Shutthanandan, J., Tropospheric Chemistry of Internally Mixed Sea Salt and Organic Particles: Surprising Reactivity of NaCl with Weak Organic Acids. *J. Geophys. Res. Atmos.* **2012,** *117*, (D15).
312. Aluwihare, L. I.; Repeta, D. J.; Chen, R. F., A Major Biopolymeric Component to Dissolved Organic Carbon in Surface Sea Water. *Nature* **1997,** *387*, (6629), 166-169.
313. Henrichs, S. M.; Williams, P. M., Dissolved and Particulate Amino Acids and Carbohydrates in the Sea Surface Microlayer. *Mar. Chem.* **1985,** *17*, (2), 141-163.

314. Larsson, K.; Odham, G.; Södergren, A., On Lipid Surface Films on the Sea. I. A Simple Method for Sampling and Studies of Composition. *Mar. Chem.* **1974,** *2*, (1), 49-57.
315. Hung, C.-C.; Tang, D.; Warnken, K. W.; Santschi, P. H., Distributions of Carbohydrates, Including Uronic Acids, in Estuarine Waters of Galveston Bay. *Mar. Chem.* **2001,** *73*, (3), 305-318.
316. Skoog, A.; Benner, R., Aldoses in Various Size Fractions of Marine Organic Matter: Implications for Carbon Cycling. *Limnol. Oceanogr.* **1997,** *42*, (8), 1803-1813.
317. Mopper, K.; Dawson, R.; Liebezeit, G.; Ittekkot, V., The Monosaccharide Spectra of Natural Waters. *Mar. Chem.* **1980,** *10*, (1), 55-66.
318. Callaghan, A. H.; Deane, G. B.; Stokes, M. D., Two Regimes of Laboratory Whitecap Foam Decay: Bubble-plume Controlled and Surfactant Stabilized. *J. Phys. Oceanogr.* **2013,** *43*, (6), 1114-1126.
319. García-Flor, N.; Guitart, C.; Ábalos, M.; Dachs, J.; Bayona, J.; Albaigés, J., Enrichment of Organochlorine Contaminants in the Sea Surface Microlayer: An Organic Carbon-driven Process. *Mar. Chem.* **2005,** *96*, (3), 331-345.
320. Wurl, O.; Holmes, M., The Gelatinous Nature of the Sea-surface Microlayer. *Mar. Chem.* **2008,** *110*, (1), 89-97.
321. Erickson, H. P., Size and Shape of Protein Molecules at the Nanometer Level Determined by Sedimentation, Gel Filtration, and Electron Microscopy. *Biol. Proced. Online* **2009,** *11*, (1), 32.
322. Ogura, N., Molecular Weight Fractionation of Dissolved Organic Matter in Coastal Seawater by Ultrafiltration. *Mar. Biol.* **1974,** *24*, (4), 305-312.
323. McCarthy, M.; Hedges, J.; Benner, R., Major Biochemical Composition of Dissolved High Molecular Weight Organic Matter in Seawater. *Mar. Chem.* **1996,** *55*, (3-4), 281-297.
324. Cloern, J. E., Phytoplankton Bloom Dynamics in Coastal Ecosystems: A Review with Some General Lessons from Sustained Investigation of San Francisco Bay, California. *Rev. Geophys.* **1996,** *34*, (2), 127-168.
325. Azam, F.; Malfatti, F., Microbial Structuring of Marine Ecosystems. *Nature Rev. Microbiol.* **2007,** *5*, (10), 782-791.
326. Norrman, B.; Zwelfel, U. L.; Hopkinson, C. S.; Brian, F., Production and Utilization of Dissolved Organic Carbon During an Experimental Diatom Bloom. *Limnol. Oceanogr.* **1995,** *40*, (5), 898-907.
327. Frimmel, F., Characterization of Natural Organic Matter as Major Constituents in Aquatic Systems. *J. Contam. Hydrol.* **1998,** *35*, (1), 201-216.
328. Jiao, N.; Herndl, G. J.; Hansell, D. A.; Benner, R.; Kattner, G.; Wilhelm, S. W.; Kirchman, D. L.; Weinbauer, M. G.; Luo, T.; Chen, F., Microbial Production of Recalcitrant Dissolved Organic Matter: Long-term Carbon Storage in the Global Ocean. *Nature Rev. Microbiol.* **2010,** *8*, (8), 593-599.
329. Amon, R. M.; Benner, R., Combined Neutral Sugars as Indicators of the Diagenetic State of Dissolved Organic Matter in the Arctic Ocean. *Deep Sea Res Part 1 Oceanogr Res Pap.* **2003,** *50*, (1), 151-169.
330. Dai, X. F.; Shi, X. C.; Gao, X.; Liang, J.; Zhang, X. H., Salipiger Nanhaiensis sp nov., a Bacterium Isolated from Deep Sea Water. *Int. J. Syst. Evol. Microbiol.* **2015,** *65*, 1122-1126.

331. Pramanik, A.; Sundararaman, M.; Das, S.; Ghosh, U.; Mukherjee, J., Isolation and Charcterization of Cyanobacteria Possessing Antimicrobial Activity from the Sundarbans, The World's Largest Tidal Mangrove Forest. *J. Phycol.* **2011,** *47*, (4), 731-743.
332. Pérez-Bibbins, B.; Torrado-Agrasar, A.; Salgado, J. M.; Mussatto, S. I.; Domínguez, J. M., Xylitol Production in Immobilized Cultures: A Recent Review. *Crit. Rev. Biotechnol.* **2016,** *36*, (4), 691-704.
333. Handa, N.; Yanagi, K., Studies on Water-extractable Carbohydrates of the Particulate Matter from the Northwest Pacific Ocean. *Mar. Biol.* **1969,** *4*, (3), 197-207.
334. Hecky, R.; Mopper, K.; Kilham, P.; Degens, E., The Amino Acid and Sugar Composition of Diatom Cell-walls. *Mar. Biol.* **1973,** *19*, (4), 323-331.
335. Gershey, R. M., Characterization of Seawater Organic Matter Carried by Bubble-generated Aerosols. *Limnol. Oceanogr* **1983,** *28*, (2), 309-319.
336. Chrost, R.; Faust, M., Organic Carbon Release by Phytoplankton: Its Composition and Utilization by Bacterioplankton. *J. Plankton Res.* **1983,** *5*, (4), 477-493.
337. Cowie, G. L.; Hedges, J. I., Carbohydrate Sources in a Coastal Marine Environment. *Geochim. Cosmochim. Acta* **1984,** *48*, (10), 2075-2087.
338. Ogura, N., High Molecular Weight Organic Matter in Seawater. *Mar. Chem.* **1977,** *5*, (4-6), 535-549.
339. Marty, J.; Žutić, V.; Precali, R.; Saliot, A.; Ćosović, B.; Smodlaka, N.; Cauwet, G., Organic Matter Characterization in the Northern Adriatic Sea with Special Reference to the Sea Surface Microlayer. *Mar. Chem.* **1988,** *25*, (3), 243-263.
340. Burrows, S. M.; Gobrogge, E.; Fu, L.; Link, K.; Elliott, S. M.; Wang, H.; Walker, R., OCEANFILMS-2: Representing Coadsorption of Saccharides in Marine Films and Potential Impacts on Modeled Marine Aerosol Chemistry. *Geophys. Res. Lett.* **2016**.
341. Reid, J. S.; Eck, T. F.; Christopher, S. A.; Koppmann, R.; Dubovik, O.; Eleuterio, D.; Holben, B. N.; Reid, E. A.; Zhang, J., A Review of Biomass Burning Emissions part III: Intensive Optical Properties of Biomass Burning Particles. *Atmos. Chem. Phys.* **2005,** *5*, (3), 827-849.
342. Ramanathan, V.; Crutzen, P.; Kiehl, J.; Rosenfeld, D., Aerosols, Climate, and the Hydrological Cycle. *Science* **2001,** *294*, (5549), 2119-2124.
343. Carslaw, K.; Lee, L.; Reddington, C.; Pringle, K.; Rap, A.; Forster, P.; Mann, G.; Spracklen, D.; Woodhouse, M.; Regayre, L., Large Contribution of Natural Aerosols to Uncertainty in Indirect Forcing. *Nature* **2013,** *503*, (7474), 67-71.
344. Lipsky, E. M.; Robinson, A. L., Effects of Dilution on Fine Particle Mass and Partitioning of Semivolatile Organics in Diesel Exhaust and Wood Smoke. *Environ. Sci. Technol.* **2006,** *40*, (1), 155-162.
345. Vakkari, V.; Kerminen, V. M.; Beukes, J. P.; Tiitta, P.; Zyl, P. G.; Josipovic, M.; Venter, A. D.; Jaars, K.; Worsnop, D. R.; Kulmala, M., Rapid Changes in Biomass Burning Aerosols by Atmospheric Oxidation. *Geophys. Res. Lett.* **2014,** *41*, (7), 2644-2651.